



National Library  
of Canada

Bibliothèque nationale  
du Canada

Canadian Theses Service

Service des thèses canadiennes

Ottawa, Canada  
K1A 0N4

## NOTICE

The quality of this microform is heavily dependent upon the quality of the original thesis submitted for microfilming. Every effort has been made to ensure the highest quality of reproduction possible.

If pages are missing, contact the university which granted the degree.

Some pages may have indistinct print especially if the original pages were typed with a poor typewriter ribbon or if the university sent us an inferior photocopy.

Previously copyrighted materials (journal articles, published tests, etc.) are not filmed.

Reproduction in full or in part of this microform is governed by the Canadian Copyright Act, R.S.C. 1970, c. C-30.

## AVIS

La qualité de cette microforme dépend grandement de la qualité de la thèse soumise au microfilmage. Nous avons tout fait pour assurer une qualité supérieure de reproduction.

S'il manque des pages, veuillez communiquer avec l'université qui a conféré le grade.

La qualité d'impression de certaines pages peut laisser à désirer, surtout si les pages originales ont été dactylographiées à l'aide d'un ruban usé ou si l'université nous a fait parvenir une photocopie de qualité inférieure.

Les documents qui font déjà l'objet d'un droit d'auteur (articles de revue, tests publiés, etc.) ne sont pas microfilmés.

La reproduction, même partielle, de cette microforme est soumise à la Loi canadienne sur le droit d'auteur, SRC 1970, c. C-30.

On Weighted  
Quadrature Amplitude Modulation:  
Power-Bandwidth Performance,  
Synchronization and Detection

by

Andy D. Kucar

A thesis  
presented to the University of Ottawa  
in fulfillment of the  
thesis requirement for the degree of  
Doctor of Philosophy

in

Ottawa, Ontario

Permission has been granted to the National Library of Canada to microfilm this thesis and to lend or sell copies of the film.

The author (copyright owner) has reserved other publication rights, and neither the thesis nor extensive extracts from it may be printed or otherwise reproduced without his/her written permission.

L'autorisation a été accordée à la Bibliothèque nationale du Canada de microfilmer cette thèse et de prêter ou de vendre des exemplaires du film.

L'auteur (titulaire du droit d'auteur) se réserve les autres droits de publication; ni la thèse ni de longs extraits de celle-ci ne doivent être imprimés ou autrement reproduits sans son autorisation écrite.

ISBN 0-315-46793-2



UNIVERSITÉ D'OTTAWA  
UNIVERSITY OF OTTAWA

## ACKNOWLEDGEMENT

The author would like to gratefully acknowledge the help provided by many individuals during the course of this research.

Sincere thanks go to his supervisor, Dr. Kamilo Feher, for his supervising; encouragement and support. A special appreciation goes to Dr. Willem Steenaart and Dr. Peter Galko for their invaluable help and understanding.

Fruitful discussions with the members of author's candidacy and thesis defence committees: Dr. A. Javed, Dr. J. Wight, Dr. W. McGee, Dr. W. Steenaart, and Dr. P. Goud are greatly appreciated.

Thanks is also extended to M.X. Chen, J. Coll, H. Girard, M. Hamze, D. Hatzinakos, P. Hill, Z.Z. Lei, P. Leung, J.X. Li, D. Makrakis, P. Mathiopoulos, M.S. Murthy, K. Nagaraj, H. Ohnishi, D. Prendergast, I. Sasase, M. Sato, R. Scott, K. Sreenath, M. St-Amand, I. Tezcan, J. Thorpe, K.T. Wu, A. Yongacoglu, and R. Zakarevicius for their assistance and support.

The help of many other individuals at the University of Ottawa, Telesat and Iskra, where the author was affiliated during his study, is deeply appreciated.

The author has been privileged to work with Dr. J. Vugrinec, whose honesty, hard dedicated work, broad knowledge and friendly human approach stimulated this contribution.

Finally, the author is deeply embeded to his spouse Mira for her timely support and understanding, and to their lovely daughters Dorothy and Kristina for their patience and cooperation. The author's brother Edward, parents, and the whole family deserve a special appreciation for their invaluable contributions.

**ABSTRACT**

This thesis investigates the performance characteristics of the newly introduced weighted quadrature amplitude modulation (WQAM) family and its corresponding new receivers.

A WQAM signal format consists of two quadrature components of the carriers that have generally unequal powers, and are modulated with independent data streams of different rates and different pulse shapes — composed of the rectangular and cosine waveforms, in general. Modulation schemes such as quadrature phase shift keying (QPSK), staggered QPSK (SQPSK), minimum shift keying (MSK), staggered quadrature overlapped raised cosine (SQORC), unbalanced QPSK, and M-ary QAM (MQAM) are all members of the WQAM family.

In order to reduce the adjacent channel interference, by using the gradient search technique, a few new pulse shapes giving a narrow mainlobe and minimal sidelobe levels are found.

The performance of 4-state WQAM schemes is evaluated in the adjacent channel interference linear and nonlinear channel environments. The results indicate that one of the new staggered WQAM schemes outperforms other known members of the WQAM family, i.e. (S)QPSK, MSK and (S)QORC in almost all practical situations.

The impact of amplitude and group delay distortions on MQAM schemes with more than 4 states is evaluated. Staggered QAM schemes perform better in the presence of linear group delay impairments, but nonstaggered schemes are less sensitive to linear amplitude gain impairments.

The correct detection of WQAM signals requires accurate carrier phase and symbol timing at the receiver. Therefore, a composite phase and timing estimation and data detection of WQAM signal sets is analyzed. By using a maximum likelihood approach, four new joint phase and timing estimators, for balanced and unbalanced WQAM schemes, are derived. At high signal-to-noise ratios, phase estimator and detector schemes merge into the classical decision feedback carrier recovery loop (DFCRL). The performance of this loop, employing an integrate-and-sample device in each quadrature arm (active loop), is evaluated in the presence of both carrier uncertainty  $\phi$  and timing uncertainty  $\lambda$ .

The performance of overlapped schemes is degraded if classical carrier recovery schemes are employed, e.g. by 1.09 dB if SQORC is used. The theoretical results are experimentally verified on our Intersymbol-Jitter-Free (IJF) 64 kb/s modem. New equalized DFCRL which employs a simple 3-tap transversal equalizer in each quadrature arm is proposed for the carrier recovery and the detection of overlapped schemes. Our new loop does not exhibit the performance degradation associated with classical schemes.

Using a maximum-a posteriori probability approach and knowledge of the phase uncertainty  $\phi$ , timing uncertainty  $\lambda$ , and nonlinearity surface of the loop  $h(\phi, \lambda)$  — accumulated over corresponding observation intervals — improved loops, i.e. crosstalk cancellation DFCRL, timing intersymbol interference cancellation DFCRL, and FEEDLOOP, are introduced and analyzed. The theoretical results are verified by the Monte Carlo simulation. These loops

perform almost as well as a continuous wave (pilot tone) carrier recovery loop, do not exhibit quadrant ambiguities, and might be employed for phase and timing estimation and the detection of balanced and unbalanced WQAM schemes. The advantages of the new loops over the classical one become greater at lower probabilities of error and when higher state schemes are employed. For example at  $P_e = 10^{-6}$  and in the presence of a normalized loop detuning of 0.7, the crosstalk cancellation loop (and FEEDLOOP) outperforms the classical one by 2.4 dB, assuming QPSK modulation is employed.

The impact of phase noise on the performance of MQAM, M-ary phase shift keying and M-ary quadrature partial response systems in a Gaussian noise environment is computed. For all cases the degradation due to phase noise is found to be less than 1 dB if a carrier-to-phase noise ratio in a double-sided Nyquist bandwidth  $(C/N)_p$  is more than 10 dB higher than the carrier-to-thermal noise ratio  $(C/N)_c$  required for the probability of error performance  $P_e = 10^{-6}$ . Performance graphs are presented which enable a fast first order approximation of the phase noise requirements of a system to be estimated. Our engineering rule-of-thumb approximations are in a close agreement with the results of measurements.

## CONTENTS

Acknowledgment .....	v
Abstract .....	vii
Contents .....	x
List of Abbreviations .....	xiii
List of Figures .....	xvii
List of Tables .....	xxii
1. Introduction .....	1
1.1 The demand for power-bandwidth efficiency .....	2
1.2 The demand for accurate carrier phase and symbol timing estimation, and detection .....	4
1.3 Thesis outline .....	6
2. 4-state WQAM schemes .....	9
2.1 System description and spectrum optimization .....	11
2.2 Performance in ACI environment .....	18
2.2.1 Linear channel .....	18
2.2.2 Hardlimited channel .....	21
2.3 Conclusion .....	23
3. 256 and 1024QAM schemes .....	24
3.1 System considerations .....	26
3.2 Computer simulation model .....	27
3.3 Results .....	30
3.4 Conclusion .....	41
4. On composite phase and timing estimation and detection of weighted QAM signals .....	42
4.1 System description and optimization strategy .....	44
4.2 Maximum likelihood (ML) approach .....	48
4.2.1 Classical DFRC loop .....	63
4.2.2 Equalized DFRC loop .....	72

4.3	Maximum a posteriori (MAP) approach	79
4.3.1	Crosstalk cancellation DFRC loop	81
4.3.2	Timing ISI cancellation DFRC loop	89
4.3.3	FEEDLOOP	91
4.4	Conclusion	94
5.	Performance of M-ary modulation systems in the presence of phase noise	96
5.1	Phase noise characterization	98
5.2	Performance evaluation	99
5.3	Conclusion	106
6.	Thesis summary	107
7.	Research proposal	110
8.	References	112
8.1	Books	114
8.2	Special issues	116
8.3	Other publications	117
A.	Computer programs printout	128

## LIST OF ABBREVIATIONS

ACI	.....	Adjacent Channel Interference
AM/AM	.....	Amplitude Modulation to Amplitude Modulation Transfer due to Nonlinearity
AM/PM	.....	Amplitude Modulation to Phase Modulation Transfer due to Nonlinearity
BLQAM	.....	Blackman Quadrature Amplitude Modulation (QAM scheme employing the Blackman window as an elementary pulse shape)
BPSK	.....	Binary Phase Shift Keying
CCDFCRL	.....	Crosstalk Cancellation Decision Feedback Carrier Recovery
CCI	.....	Cochannel Interference
$(C/N)$	.....	Carrier-to-noise ratio in a specified bandwidth
$(C/N)_6$	.....	Carrier-to-thermal noise ratio in a specified bandwidth required for the probability of error performance $P_e = 10^{-6}$
$(C/N)_p$	.....	Carrier-to-phase noise ratio in a specified bandwidth
CR	.....	Carrier Recovery
CW	.....	Continuous Wave
DA	.....	Data Aided (Approach)
DFCRL	.....	Decision Feedback Carrier Recovery Loop
DTTL	.....	Data Transition Tracking Loop
FEC	.....	Forward Error Correction (Codes)
FEEDLOOP	.....	Feedback, Estimation of phase, Estimation of timing, Decision LOOP (an acronym)
GD	.....	Group Delay
HL	.....	Hard Limiter
HMQAM	.....	Hamming Quadrature Amplitude Modulation (QAM scheme employing the Hamming window as an elementary pulse shape)
HPA	.....	High-Power Amplifier
IJF	.....	Intersymbol Jitter Free (Fehler's QPSK)
ISD	.....	Integrate-Sample-and-Dump (Circuit)
ISI	.....	Intersymbol Interference
LO	.....	Local Oscillator
LPAM	.....	L-ary Pulse Amplitude Modulation
MAP	.....	Maximum a Posteriori
ML	.....	Maximum Likelihood
MMSK	.....	Modified Minimum Shift Keying

MPSK	M-ary Phase Shift Keying
MQAM	M-ary Quadrature Amplitude Modulation
MQPR	M-ary Quadrature Partial Response
MSK	Minimum Shift Keying
P/S	Parallel-to-Serial Converter
$P_e$	Probability of Error
$P(e \phi)$	Conditional Probability of Error (conditioned on the phase uncertainty $\phi$ )
QAM	Quadrature Amplitude Modulation
QPSK	Quadrature Phase Shift Keying
QORC	Quadrature Overlapped Raised Cosine
RX	Receiver
SCPC	Single Channel per Carrier (Satellite System)
sign(a)	Signum of the Quantity a
SNR	Signal-to-Noise Ratio
S/N	Signal-to-Noise Ratio
$SNR_{IF}$	Signal-to-Noise Ratio within the Intermediate Frequency (IF) Bandwidth
SP	Signal Processor, Signal Processing
S/P	Serial-to-Parallel Converter
SQAM	Staggered Quadrature Amplitude Modulation
SQPSK	Staggered Quadrature Phase Shift Keying
SQORC	Staggered Quadrature Overlapped Raised Cosine
SSB	Single Sideband
S3MQAM	Staggered (Offset) Quadrature Amplitude Modulation scheme employing the class 3 minimal window as an elementary pulse shape
TDA	Transition Detector in the A Channel
TDB	Transition Detector in the B Channel
TR	Timing Recovery
TWTA	Travelling Wave Tube Amplifier
TX	Transmitter
UD	Uncertainty Diagram
$U_\phi$	Phase Uncertainty (Diagram)
VCO	Voltage Controlled Oscillator
VCC	Voltage Controlled Clock
WQAM	Weighted Quadrature Amplitude Modulation
3MQAM	Quadrature Amplitude Modulation scheme employing the class 3 Minimal window as an elementary pulse shape
4MQAM	Quadrature Amplitude Modulation scheme employing the class 4 minimal window as an elementary pulse shape



*List of Abbreviations*

$\lambda$	.....	timing uncertainty
$\phi$	.....	phase uncertainty
$h(\phi, \lambda)$	.....	nonlinearity surface of the loop
$p(\phi, \lambda)$	.....	probability density function of the process $\{\phi, \lambda\}$
$\rho \equiv SNR_L$	.....	Signal-to-Noise Ratio within the loop bandwidth

LIST OF FIGURES

Figure 1.1. The flowchart of the thesis .....	7
Figure 2.1. The weighted quadrature amplitude modulation system .....	12
Figure 2.2. The signal shapes (windows) of the WQAM schemes .....	16
Figure 2.3. The power spectral densities of the WQAM schemes .....	17
Figure 2.4. The simulation model of the QAM system .....	19
Figure 2.5. The linear channel performance of the WQAM schemes .....	20
Figure 2.6. The hardlimited channel performance of the WQAM schemes .....	22
Figure 3.1. The computer model of the MQAM system .....	29
Figure 3.2. The performance degradation of the 256 and the 1024QAM (1.544/1.6) Mb/s systems versus the linear group delay impairments .....	31
Figure 3.3. The performance degradation of the 256 and the 1024QAM (1.544/1.6) Mb/s systems versus the parabolic group delay impairments .....	32
Figure 3.4. The performance degradation of the 256 and the 1024QAM (1.544/1.6) Mb/s systems versus the linear amplitude gain impairments .....	33
Figure 3.5. The performance degradation of the 256 and the 1024QAM (1.544/1.6) Mb/s systems versus the parabolic amplitude gain impairments .....	34
Figure 3.6. The performance degradation of the 1024QAM (2.048/2.1) Mb/s systems versus the group delay impairments .....	36
Figure 3.7. The performance degradation of the 1024QAM (2.048/2.1) Mb/s systems versus the amplitude gain impairments .....	37

Figure 3.8.	The 256QAM 0.2 MBd system with the $\alpha = 0.2$ filtering	38
Figure 3.9.	The S1024QAM 0.21 MBd system with the $\alpha = 0.14$ filtering	39
Figure 3.10.	The 1024QAM 0.21 MBd system with the $\alpha = 1.0$ filtering	40
Figure 4.1.	The typical conditional probability of error $P(e \phi)$ , the probability density function $p(\phi)$ , and the average probability of error $P_e$ curves of the MQAM schemes	45
Figure 4.2.	The joint phase and timing estimator for the WQAM schemes, which corresponds to the eqs. (4.20 a-c) in the text	54
Figure 4.3.	The joint phase and timing estimator for the 4 state 2x2 baseband level WQAM schemes, which corresponds to the eqs. (4.28 a-c) in the text	56
Figure 4.4.	The joint phase and timing estimator for the QPSK schemes, which corresponds to the eqs. (4.29 a-c) in the text	58
Figure 4.5.	The joint phase and timing estimator for the MSK schemes, which corresponds to the eqs. (4.30 a-c) in the text	60
Figure 4.6.	The classical decision feedback carrier recovery loop	62
Figure 4.7.	The $P(e \phi)$ performance of the MQAM schemes	65
Figure 4.8.	The $P(e \lambda)$ performance of the EPAM schemes	66
Figure 4.9.	The 256QAM uncertainty diagram	68
Figure 4.10.	The QPSK nonlinearity surface	70
Figure 4.11.	The SQPSK nonlinearity surface	71
Figure 4.12.	The autocorrelation functions of the WQAM schemes	73
Figure 4.13.	a) The SQORC signal shapes. b) The average probability of error performance	

measurements (•) of the IJF (SQORC) modem employing the classical carrier recovery loop .....	74
Figure 4.14. The SQORC uncertainty diagram when employing the classical DFCRL .....	75
Figure 4.15. The equalized decision feedback carrier recovery loop .....	77
Figure 4.16. The SQORC uncertainty diagram when employing the equalized DFCRL .....	78
Figure 4.17. a) The QAM degradation model of the loop caused impairments due to the phase uncertainty $\phi$ and the timing uncertainty $\lambda$ . b) The corresponding equalization model .....	80
Figure 4.18. The crosstalk cancellation DFCRL .....	82
Figure 4.19a The (S)QPSK nonlinearity curves employing the crosstalk cancellation decision feedback carrier recovery loop .....	83
Figure 4.19b The MQAM nonlinearity curves when employing the classical decision feedback carrier recovery loop .....	84
Figure 4.20. The QPSK $\log_{10} P_e$ performance versus the carrier-to-noise ratio C/N in dB in the double-sided Nyquist bandwidth and the normalized loop detuning (loop stress) $\beta_N$ as a parameter, when employing the classical or the crosstalk cancellation decision feedback carrier recovery loop .....	87
Figure 4.21. The 4QAM and the 16QAM $\log_{10} P_e$ performance versus the normalized loop detuning (loop stress) $\beta_N$ , when employing the classical or the crosstalk cancellation decision feedback carrier recovery loop .....	88
Figure 4.22. The timing intersymbol interference cancellation DFCRL .....	90
Figure 4.23. The FEEDLOOP .....	92
Figure 4.24. The 256QAM uncertainty diagram when employing the FEEDLOOP .....	93
Figure 5.1. The average probability of error performance of the M-ary schemes versus the carrier-to-thermal noise ratio .....	100

Figure 5.2. The 256QAM average probability of error performance versus the carrier-to-thermal noise ratio with the carrier-to-phase noise ratio as a parameter 101

Figure 5.3. The degradation of the MPSK systems in dB, with respect to the theoretical value necessary to achieve the  $P_e = 10^{-6}$  performance, versus the carrier-to-phase noise ratio in the double-sided Nyquist bandwidth in dB ..... 102

Figure 5.4. The degradation of the MQAM systems in dB, with respect to the theoretical value necessary to achieve the  $P_e = 10^{-6}$  performance, versus the carrier-to-phase noise ratio in the double-sided Nyquist bandwidth in dB ..... 103

Figure 5.5. The degradation of the MQPR systems in dB, with respect to the theoretical value necessary to achieve the  $P_e = 10^{-6}$  performance, versus the carrier-to-phase noise ratio in the double-sided Nyquist bandwidth in dB ..... 104

# LIST OF TABLES

*List of Tables*      xxiii

Table 2.1. The summary of the WQAM system performance .....	15
Table 3.1. The 256 and the 1024QAM system considerations .....	26

1

1

## INTRODUCTION

2

1

## 1.1 DEMAND FOR POWER-BANDWIDTH EFFICIENCY

The available radio frequency spectrum is a limited natural resource, which demands that efficient transmission of information be done. In a satellite system the maximum available power utilization is of primary concern, which requires a power efficient modulation schemes to be employed [B1]-[B11]. An efficient power utilization requires a spacecraft traveling wave tube amplifier (TWTA), or solid-state power amplifier (SSPA), and possibly an earth station high-power amplifier (HPA) to be operated in a nonlinear mode, which causes intermodulation, AM/AM and AM/PM transfer, and spectrum regeneration. To avoid a spectrum spillover into the neighboring channels — which will cause adjacent channel interference (ACI) — a careful design of the signal shaping filters in the modem, the output filter which follows the HPA, transponder input and output multiplex filters, and possibly linearization of the HPA and TWTA needs to be done. However, tight filtering might cause increased intersymbol interference (ISI). Multipath propagation within adjacent transponders on the spacecraft and reuse of frequency by other satellite or terrestrial links will cause a further degradation of the system performance. In this environment, nearly constant envelope modulation schemes with 4 or 8 states and a spectral efficiency of about 1 bit/s/Hz are used.

In cable, telephone line, and terrestrial radio systems (except a mobile radio) the bandwidth efficiency is of primary concern, which leads to the use of high-level modulation schemes [S4], [S6]. 256 state schemes with a spectral efficiency in the range of 6 bit/s/Hz are the field leaders. Such schemes are sensitive to amplitude and group delay imperfections associated with practical (analog) filters, selective fading channels, ACI and cochannel interference (CCI), and phase and timing uncertainties.

During the past years, a tremendous amount of effort has been devoted to this subject. This includes novel modulation schemes, which perform well in a complex ACI and CCI environment [S1], [S3], [S5]; power efficient coding but at the expense of bandwidth efficiency [B19]; Ungerböck trellis coding in which an increased power efficiency is achieved without sacrifice of the bandwidth efficiency, but at the expense of the increased number of signal states and therefore increased sensitivity to carrier and timing uncertainties [P11], [S6]; combinations of modulation and coding, different linearization techniques to improve performance of a modulator-power amplifier combination [B10], [S3] — all these at the transmitter — and different carrier and timing recovery schemes with and without equalization at the receiver [B3], [S7]-[S8].

Many investigations into new modulation schemes (pulse shapes) have been based on trial-and-error methods. After a "new" pulse shape (modulation scheme) has been found, heuristically, the analysis — usually supported by computer simulation — followed. The procedure

was iterated until the "best" results were achieved. However, an optimal pulse shape for non-linearly amplified systems has not been described in the literature. Chapter 2 of this thesis deals with this problem in a different way. The idea and details are presented in the thesis outline and Chapter 2, respectively.

The bandwidth efficient modulation schemes usually operate in a linear channel environment, and the practical constraints differ significantly from those systems which operate in a power limited environment. Some of the typical problems, i.e. group delay and amplitude linearity impairments, estimation of the carrier phase and timing and detection, and degradation due to phase noise of the frequency sources are tackled in Chapter 3, Chapter 4 and Chapter 5, respectively.

## 1.2 DEMAND FOR ACCURATE CARRIER PHASE AND TIMING ESTIMATION, AND DETECTION

The correct detection of WQAM signals requires accurate carrier phase and symbol timing. It is desired to estimate these parameters directly from measurements on the received data signal. Since WQAM schemes are of the suppressed carrier type, a nonlinear operation on the receiver data is necessary. When the number of states or the imbalance increases, estimation becomes more complex and a higher sensitivity to any phase uncertainty  $\phi$  and timing uncertainty  $\lambda$  might be expected. Some bandwidth and power efficient modulation schemes employ pulse weighting and overlapping to improve performance in nonlinear, ACI and CCI environments, which impose additional constraints on the receiver.

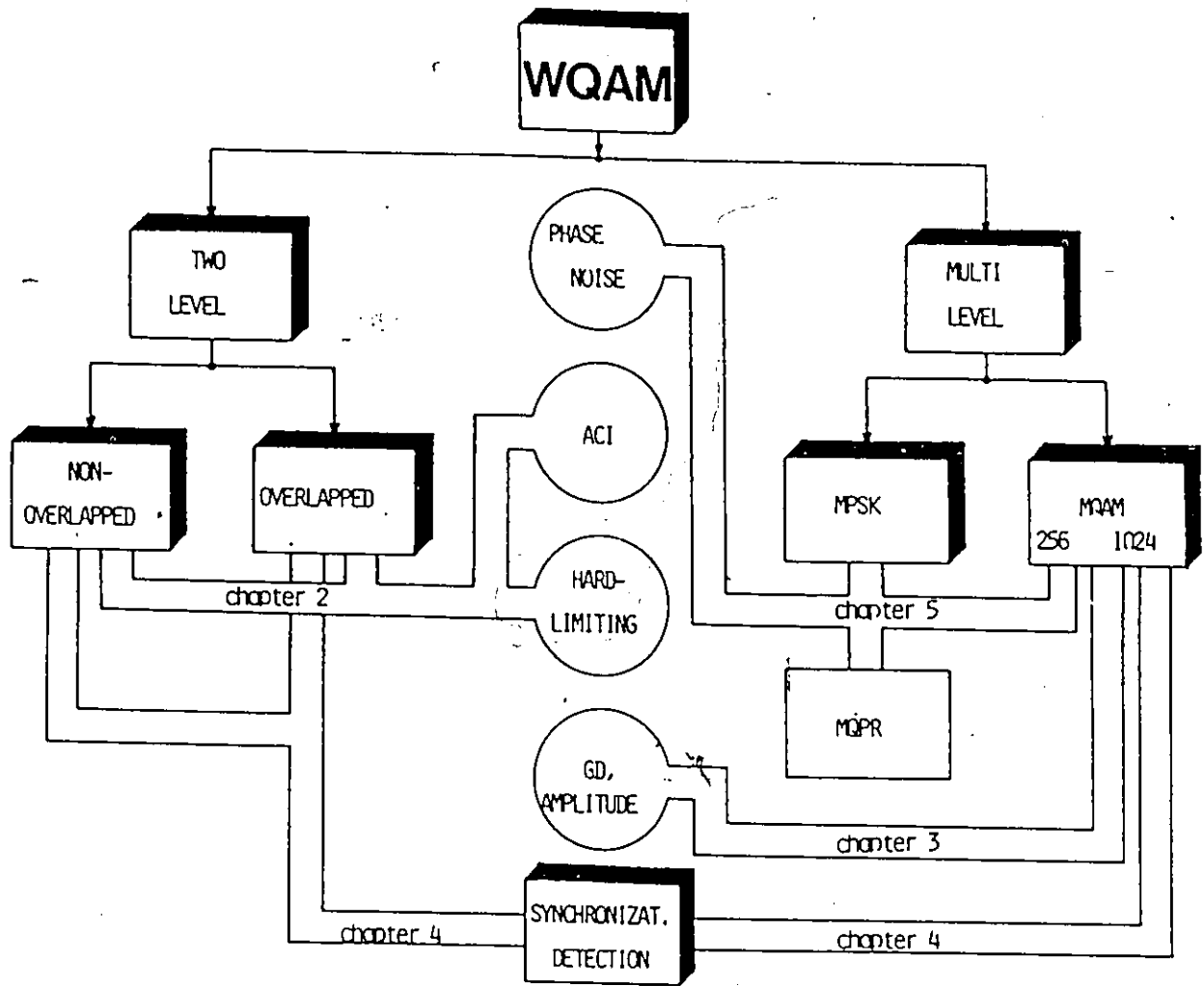
Numerous techniques for carrier and timing (clock) information recovery, based on a maximum likelihood (ML) or a maximum a posteriori (MAP) probability approach, have been analyzed. Among others, references [B3], [S7]–[S8] excellently summarize these efforts. Carrier recovery (CR) loops for an unbalanced QPSK scheme are analyzed in [P127]–[P130]. New CR loops for overlapped schemes are proposed in [P115]–[P116]. However, studies [P131]–[P136] show the superiority of a joint estimation of phase and timing, to which attention is devoted in Chapter 4 of this contribution. Kobayashi [P131] proposed a joint estimator and detector for QAM and SSB schemes which employs a decision-directed feedback. The proposed ML receiver is a recursive type which minimizes the probability of error of an entire data sequence and estimates phase and timing. Gaussian and generally unknown channels which invoke an adaptive receiver are analyzed. Falconer and Salz [P132] showed that the receiver of [P131] does not necessarily produce minimum symbol error probability. An ML receiver is proposed where phase and timing estimates are updated on a symbol-per-symbol basis, rather than by an average taken over an entire data sequence. Mengali [P133] analyzed two different recursive methods for carrier phase and timing acquisition. The coupling between phase and timing is discussed in view of its effects upon the stability and convergence rate of the synchronization algorithm. Franks [P134], and Meyers and Franks [P135] examined a joint carrier phase and symbol timing estimation in SSB and MQAM schemes. The importance of cyclostationarity for CR and timing recovery (TR) is highlighted and new joint CR+TR ML based estimators are suggested. Poklemba [P136] presented a similar, although different, practical realization of a joint estimator-detector for the QPSK signal set. Kam [P83] pointed out some of the shortcomings of previous approaches and suggested a new ML receiver.

Most of the previous approaches dealt with optimization of phase and timing estimators and eventually the conditional probability of error for small uncertainties  $\phi$  and  $\lambda$ . However, in practice, an average probability of error  $P_e = \int_{\phi} \int_{\lambda} P(e|x, y) p(x, y) dx dy$  is more important. Optimization of the system performance corresponds to the minimization of

the average probability of error  $P_e$ , which is equivalent to the minimization of the product  $P(e|\phi, \lambda) p(\phi, \lambda)$ . Herein, the product of this conditional probability of error  $P(e|\phi, \lambda)$  times the probability density function  $p(\phi, \lambda)$  of a joint estimator shall be minimized over the entire range of  $\phi$  and  $\lambda$ . The probability density function  $p(\phi, \lambda)$  of the decision feedback loop is difficult to obtain in a closed form. Therefore, we describe  $p(\phi, \lambda)$  by the nonlinearity surface of the loop  $h(\phi, \lambda)$ , the importance and meaning of which is explained further, later. By knowing  $P(e|\phi, \lambda)$  and  $h(\phi, \lambda)$  we are able to minimize  $P_e$  and therefore improve the overall system performance.

### 1.3 THESIS OUTLINE

The flowchart of the thesis is presented in Fig.1.1. In Chapter 2 the WQAM family is introduced. First, attention is focused on the pulse shaping and overlapping at the transmitter to keep the spectral density main lobe as narrow as possible while at the same time minimizing the sidelobe level within the prescribed bandwidth. Although coding might be combined with the WQAM schemes to improve their performance even further, coding analysis is outside the scope of this contribution. Our signal shape consists of weighted rectangular and cosine functions only, which allows an easy practical implementation of the modem even at the highest data rates. We use the gradient search technique to minimize sidelobe levels within an equivalent baseband  $|fT_s| = 0$  to 5 (this corresponds to 1 to 2 adjacent channels in practice). The results of this minimization are the values of the weighting coefficients in the WQAM modulator, the meaning of which will be further explained, later. It might be expected that such a modulation scheme with low sidelobes will perform well in an ACI environment. Results which follow show that this hypothesis is correct. A comparison of 4 state WQAM schemes — new and known — is given, including signal shapes, power spectral densities, and performance in the linear and nonlinear ACI environments — typical for satellite systems.



Fla.1.1. The flowchart of the thesis.

WQAM schemes with more than 4 states might combine different signal shapes at different signal levels to improve the performance in a particular environment. As an example of a possible application of high level WQAM schemes, in Chapter 3, a brief feasibility study of the transmission of North American T1 (DS1) 1544 kb/s or CCITT 2048 kb/s data stream over the analog 240 kHz wide CCITT supergroup is performed. The performance of the simplest, rectangular window, 256 and 1024 state, staggered and nonstaggered QAM schemes is analyzed in the presence of amplitude and group delay imperfections — typically associated with the supergroup filters.

In Chapter 2 and Chapter 3 a perfect knowledge of the carrier phase and symbol timing was assumed. However, this information is not available at the receiver in advance. Before any decision has to be made, the receiver must establish the correct phase and timing reference. This problem is considered in Chapter 4. First, by using a ML approach, four new joint phase and timing estimators are derived. Then, based on the knowledge of  $\phi$ ,  $\lambda$ , and estimator-detector behavior accumulated over the observation interval(s), MAP detectors are derived. Since both phase and timing estimates depend on the probability of correct decision, this improved decision leads to an improved estimation, etc. As a result, a few new structures are suggested which cancel (or at least significantly attenuate) data-dependent pattern jitter, i.e. these loops perform nearly as well as a continuous wave (CW) loop.

The performance of any coherent digital modulation system is degraded by an excessive amount of phase noise. In this contribution the term phase noise is synonymous with non-thermal random interference such as phase noise of the frequency sources (local oscillators, up/down converters, voltage controlled oscillators), etc. In the past a considerable effort has been devoted by various authors to this subject [B3], [B13], [B15], [B16], [B20]. However, an exact mathematical solution for modulation schemes with more than 4 states has not been published. In Chapter 5 we adopt a practical approach, which yields useful performance curves in which the degradation due to phase noise can be readily seen.

Chapter 6 summarizes the thesis results. In the Chapter 7 a brief research proposal for the future work is outlined. This contribution concludes with an extensive list of references, and a printout of the computer programs.

## 4-state WQAM schemes

A brief outline of the chapter follows. In Section 2.1 the WQAM system is introduced. A family of weighted cosine pulse shapes is defined. The general expressions for power spectral density are given. The new modulation schemes termed 3M-, 4M-, HM- and BLQAM are introduced. In Section 2.2 the performance of the WQAM schemes is evaluated in linear and hardlimited channels and in the presence of ACI by means of a computer simulation. A comparison of new and known modulation schemes is given in the table and graphs.

## 2.1. SYSTEM DESCRIPTION AND SPECTRUM OPTIMIZATION

A weighted quadrature amplitude modulation signal  $s(t)$  with data rates  $R_A = 1/T_A$  and  $R_B = 1/T_B$ , where  $A$  and  $B$  represent the in-phase and quadrature channels respectively, Fig.2.1.(a), is

$$s(t) = \sqrt{P_A} \sum_i \alpha_i w_A(t - iT_A) \cos(2\pi f_c t) + \sqrt{P_B} \sum_j \beta_j w_B[t - (jT_B + \delta)] \sin(2\pi f_c t) \quad (2.1)$$

The quantities  $P_A$  and  $P_B$  are the signal powers,  $\alpha_i$  and  $\beta_j$  are independent binary ( $\pm 1$ ) random data sequences which could be obtained from an information sequence through a serial-to-parallel converter,  $w_A(t)$  and  $w_B(t)$  are the pulse shaping functions (weights, windows) in channels  $A$  and  $B$ , defined in the interval  $(0, T_A)$  and  $(0, T_B)$ , respectively,  $f_c$  is the carrier frequency, and  $\delta$  is an arbitrary delay in the  $B$  channel. The present concept might be applied to multilevel, multistate systems, where, in general, different pulse shapes might be employed on different baseband levels. As an example,  $M$ -ary QAM schemes employ  $\alpha_i, \beta_j \in \{-(L-1), \dots, -1, +1, \dots, +(L-1)\}$  and rectangular signal shape on every baseband signal level. By allowing  $P_A \neq P_B$  and  $R_A \neq R_B$  an (intentionally) unbalanced system might be analyzed, or the effects of imbalance on the performance of balanced systems might be estimated. Generally  $P_A \neq P_B$  and  $R_A \neq R_B$ ; i.e., the QAM system is unbalanced. In this chapter, we limit our attention to the 4-state balanced system with  $P_A = P_B = P$ ,  $R_A = R_B = R = 1/2T = 1/T_S$  and  $w_A(t) = w_B(t) = w(t)$ , particularly the nonstaggered schemes with  $\delta = 0$  and the staggered schemes with  $\delta = T = T_S/2$ . The equivalent baseband power spectral density of the WQAM signal  $s(t)$  is [B15,p.120]

$$S_b(f) = \frac{2}{T_S} |W(f)|^2 \quad (2.2)$$

where  $W(f)$  is the Fourier transform of the baseband signal pulse shape  $w(t)$ .

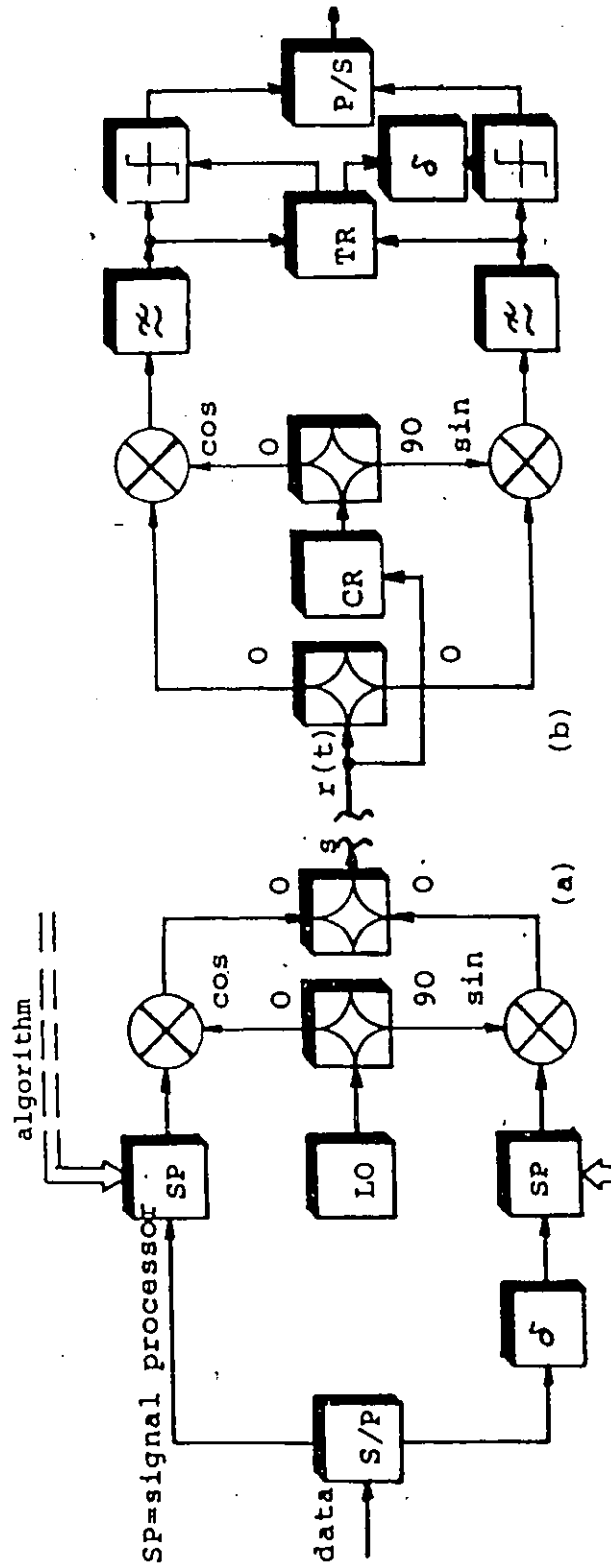


Figure 2.1. The weighted quadrature amplitude modulation system: a) Transmitter, b) Receiver.

We define the weighted cosine pulse shape as

$$w_n(t) \stackrel{\text{def}}{=} \begin{cases} \sum_{i=1}^n g_i \cos\left(\frac{\pi t K_i}{L_i}\right), & \text{for } |t| \leq L_i/2, \\ 0, & \text{for } |t| > L_i/2, \end{cases} \quad (2.3a)$$

where

$$K_1 = 0, \quad \sum_{i=1}^n g_i = 1. \quad (2.3b)$$

The quantity  $g_i$  is the weighting factor ( $g_i = a_i$ , or  $g_i = b_i$ , refers to the A or B channel, respectively),  $K_i$  is the frequency parameter,  $L_i$  is the overlapping factor normalized to the symbol duration  $T_s$  and  $n$  is the class of the signal pulse shape. The Fourier transform of the weighted cosine signal is

$$\begin{aligned} W_n(f) &= \int_{-L_i/2}^{L_i/2} w_n(t) \exp(-j2\pi ft) dt \\ &= \frac{1}{2} \sum_{i=1}^n a_i L_i \left[ W_{io}\left(fL_i - \frac{K_i}{2}\right) + W_{io}\left(fL_i + \frac{K_i}{2}\right) \right] \end{aligned} \quad (2.4)$$

where

$$W_{io} = \frac{\sin \pi x}{\pi x} = \text{sinc}(\pi x) \quad (2.5)$$

The right choice of  $g_i$ ,  $K_i$  and  $L_i$  parameters depends on the desirable goal. Here, our primary concern is the spectral density with narrow mainlobe and minimal sidelobe levels within  $|fT_s| = 0$  to 5. Since the signal with larger overlapping factor  $L_i$  possesses the narrower spectrum,  $L = L_i$  could be one of additional practical constraints. On the other hand, the signal with large  $L$  causes intersymbol interference at the sampling point. A further increase in  $L$  leads to a multilevel signal. The signal  $w_n(t)$  with a smooth transitions from maximum to zero and a good compromise between the mainlobe width and the sidelobe levels suggests the  $K_i$  to be an even integer. As an example, assume the overlapping factor  $L_i = L$ , and  $n = 3$ . The Fourier transform  $W_3(f)$  of the class 3 signals,  $n = 3$  in (2.4), is

$$\begin{aligned} W_3(f) &= \underbrace{\left[ \frac{\sin(\pi f L/2)}{(\pi f L/2)} \right]}_{\text{QPSK like}} \underbrace{\left[ \frac{\cos(\pi f L/2)}{(fL)^2 - 1} \right]}_{\text{MSK like}} \\ &\times L \frac{4a_1 - (5a_1 - 4a_2 + a_3)(fL)^2 + (a_1 - a_2 + a_3)(fL)^4}{(fL)^2 - 1} \end{aligned} \quad (2.6)$$

The spectral density consists of a QPSK-like factor, a MSK-like factor, and a third factor which can be optimized to obtain a better spectral performance. Our results, reported in

Section 2.2, indicate that the signals obtained for the linear channel also have a good performance in non-linearly amplified (hardlimited) systems. The performance of modulation schemes is summarized in Table 2.1. The pulse shape which gives minimum sidelobes within the  $|fT_s| = 0$  to 5 frequency band is termed as the minimum. The choice of a pulse duration  $L$  will depend on an expected amount of ACI, frequency separation, and filter strategy. The subclass of windows termed as minimum, with  $L = T_s$  is also known as the Blackman-Harris family [P63]. If  $L > T_s$  the consecutive pulses will overlap, and the new elementary waveshape within the interval  $(-T_s/2, T_s/2)$  will generally be asymmetric about the plane  $t = 0$ . The + and - pulses will also be asymmetric. However, the symmetry is maintained in average.

The QPSK, BPSK, and MQAM schemes analyzed in Chapter 3, are using rectangular signal shape (Dirichlet window). The MSK consists of Hann 1 signal in each of two quadrature channels, and the  $B$  channel is additionally staggered by  $T_s/2$  to maintain a constant envelope of the signal  $s(t)$ , Fig. 2.1. However, all other modulation schemes employ overlapping techniques (overlapping factor  $L > 1$ ) to obtain a narrower spectrum. The envelope of signal  $s(t)$  is not constant in general. But spectrum sidelobes of schemes with the nonconstant envelope are far below the spectrum sidelobes of schemes with the constant envelope. They remain low even after hardlimiting, Fig. 2.3. The QORC scheme employs the Hann 2 signal window with the overlapping factor  $L = 2T_s$ . Further reduction of sidelobes level is achieved by employing the Hamming weighting and overlapping, i.e. the HMQAM.

In [P56] the MMSK signal family was introduced and the particular scheme with parameter  $A=0.8$  was found to be the best, based on a trial-and-error method. However, the BLQAM which is equivalent to the MMSK scheme with  $A=0.84$  seems to be the best.

The sidelobe level of the 3MQAM scheme is 12.7 dB lower than the BLQAM's and far below the QORC's. Additional sidelobe level reduction could be achieved at the expense of a wider mainlobe, i.e., by employing the 4MQAM.

The signal shapes  $w_n(t)$  and the corresponding power spectral densities are given in Fig. 2.2. and Fig. 2.3, respectively.

The 3MQAM outperforms MSK in the whole frequency band, as well the QPSK, except around the first zero of the QPSK at  $fT_s = 1$ . From  $fT_s = 1.17$  up, the sidelobes of 3MQAM are below the QORC. The 3MQAM represents a good compromise between the mainlobe width and the sidelobes level.

	Name of the window	1, zero width	Sidelobe level, dB <sub>r</sub>	Duration L/T	QAM name	a <sub>1</sub> K <sub>1</sub>	a <sub>2</sub> K <sub>2</sub>	a <sub>3</sub> K <sub>3</sub>	a <sub>4</sub> K <sub>4</sub>
1	Rectangular (Dirichlet)	1.00	-13.0	1.0	QPSK SQPSK	1.00000 0.00000	-	-	-
2	Cosine1 (Hann 1)	1.50	-23.0	1.0	MSK	-	1.00000	-	-
2	Cosine2 (Hann 2)	1.00	-31.4	2.0	QORC (IJF)	0.50000 0.00000	0.50000 2.00000	-	-
2	Hamming	1.17	-42.6	1.7	HMQAM	0.54000 0.00000	0.46000 2.00000	-	-
3	Blackman	1.50	-58.1	2.0	BLOAM	0.42000 0.00000	0.50000 2.00000	0.08000 4.00000	-
3	Minimum Bl.-Harris3	1.50	-70.8	2.0	3MQAM	0.42323 0.00000	0.49755 2.00000	0.07922 4.00000	-
4	Minimum Bl.-Harris4	2.00	-92.0	2.0	4MQAM	0.35875 0.00000	0.48829 2.00000	0.14128 4.00000	0.01168 6.00000

Table 2.1. The summary of WQAM system performance.

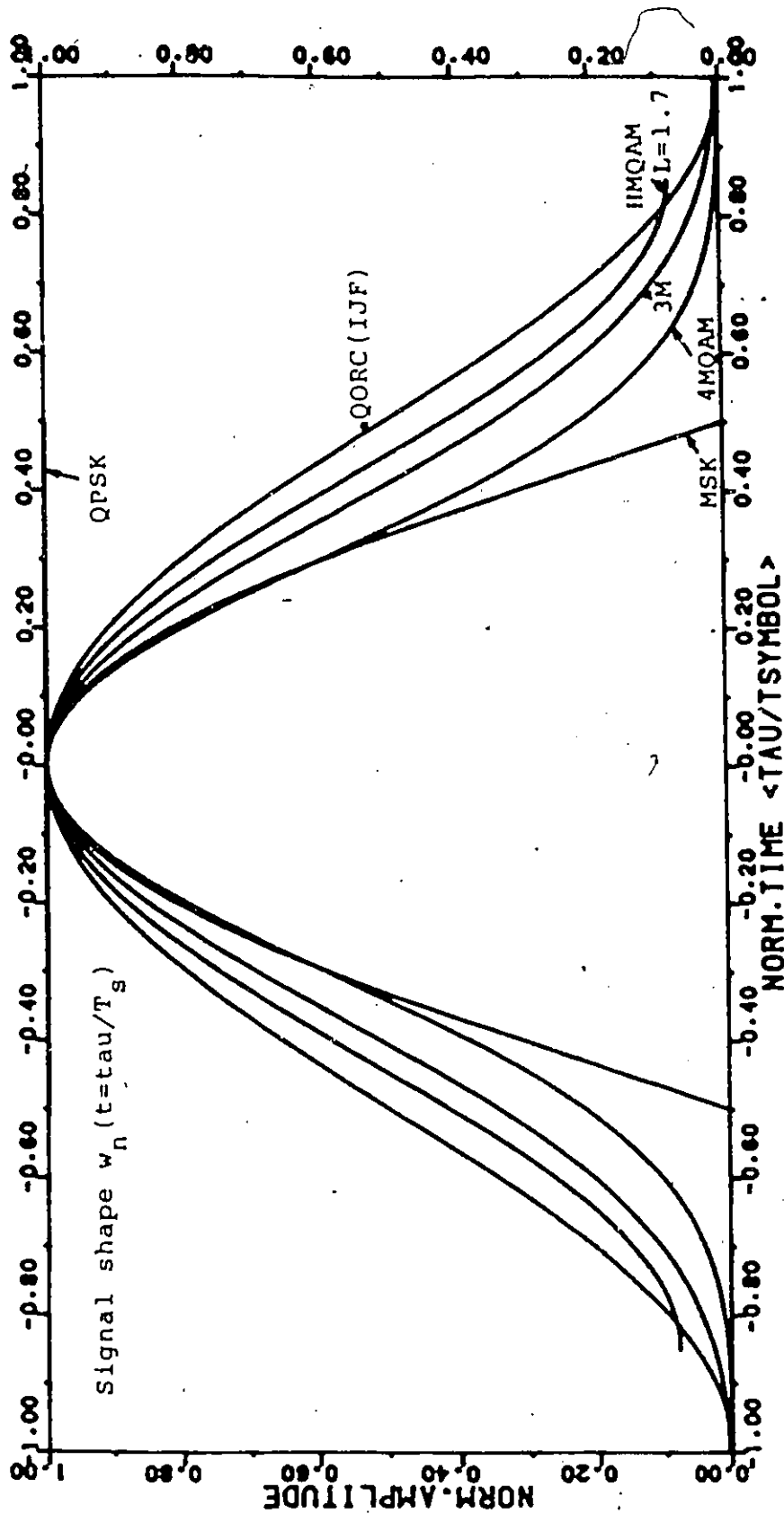


Figure 2.2. The signal shapes (windows) of the WQAM schemes: The QPSK (Dirichlet), MSK (cosine, Hann 1) — both the one symbol duration —, the 11MQAM (Hanning)  $L = 1.7 T_s$  symbol duration, the QORC, i.e. IJF (cosine squared, Hann 2), the 3MQAM (minimum class 3), and the 4MQAM (minimum class 4) modulation schemes — all two symbols duration.

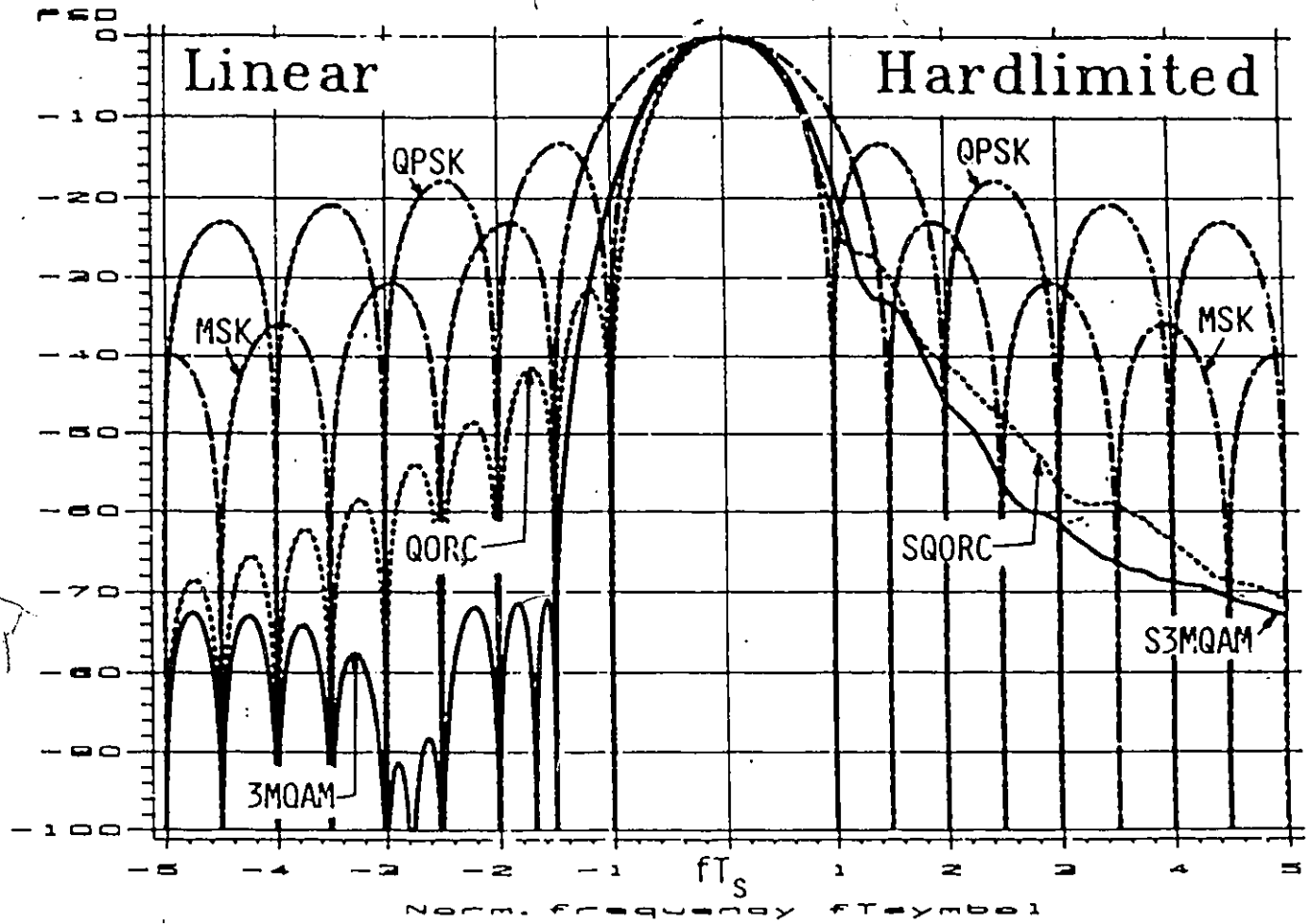


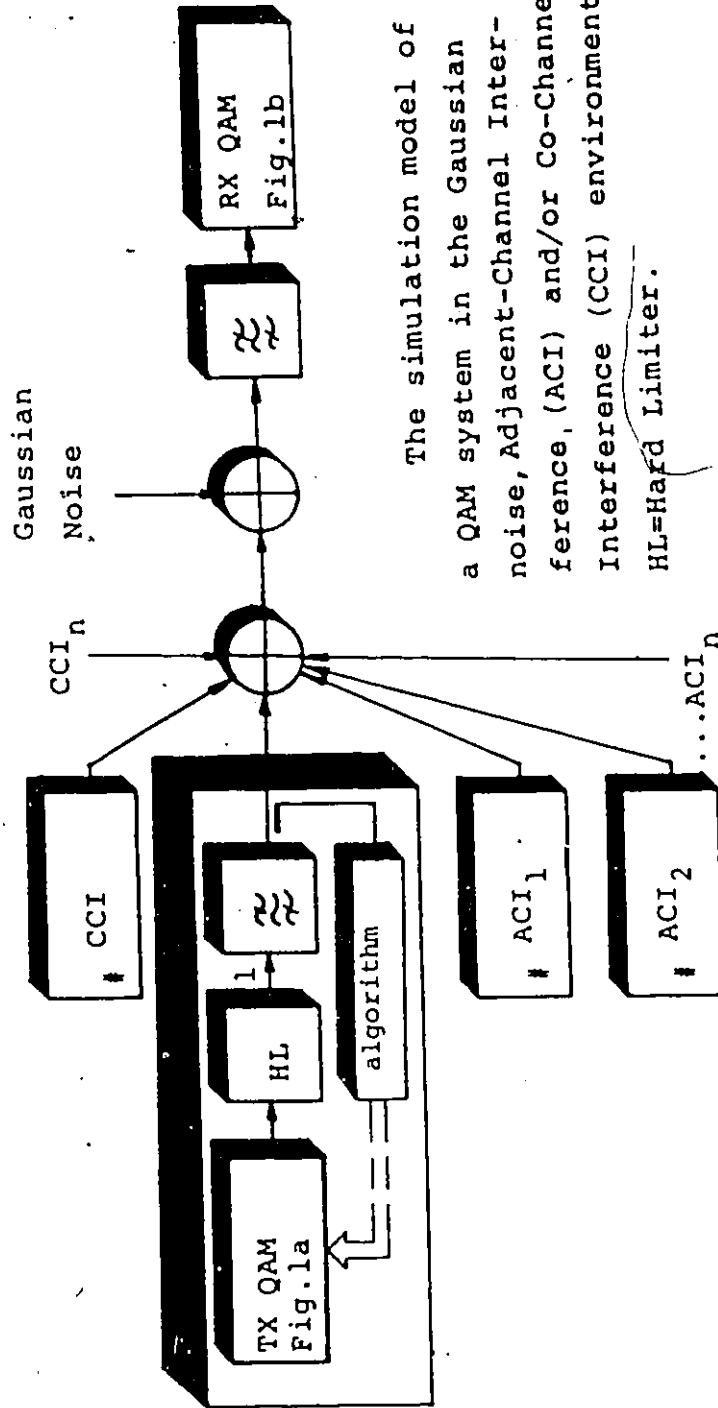
Figure 2.3. The power spectral densities of WQAM schemes. Ordinata in dB.

## 2.2 PERFORMANCE IN ACI ENVIRONMENT

To evaluate the performance of WQAM schemes in ACI environment the computer simulation procedure with the following assumptions is used. The WQAM receiver is illustrated in Fig.2.1(b). Here ideal carrier recovery (CR) and symbol timing recovery (STR) are assumed. The simulation model of a system is given in Fig.2.4. A 5th order phase equalized (constant group delay) Butterworth filter with single-sided bandwidth  $B_1 T_S = 0.55$  is assumed in every channel. The interferer's phases and symbol timings are randomized over the interval  $(0, 2\pi)$  and  $(0, T_S)$  respectively.

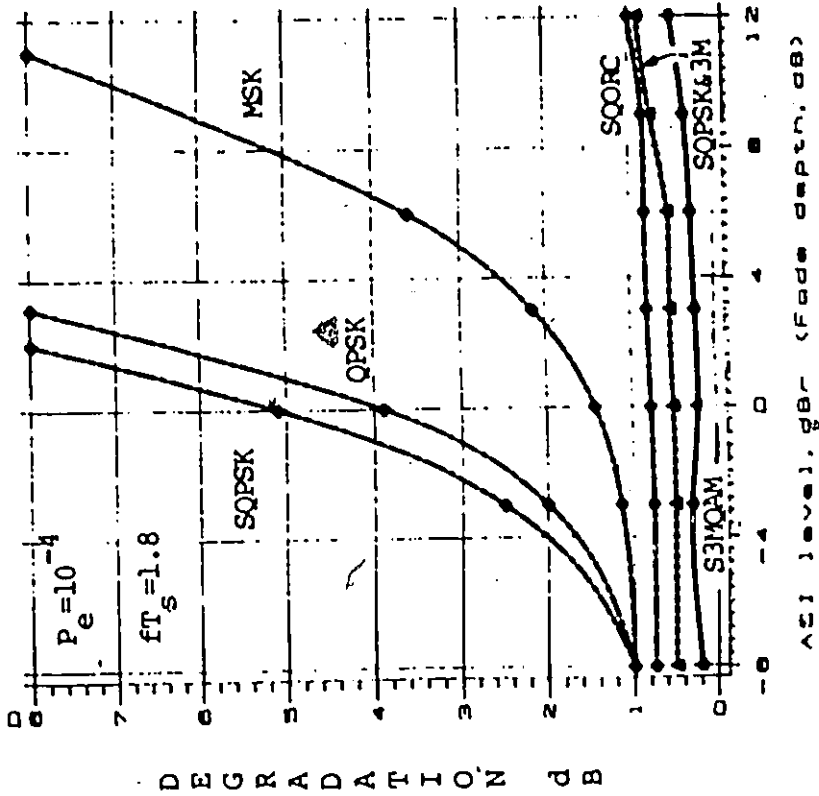
### 2.2.1 Linear channel

In the linear channel system model the hardlimiter in Fig.2.4 is by-passed. The performance of the WQAM systems vs. the normalized channel spacing frequency in the presence of two ACIs with the power level  $I_1 = I_2 = 0$  dB, equal to the power of the main channel, is summarized in Fig.2.5.(a). The performance of WQAM systems vs. the ACI interference level, i.e. the relative fading depth, is given in Fig.2.5.(b). The staggered S3MQAM using simple Butterworth filter is performing well even in the presence of strong ACI and outperforms QPSK, SQPSK, SQORC(SIJF) [B8],[P52], and MMSK [P56].

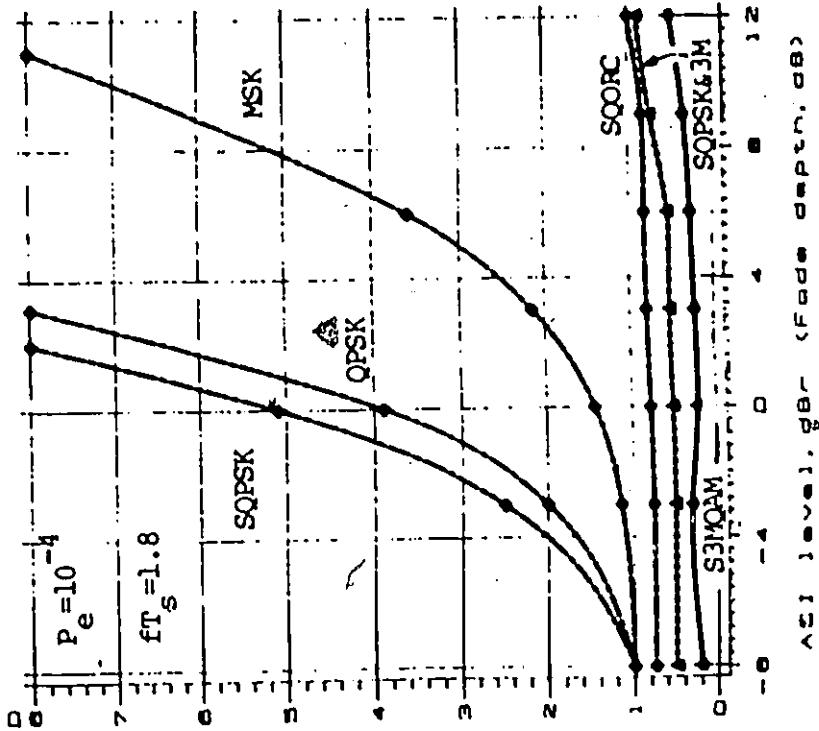


The simulation model of a QAM system in the Gaussian noise, Adjacent-Channel Interference, (ACI) and/or Co-Channel Interference (CCI) environment. HL=Hard Limiter.

Figure 2.4. The simulation model of a QAM system.



a) The performance of the WQAM systems versus the normalized channel spacing frequency  $fT_s$  in the presence of two equal power adjacent channel interferers.



b) The performance of the WQAM systems versus the adjacent channel interferers' level in dB (or flat fading depth in dB).

The ordinates represent the degradation in dB, relative to the theoretical value  $E_b/N_0 = 8.4$  dB at  $P_e = 10^{-4}$ . The (S)QPSK, MSK, (S)QORC, and (S)3MQAM — all, main channel and interferences are of the same type, correspondingly. The SQPSK & 3M labeled curve represents SQPSK main channel and two ACI interferences of the S3MQAM type.

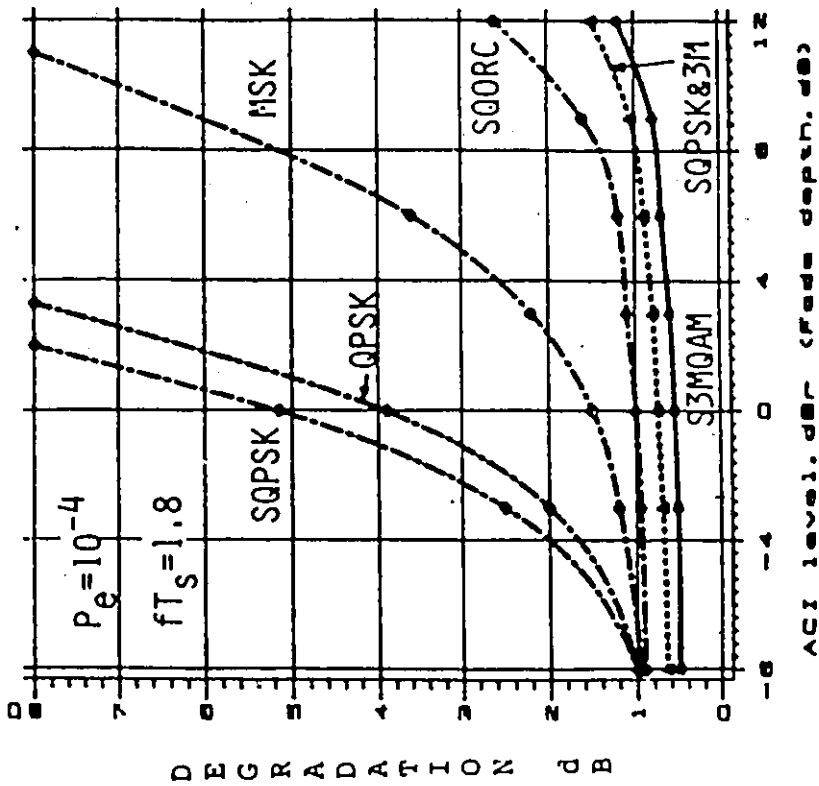
Figure 2.5. The linear channel performance of WQAM schemes.

### 2.2.2 Hardlimited channel

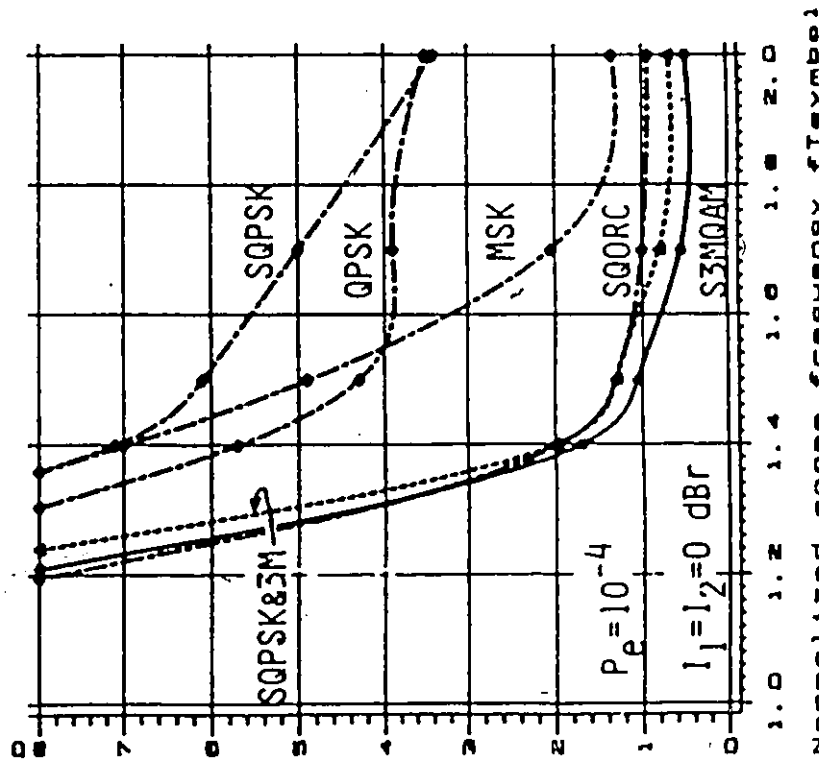
The power spectral density of the signal  $s(t)$ , Point 1 after the hardlimiter in Fig.2.4, is given in Fig.2.3. The sidelobes of S3MQAM scheme are about 10 dB below those of the SQORC and far below QPSK and MSK. In the present filtering strategy configuration, the constant envelope signals (QPSK, SQPSK and MSK) perform in exactly the same way as in the case of linear channel. The performance of the WQAM systems vs. the normalized channel space frequency and in the presence of two ACIs with the power level  $I_1 = I_2 = 0$  dB, equal to the level of the main channel, is summarized in Fig.2.6.(a). The performance of the WQAM system vs. the ACI interference level, i.e. a relative flat fading depth, is illustrated in Fig.2.6.(b).

The S3MQAM outperforms all competitors if a normalized space frequency of adjacent channels is larger than  $1.35 fT_5$ . As the fade depth increases the advantage of the S3MQAM becomes more obvious. As an example, at the fade depth of 12 dB, S3MQAM outperforms SQORC (LJF) modulation scheme by more than 1 dB, Fig.2.6b.

Single channel per carrier (SCPC) satellite systems above 10 GHz, and terrestrial and satellite systems for mobile, maritime, and aeronautical services, are some of the typical examples where these schemes might find an application. In practice, observed —main— channel might be faded due to the rain (above 10 GHz satellite SCPC systems) or due to the shadowing (mobile radio), while neighboring channels do not experience either fading or shadowing. Under these circumstances the main channel is experiencing an attenuation of the signal level, and in addition it must cope with an increased ACI. As it is shown, our new S3MQAM scheme outperforms its competitors under these practical conditions.



a) The performance of the WQAM systems versus the normalized spacing frequency  $fT_s$  in the presence of two equal power adjacent channel interferences.



b) The performance of the WQAM systems versus the adjacent channel interferers' level in dB (or flat fading depth in dB).

The ordinates represent the degradation in dB, relative to the theoretical value  $E_b/N_c = 8.4$  dB at  $P_e = 10^{-4}$ . The (S)QPSK, MSK, (S)QORC, and (S)3MQAM — all, main channel and interferences are of the same type, correspondingly. The SQPSK & 3M labeled curve represents SQPSK main channel and two ACI interferences of the S3MQAM type.

Figure 2.6. The hardlimited channel performance of WQAM schemes.

## 2.3 CONCLUSION

In this chapter the weighted quadrature amplitude modulation (WQAM) was introduced. By using the gradient search technique, a family of pulse shapes with a narrow mainlobe and minimal sidelobe levels within an equivalent baseband  $|fT_s| = 0$  to 5 (this corresponds to 1 to 2 adjacent channels in practice) was found. The performance of 4-state WQAM schemes was evaluated in the ACI linear and nonlinear channel environments, with the channel spacing and fading depth (signal attenuation) as parameters, by means of the computer simulation. One of the new staggered WQAM schemes, termed S3MQAM, outperforms other known members of the WQAM family, i.e. (S)QPSK, MSK and (S)QORC in almost all practical situations. By using the S3MQAM scheme more compact spacing —more efficient transmission, i.e. more b/s/Hz— than before might be possible.

256 and 1024QAM schemes

The WQAM family was introduced in the previous chapter. The performance of 4 state WQAM schemes was evaluated in the presence of ACI. In this chapter the performance of the 256 and the 1024QAM schemes, which employ rectangular window (pulse shape) at each symbol level, is evaluated in the presence of amplitude and group delay impairments. These are the typical impairments associated with the practical (analog) filters employed in the radio and cable systems.

An outline of the chapter follows. In Section 3.1 an overview of system considerations is given. The computer simulation model is presented in Section 3.2. The chapter concludes with the results of the computer simulation.

### 3.1 SYSTEM CONSIDERATIONS

To transmit 1544 (2048) kb/s over a 240 kHz wide CCITT supergroup, a digital modulation scheme with a spectral efficiency better than  $1544(2048)/240=6.43$  (8.53) b/s is required. To achieve this, (S)256QAM and (S)1024QAM schemes, with a theoretically maximum spectral efficiency of 8 b/s/Hz and 10 b/s/Hz respectively, are considered in this chapter. Forward error correcting (FEC) coding might be employed, which will bring the corresponding channel rate to the 1.6 Mb/s (2.1 Mb/s). Throughout this chapter the information rate of 1544 (2048) kb/s is associated with a channel rate of 1.6 (2.1) Mb/s. The 1.6 Mb/s might be transmitted by the 256QAM scheme, which will give the symbol rate of 0.2 MBaud and the spectral efficiency of 6.67 b/s/Hz. Should 1024QAM scheme be used, the symbol rate will be 0.16 MBaud, Table 3.1. In this case the less steep cosine filter with  $\alpha = 0.5$  would be sufficient ( $\alpha = 0.2$  if 256QAM is employed). The 2.1 Mb/s bit rate requires the 1024QAM to be employed, which gives the symbol rate of 0.21 MBaud, noise bandwidth of 210 kHz, channel spectral efficiency of 8.75 b/s/Hz and  $\alpha = 0.14$  filters, Table 3.1.

Mb/s	256QAM			1024QAM		
	MBaud	$\alpha$	b/s/Hz	MBaud	$\alpha$	b/s/Hz
1.6	0.20	0.20	6.67	0.16	0.50	6.67
2.1	—	—	—	0.21	0.14	8.75

### 3.2 COMPUTER SIMULATION MODEL

In practice, at the transmitter the 1.544 (2.048) Mb/s data stream might be interleaved and FEC encoded to 1.6 (2.1) Mb/s and split into two streams by a serial-to-parallel converter S/P. Each stream might be differentially and Gray encoded into the 16 (32) level signals with the symbol rate of 200 (210) kBaud. These signals are fed into the  $\alpha = 0.2$  ( $\alpha = 0.14$ ) cosine filters and modulated by the in-phase and quadrature signals.

256QAM (1024QAM) signal is fed to the in-phase and quadrature receiver. The in-phase signal is used to extract the symbol timing clock. After demodulation, the baseband adaptive transversal equalizer might be applied to equalize the impairments caused by the supergroup-through-connect filters and other system impairments. After Gray and differential decoding, the in-phase and quadrature signals are parallel-to-serial converted into a 1.6 (2.1) Mb/s signal. This signal is de-interleaved and FEC decoded and becomes the 1.544 (2.048) Mb/s replica of the original signal.

To be able to simulate the influence of amplitude and group delay impairments on the 256QAM and 1024QAM systems we adopted a simplified computer model without coding and equalization and with the following properties: the pseudo-random data has period of  $2^{31} - 1$ , a half million samples is used for every run, the carrier frequency is set to the zero, an ideal carrier recovery is assumed, Gaussian noise is included analytically and the timing recovery has the memory which is 256 symbols long, i.e. practically perfect timing exists. †

The computer model of the M-ary quadrature amplitude modulation, MQAM, system is given in Fig. 3.1. The input data stream  $d(t)$  with the data rate of 1.6 (2.1) Mb/s is split, by using the serial-to-parallel converter S/P, into the two independent data streams  $A(t)$  and  $B(t)$ , respectively. The  $B(t)$  could be staggered by a time delay  $\delta = T_S/2$ , where  $T_S$  is the time period of  $B(t)$ .  $A(t)$  and  $B(t)$  are processed in the  $2 \rightarrow L$  level converter,  $x/\sin x$  and  $\sqrt{\alpha}$  cosine filter to give the corresponding signals  $a(t)$  and  $b(t)$ , respectively.  $M = L \times L$  and  $\alpha$  is the roll-off factor of the cosine filter. The corresponding parameters are given in Table 3.1. The channel is represented by the filter  $H(f)$  and the white Gaussian noise. In the practice, the cascade of supergroup (SG)-through-connect filters might have a significant impact on the performance of transmission. At the receiver the in-phase and quadrature channels are fed into the  $\sqrt{\alpha}$  cosine filters. Assuming wide  $H(f)$ , this filtering will satisfy both Nyquist and matched filter criteria, i.e. an optimum reception. If this is not the case, an adaptive equalizer should be employed. The carrier recovery and timing recovery circuits provide the correct phase and timing instants to make a correct decision. Finally, by  $L \rightarrow 2$  mapping and the parallel-to-serial conversion P/S an estimation of the original data,  $\hat{d}(t)$ , is

† The carrier recovery and timing recovery schemes are analyzed in the Chapter 4.

available.

The results previously achieved by this computer model were in a close agreement with the measured results made on different hardware models with up to 256 states. Here, we present the performance of 256QAM and 1024QAM modems in the presence of amplitude or group delay imperfections similar to those associated with practical SG-through-connect filters.

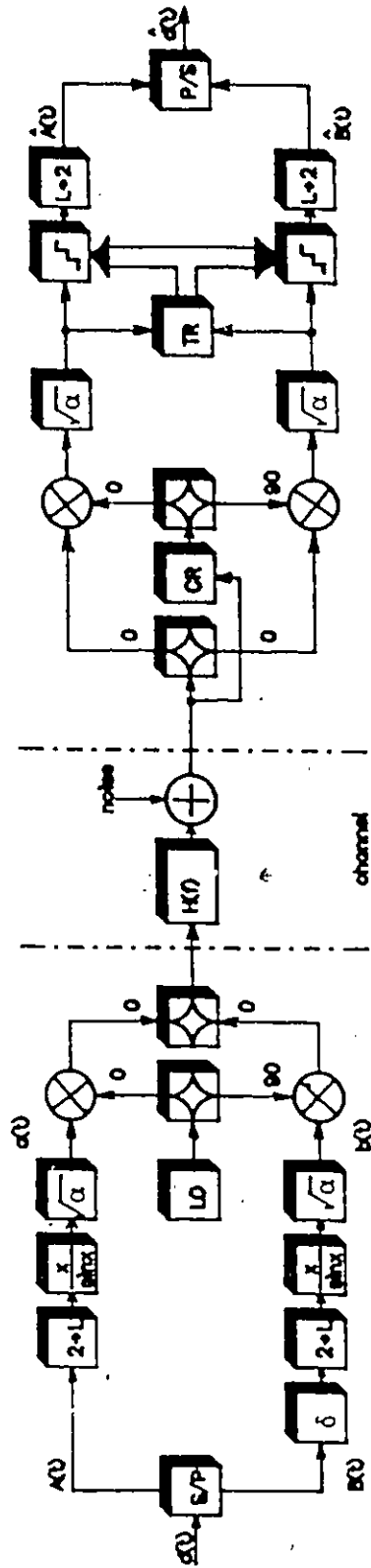


Figure 3.1.1. The computer model of MQAM system.

### 3.3. RESULTS

Three sets of results are presented. First, the performance of the 1.6 Mb/s modems using 256QAM schemes and a symbol rate of 0.2 MBaud is compared with the 1.6 Mb/s modems using 1024QAM schemes with a symbol rate of 0.16 MBaud.

- The degradation in dB is the difference between the carrier-to-noise ratio ( $C/N$ ) required to achieve the  $P_e = 10^{-6}$  performance when group delay or amplitude imperfections exist, and the ( $C/N$ )  $\doteq$  33 dB needed to achieve the same probability of error performance  $P_e$  with the 256QAM scheme in an ideal Gaussian channel environment.

The performance of 256QAM and 1024QAM systems in the presence of linear group delay is summarized in Fig.3.2. † Staggered schemes seem to be less sensitive to the linear group delay imperfections than their nonstaggered counterparts. In the presence of strong group delay impairments the S1024QAM, with more relaxed filter  $\alpha = 0.5$ , outperforms (S)256QAM schemes with  $\alpha = 0.2$ . In the Hermitian symmetric channel (parabolic group delay as given in Fig.3.3 and parabolic amplitude gain as given in Fig.3.5) the staggered and nonstaggered schemes perform equally. However, in the presence of the linear amplitude gain impairments nonstaggered schemes outperform their staggered counterparts, Fig.3.4, i.e. 256QAM gives the best performance and it is followed by S256QAM, 1024QAM and S1024QAM. Usually amplitude distortions are less difficult to be equalized, which might prefer staggered schemes to be employed.

---

† The definition of group delay and amplitude gain corresponds to that given in [B8, p.185].  
1 dB higher implementation margin for the 1024QAM schemes is assumed in figures which follow.

# 1.544 Mb/s @ 240 kHz SG

Linear group delay  $\mu\text{s}/240 \text{ kHz}$

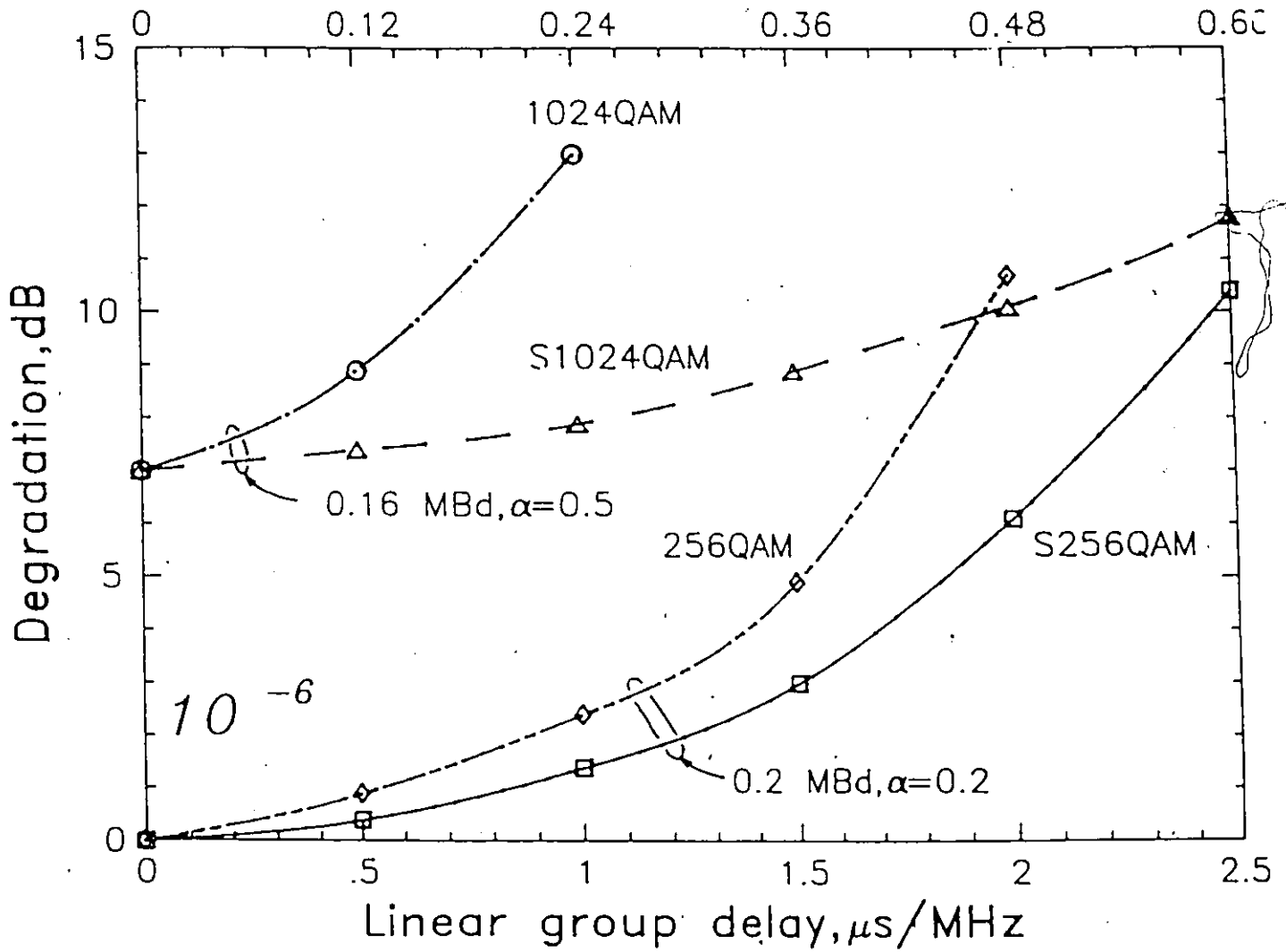


Figure 3.2. The performance degradation of the 256 and 1024QAM (1.544/1.6) Mb/s systems versus the linear group delay impairments. The degradation in dB is the difference between the C/N necessary to achieve the  $P_e = 10^{-6}$  performance when impairments are present, and the  $C/N \approx 33$  dB giving  $P_e = 10^{-6}$  without impairments.

1.544 Mb/s @ 240 kHz SG

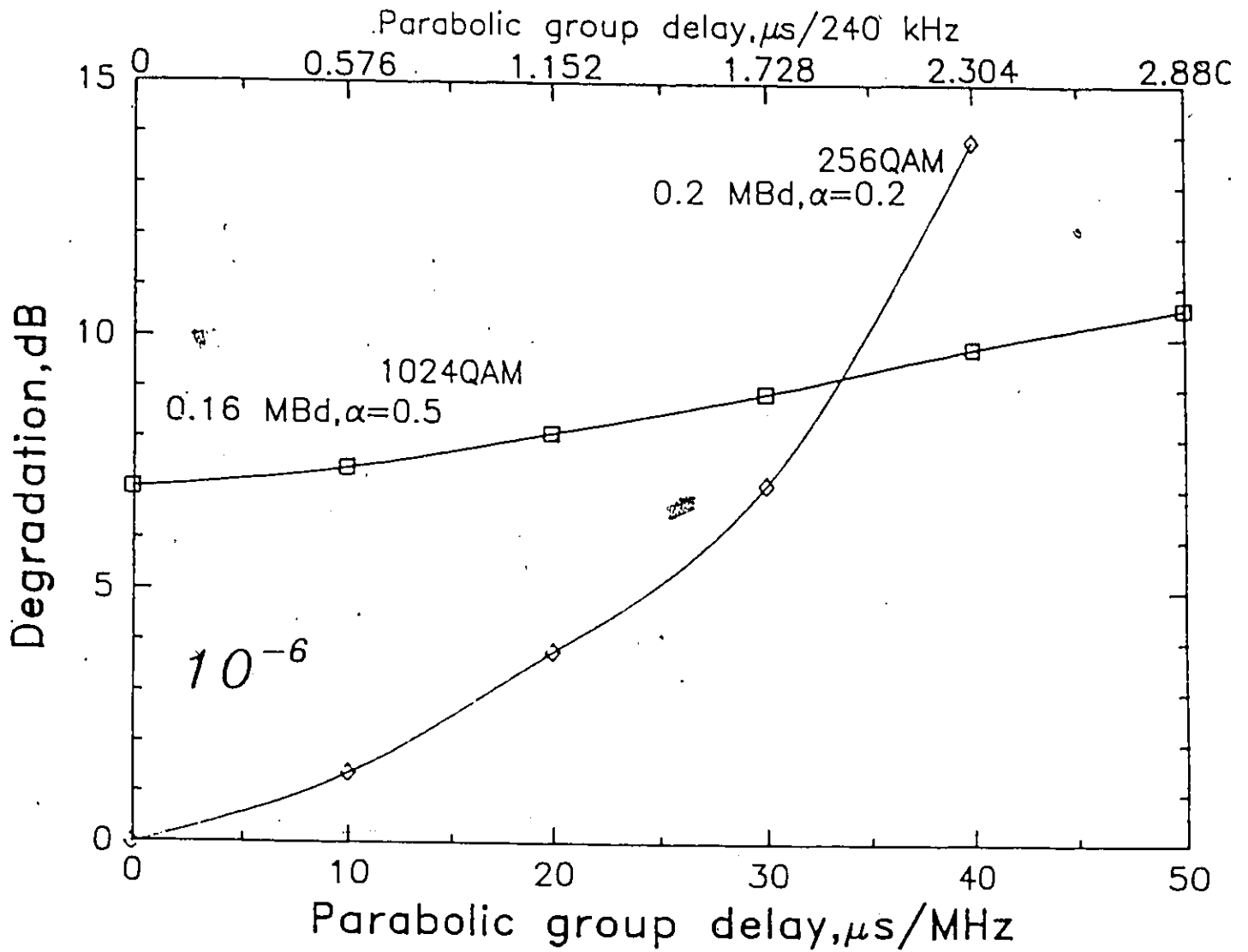


Figure 3.3. The performance degradation of the 256 and 1024QAM (1.544/1.6) Mb/s systems versus the parabolic group delay impairments. The degradation in dB is the difference between the C/N necessary to achieve the  $P_e = 10^{-6}$  performance when impairments are present, and the  $C/N \approx 33$  dB giving  $P_e = 10^{-6}$  without impairments.

1.544 Mb/s @ 240 kHz SG

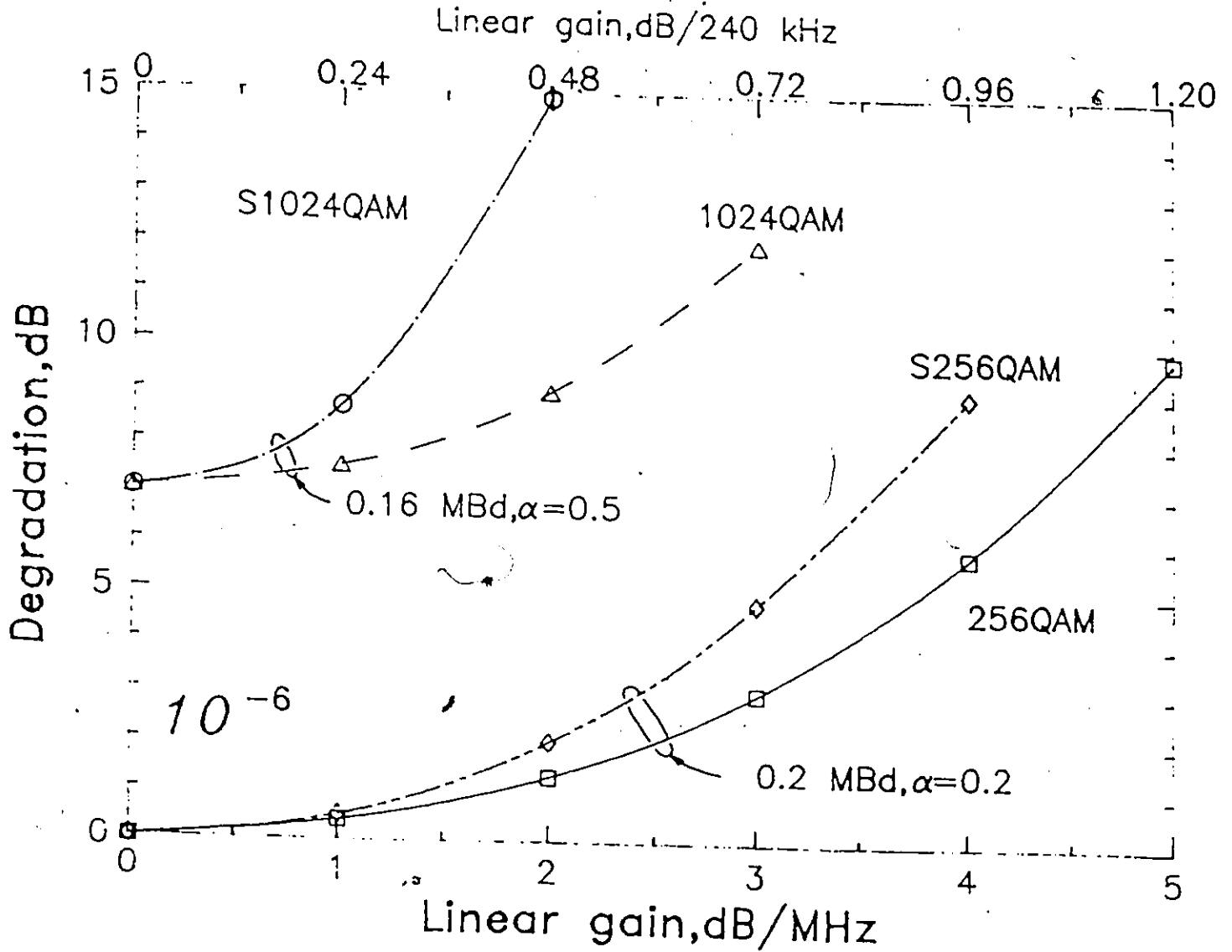


Figure 3.4. The performance degradation of the 256 and 1024QAM (1.544/1.6) Mb/s systems versus the linear amplitude gain impairments. The degradation in dB is the difference between the C/N necessary to achieve the  $P_e = 10^{-6}$  performance when impairments are present, and the  $C/N \approx 33$  dB giving  $P_e = 10^{-6}$  without impairments.

1.544 Mb/s @ 240 kHz SG

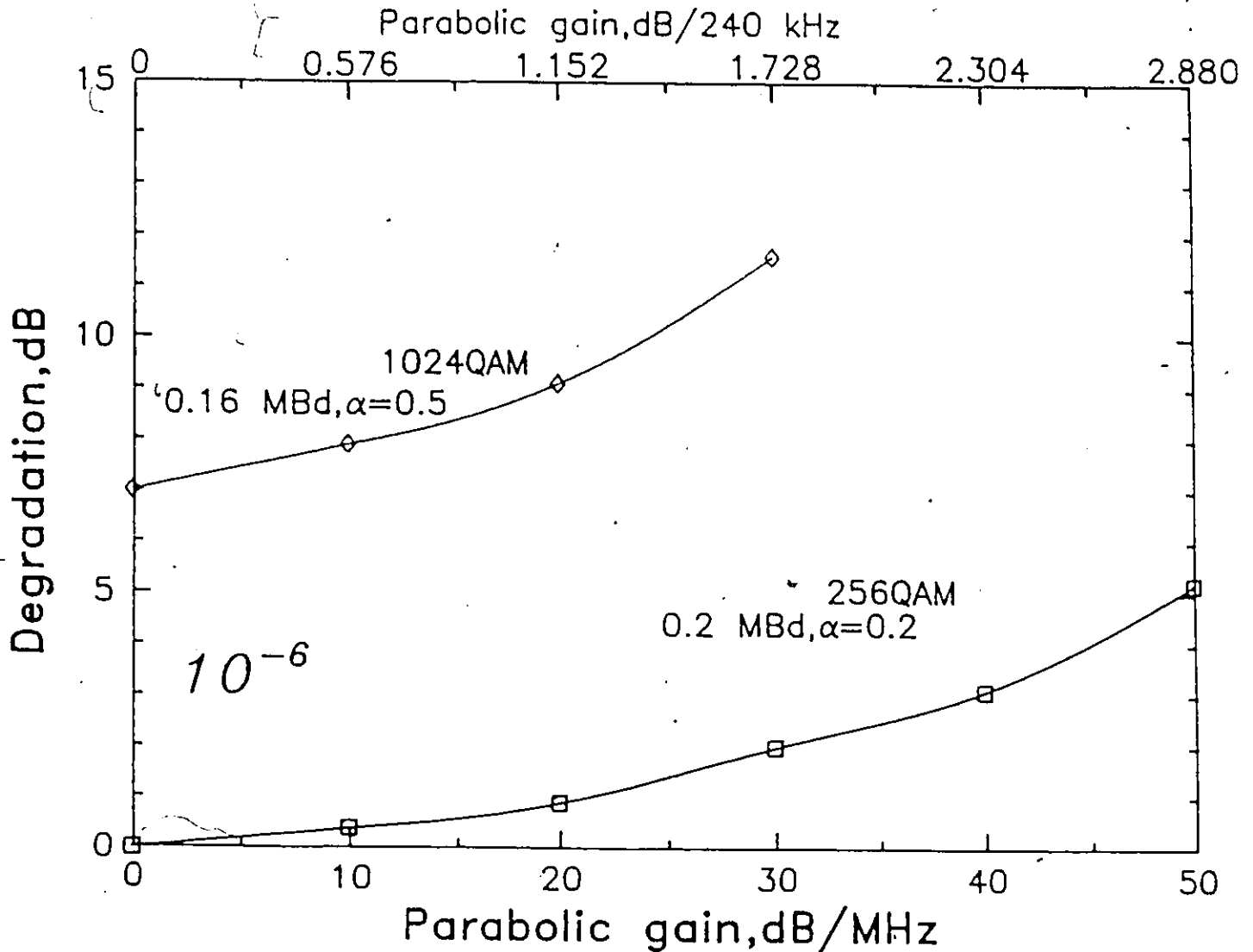


Figure 3.5. The performance degradation of the 256 and 1024QAM (1.544/1.6) Mb/s systems versus the parabolic amplitude gain impairments. The degradation in dB is the difference between the C/N necessary to achieve the  $P_e = 10^{-6}$  performance when impairments are present, and the C/N  $\approx 33$  dB giving  $P_e = 10^{-6}$  without impairments.

Second, the performance of the 2.1 Mb/s modems using the 1024QAM schemes is given.

- The degradation in dB is the difference between the  $(C/N)$  required to achieve the  $P_e = 10^{-6}$  performance when group delay or amplitude imperfections exist, and the  $(C/N) \doteq 39$  dB needed to achieve the same  $P_e$  performance with the 1024QAM system in an ideal Gaussian noise channel.

The staggered schemes seem to be less sensitive to the linear group delay while there is no difference in the performance in the presence of parabolic distortions, Fig.3.6. However, the nonstaggered schemes perform better in the presence of linear amplitude gain distortion, Fig.3.7.

Third, the computer generated eye diagram of the 256QAM system in the presence of  $1.5 \mu\text{s}/\text{MHz}$  group delay is given in Fig.3.8 (a). The central eyes are quite open, while the timing eyes are smeared, i.e. timing jitter exists. The eye diagram of the same system but without group delay distortion is given in Fig.3.8 (b). In the S1024QAM system with the  $0.5 \mu\text{s}/\text{MHz}$  linear group delay and  $\alpha = 0.14$  cosine filter middle eyes are much narrower, intersymbol interference is present, while the small timing eyes are totally smeared, i.e. a strong timing jitter exists, Fig.3.9. However, this will not be the case in an ideal  $\alpha = 1.0$  Nyquist channel, i.e. both sampling and timing eyes are fully open, Fig.3.10. Obviously, high level modulation schemes are very sensitive to any timing recovery uncertainty.

2.048 Mb/s @ 240 kHz SG

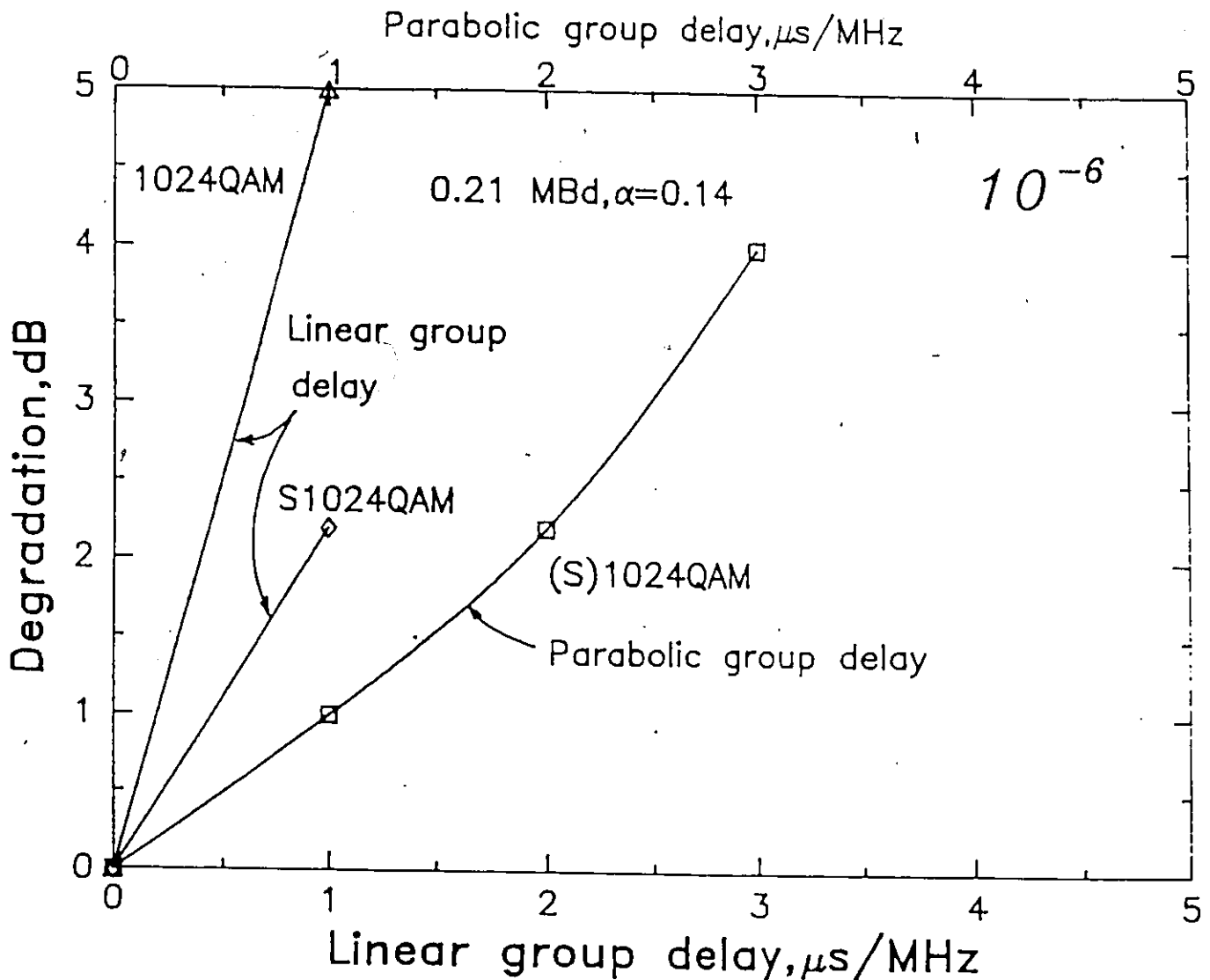


Figure 3.6. The performance degradation of 1024QAM (2.048/2.1) Mb/s systems versus the group delay impairments. The degradation in dB is the difference between the C/N necessary to achieve the  $P_e = 10^{-6}$  performance when impairments are present, and the  $C/N \approx 39$  dB giving  $P_e = 10^{-6}$  without impairments.

## 2.048 Mb/s @ 240 kHz SG

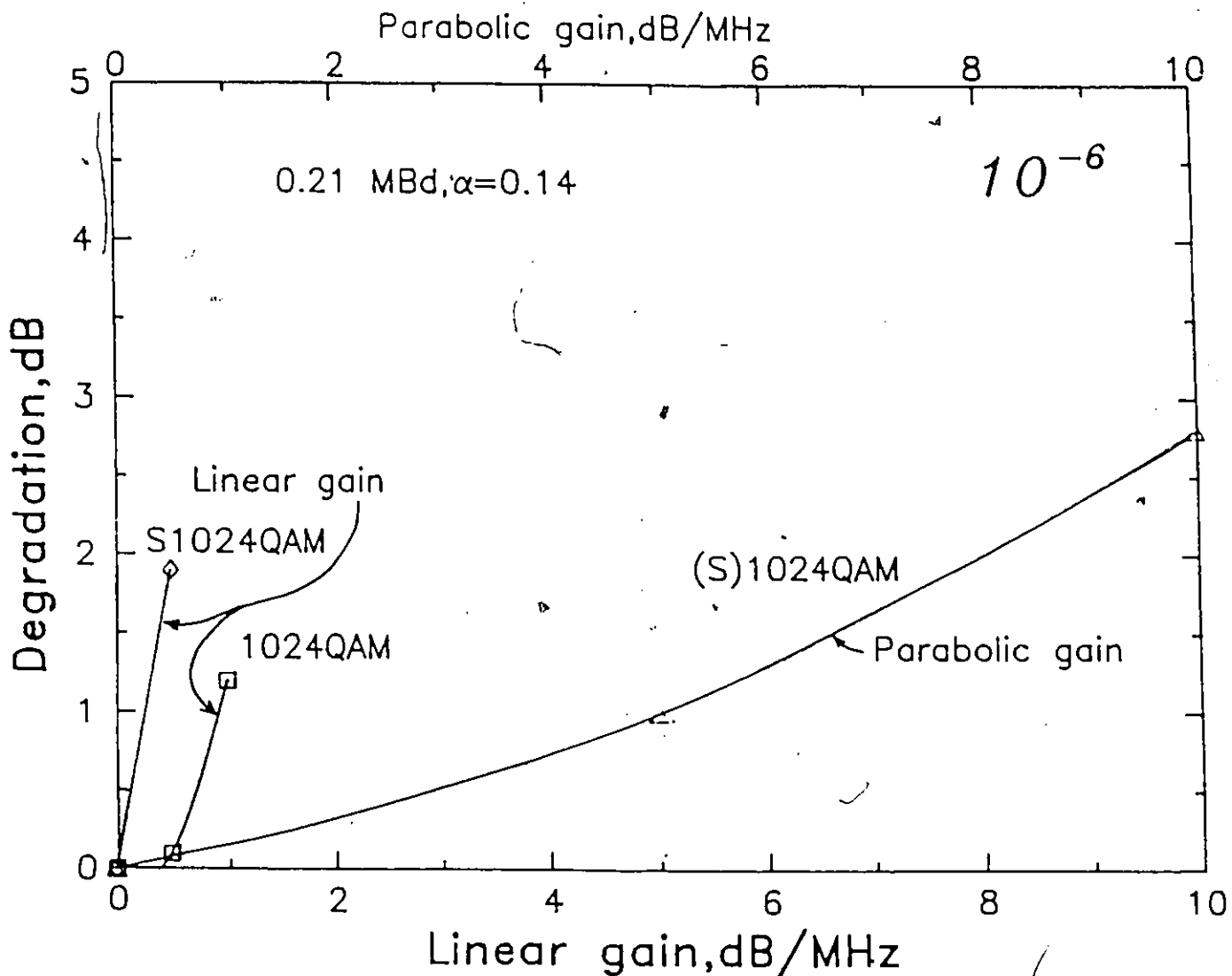
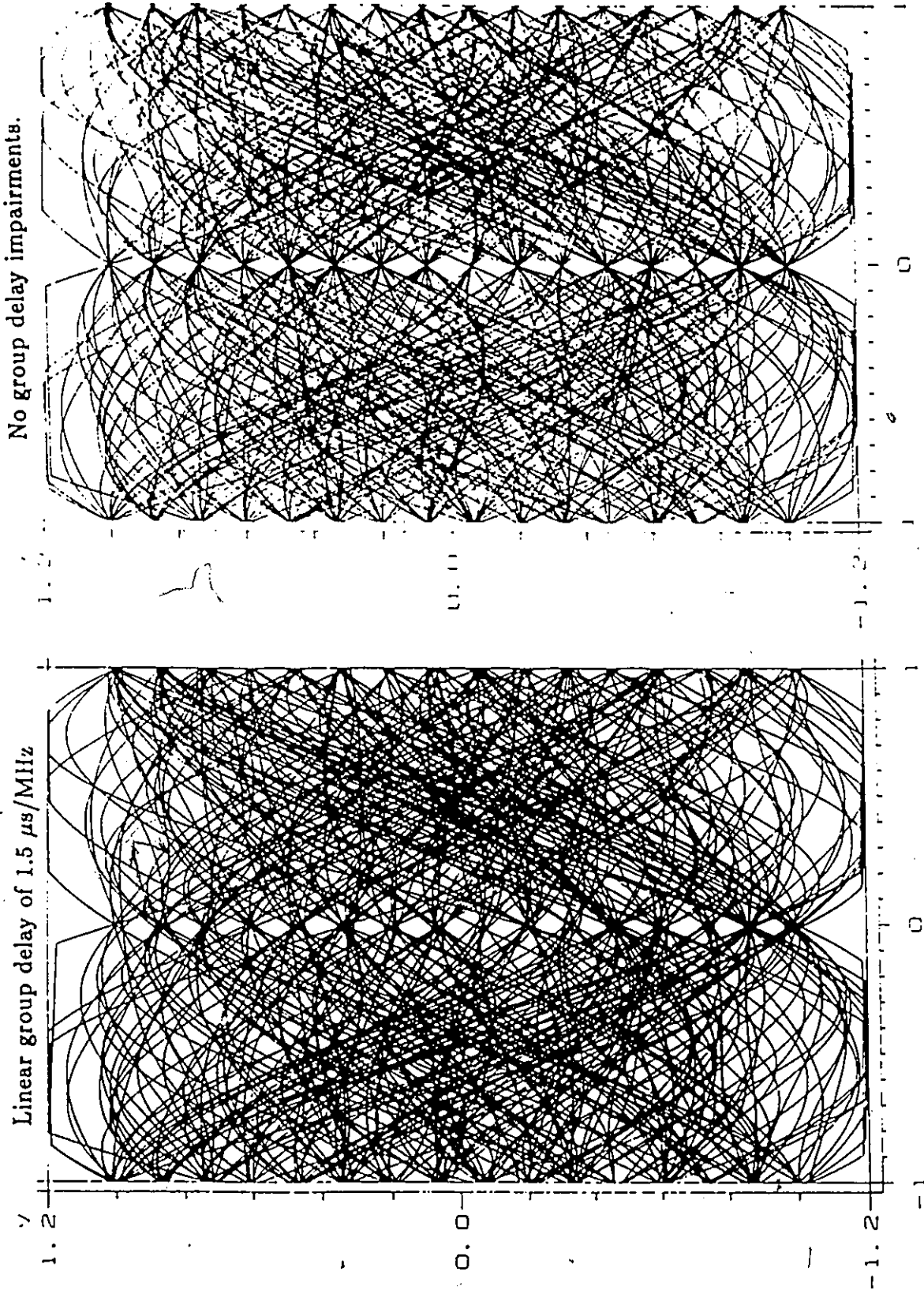


Figure 3.7. The performance degradation of the 1024QAM (2.048/2.1) Mb/s systems versus the amplitude gain impairments. The degradation in dB is the difference between the C/N necessary to achieve the  $P_e = 10^{-6}$  performance when impairments are present, and the  $C/N \approx 39$  dB giving  $P_e = 10^{-6}$  without impairments.



Norm. time (1/symbol)

Figure 3.8. The 256QAM 0.2 MBd system with the  $\alpha = 0.2$  filtering. The computer generated eye diagrams.

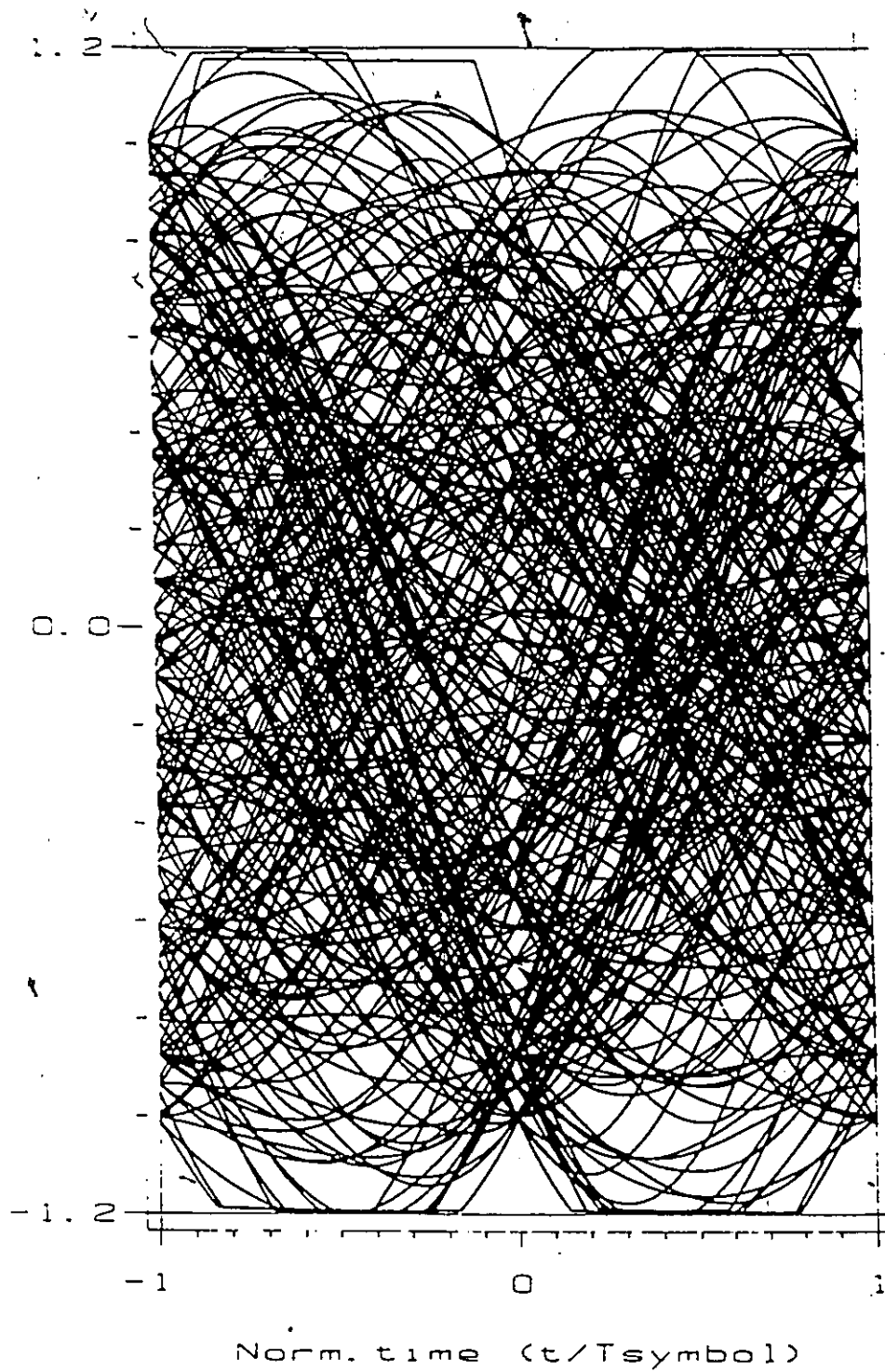


Figure 3.9. The S1024QAM 0.21 MBd system with the  $\alpha = 0.14$  filtering. Linear group delay of  $0.5 \mu\text{s}/\text{MHz}$ . The computer generated eye diagram.

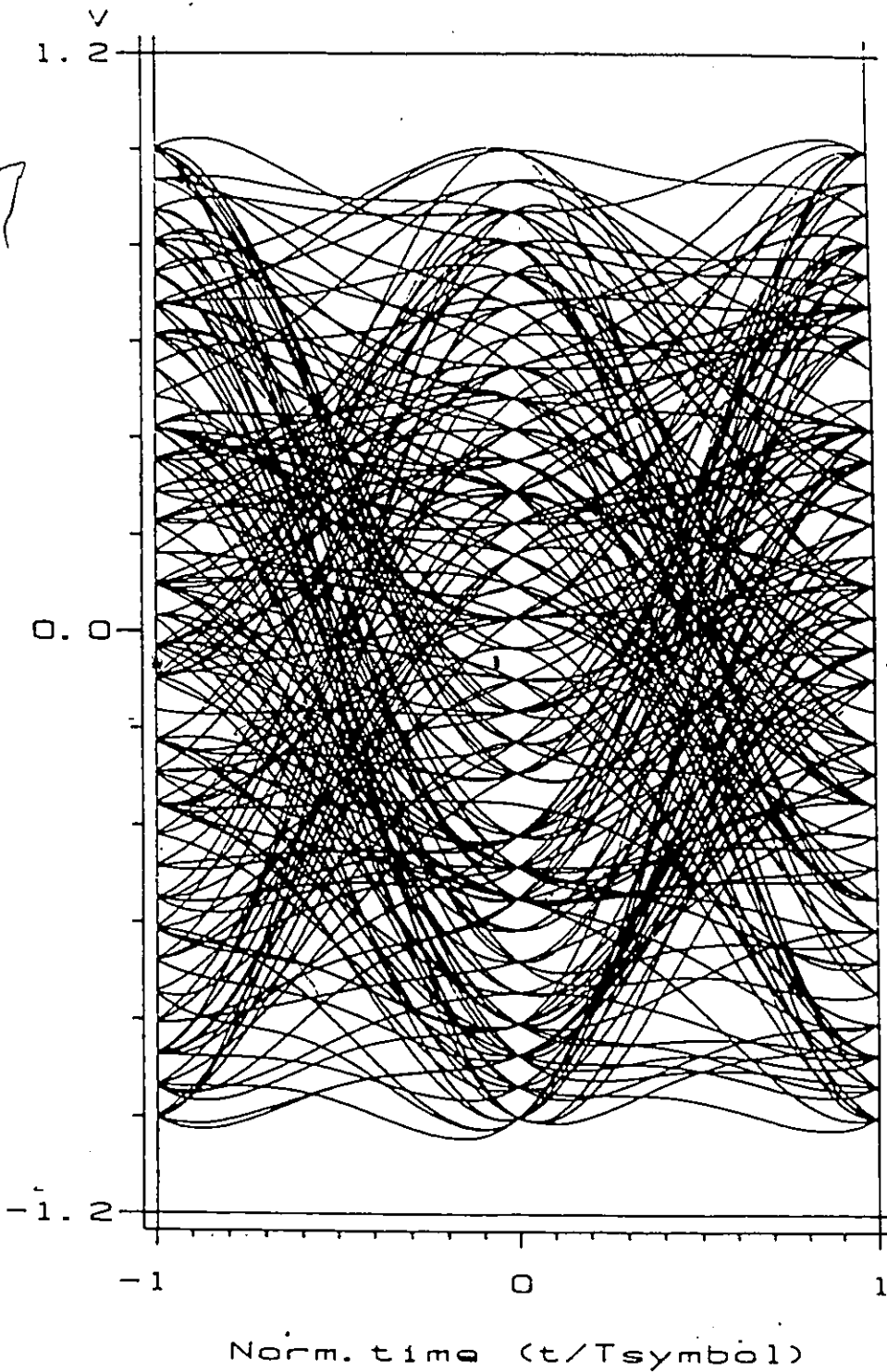


Figure 3.10. The 1024QAM 0.21 MBd system with the  $\alpha = 1.0$  filtering. No group delay impairments. The computer generated eye diagram.

### 3.4. CONCLUSION

In this chapter the performance analysis of 256 and 1024QAM schemes is performed in the presence of amplitude and group delay impairments. A brief feasibility study of the transmission of North American T1 (DS1) 1544 kb/s or CCITT 2048 kb/s data stream over the analog 240 kHz wide CCITT supergroup is given. Staggered QAM schemes perform better in the presence of linear group delay impairments, but nonstaggered schemes are less sensitive to linear amplitude gain impairments.

In this, and the previous chapter, it has been assumed that the receiver is provided with a perfect knowledge of the carrier phase and the timing instants. However, in practice, this information is not available in advance. Before any decision is to be made, the receiver must establish, by itself, a proper phase and timing. This topic is the concern of our next chapter.

ON COMPOSITE  
PHASE AND TIMING ESTIMATION  
AND DETECTION  
OF WEIGHTED QAM SIGNALS

In Chapter 2 the WQAM family has been introduced. Its performance has been analyzed in the presence of different impairments such as: ACI, hardlimiter nonlinearity (Chapter 2), amplitude and group delay (Chapter 3) imperfections. An exact knowledge of the carrier phase and symbol timing(s) has been assumed. However, in practice, this is not the case and prior any decision has to be made, the proper carrier phase and symbol timing(s) need to be established. In this chapter, we search for new (improved) receivers for composite phase and timing estimation and detection of WQAM signals, and then, compare their performance with the known (conventional) ones.

An outline of the chapter follows. The WQAM signal has been defined in (2.1). However, for the purposes of this chapter a more precise definition is necessary. This, and the Bayes-based optimization strategy are given in the Section 4.1. Section 4.2 deals with ML-based classical- and equalized DFCRL. The performance of these loops is presented in the form of an uncertainty diagram (UD) and a nonlinearity surface. Finally, MAP-based crosstalk cancellation DFCRL, timing intersymbol interference (ISI) cancellation DFCRL, and FEEDLOOP are presented in Section 4.3.

#### 4.1. SYSTEM DESCRIPTION AND OPTIMIZATION STRATEGY

A weighted quadrature amplitude modulation signal  $s(t, \alpha, \beta, \epsilon_1, \epsilon_2, \theta)$  with data rates  $R_A = 1/T_A$  and  $R_B = 1/T_B$  in the in-phase and quadrature channels respectively, can be represented by

$$s(t, \alpha, \beta, \epsilon_1, \epsilon_2, \theta) = \sqrt{P_A} \sum_i \underbrace{\alpha_i w_A[t - iT_A + \epsilon_1(t)]}_x \cos[2\pi f_c t + \theta(t)] \\ + \sqrt{P_B} \sum_j \underbrace{\beta_j w_B[t - (jT_B + \delta) + \epsilon_2(t)]}_y \sin[2\pi f_c t + \theta(t)], \\ i, j \in \{I\} \quad (4.1)$$

Quantities  $P_A$  and  $P_B$  are the signal powers,  $\alpha$  and  $\beta$  are independent random data sequences,  $w_A(t)$  and  $w_B(t)$  are the pulse shaping functions (weights, windows) in channels  $A$  and  $B$ , defined on the interval  $(-T_A/2, +T_A/2)$  and  $(-T_B/2, +T_B/2)$ , respectively,  $f_c$  is the carrier frequency, and  $\delta$  is an arbitrary delay in the  $B$  channel.  $\epsilon_1(t)$  and  $\epsilon_2(t)$  are random timing offsets assumed to be uniformly distributed on the interval  $(-T_A/2, +T_A/2)$  and  $(-T_B/2, +T_B/2)$ , respectively— and independent of each other in general, and  $\theta(t)$  is the random carrier phase assumed to be uniformly distributed on the interval  $(-\pi, +\pi)$ . Summations over  $i, j$  extend over the set of all integers  $\{I\}$ . In the text which follows we use abbreviations  $\epsilon_1 = \epsilon_1(t)$ ,  $\epsilon_2 = \epsilon_2(t)$  and  $\theta = \theta(t)$ .

We would like to minimize the average probabilities of error  $P_{eA}, P_{eB}$ , where

$$P_{eA} = \int_{\phi} \int_{\lambda_1} P(e|x, y) p(x, y) dx dy \quad (4.2a)$$

$$P_{eB} = \int_{\phi} \int_{\lambda_2} P(e|x, y) p(x, y) dx dy \quad (4.2b)$$

Quantities  $P(e|x = \phi, y = \lambda_1)$  and  $P(e|x = \phi, y = \lambda_2)$  are the conditional error rates — where errors are committed by the decision devices within the loop and are conditioned on the phase uncertainty  $\phi = \theta - \hat{\theta}$  and the timing uncertainties  $\lambda_1 = \epsilon_1 - \hat{\epsilon}_1$  and  $\lambda_2 = \epsilon_2 - \hat{\epsilon}_2$ , respectively.  $\hat{\theta}, \hat{\epsilon}_1$ , and  $\hat{\epsilon}_2$  are estimates of the phase and timings as provided by the corresponding loops.  $p(x = \phi, y = \lambda_1)$  and  $p(x = \phi, y = \lambda_2)$  are the corresponding probability density functions. Typical  $P(e|\phi, \lambda = 0)$  and  $p(\phi, \lambda = 0)$  functions are given in Fig.4.1.

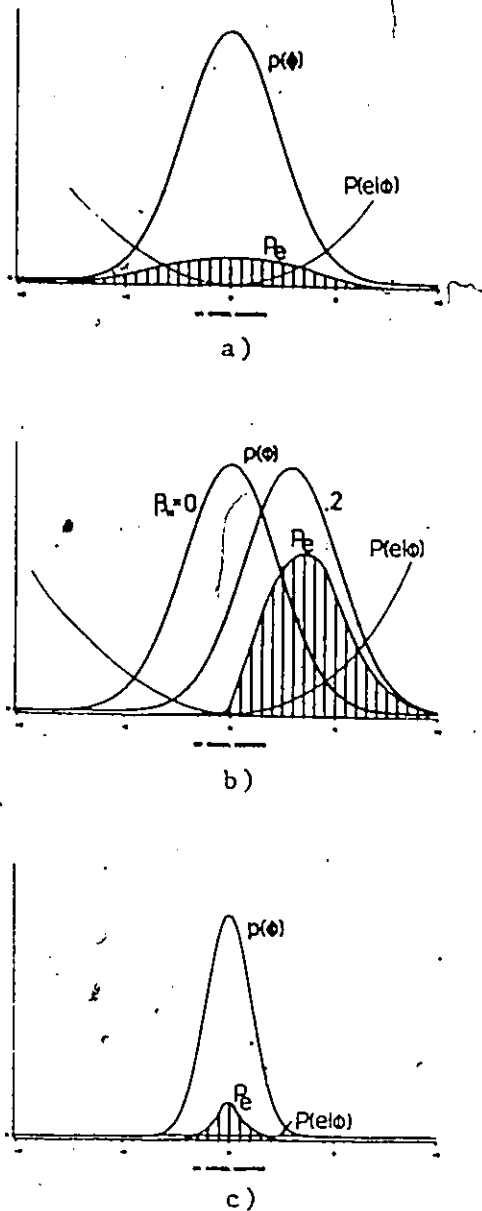


Figure 4.1. The typical conditional probability of error  $P(e|\phi)$ , probability density function  $p(\phi)$ , and average probability of error  $P_e$  curves of the MQAM scheme employing: a) classical carrier recovery loop (e.g. classical decision feedback carrier recovery loop DFCRL) with normalized loop detuning  $\beta_N = 0$ , b) classical DFCRL with  $\beta_N = 0.2$ , and c) crosstalk cancellation DFCRL. The values of corresponding  $P(e|\phi)$  curves are enlarged for illustrative purposes. In practice they are as low as  $10^{-12}$  at  $\phi \approx 0$ , and approach to 1 as  $\phi \rightarrow 45^\circ$ .

The minimization of the  $P_{eA}, P_{eB}$  is equivalent to the minimization of the corresponding products under the double integrals in (4.2a-b). Therefore, we would like to minimize these products over the entire range of  $\{\phi, \lambda\}$ . Both, yet unknown, functions depend on the known WQAM signal constellation and, yet unknown, circuit design which we would like to find. To achieve this, a Bayes estimate is used with the following cost functions:  $C_{ii} = 0$  for a correct decision and  $C_{ij} = 1, i \neq j$  for an erroneous decision [B22]. Although a similar analysis might be found in many books related to communications, our approach has a few differences which lead to new solutions. These differences are emphasized in the text which follows, including analysis of a few new receivers. A few preliminaries need to be established. The received signal  $r(t)$  consists of the signal  $s(t)$  and the band-limited ( $-B_{IF}/2$  to  $+B_{IF}/2$ ) white Gaussian noise with single sided spectral density  $N_o$ , i.e.

$$r(t) = s(t) + n(t) \quad (4.3)$$

where, for convenience, we have dropped the dependance of  $s(t)$  and thus  $r(t)$  on  $\alpha, \beta, \epsilon_1, \epsilon_2, \theta$ . We assume that the receiving  $IF$  filter  $H(f)$  is wide enough to cause no additional shaping of the signal pulse, and narrow enough to allow a narrowband representation of the noise  $n(t)$ , i.e.

$$n(t) = n_c(t) \cos(2\pi f_c t + \theta) + n_s(t) \sin(2\pi f_c t + \theta) \quad (4.4)$$

Furthermore, we assume that  $H(f)$  is symmetric around  $f_c$ , i.e. the in-phase noise component  $n_c(t)$  and quadrature component  $n_s(t)$  are statistically independent. In practice, a tight filtering might be imposed on both the transmitter and receiver side accompanied with nonlinearities, adjacent and cochannel interferences (ACI and CCI), selective fading, and other impairments. However, taking into account all of these factors at the same time leads to extremely complex expressions which remain to be solved. We limit our attention to a more tractable situation, where the WQAM signal is immersed in white Gaussian noise only. A responsibility of the receiver will be based on observation of  $r(t)$  as given in (4.3), decide which of data pairs  $(\alpha, \beta)$  are sent. However first, both phase coherence and timing synchronization need to be established. Composite phase and timing estimation and detection analysis is performed as follows. We use the sampled data approach [B21].  $r(t)$  is uniformly sampled on the interval  $(0, T_N)$   $N$  times. The spacing between samples is  $\Delta t = t_k - t_{k-1} = 1/2B_{IF}$ , which creates independent samples. Now, (4.3) might be written in the sampled form

$$\vec{r} = \vec{s} + \vec{n} \quad (4.5)$$

Quantities  $\vec{r}$  and  $\vec{s}$  are the  $N$ -dimensional vectors of the received and transmitted signal, respectively, and  $\vec{n}$  is the  $N$ -dimensional noise vector, the components of which are statistically independent zero-mean Gaussian random variables with variances  $N_o B_{IF}$ . Without loss of generality, we assume that a decision on  $r(t)$  occurs at  $t_k = k$ , i.e. at the  $k$ -th data

symbol. Carrier phase is observed on the interval  $[k-1-T_c, k-1]$  where, with very little loss of generality, it might be assumed that  $T_c = V_{Ac}T_A$ .  $V_{Ac}$  is an integer such that  $V_{Ac} > 1$ , where the first subscript  $A$  refers to the  $A$  channel and the second subscript  $c$  refers to the carrier phase estimation. We arbitrarily assume that  $T_B = \xi T_A$  and  $\xi \geq 1$ , i.e. symbol rate  $R_A$  in the  $A$  channel is equal to or higher than  $R_B$ . During the interval  $[k-1-T_c, k-1]$  there are  $V_{Ac}$  symbols  $(\alpha_{k-1-T_c}, \alpha_{k-T_c}, \dots, \alpha_{k-1})$  in the  $A$  channel if  $\epsilon_1 = 0$ ,  $V_{Ac} + 1$  symbols (the right most part of  $\alpha_{k-2-T_c}, \alpha_{k-1-T_c}, \dots, \alpha_{k-2}$ , the left most part of  $\alpha_{k-1}$ ) if  $\epsilon_1 < 0$ , and  $V_{Ac} + 1$  symbols (the right most part of  $\alpha_{k-1-T_c}, \alpha_{k-T_c}, \dots, \alpha_{k-1}$ , the left most part of  $\alpha_k$ ) if  $\epsilon_1 > 0$ . The data stream in the  $B$  channel is generally not aligned to the stream in the  $A$  channel. Depending on the data rate ratio  $\xi$ , static offset  $\delta$ , and amount of random offsets  $\epsilon_1$  and  $\epsilon_2$ , different combinations exist. Generally,  $V_{Bc} + 1 = V_{Ac}/\xi + 1$  symbols in the  $B$  channel belong to the observation interval  $[k-1-T_c, k-1]$ . Timing epochs  $\epsilon_1$  and  $\epsilon_2$  are observed on the interval  $[k-1-T_A, k-1]$  and  $[k-1-T_B + \Delta\epsilon, k-1 + \Delta\epsilon]$  respectively, where  $\Delta\epsilon$  accounts for the relative offset between  $\epsilon_1$  and  $\epsilon_2$ .

With these preliminaries, the Bayes estimate of  $\epsilon_1, \epsilon_2$  and  $\theta$  might be derived as follows: Choose  $\epsilon_1 = \hat{\epsilon}_1$ ,  $\epsilon_2 = \hat{\epsilon}_2$  and  $\theta = \hat{\theta}$  such that the conditional density function of the parameters  $\alpha, \beta, \epsilon_1, \epsilon_2, \theta$  given observation vector  $\bar{r}$ , i.e.  $f(\epsilon_1, \epsilon_2, \theta | \bar{r})$ , is maximum. Such an estimator is called nondata-aided (NDA), while a data-aided (DA) estimator employs data estimates  $\hat{\alpha}$  and  $\hat{\beta}$  instead. We use Bayes formula [B22]

$$f(\epsilon_1, \epsilon_2, \theta | \bar{r}) = \frac{\langle f(\bar{r} | \alpha, \beta, \epsilon_1, \epsilon_2, \theta) \rangle f(\epsilon_1, \epsilon_2, \theta)}{f(\bar{r})} \quad (4.6)$$

where  $\langle \cdot \rangle$  represents the statistical average on data  $\alpha, \beta$ . Since  $f(\bar{r})$  is independent of  $\epsilon_1, \epsilon_2$ , and  $\theta$ , the Bayes estimate of  $\epsilon_1, \epsilon_2$ , and  $\theta$  might be restated as follows: Choose  $\epsilon_1 = \hat{\epsilon}_1$ ,  $\epsilon_2 = \hat{\epsilon}_2$ , and  $\theta = \hat{\theta}$  such that the product  $\langle f(\bar{r} | \alpha, \beta, \epsilon_1, \epsilon_2, \theta) \rangle \cdot f(\epsilon_1, \epsilon_2, \theta)$  is maximum. Usually,  $f(\epsilon_1, \epsilon_2, \theta)$  is assumed to be uniformly distributed over the  $(\epsilon_1, \epsilon_2, \theta)$  hyperplane, which leads to the following criterion: Choose  $\epsilon_1 = \hat{\epsilon}_1$ ,  $\epsilon_2 = \hat{\epsilon}_2$ , and  $\theta = \hat{\theta}$  such that  $\langle f(\bar{r} | \alpha, \beta, \epsilon_1, \epsilon_2, \theta) \rangle$  is maximum. We call this estimator maximum likelihood (ML), since the ML estimate corresponds mathematically to the limiting case of a maximum a posteriori (MAP) estimate in which the a priori knowledge approaches zero, i.e.  $\epsilon_1, \epsilon_2$  and  $\theta$  are uniformly distributed, [B22, p.65]. Note that many authors treat  $\epsilon_1, \epsilon_2$ , and  $\theta$  as deterministic but unknown quantities in their ML approaches.  $f(\bar{r} | \alpha, \beta, \epsilon_1, \epsilon_2, \theta)$  is an a posteriori probability and very often such an estimator is (incorrectly) called MAP. Later, we use the knowledge of  $\epsilon_1, \epsilon_2$ , and  $\theta$  accumulated over corresponding observation intervals to develop improved estimator-detectors, which will be called MAP.

## 4.2. MAXIMUM LIKELIHOOD (ML) APPROACH

We maximize the likelihood function

$$\Lambda(\vec{r}|\epsilon_1, \epsilon_2, \theta) = \ln\{f(\vec{r}|\alpha, \beta, \epsilon_1, \epsilon_2, \theta)\}, \quad (4.7)$$

denote the corresponding  $\epsilon_1, \epsilon_2$ , and  $\theta$  with  $\hat{\epsilon}_1, \hat{\epsilon}_2$ , and  $\hat{\theta}$ , and name the respective estimator as ML. The analysis proceeds as follows: Conditioned on  $\alpha, \beta, \epsilon_1, \epsilon_2$ , and  $\theta$ , the random vector  $\vec{r}$  is  $N$ -dimensional Gaussian with mean value which is equal to the vector  $\vec{s}$ , i.e.

$$f(\vec{r}|\alpha, \beta, \epsilon_1, \epsilon_2, \theta) = \frac{\exp[-(1/2)(\vec{r} - \vec{s})^T K_n^{-1}(N)(\vec{r} - \vec{s})]}{(2\pi)^{N/2} |K_n(N)|^{1/2}} \quad (4.8)$$

Quantity  $K_n(N) = I(N)N_o B_{IF}$  is the noise covariance matrix,  $I(N)$  is the  $N$ -dimensional identity matrix, superscript  $T$  denotes transpose, and dependence of  $f(\vec{r}|\alpha, \beta, \epsilon_1, \epsilon_2, \theta)$  on  $\alpha, \beta, \epsilon_1, \epsilon_2$ , and  $\theta$  occurs in the vector  $\vec{s}$ . A more complex channel might be represented by a complex matrix  $K(N)$ , while a corresponding equalizer will be represented by its inverse  $K^{-1}(N)$ . However, analysis of such a system is out of the scope of this contribution. Since the components of vector  $\vec{r}$  are mutually independent

$$f(\vec{r}|\alpha, \beta, \epsilon_1, \epsilon_2, \theta) = (2\pi N_o B_{IF})^{-N/2} \exp\left(-\frac{1}{N_o} \sum_{k=1}^N |r_k|^2 \Delta t\right) \times \exp\left(-\frac{1}{N_o} \sum_{k=1}^N |s_k|^2 \Delta t + \frac{2}{N_o} \sum_{k=1}^N r_k s_k \Delta t\right) \quad (4.9)$$

where  $r_k = r(t_k)$  and  $s_k = s(t_k)$ .  $r_k$  does not depend on  $\alpha, \beta, \epsilon_1, \epsilon_2$ , and  $\theta$  and might be absorbed within a constant. Very often,  $s(t)$  has been assumed to be a constant envelope process and a maximization of the terms in the last sum of (4.9) followed. This is valid for a rather limited number of systems such as nonfiltered QPSK, MSK, and MPSK. Any filtering of such a system introduces envelope fluctuations, which require an equalization to be employed at the receiver end. Here, we do not consider problems related to the filtering and equalization. However, an envelope fluctuation is inherited within the elementary structure of the multilevel and overlapped schemes and this must be taken into consideration. We explore this problem in Section 4.2.2. In this section a constant envelope process is assumed. Using (4.9), the likelihood function  $\Lambda(\vec{r}|\epsilon_1, \epsilon_2, \theta)$  might be written as

$$\Lambda(\vec{r}|\epsilon_1, \epsilon_2, \theta) = \sum_V \ln \sum_{i,j} e^{\Gamma} + C_1 \quad (4.10)$$

where summation over  $V$  denotes estimation on interval  $[k - (V + 2), k - 1]$ , summation over  $i, j$  denotes averaging over all possible data patterns  $\{\alpha_i, \beta_j\}$ , and  $\Gamma$  will be described in (4.13), and  $C_1$  is a constant which includes the a priori probabilities of the sequences  $\alpha$  and  $\beta$ . Necessary but not sufficient conditions that must be satisfied by  $\epsilon_1, \epsilon_2$ , and  $\theta$  in order to be an ML estimate are

$$\left. \frac{\partial \Lambda(\bar{r}|\epsilon_1, \epsilon_2, \theta)}{\partial \theta} \right|_{\theta=\hat{\theta}, \epsilon_1=\hat{\epsilon}_1, \epsilon_2=\hat{\epsilon}_2} = 0 \quad (4.11a)$$

$$\left. \frac{\partial \Lambda(\bar{r}|\epsilon_1, \epsilon_2, \theta)}{\partial \epsilon_1} \right|_{\theta=\hat{\theta}, \epsilon_1=\hat{\epsilon}_1, \epsilon_2=\hat{\epsilon}_2} = 0 \quad (4.11b)$$

$$\left. \frac{\partial \Lambda(\bar{r}|\epsilon_1, \epsilon_2, \theta)}{\partial \epsilon_2} \right|_{\theta=\hat{\theta}, \epsilon_1=\hat{\epsilon}_1, \epsilon_2=\hat{\epsilon}_2} = 0 \quad (4.11c)$$

In addition to (4.11a-c) the following conditions apply

$$\begin{vmatrix} \partial^2 \Lambda / \partial \epsilon \partial \theta & \partial^2 \Lambda / \partial \epsilon^2 \\ \partial^2 \Lambda / \partial \theta^2 & \partial^2 \Lambda / \partial \epsilon \partial \theta \end{vmatrix} < 0. \quad (4.11d)$$

$\Lambda$  has a maximum if  $\partial^2 \Lambda / \partial \epsilon^2 < 0$  and  $\partial^2 \Lambda / \partial \theta^2 < 0$  at  $(\epsilon_o, \theta_o)$ -this corresponds to a stable and correct (desirable) lock point of a recovery loop.  $\Lambda$  has a minimum if  $\partial^2 \Lambda / \partial \epsilon^2 > 0$  and  $\partial^2 \Lambda / \partial \theta^2 > 0$  at  $(\epsilon_o, \theta_o)$ -this corresponds to a false lock point of a recovery loop. Here we have tacitly assumed that the function  $\Lambda(\bar{r}|\epsilon_1, \epsilon_2, \theta)$  is differentiable over all  $\{\epsilon_1, \epsilon_2, \theta\}$ , i.e. the first and second derivatives with respect to the  $\epsilon_1, \epsilon_2, \theta$  exist. However, this might not be true, in general, and any singularity must be taken into consideration. As an example: The derivative of a rectangular pulse must be precisely defined for  $t = +T_S/2$  as  $(a_k - a_{k+1})/2$ ; the derivative of  $++$  ( $--$ ) sequence of MSK, (Hann1 pulse) has a discontinuity in the vicinity of  $t = T_S/2$ , i.e. the step from  $-1$  to  $+1$  ( $+1$  to  $-1$ ), and must be defined as zero for  $t = T_S/2$  for both cases; etc. Then, (4.11a-c) become

$$\frac{\partial \Lambda(\bar{r}|\epsilon_1, \epsilon_2, \theta)}{\partial \theta} = \sum_V \frac{\sum_{i,j} (\partial \Gamma / \partial \theta) e^\Gamma}{\sum_{i,j} e^\Gamma} \quad (4.12a)$$

$$\frac{\partial \Lambda(\bar{r}|\epsilon_1, \epsilon_2, \theta)}{\partial \epsilon_1} = \sum_V \frac{\sum_{i,j} (\partial \Gamma / \partial \epsilon_1) e^\Gamma}{\sum_{i,j} e^\Gamma} \quad (4.12b)$$

$$\frac{\partial \Lambda(\bar{r}|\epsilon_1, \epsilon_2, \theta)}{\partial \epsilon_2} = \sum_V \frac{\sum_{i,j} (\partial \Gamma / \partial \epsilon_2) e^\Gamma}{\sum_{i,j} e^\Gamma} \quad (4.12c)$$

By using (4.1 and 4.8), a nondata-aided approach gives

$$\Gamma = -\frac{1}{N_o} \int [P_A x^2(V, \epsilon_1) + P_B y^2(V, \epsilon_2)] + [P_A x^2(V, \epsilon_1) - P_B y^2(V, \epsilon_2)] \cos 2(2\pi f_c t + \theta) dt \\ + \frac{2}{N_o} \int [\sqrt{P_A} r(t) x(V, \epsilon_1) \cos(2\pi f_c t + \theta) + \sqrt{P_B} r(t) y(V, \epsilon_2) \sin(2\pi f_c t + \theta)] dt \quad (4.13)$$

$$\frac{\partial \Gamma}{\partial \theta} = \frac{1}{N_o} \int [P_A x^2(V, \epsilon_1) - P_B y^2(V, \epsilon_2)] \sin 2(2\pi f_c t + \theta) dt \\ - \frac{2}{N_o} \int [\sqrt{P_A} r(t) x(V, \epsilon_1) \sin(2\pi f_c t + \theta) - \sqrt{P_B} r(t) y(V, \epsilon_2) \cos(2\pi f_c t + \theta)] dt \quad (4.14)$$

$$\frac{\partial \Gamma}{\partial \epsilon_1} = -\frac{P_A}{N_o} \int x(V, \epsilon_1) \frac{\partial x(V, \epsilon_1)}{\partial \epsilon_1} [1 + \cos 2(2\pi f_c t + \theta)] dt \\ + \frac{2\sqrt{P_A}}{N_o} \int r(t) \frac{\partial x(V, \epsilon_1)}{\partial \epsilon_1} \cos(2\pi f_c t + \theta) dt + L_{AS} + L_{AC} \quad (4.15)$$

$$\frac{\partial \Gamma}{\partial \epsilon_2} = -\frac{P_B}{N_o} \int y(V, \epsilon_2) \frac{\partial y(V, \epsilon_2)}{\partial \epsilon_2} [1 - \cos 2(2\pi f_c t + \theta)] dt \\ + \frac{2\sqrt{P_B}}{N_o} \int r(t) \frac{\partial y(V, \epsilon_2)}{\partial \epsilon_2} \sin(2\pi f_c t + \theta) dt + L_{BS} + L_{BC} \quad (4.16)$$

where the summation over  $k$  is approximated with an integral

$$\sum_{k=1}^N r(t_k) w(t - iT_s + \epsilon) \frac{\cos}{\sin} (2\pi f_c t + \theta) \Delta t = \\ \int_{-T_s/2 + iT_s - \epsilon T_s/2}^{+T_s/2 + iT_s - \epsilon T_s/2} r(t_k) w(t + \epsilon) \frac{\cos}{\sin} (2\pi f_c t + \theta) dt, \quad S = A, B \quad (4.17)$$

and for convenience the integral limits are omitted.  $L_{AS}, L_{AC}, L_{BS}, L_{BC}$  are terms due to Leibniz' rule given as

$$L_{AS} = \frac{2\sqrt{P_A} T_A}{N_o \pi} r(t) \cos(2\pi f_c t + \theta)$$

$$[x(iT_A - T_A/2 - \epsilon_1 T_A/\pi) - x(iT_A + T_A/2 - \epsilon_1 T_A/\pi)] p_A \quad (4.18a)$$

$$L_{AC} = \frac{P_A}{N_o} [x^2(iT_A - T_A/2 - \epsilon_1 T_A/\pi) - x^2(iT_A + T_A/2 - \epsilon_1 T_A/\pi)] p_A \quad (4.18b)$$

$$L_{BS} = \frac{2\sqrt{P_B} T_B}{N_o \pi} r(t) \sin(2\pi f_c t + \theta) \\ [y(jT_B - T_B/2 - \epsilon_2 T_B/\pi) - y(jT_B + T_B/2 - \epsilon_2 T_B/\pi)] p_B \quad (4.19a)$$

$$L_{BC} = \frac{P_B}{N_o} [y^2(jT_B - T_B/2 - \epsilon_2 T_B/\pi) - y^2(jT_B + T_B/2 - \epsilon_2 T_B/\pi)] p_B \quad (4.19b)$$

where  $p_A$  and  $p_B$  are the probabilities of symbol transitions in the A and B channel, respectively. Note that for  $\epsilon_i > 0$ , two symbols, the  $k$ -th and  $(k-1)$ -th, are involved in (4.18a-4.19b).

Equations (4.12a-c) are highly nonlinear, and explicit solutions for  $\epsilon_1, \epsilon_2$ , and  $\theta$  seem to be, at least, very complex if not impossible. Therefore, an ML estimator might not be practically realizable in general. Furthermore, these equations are not independent, which suggests that a joint carrier and timing(s) solution might offer better results than separate solutions. In the following, we concentrate on some simplifications, which might lead to easier practical realizations. The integrals in (4.14-4.16) which contain double frequency terms equal zero if the carrier frequency  $f_c$  is an integer multiple of data rates  $R_A, R_B$ . They are negligible if  $f_c \gg R_A, R_B$  and will be ignored in our analysis. Usually, the signal set in each quadrature channel is symmetric. Then, (4.12a-c) might be written as

$$\frac{\partial \Lambda(\vec{r}|\epsilon_1, \epsilon_2, \theta)}{\partial \theta} = 0 = \sum_V \frac{N(\theta)}{D_o} \quad (4.20a)$$

$$\frac{\partial \Lambda(\vec{r}|\epsilon_1, \epsilon_2, \theta)}{\partial \epsilon_1} = 0 = \sum_V \frac{N(\epsilon_1)}{D_o} \quad (4.20b)$$

$$\frac{\partial \Lambda(\vec{r}|\epsilon_1, \epsilon_2, \theta)}{\partial \epsilon_2} = 0 = \sum_V \frac{N(\epsilon_2)}{D_o} \quad (4.20c)$$

$$D_o = \sum_{i,j} e^\Gamma \quad (4.21a)$$

$$\Rightarrow \sum_{i,j} W_i \cosh(C_x) W_j \cosh(S_y) \quad (4.21b)$$

In (4.21a),  $i, j \in \{I\}$ , and the  $\Gamma$  term is given in (4.13). However, due to symmetry of the signal set, summations over  $i, j$  in (4.21b) and the equations which follow extend over

nonnegative integers only.

$$N(\theta) = 4 \sum_{i,j} [-S_x \sinh(C_x) \cosh(S_y) + C_y \cosh(C_x) \sinh(S_y)] \quad (4.22)$$

$$\begin{aligned} N(\epsilon_1) = 4 \sum_{i,j} & \left( \left[ -\frac{P_A}{N_o} \int x(V, \epsilon_1) \frac{\partial x(V, \epsilon_1)}{\partial \epsilon_1} dt + L_{AC} \right] W_i \cosh(C_x) W_j \cosh(S_y) \right. \\ & \left. + \left[ \frac{2\sqrt{P_A}}{N_o} \int \frac{\partial x(V, \epsilon_1)}{\partial \epsilon_1} r(t) \cos(2\pi f_c t + \theta) dt + L_{AS} \right] W_i \sinh(C_x) W_j \cosh(S_y) \right) \end{aligned} \quad (4.23)$$

$$\begin{aligned} N(\epsilon_2) = 4 \sum_{i,j} & \left( \left[ -\frac{P_B}{N_o} \int y(V, \epsilon_2) \frac{\partial y(V, \epsilon_2)}{\partial \epsilon_2} dt + L_{BC} \right] W_i \cosh(C_x) W_j \cosh(S_y) \right. \\ & \left. + \left[ \frac{2\sqrt{P_B}}{N_o} \int \frac{\partial y(V, \epsilon_2)}{\partial \epsilon_2} r(t) \cos(2\pi f_c t + \theta) dt + L_{BS} \right] W_i \cosh(C_x) W_j \sinh(S_y) \right) \end{aligned} \quad (4.24)$$

where

$$W_i = \exp\left[-\frac{P_A i^2}{2N_o} \int x^2(V, \epsilon_1) dt\right] \quad (4.25a)$$

$$W_j = \exp\left[-\frac{P_B j^2}{2N_o} \int y^2(V, \epsilon_2) dt\right] \quad (4.25b)$$

are weighting factors proportional to the negative exponent of the signal-to-noise ratio (SNR) in the corresponding baseband levels, and

$$C_x = \frac{2\sqrt{P_A} i}{N_o} \int r(t) x(V, \epsilon_1) \cos(2\pi f_c t + \theta) dt \quad (4.26a)$$

$$C_y = \frac{2\sqrt{P_B} j}{N_o} \int r(t) y(V, \epsilon_2) \cos(2\pi f_c t + \theta) dt \quad (4.26b)$$

$$S_x = \frac{2\sqrt{P_A} i}{N_o} \int r(t) x(V, \epsilon_1) \sin(2\pi f_c t + \theta) dt \quad (4.26c)$$

$$S_y = \frac{2\sqrt{P_B} j}{N_o} \int r(t) y(V, \epsilon_2) \sin(2\pi f_c t + \theta) dt \quad (4.26d)$$

Leibnitz's terms and derivatives are now related to the nonnegative  $i, j$ . Then, (4.20a-c) suggest a closed-loop structure for the joint carrier phase estimate  $\theta$  and timing estimates  $\epsilon_1, \epsilon_2$

given in Fig.4.2. In this and following figures, timing information paths to the integrals and delay elements necessary for a proper operation of the loops are omitted for the reason of clarity. Note that the timing loop consists of two essential parts: the first one which represents the first continuous part in (4.15-4.16) and the second one which represents Leibniz's transitional parts (4.18a-4.19b). The transitional part only is the essence of a digital data transition tracking loop (DTTE) [B16]. The probability of no transition of MQAM schemes equals  $1/L$ , where  $L$  is the number of baseband levels, which suggests that this part might be essential for a TR device for multilevel schemes. The transitional part of rectangular schemes is independent of  $\epsilon$ , whereas it increases as  $\epsilon$  increases for MSK, an example of a nonrectangular scheme.

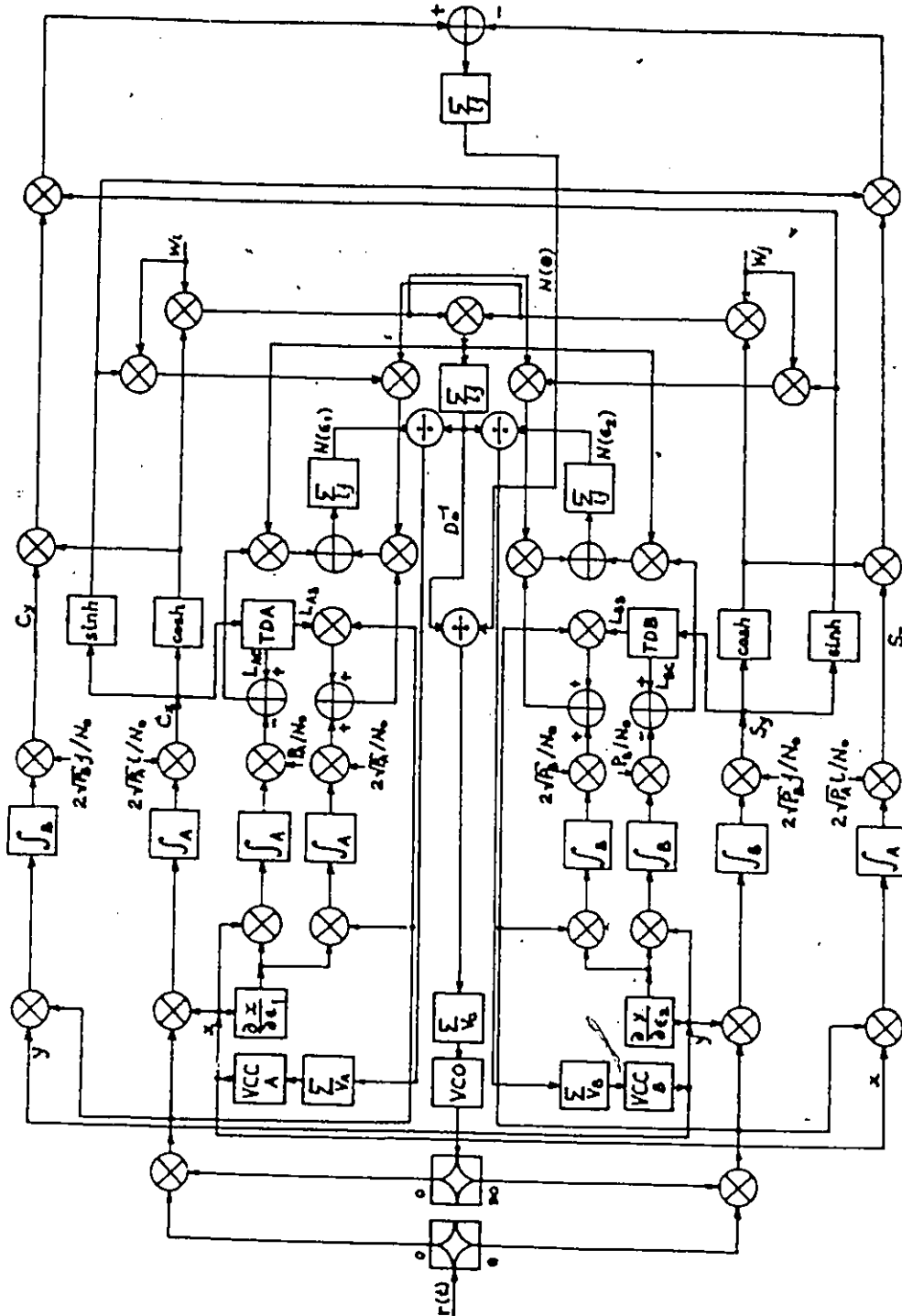


Figure 4.2. The joint phase and timing estimator for WQAM schemes, which corresponds to eqs. (4.11 a-c) in the text.

By approximating the continuous derivative by a finite difference, i.e.,

$$\begin{aligned} \frac{\partial \Lambda(\bar{r}|\epsilon_1, \epsilon_2, \theta)}{\partial \epsilon} &\doteq \frac{\Lambda(\epsilon + \Delta\epsilon/2) - \Lambda(\epsilon - \Delta\epsilon/2)}{\Delta\epsilon} \\ &= \sum_V \frac{\ln \sum_{i,j} \exp(+\Delta\epsilon) - \ln \sum_{i,j} \exp(-\Delta\epsilon)}{\Delta\epsilon} \end{aligned} \quad (4.27a)$$

$$\Rightarrow \sum_V \frac{\ln \sum_{i,j} \cosh(+\Delta\epsilon) - \ln \sum_{i,j} \cosh(-\Delta\epsilon)}{\Delta\epsilon} \quad (4.27b)$$

where  $\{\pm\Delta\epsilon\}$  correspond to  $\Gamma(\epsilon \pm \Delta\epsilon/2)$  respectively, an early-late gate loop [B3] is suggested. The summations in (4.27a) assume that  $i, j \in \{I\}$  while the summations in (4.27b) assume nonnegative  $i, j$ .

The structure given in Fig.4.2 seems to be complex, and the hyperbolic sine and hyperbolic cosine functions might not be practical to realize. The approximations  $\sinh(x) \doteq x$ ,  $\cosh(x) \doteq 1 + x^2/2$  for small  $x$  (low SNR) and  $\cosh(x) \doteq \text{sign}(x) \sinh(x)$  for large  $x$  (high SNR) might be employed to simplify the loop. However, we proceed in a different way. For 4-state 2x2 baseband levels schemes, (4.20a-c) reduce to

$$\frac{\partial \Lambda(\bar{r}|\epsilon_1, \epsilon_2, \theta)}{\partial \theta} = 0 = \sum_V [-S_x \tanh(C_x) + C_y \tanh(S_y)] \quad (4.28a)$$

$$\begin{aligned} \frac{\partial \Lambda(\bar{r}|\epsilon_1, \epsilon_2, \theta)}{\partial \epsilon_1} = 0 &= \sum_V \left( -\frac{P_A}{N_o} \int x(V, \epsilon_1) \frac{\partial x(V, \epsilon_1)}{\partial \epsilon_1} dt \right. \\ &\quad \left. + \left[ \frac{2\sqrt{P_A}}{N_o} \int \frac{\partial x(V, \epsilon_1)}{\partial \epsilon_1} r(t) \cos(2\pi f_c t + \theta) dt + L_{AS} \right] \tanh(C_x) \right) \end{aligned} \quad (4.28b)$$

$$\begin{aligned} \frac{\partial \Lambda(\bar{r}|\epsilon_1, \epsilon_2, \theta)}{\partial \epsilon_2} = 0 &= \sum_V \left( -\frac{P_B}{N_o} \int y(V, \epsilon_2) \frac{\partial y(V, \epsilon_2)}{\partial \epsilon_2} dt \right. \\ &\quad \left. + \left[ \frac{2\sqrt{P_B}}{N_o} \int \frac{\partial y(V, \epsilon_2)}{\partial \epsilon_2} r(t) \sin(2\pi f_c t + \theta) dt + L_{BS} \right] \tanh(S_y) \right) \end{aligned} \quad (4.28c)$$

(4.28a-c) suggest a device as given in Fig.4.3. Without the TR part (i.e. 4.28b and 4.28c) and for rectangular signal shapes, this becomes a CR loop as given in [P127].

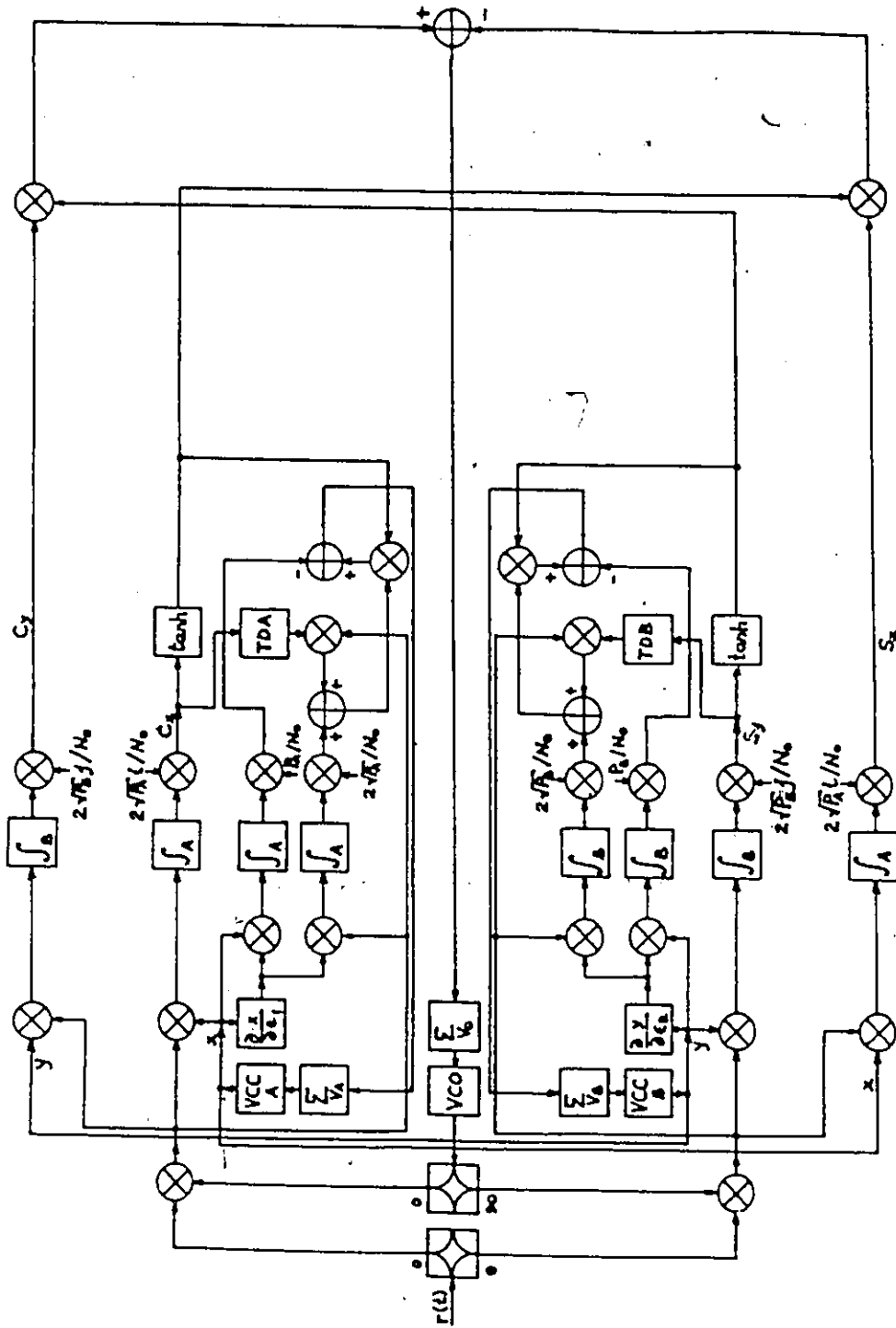


Figure 4.3. The joint phase and timing estimator for 4 state 2x2 baseband level WQAM schemes, which corresponds to eqs. (4.28 a-c) in the text.

We will not pursue unbalanced schemes further. However, note that QAM schemes with more than 4 states are balanced only on average i.e. the average power in the A channel is equal to the average power in the B channel, but they are not balanced on a per-symbol-basis. As an example, a 256QAM scheme exhibits the maximum imbalance of 15/1 when a baseband level of 1 in the A channel is accompanied with the level of 15 in the B channel and vice versa. Similarities between unbalanced schemes and MQAM schemes may be observed on the corresponding nonlinearity curves for unbalanced schemes [P127]-[P130] and MQAM schemes [P122]-[P125]. For 4 state balanced schemes with  $P_A = P_B, R_A = R_B = 1/T_S, C_x = C_y, S_x = S_y$  and rectangular signal shapes, (4.28a-c) reduce to

$$\frac{\partial \Lambda(\vec{r}|\epsilon_1, \epsilon_2, \theta)}{\partial \theta} = 0 = \sum_V [-S_x \tanh(C_x) + C_x \tanh(S_x)] \quad (4.29a)$$

$$\begin{aligned} \frac{\partial \Lambda(\vec{r}|\epsilon_1, \epsilon_2, \theta)}{\partial \epsilon} = 0 = & \sum_V \left( -\sqrt{P_A} \int x(V, \epsilon) \frac{\partial x(V, \epsilon)}{\partial \epsilon} dt \right. \\ & + \tanh(C_x) \int \frac{\partial x(V, \epsilon)}{\partial \epsilon} r(t) \cos(2\pi f_c t + \theta) dt \\ & + \tanh(S_x) \int \frac{\partial y(V, \epsilon)}{\partial \epsilon} r(t) \sin(2\pi f_c t + \theta) dt \\ & \left. + L_{AS} \tanh(C_x) + L_{BS} \tanh(S_x) \right) \quad (4.29b) \end{aligned}$$

which suggests the device given in Fig.4.4. The nonlinearity  $\tanh(x)$  might be approximated by  $x - x^3/3! + \dots$  for low SNRs and by  $sign(x)$  for high SNRs. The high SNR loop approximation without the timing part is called a **DFCRL** since decisions on  $\alpha, \beta$ , i.e.  $\hat{\alpha}, \hat{\beta}$  are used to (partly) wipe off the data. This type of loop is often called data-aided. However, a DA approach is not used here and this solution is, therefore, not necessary optimal in a DA sense. The DA approach calls for data estimates  $\hat{\alpha}$  and  $\hat{\beta}$  in (4.6-4.7). Both  $\hat{\alpha}$  and  $\hat{\beta}$  depend on  $\epsilon_1, \epsilon_2$ , in a yet unknown way and a strict DA approach seems to be rather difficult. Later we discuss this dependence and a few improved circuits are suggested.

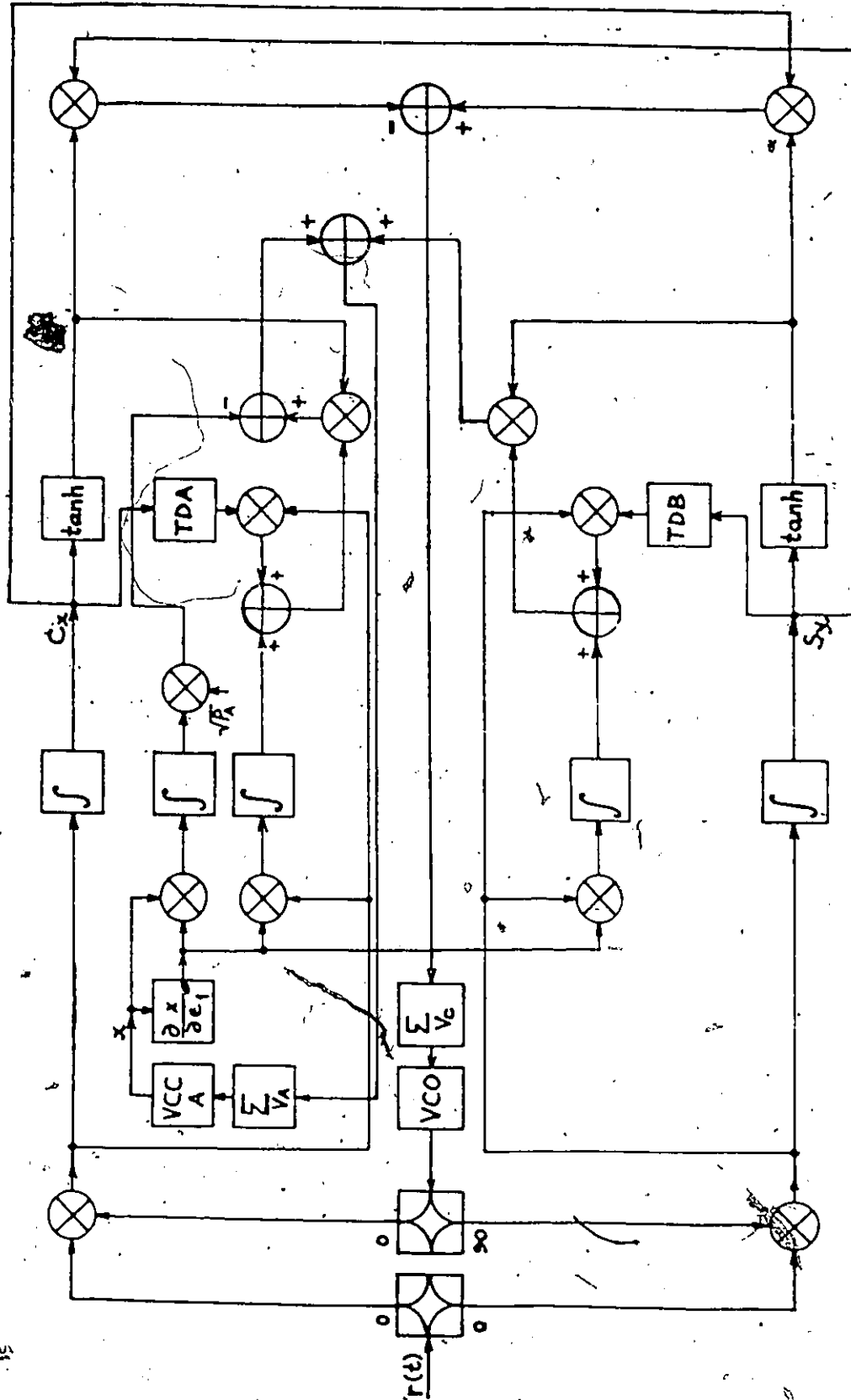


Figure 4.4. The joint phase and timing estimator for QPSK schemes, which corresponds to eqs. (4.29 a-c) in the text.

MSK is an example of schemes with a nonrectangular signal shape. By using (4.26a-d) and (4.28a-c) the phase and timing estimation equations become

$$\begin{aligned} \frac{\partial \Lambda(\bar{r}|c_1, \epsilon_2, \theta)}{\partial \theta} = 0 &= \sum_V \left( - \int \cos\left(\frac{\pi t}{T} + \epsilon\right) r(t) \sin(2\pi f_c t + \theta) dt \right. \\ &\times \tanh\left[\frac{2\sqrt{P_A}}{N_o} \int \cos\left(\frac{\pi t}{T} + \epsilon\right) r(t) \cos(2\pi f_c t + \theta) dt\right] \\ &+ \int \sin\left(\frac{\pi t}{T} + \epsilon\right) r(t) \cos(2\pi f_c t + \theta) dt \\ &\left. \times \tanh\left[\frac{2\sqrt{P_B}}{N_o} \int \sin\left(\frac{\pi t}{T} + \epsilon\right) r(t) \sin(2\pi f_c t + \theta) dt\right] \right) \quad (4.30a) \end{aligned}$$

$$\begin{aligned} \frac{\partial \Lambda(\bar{r}|c_1, \epsilon_2, \theta)}{\partial \epsilon} = 0 &= \sum_V \left( - \left[ \int \sin\left(\frac{\pi t}{T} + \epsilon\right) r(t) \cos(2\pi f_c t + \theta) dt + L_{AS} \right] \right. \\ &\times \tanh\left[\frac{2\sqrt{P_A}}{N_o} \int \cos\left(\frac{\pi t}{T} + \epsilon\right) r(t) \cos(2\pi f_c t + \theta) dt\right] \\ &+ \left[ \int \cos\left(\frac{\pi t}{T} + \epsilon\right) r(t) \sin(2\pi f_c t + \theta) dt + L_{BS} \right] \\ &\left. \times \tanh\left[\frac{2\sqrt{P_B}}{N_o} \int \sin\left(\frac{\pi t}{T} + \epsilon\right) r(t) \sin(2\pi f_c t + \theta) dt\right] \right) \quad (4.30b) \end{aligned}$$

The corresponding joint estimator is given in Fig.4.5. Note the similarity of our estimator with that given in [P138, Fig.3]. Our scheme uses additional transition detectors TDA and TDB to improve timing performance by accounting for the Leibniz terms. Since MSK is using  $\cos(x)$  and  $\sin(x)$  pulse shapes in *A* and *B* channels respectively, the derivatives suggested in (4.28a-c) are realized by employing the respective crossarm signals. In a data-aided approach, at high SNR,  $\tanh(x) \doteq \text{sign}(x)$  is used. The extension of this concept to other WQAM schemes is straightforward.

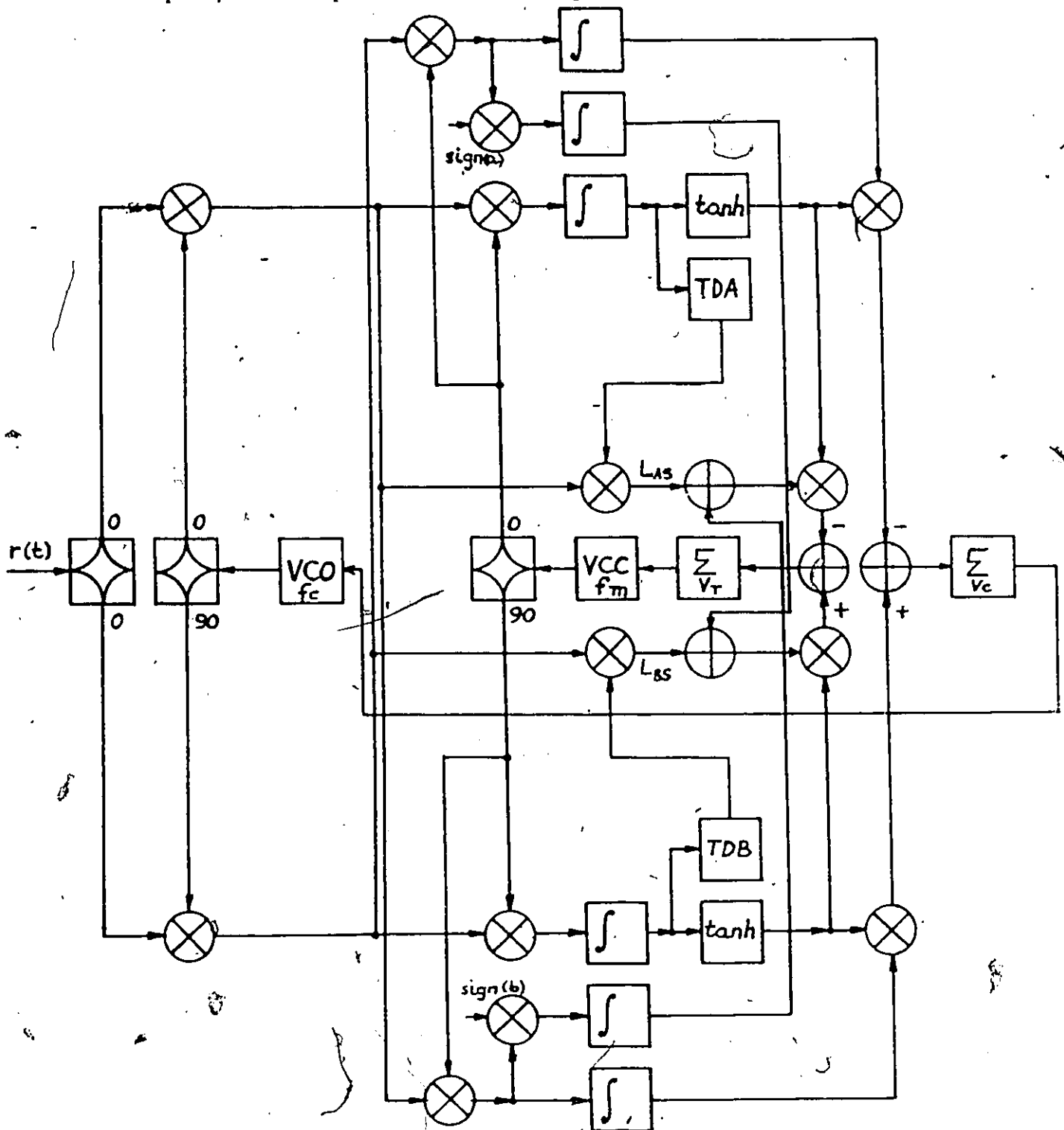


Figure 4.5. The joint phase and timing estimator for MSK schemes, which corresponds to eqs. (4.30 a-c) in the text.

Now, we proceed with the CR structures analysis. When schemes with more than 4 states are employed, a term within the second sum in (4.9) suggests that a quantizer

$$Q_k(x) = \begin{cases} kd, & \text{for } (k-1)d \leq x < (k+1)d; \\ (L-1)d, & \text{for } (L-2)d \leq x < \infty; \\ -(L-1)d, & \text{for } -\infty < x \leq -(L-2)d. \end{cases} \quad k = 0 \pm 2, \pm 4, \dots \pm (L-3); \quad (4.31)$$

be used as a decision device. This loop, Fig.4.6, which we call the classical DFCRL, serves as a reference to which all new schemes are compared. This type of loop with an integrate-sample-and-dump (ISD) circuit (box noted with an integral) within the loop arms is called active, while the other one, employing a lowpass filter instead, is called passive. We analyze the former one only and note that an active loop performs better than a passive one, at least for  $\phi, \lambda \neq 0$ . Usually, an active loop with ideal sampling is assumed. Since this might not be a practical case, we analyze the loop performance in the presence of both CR uncertainty  $\phi$  and TR uncertainty  $\lambda$ , which to the best of our knowledge has not been published in the open literature, yet.

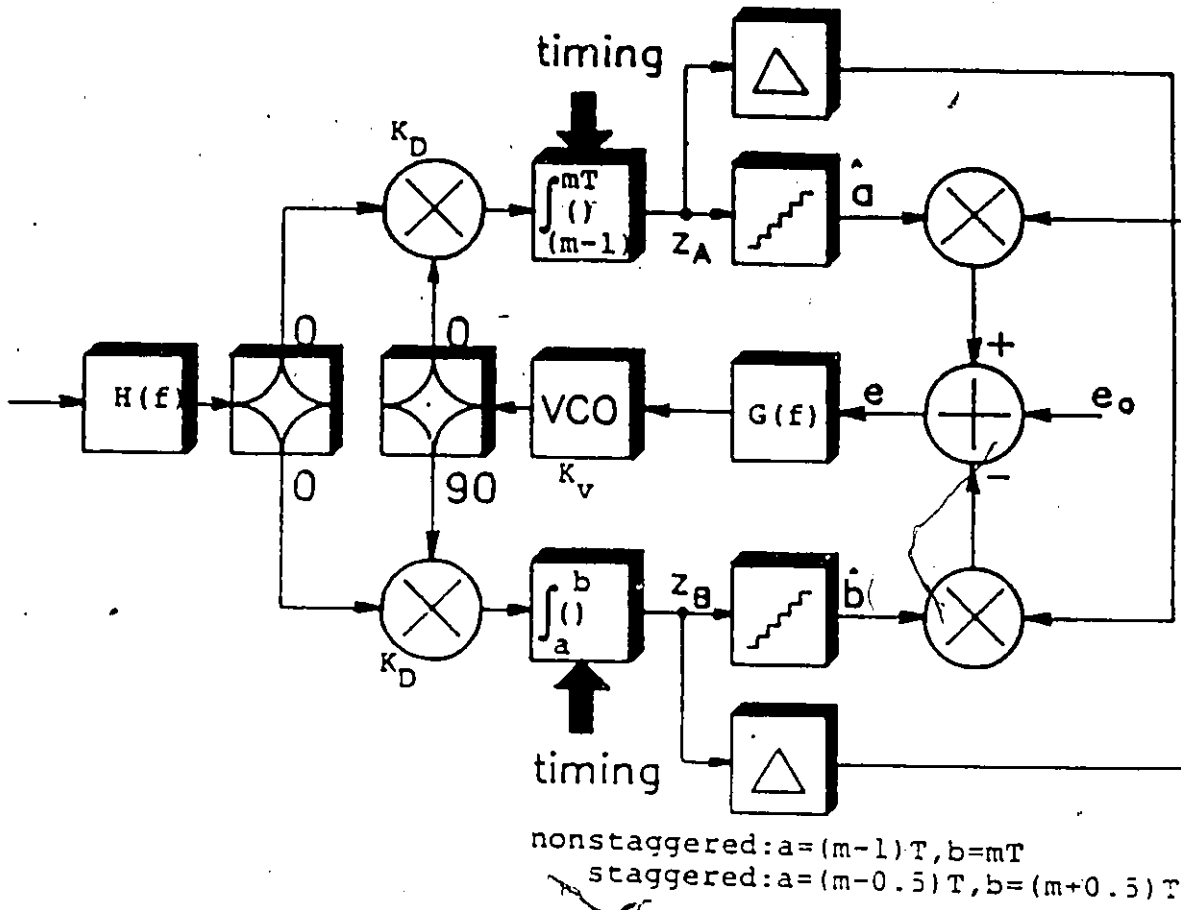


Figure 4.6. The classical decision feedback carrier recovery loop.

### 4.2.1. CLASSICAL DECISION FEEDBACK CR LOOP

The block diagram of the classical DFCRL is given in Fig.4. Combining both CR and TR uncertainties, † signal  $z_A(t)$  at the decision device input is:

$$z_A(t) = a_m w_A [t - (m-1)T - \epsilon] \cos \phi + b_n w_B [t - (n-1)T - \epsilon] \sin \phi + \nu_A \quad (4.32)$$

where  $\nu_A$  is the sample of Gaussian noise in the A channel. The conditional probability of error of an MQAM scheme is

$$U(\phi, \lambda) = P(e|\phi, \lambda) = P[e|\phi, \lambda, a_m = m = -(L-1)] \\ + P[e|\phi, \lambda, a_m = m = +(L-1)] + P[e|\phi, \lambda, |a_m = m| < (L-1)] \quad (4.33)$$

$$P[e|\phi, \lambda, a_m = m = \pm(L-1), a_{m-1} = u, b_n = n, b_{n-1} = v] =$$

$$Q[\gamma\{- (L-2) + [(L-1)R_A(|\lambda|) + uR_A(1-|\lambda|)] \cos \phi + [nR_B(|\lambda|) + vR_B(1-|\lambda|)] \sin \phi\}] \quad (4.34)$$

$$P[e|\phi, \lambda, |a_m = m| < (L-1), a_{m-1} = u, b_n = n, b_{n-1} = v] =$$

$$Q[\gamma\{-(m-1) + [mR_A(|\lambda|) + uR_A(1-|\lambda|)] \cos \phi + [nR_B(|\lambda|) + vR_B(1-|\lambda|)] \sin \phi\}] + \\ Q[\gamma\{+(m+1) - [mR_A(|\lambda|) + uR_A(1-|\lambda|)] \cos \phi - [nR_B(|\lambda|) + vR_B(1-|\lambda|)] \sin \phi\}] \quad (4.35)$$

The quantities  $P(e|x, y, \dots)$  are the conditional probabilities of error conditioned on  $x, y, \dots$  respectively,  $Q[x]$  is the Gaussian probability function [B26, 26.2.3],  $\gamma$  is the average signal-to-noise ratio at the decision device input, and  $R_A(x)$  and  $R_B(x)$  are the crosscorrelation functions of reference signal and data in A and B channel respectively, in the corresponding TR loops. To distinguish between different conditional probabilities, the conditional probability of error  $P(e|\phi, \lambda)$  is called the **uncertainty diagram**  $U(\phi, \lambda)$ , the meaning and importance of which will be explained further, later on. The conditional probability of error of staggered schemes is given by (4.33-4.35) if  $R_B(|\lambda|)$  and  $R_B(1-|\lambda|)$  are replaced by  $R_B(1/2 + |\lambda|)$  and  $R_B(1/2 - |\lambda|)$ , respectively.

The conditional probability of error performance  $P(e|\phi)$  of MQAM schemes, conditioned on a CR uncertainty  $\phi$  is summarized in Fig.4.7. For comparison purposes, a probability of

† We assume that the receiving filter  $H(f)$  is wide enough to cause no significant pulse reshaping, and narrow enough to allow the narrow-band representation of additive white Gaussian noise of the channel. The loop bandwidth is much narrower than the data bandwidth. The loop is initially locked. As a consequence, the phase process  $\phi$  in the loop varies much more slowly than the signal and the noise process correlation time is much less than the length of the symbol interval, i.e. the noise is practically white.

error of  $10^{-10}$  is assumed. This corresponds to a typical non-faded value in terrestrial radio. To emphasize threshold crossings, the absolute value of arguments within the  $Q(x)$  function, i.e.  $Q(|x|)$ , is used. The corresponding angles represent phase errors which cause threshold boundary crossings, i.e. erroneous decisions.

We will attempt to relate these theoretically obtained curves to some practical cases as follows. As an example, an absolute CR phase uncertainty of 2 degrees causes a minimal degradation of the conditional probability of error, if BPSK is employed, see Fig.4.7. However, the same 2 degrees uncertainties causes the degradation from  $10^{-10}$  to  $10^{-3}$  if 256QAM scheme is concerned. The corresponding average probability of error  $P_e$  depends further on the probability density function  $p(\phi)$ , which is dictated by the loop design. For this type of loop and an MQAM signal constellation, an exact expression for  $p(\phi)$  is very difficult to obtain, and — in our best knowledge — is not known. As a consequence,  $P_e$  is not known either. Therefore, for the practical purposes we will give some examples. If  $p(\phi)$  is uniformly distributed, a receiver does not have the information about the carrier phase and coherent detection is not possible. If  $p(\phi) = \delta(\phi)$ , where  $\delta$  is the delta function, the conditional probability of error  $P(e|\phi)$  equals the average  $P_e$  and the ordinate in Fig.4.7 reads as  $P_e$ . This occurs when the impairment dynamic is faster than the loop bandwidth, but slower than the data bandwidth, i.e. the phase error is virtually constant over a number of data symbols. A practical loop emphasizes the angles close to zero degrees. Therefore,  $P_e$  results better than those given in Fig.4.7 might be expected. Fig.4.7 gives an estimate of maximum tolerable imperfections of the loop components, such as phase detector, amplifier and filter responses, d.c. wandering, etc. Obviously, as the number of levels (states) increases, these imperfections cause an increased degradation in the  $P_e$  performance. In Section 4.3 we search for loops which are less prone to these effects. There, the  $P_e$  performance of the classical DFCRL is given and compared with new improved loops.

The L-ary pulse amplitude modulation, LPAM ( $M=L \times L$ ), conditional probability of error performance  $P(e|\lambda)$  is summarized in Fig.4.8. To emphasize threshold crossings the absolute value of arguments within the  $Q(x)$  function, i.e.  $Q(|x|)$ , is used. The corresponding fractions represent timing errors, normalized to the symbol duration, which cause erroneous decisions. A timing uncertainty of 1/30 of the symbol duration causes a performance degradation in probability of error from  $10^{-10}$  to  $10^{-9}$  in a two level baseband signal modulation scheme (BPSK, QPSK), but an erroneous decision in a 16 (256QAM) or higher level scheme.

The meaning of this figure is similar to that of Fig.4.7.

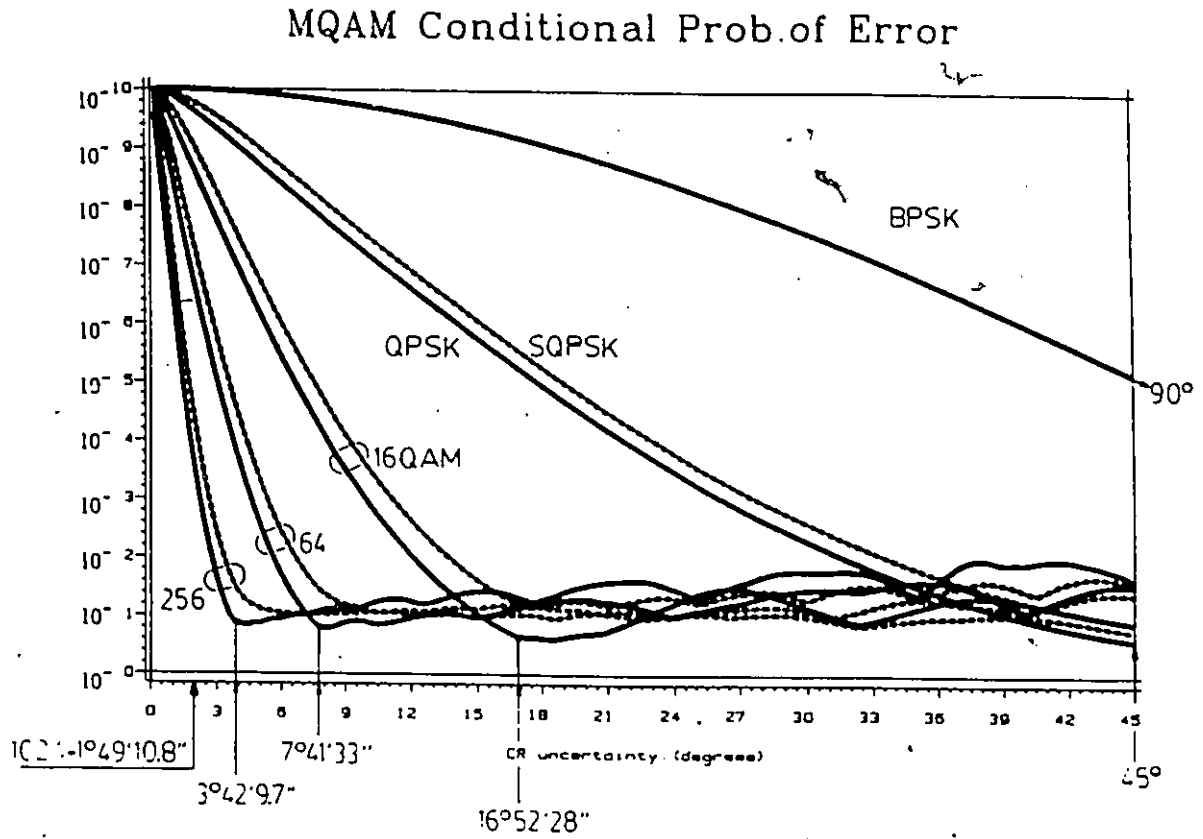


Figure 4.7. The  $P(e|\phi)$  performance of MQAM schemes. The performance of  $10^{-10}$  is taken as the reference. To emphasize threshold crossings, the absolute value of arguments within the  $Q(x)$  function, i.e.  $Q(|x|)$ , is used.

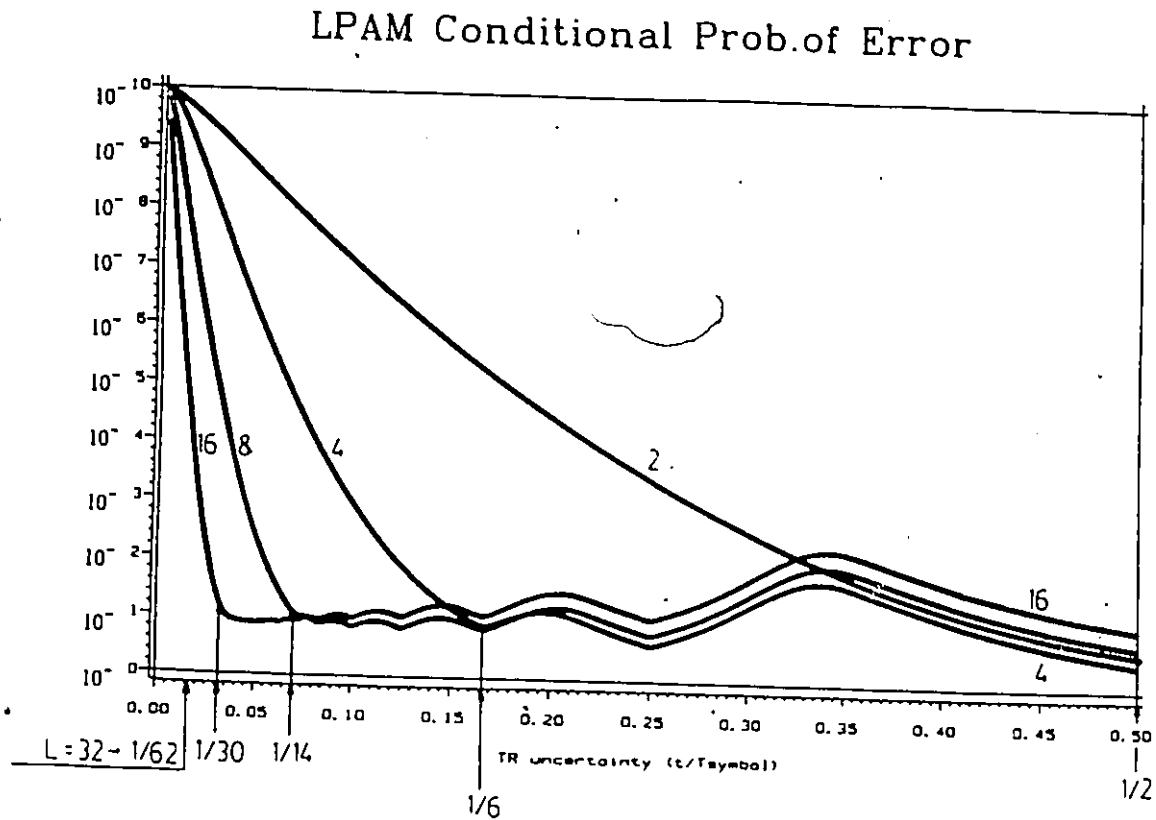


Figure 4.8. The  $P(e|\lambda)$  performance of the LPAM schemes. The performance of  $10^{-10}$  is taken as the reference. To emphasize threshold crossings, the absolute value of arguments within the  $Q(x)$  function, i.e.  $Q(|x|)$ , is used.

The combined effect of the phase and timing uncertainties on the system performance is given by (4.33–4.35). To get a better understanding of the nature of (4.33–4.35), we plotted them using two different forms: the uncertainty diagram (UD)  $U(\phi, \lambda)$  and the equal probability of error or the isoper curves. To emphasize threshold crossings,  $Q(x)$  is sometimes replaced by  $Q(|x|)$ .  $U(\phi, \lambda)$  exhibits a periodicity of  $2\pi$  radians, while  $U(|\phi, \lambda|)$  of the BPSK and QAM schemes have periods of  $\pi$  and  $\pi/2$ , respectively. The UD and isoper curves of the 256QAM scheme are given as an example in Fig.4.9a-b. These figures show a high sensitivity to any phase and timing uncertainty assuming that a classical DFCRL is used. The UD and isoper curves of the BPSK, 4PAM, QPSK, SQPSK and 16QAM schemes are given in [P117]. Similar curves for four level modulation schemes are generated by Harris and Kristiansen [P118] using a computer simulation technique. Further results are given in [P119]–[P121].

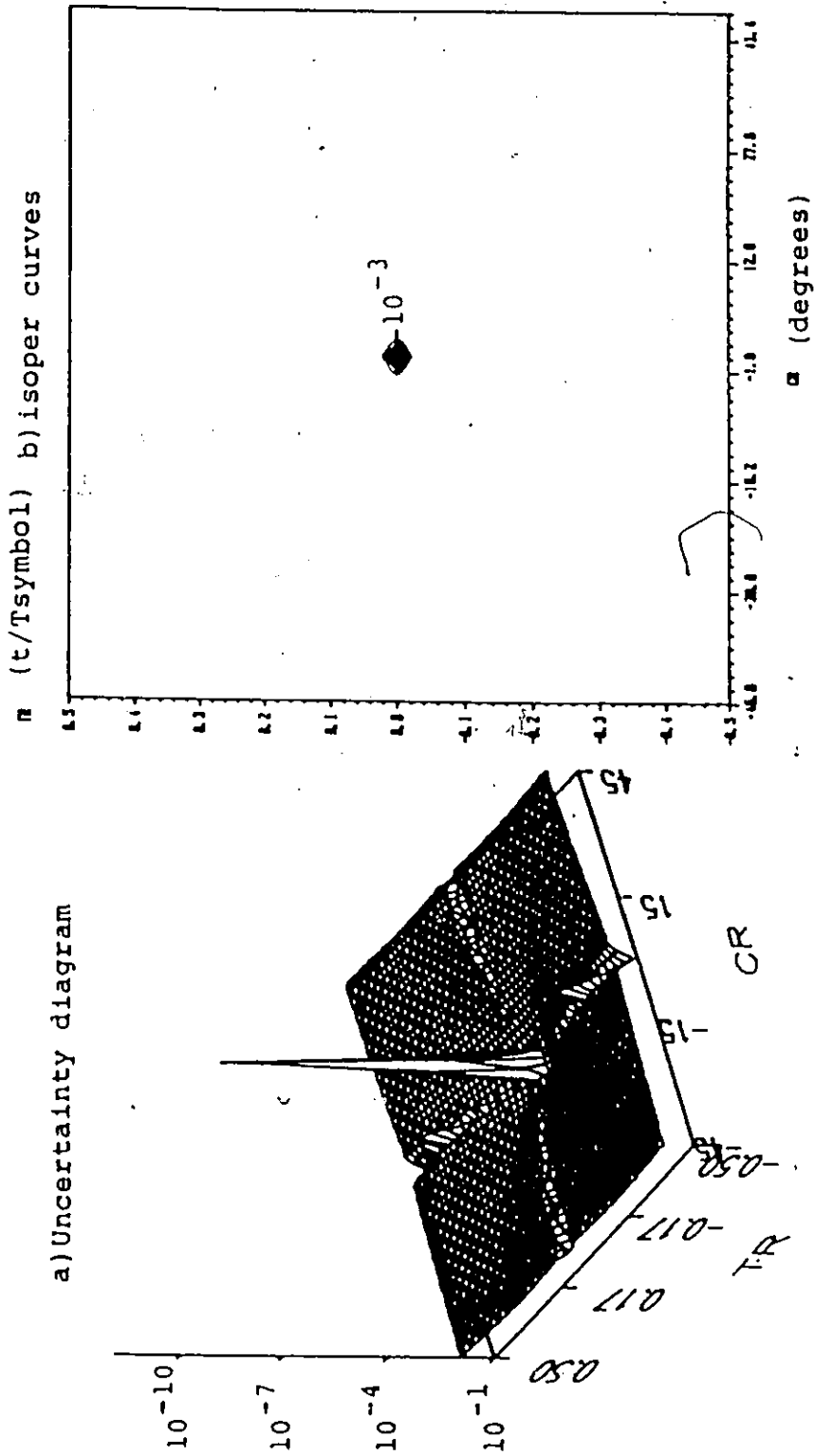


Figure 4.9. The 256QAM uncertainty diagram. The performance of  $10^{-10}$  is taken as the reference.

More detailed analysis of the loop behavior including the probability density function, average probability of error, slipping rate, and acquisition properties is out of the scope of this presentation. However, most of these quantities, including  $p(\phi, \lambda)$  are functions of a nonlinearity surface which will be briefly assessed. The integro-differential equation of the loop is

$$\dot{\phi}(t) = \dot{\theta}(t) - K_o F(p) e^{-p\Delta} P_{av} \left( [-g_1(\phi, \lambda) \sin \phi + g_2(\phi, \lambda) \cos \phi] + \nu \sqrt{N_c(\phi, \lambda) N_o} \right) \quad (4.36)$$

where  $P_{av} = 2(M - 1)/3$  is the average signal power, the dot represents the derivative with respect to the time variable  $t$ ,  $F(p)$  is the transfer function of the loop filter,  $K_o$  is the equivalent loop gain,  $\Delta$  is the delay within the loop, functions  $g_1, g_2$  and  $N_c$  are

$$g_1(\phi, \lambda) = \langle a\hat{a} + b\hat{b} | \phi, \lambda \rangle / P_{av} \quad (4.37)$$

$$g_2(\phi, \lambda) = \langle \hat{a}b - \hat{b}a | \phi, \lambda \rangle / P_{av} \quad (4.38)$$

$$N_c(\phi, \lambda) = \langle \hat{a}^2 + \hat{b}^2 | \phi, \lambda \rangle / P_{av} \quad (4.39)$$

$\nu$  is a Gaussian random variable, and  $\langle \cdot \rangle$  represents the time average. The function

$$h(\phi, \lambda) = 2 \frac{-g_1(\phi, \lambda) \sin \phi + g_2(\phi, \lambda) \cos \phi}{N_c(\phi, \lambda) N_o} \quad (4.40)$$

is termed the normalized nonlinearity surface or (two dimensional) restoring force of the CR loop, and becomes the nonlinearity S curve when  $\lambda \rightarrow 0$ . An integral of  $-h(\phi, \lambda)$  represents a potential function. The nonlinearity surface QPSK has period of  $\pi/2$  radians, Fig.4.10. However, the period of staggered QPSK is extended to  $\pi$  radians, Fig.4.11. The nonlinearity surface of the SQPSK scheme has a favorable shape in a comparison with the shape of the QPSK scheme, because of an extended linear region near the origin ( $\phi = 0, \lambda = 0$ ) and the larger period. Therefore, SQPSK will perform better (will have lower  $P_e$ ) than QPSK in the presence of phase uncertainties. Note that  $p(\phi, \lambda)$  depends on  $h(\phi, \lambda)$ , i.e.

$$p(\phi, \lambda) = C \frac{\exp[-\int_{\phi} \int_{\lambda} h(\phi, \lambda) dx dy]}{N_c(\phi, \lambda) N_o} + \text{Ito terms} \quad (4.41)$$

$p(\phi, \lambda)$  is a nonelementary function due to a nonelementary integral in its exponent. By using (4.36-4.41), solutions  $\phi_i$  (4.2a-b) might be obtained, in principal, by a numerical integration. However, for more than 4 state schemes, an excessive amount of computer time is required. Nevertheless, for comparison purposes, the nonlinearity surface  $h(\phi, \lambda)$  and uncertainty diagram  $U(\phi, \lambda)$  are better figures of merit than the corresponding average probability of error  $P_e$ . An ideal  $U(\phi, \lambda)$  is independent of  $\phi$  and  $\lambda$ , while  $h(\phi) = \sin \phi$  is a good choice.

QPSK @ 10<sup>-10</sup>

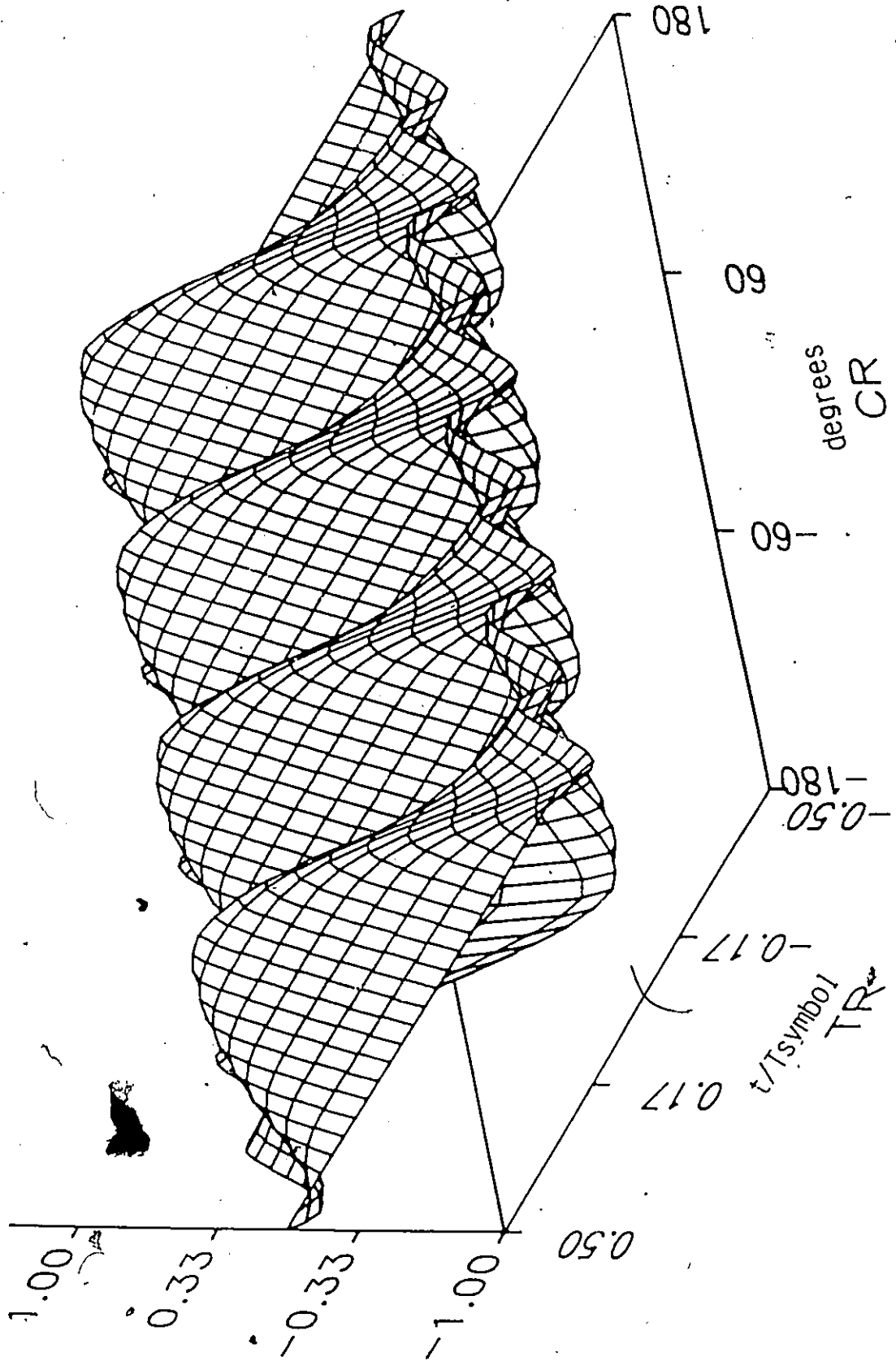


Figure 4.10. The QPSK nonlinearity surface. DFCRL

# SQPSK @ 10 -10

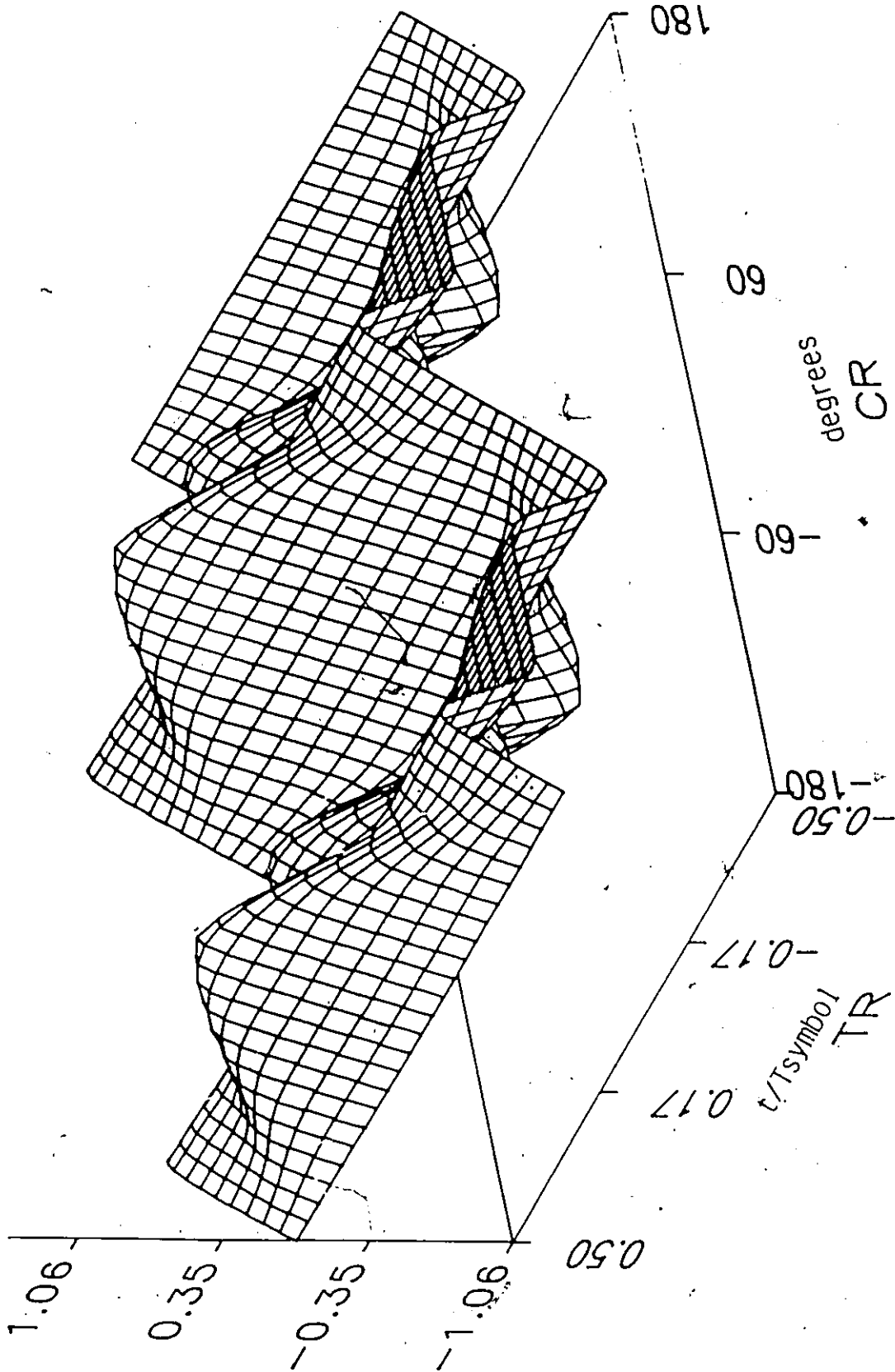


Figure 4.1.1. The SQPSK nonlinearity surface. DFCRL

### 4.2.2. EQUALIZED DFCRL

Although an equalization within the loop might be employed in any narrowband system to improve performance, here we analyze a wideband system employing an overlapped modulation scheme. Due to overlapping pulses extending beyond the  $(-T/2, +T/2)$  interval, Fig.2.2, ISI is present at the receiver. We analyze this ISI, which might be reduced by employing a simple equalizer in each of the quadrature arms of the DFCRL. Our analysis uses the SQORC (also known as Feher's IJF, [B3]) modulation scheme, Table 2.1, Fig.2.2, eqs.(2.1-2.3), as a model which might be straightforwardly applied to any other overlapped scheme. From (2.1-2.3), it is easy to show that SQORC does not have a constant envelope, i.e. the factor within the second sum in (4.9) is not a constant. Therefore, a ML approach should take this into consideration. By applying the previous, rather lengthy procedure, an ML-based receiver might be derived. Instead, we use a more effective approach based on the following logical reasoning: The autocorrelation function of an overlapped scheme spans more than a  $2T$  second interval, Fig.4.12, i.e. neighboring pulses cause ISI at the sampling point. We assume that an early-late gate loop, like a TR crosscorrelation device, is used to establish a timing reference, [B3], and sampling is made every  $T$  seconds. The crosscorrelation function of a presumably rectangular reference signal and input pulses (described by eqs. 2.3a-b), rather than the autocorrelation function given in Fig.4.12, are used for our purposes. A  $T$  seconds long pulse might have four different forms, Fig.4.13a, and an equal number of forms with opposite signum. The signal power after the ISD device (denoted with an integral in Fig.4.6), i.e. at the decision device input, varies from symbol to symbol because of non-equal pulses. The probability of error performance is dictated by a pulse with the lowest energy, i.e. a degradation of 1.09 dB might be expected. This theoretical result is experimentally verified on our IJF modem, Fig.4.13b. This translates into a conditional probability of error degradation from  $10^{-10}$  to  $10^{-8.59}$ . See the UD in Fig.4.14.

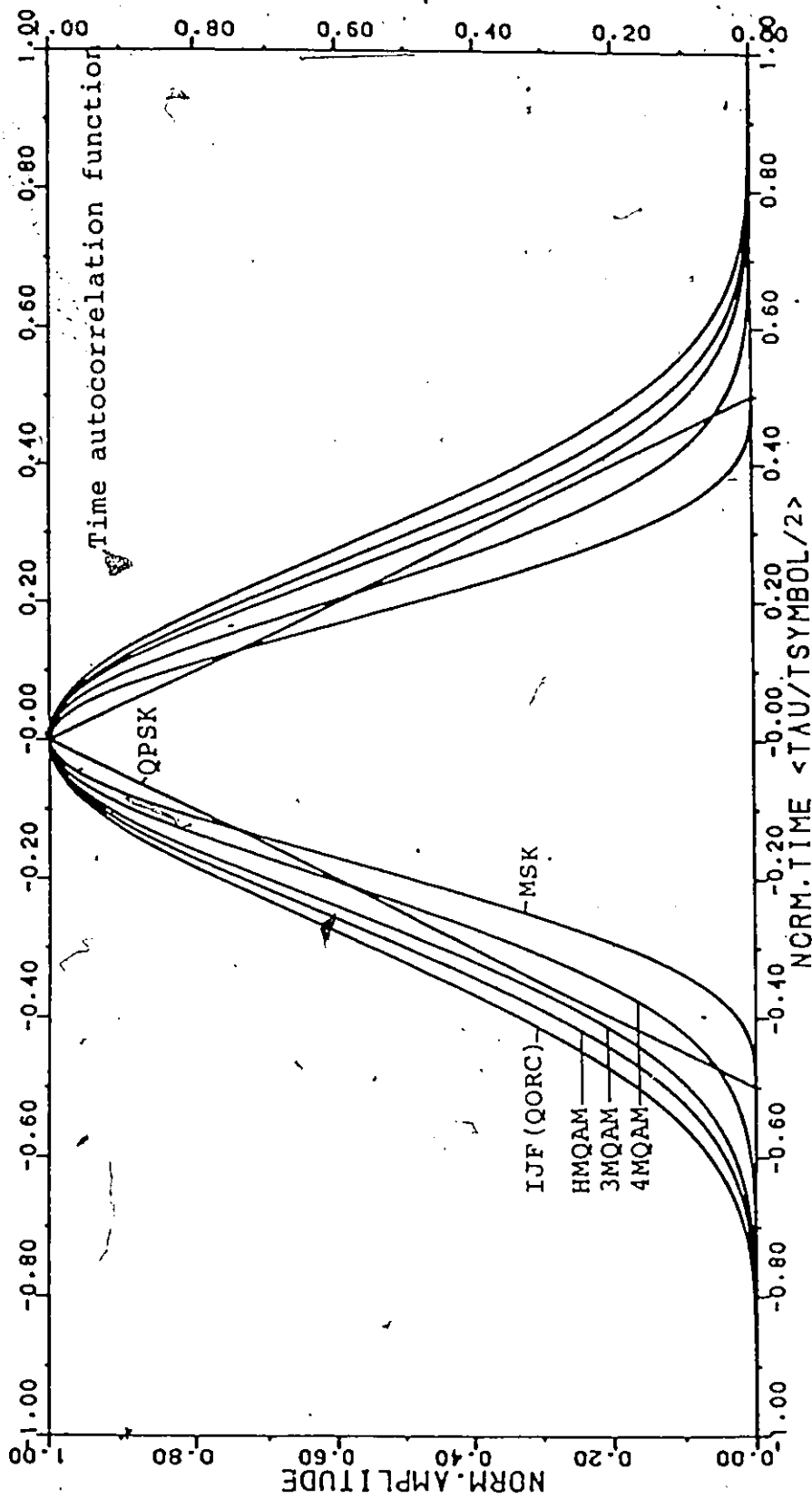


Figure 4.12. The autocorrelation functions of WQAM schemes.

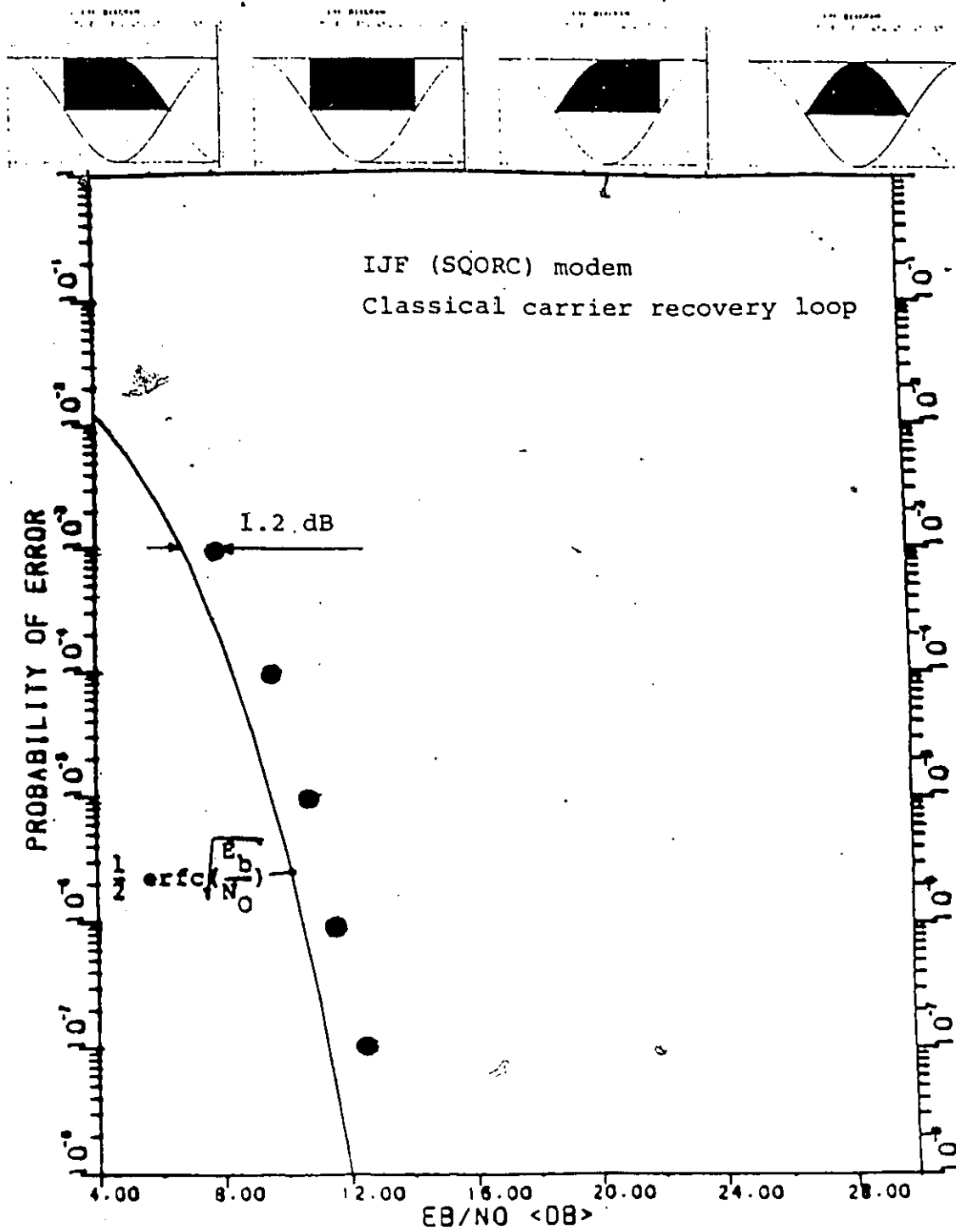


Figure 4.13. a) The SQORC signal shapes. b) The average probability of error performance measurements (•) of the IJF (SQORC) modem employing the classical carrier recovery loop.

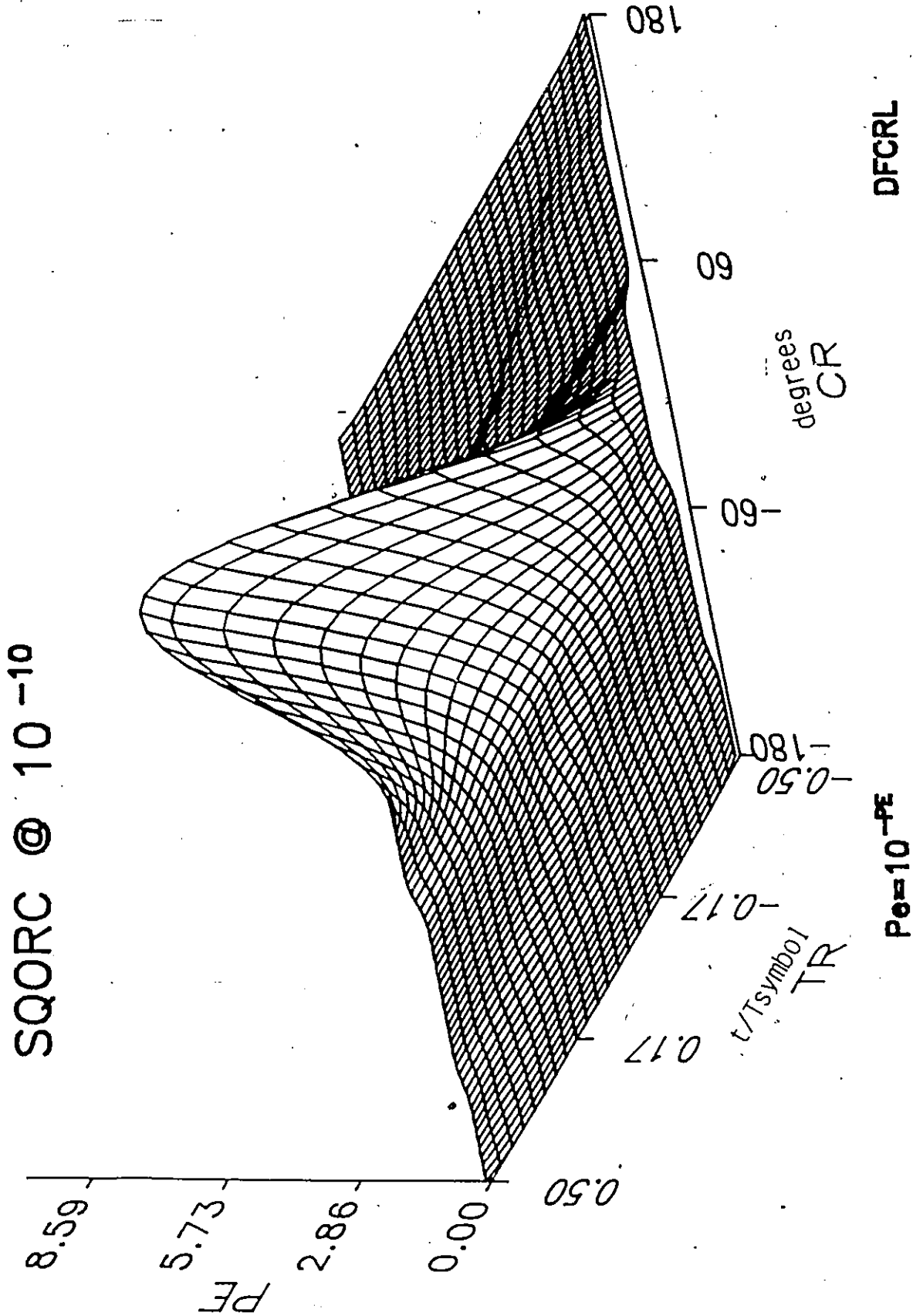


Figure 4.14. The SQORC uncertainty diagram employing the classical DFCRL. The performance of  $10^{-10}$  is taken as the reference.

To smooth the signal fluctuations of overlapped schemes at the decision device input a simple 3-tap equalizer is placed between the ISD and the decision device inside the DFCRL in Fig.4.6, which gives a new loop called equalized DFCRL, Fig.4.15. The noise after the equalizer is Gaussian but not white with variance  $\sigma_n^2 = (c_0^2 + 2c_1^2)N_0$ , where  $c_0, c_1$  are tap coefficients. As a consequence, the performance of SQORC is improved to  $10^{-9.97}$  which is a minor, rather insignificant degradation (0.03 dB) from the  $10^{-10}$  reference. The UD of SQORC using this transversal type of equalizer within the DFCRL is illustrated in Fig.4.16. Although the pulse shape of QORC schemes extends over parts of three  $T$  intervals— the right half of the  $(k-1)$ -th, all of the  $k$ -th, and the left half of the  $(k+1)$ -th interval, Fig.2.2, the energy in the  $(k-1)$ -th interval depends also on the pulse in the  $(k-2)$ -th interval, etc. Total ISI cancellation requires an infinite number of taps. However, a simple 3-tap equalizer cancels ISI almost completely. Tap coefficients actually depend on the data streams in both quadrature channels, except for  $\phi = 0$ . By employing a more complex feedforward and decision feedback equalizer, we might be able to achieve a slightly better performance than given in Fig.4.16. However, a detailed analysis of the canceller optimization is out of the scope of this contribution. An ML-based device for SQORC (and other overlapped schemes) might also be realized in a parallel form. Three pairs of in-phase and quadrature arms at frequencies  $f_c$  and  $f_c + n/T_S$  will be followed by the ISD and decision devices plus a baseband combiner. No equalizers will be needed.

We have concluded the analysis of the ML approach and proceed with the MAP approach, in which a search for new improved loops is pursued.

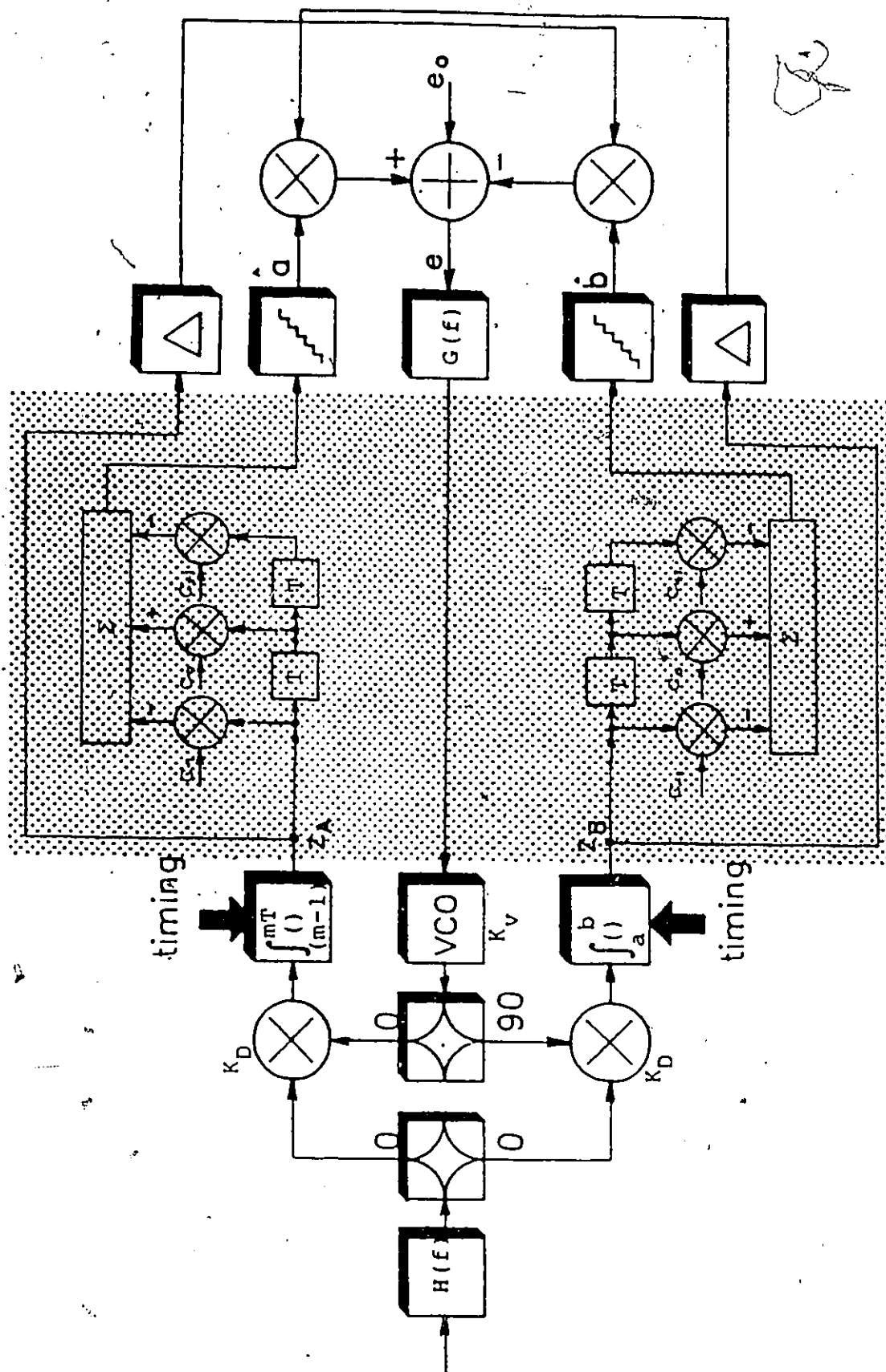


Figure 4.15. The equalized decision feedback carrier recovery loop.

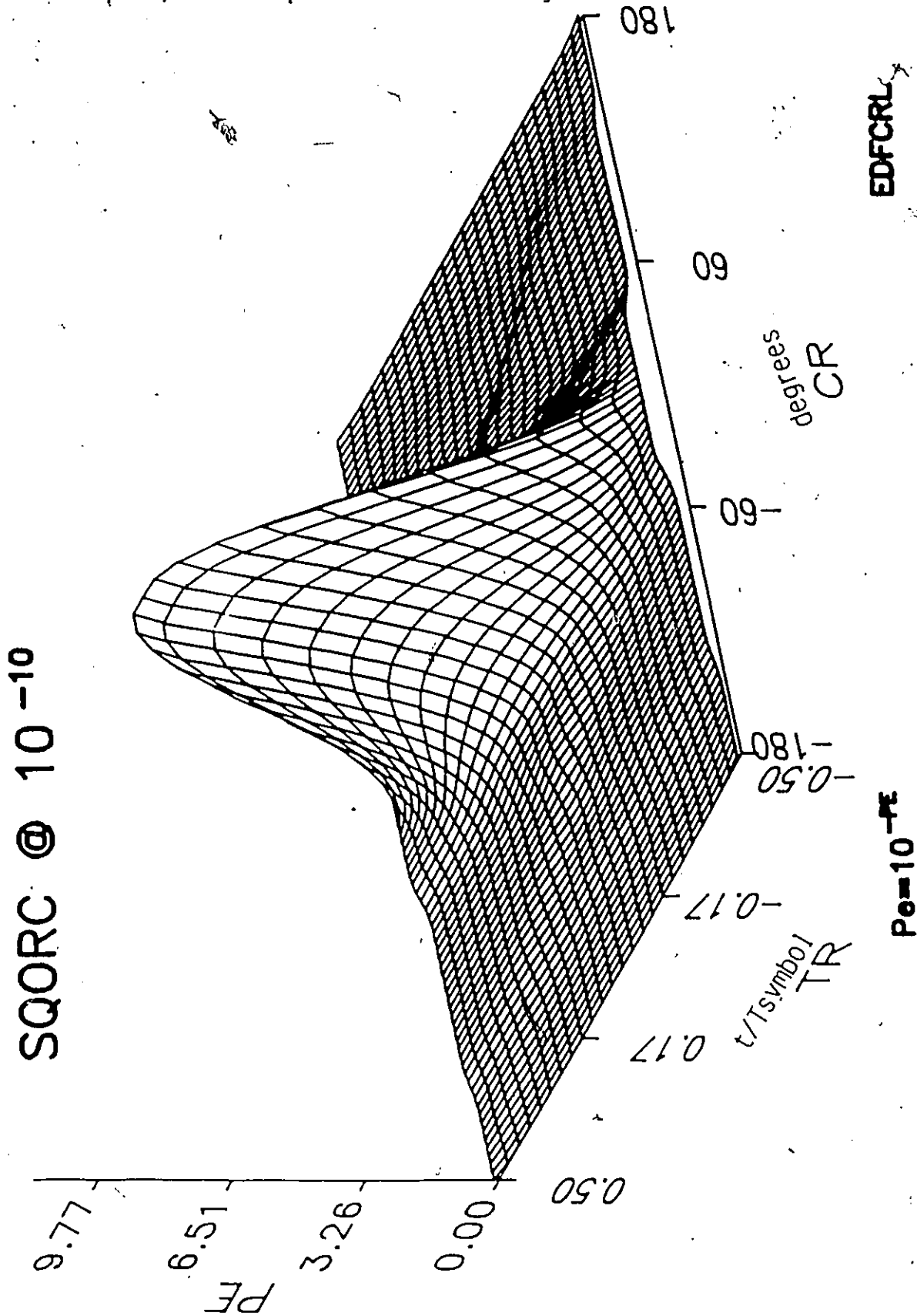


Figure 4.16. The SQORC uncertainty diagram employing equalized DFRL. The performance of  $10^{-10}$  is taken as the reference.

### 4.3 MAXIMUM A POSTERIORI (MAP) APPROACH

Previously, a uniform distribution of  $f(\epsilon_1, \epsilon_2, \theta)$  in (4.6) was assumed and ML optimization followed. A structure with the  $\tanh(x)$  nonlinearity was found, which was approximated with  $\text{sign}(x)$  for high SNR and realized with a quantizer characteristic (4.31) for schemes with more than 2-baseband levels. The corresponding loop is called classical DFCRL, Fig.4.6. However, as shown by (4.31–4.39) and Figs.4.7–4.11, this loop seems to be optimal for  $\phi = \lambda = 0$  only. In general, we might use the knowledge of  $f(\epsilon_1, \epsilon_2, \theta)$  accumulated over previous  $V_T$  and  $V_c$  symbols to improve our decision on the  $k$ -th symbol. This value of  $f(\epsilon_1, \epsilon_2, \theta)$  might be introduced in (4.6) and an MAP optimization procedure might follow. However,  $f(\epsilon_1, \epsilon_2, \theta)$  and the related  $p(\phi, \lambda)$  are nonelementary functions, which are rather difficult if not impossible to manipulate. Therefore, we use a more practical approach based on the knowledge of  $\phi, \lambda$  and  $h(\phi, \lambda)$  accumulated over previous  $V_c$  and  $V_T$  symbols respectively, as follows: According to (4.32–4.35), the phase uncertainty  $\phi$  of the loop causes an attenuation of the in-phase signal proportional to  $\cos \phi$  and a crosstalk proportional to  $\sin \phi$ . The timing uncertainty  $\lambda$  causes an attenuation of the  $k$ -th pulse (on which the decision has to be made) proportional to  $R(|\lambda|)$  and an ISI of the  $(k - 1)$ -th or  $(k + 1)$ -th neighboring pulse proportional to  $R(1 - |\lambda|)$ . A model of these degradations is shown in Fig.4.17a. Since we know the  $V_c$  symbols long estimate of  $\phi$ , say  $\hat{\phi}$ , the  $V_T$  symbols long estimate of  $\lambda$ , say  $\hat{\lambda}$ , and the  $(V_c, V_T)$  symbols long estimate of  $h(\phi, \lambda)$ , say  $\hat{h}(\phi, \lambda)$ , we might be able to compensate for these degradations, Fig.4.17b. For the purpose of this contribution, we assume perfect estimates of  $\phi, \lambda$  and  $h(\phi, \lambda)$ , i.e.  $\phi = \hat{\phi}$ ,  $\lambda = \hat{\lambda}$ , and  $h(\phi, \lambda) = \hat{h}(\phi, \lambda)$ , which might be reasonable since high SNRs within the loop bandwidth are assumed. A compensation for the  $\phi$ -caused degradation is explained in Section 4.3.1, compensation for the  $\lambda$ -caused degradation is explained in Section 4.3.2, while a hybrid compensation scheme follows in Section 4.3.3.

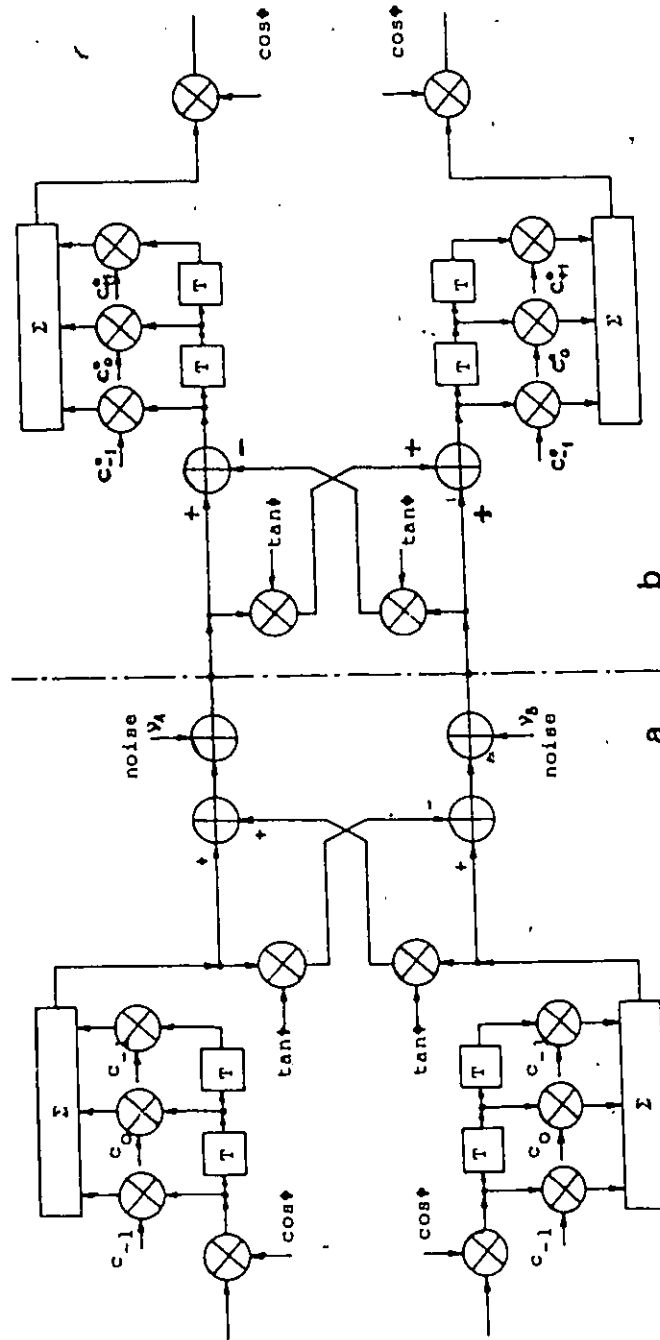


Figure 4.17. a) The degradation model for the loop caused impairments due to the phase uncertainty  $\phi$  and the timing uncertainty  $\lambda$ . b) The corresponding equalization model.

### 4.3.1 Crosstalk Cancellation DFRC Loop

The following conclusions might be drawn from (4.31-4.40): The quantizer represented by the characteristic in (4.31) is an optimum nonlinearity for  $\phi = 0$  only. However, to minimize an average probability of error  $P_e$  for any  $\phi$ , a device for which the decision is independent of  $\phi$  must be found. In addition to the already applied ML criterion, different criteria (constraints) might apply, e.g. minimum mean square error, etc. We decide to minimize  $P(e|\phi)$  over the entire range of  $\phi$ , which, as shown later, corresponds to the cancellation of pattern jitter. Although an analysis might be quite complex regarding the difficulties of an exact calculation of the noise statistics at the VCO input, we ignore this noise, which is reasonable as long as the loop bandwidth is small in comparison with the data bandwidth. Then, a new crosstalk cancellation (CC) DFRC for M-ary quadrature amplitude modulation (MQAM) signal sets is given in Fig.4.18. The loop employs two adders, two baseband amplifiers with gains equal to  $\tan \phi$ , and two adaptive quantizers (or a pair of amplifier-fix quantizer combination), which are governed by a phase error  $\phi$  of the loop, to cancel (or at least attenuate) the crosstalk. As a result, the pattern dependent jitter is cancelled (at least attenuated) and the loop performs as a continuous wave (CW) CR loop. Here, we optimize the loop performance for  $\lambda = 0$ , while a more general case  $\phi \neq 0, \lambda \neq 0$  is analyzed in Section 4.3.3. If  $K_A(\phi) = K_B(\phi) = \tan \phi$ , a signal at the A decision device input is

$$\begin{aligned} \zeta_A &= (+a_m \cos \phi + b_n \sin \phi + \nu_A) \\ &\quad - (-a_m \sin \phi + b_n \cos \phi + \nu_B) \tan \phi \\ &= \frac{a_m}{\cos \phi} + (\nu_A - \nu_B \tan \phi) \end{aligned} \quad (4.42)$$

i.e. no crosstalk occurs and the signal-to-noise ratio remains constant, since both the desired signal and noise powers are increased in the same proportion. A decision is independent of CR uncertainties, i.e. the loop operates as a CW CR loop and the nonlinearity curves equal  $\sin \phi$ , Fig.4.19a (here an ideal timing is assumed). Note that the curve labeled  $\lambda = 0.0$  corresponds also to any MQAM scheme (within a constant factor), assuming CCDFRC is employed. The nonlinearity curves ( $\lambda = 0.0$ ) of the MQAM schemes employing classical DFRC are summarized in Fig.4.19b. The advantage of our new crosstalk cancellation loop over the classical one is obvious.

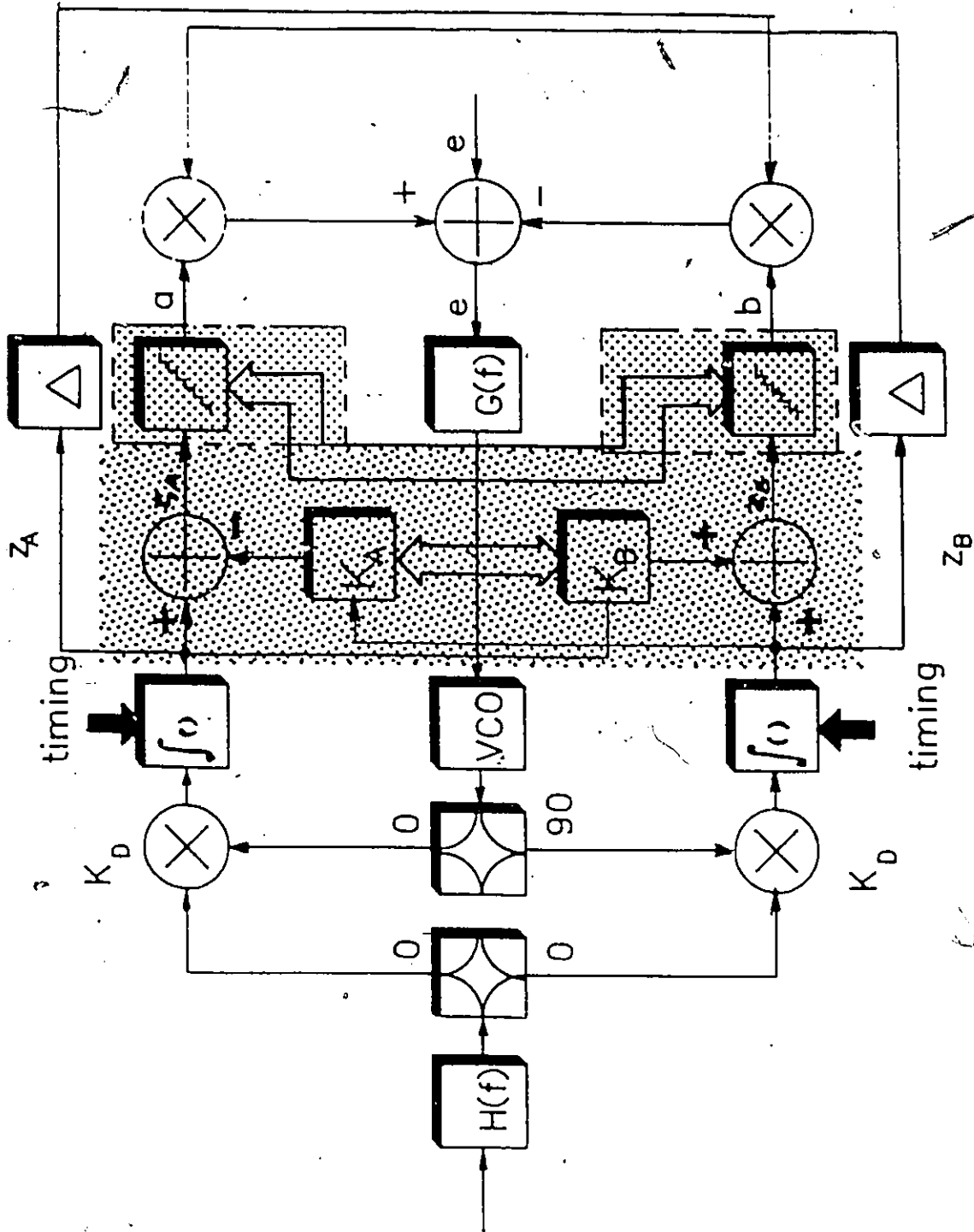


Figure 4.18. The crosstalk cancellation DFCRL.

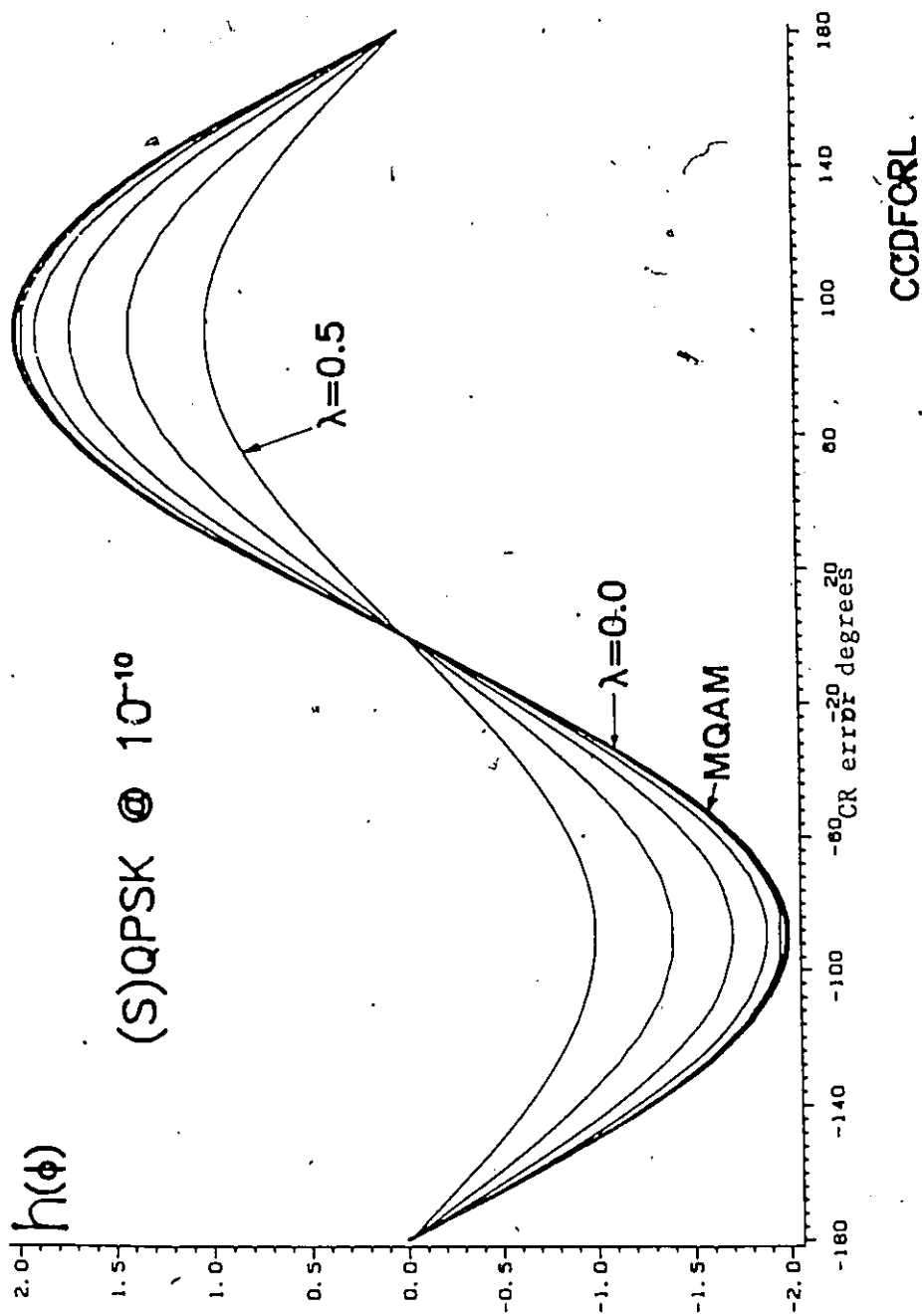


Figure 4.19a . The (S)QPSK nonlinearity curves employing the crosstalk cancellation decision feedback carrier recovery loop. The  $\lambda = 0.0$  labelled curve corresponds to the MQAM schemes also.

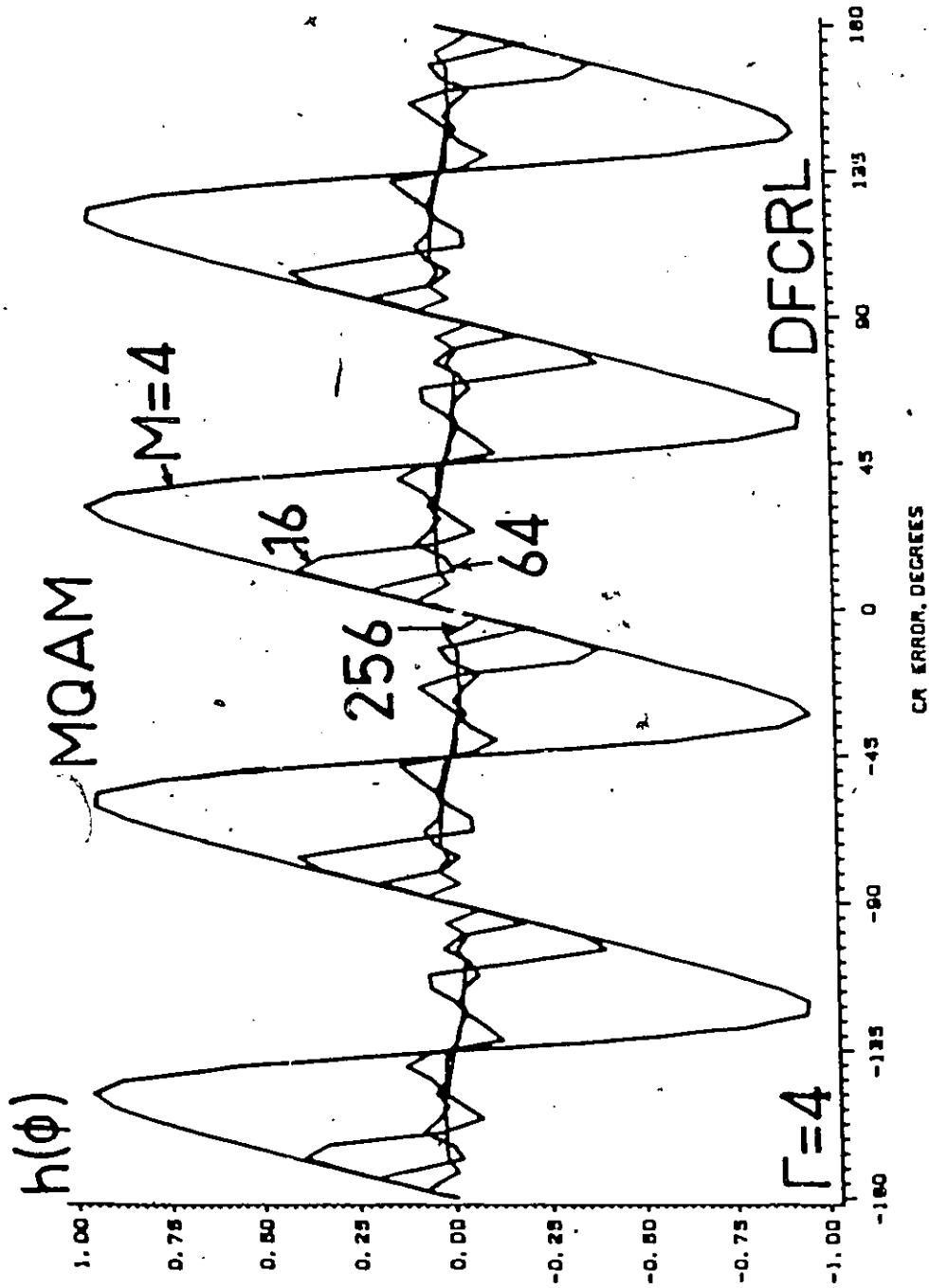


Figure 4.19b. The MQAM nonlinearity curves employing classical decision feedback carrier recovery loop. The parameter  $\Gamma = 4$  corresponds to the  $P(\epsilon|\phi) \approx 10^{-8}$ .

In our analysis of the CCDFCRL we have assumed an optimal estimation of  $\phi$ , i.e.  $\hat{\phi} = [h(\phi, \lambda = 0)]^{-1}$  where  $[h(\phi, \lambda = 0)]^{-1}$  equals the inverse of  $h(\phi, \lambda = 0)$ . A detailed analysis of this estimator is out of the scope of this presentation. However, a brief heuristic explanation follows. Let's assume that the loop is initially locked and  $\phi = 0$ . As input symbols of data are arriving into the loop arms, the phase uncertainty  $\phi(t)$  due to Gaussian noise fluctuates slowly (relative to the symbol rate) and might take any value between  $(-\pi, +\pi)$ . For small  $\phi$ ,  $h(\phi) \doteq \phi$ , i.e.  $\phi$  is directly proportional to the voltage  $h(\phi)$ . The shaded part of the loop in Fig.4.18 feeds back this (presumably correct) information on  $\phi$  accumulated over the previous  $V_c$  symbols and improves the decision at the  $k$ -th symbol, which is now virtually independent of  $\phi$ . This improved decision changes  $h(\phi)$  from the complex form given in equation (4.40) and Fig.4.19b to  $h(\phi) = \sin \phi$ , Fig.4.19a. As a final result, the pattern jitter is cancelled (practically, it is attenuated by an amount proportional to the ratio of data and loop bandwidths  $R_p = SNR_{IF}/SNR_L$ ) and, more importantly, the quadrant ambiguities previously present due to the combination of signal constellation and fixed threshold decision devices, have vanished. Similar improvement might be expected in the tracking of unbalanced schemes while employing proper gains in the quadrature arms.

The average probability of error  $P_e$  of the WQAM schemes employing CCDFCRL equals

$$P_e = \underbrace{P(e|\phi)}_{\text{constant}} \underbrace{\int_{-\pi}^{+\pi} p(\phi) d\phi}_{=1} = P(e|\phi = 0) \quad (4.43)$$

i.e. no degradation (pattern jitter) exists due to the presence of data, assuming  $P_e < 10^{-3}$ . At high  $P_e$  (above  $10^{-2}$ ) the signal  $h(\phi)$  which governs the loop is attenuated (by approximately 0.175 dB at  $P_e \approx 10^{-1}$  when 16QAM is concerned) since the decision principal is employed within the loop. However, further analysis of these effects at high  $P_e$  is out of the scope of this presentation.

In order to compare the average probability of error  $P_e$  performances of the WQAM schemes employing the classical DFCRL and those schemes employing our new crosstalk cancellation DFCRL the knowledge of the probability density function  $p(\phi)$  of the classical DFCRL is necessary. This is rather difficult task, which requires a tedious mathematical procedure to be employed in an attempt to solve the stochastic partial differential equation of the Fokker-Planck-Kolmogorov type, or a time consuming computer simulation needs to be done. On the contrary, the probability density function  $p(\phi)$  of the crosstalk cancellation DFCRL is practically equivalent to that of the CW loop and is given by [B16], Fig.4.1,

$$p(\phi) \stackrel{\rho > 10}{\approx} C \frac{\exp[\rho(\cos \phi + \beta_N \phi)]}{2\pi I_0(\rho)} \quad (4.44)$$

$\rho$  is the signal-to-noise ratio within the loop,  $C$  is the normalization constant,  $\beta_N = \beta/\rho$  is the normalized loop detuning,  $\beta$  is the absolute detuning, and  $I_0(\rho)$  is the modified Bessel

function of zero order and argument  $\rho$ . We assume that the classical DFCRL has the same probability density function  $p(\phi)$  as the CW loop (and the crosstalk cancellation DFCRL) — except for the factor four and the periodicity of  $\pi/2$  radians. The true probability density function of the classical DFCRL will have less desirable form. Therefore, our estimation might be biased in favor of the classical loop.

We were able to perform the Monte Carlo simulation of the performance of the QPSK schemes — employing both classical and crosstalk cancellation loops — at  $P_e > 10^{-4}$  and that of the 16QAM at  $P_e \approx 10^{-2}$ . We also generated the theoretical performance curves of QPSK and 16QAM schemes at  $\rho \leq 174$  (22.4 dB). The results are summarized in Figs. 20–21. In Fig. 20 the QPSK  $\log_{10} P_e$  performance versus the carrier-to-noise ratio C/N in dB in the double-sided Nyquist bandwidth and the normalized loop detuning (loop stress)  $\beta_N$  as a parameter is presented. The ratio  $R_\rho = \rho/SNR_{IF} = 10$  is assumed. This is the lower end practical value, which allows us to generate these curves. Note that typical satellite systems operate at  $SNR_{IF} > 5$  dB, i.e.  $\rho > 15$  dB. The typical terrestrial (and cable) systems operate at even higher  $SNR_{IF}$  ( $\rho \gg 15$  dB). An estimation error of 0.46 dB is assumed when the crosstalk cancellation DFCRL is employed. An ideal ambiguity resolution is assumed when the classical DFCRL is employed — a bias in the favor of the classical loop. In practice, a degradation of 0.3–0.5 dB might be expected due to the ambiguity resolution. A random d.c. wandering within the loop, channel asymmetry (e.g. during a selective fading event), or any other dynamic impairment of such kind will cause a stress in the loop and consequently a degradation of the  $P_e$  performance. The classical DFCRL suffers significant degradation, while our new loop is practically insensitive to these kind of impairments, Fig. 4.1, Fig. 4.20. At  $P_e = 10^{-6}$  and  $\beta_N = 0.7$  our new loop outperforms the classical one by 2.5 dB, assuming QPSK is employed. Results in Fig. 4.7, and Fig. 4.21 indicate that at lower  $P_e$  and for higher state modulation schemes our new loop will outperform the classical one by even higher margin.

- E.g., let's brief the necessary performance of the  $K_A(\phi)$  and  $K_B(\phi)$  devices (amplifiers). Let's assume the symbol rate equals 10 Msymbols/s. Then, the necessary bandwidth of the  $K_A(\phi)$  and  $K_B(\phi)$  devices is in the range of the tens of MHz. Usually, the loop bandwidth is a one hundred or more times narrower than the bandwidth of the data. Therefore, the phase changes  $\phi$  and the necessary dynamic changes of the  $K_A(\phi)$  and  $K_B(\phi)$  amplifiers are in the range of one hundred of kHz, or lower. The necessary gain is proportional to the  $\tan \phi$ . If  $|\phi| < 45^\circ$ ,  $K_A(\phi)$  and  $K_B(\phi)$  perform as attenuators. If the maximal available gains of  $K_A(\phi)$ ,  $K_B(\phi)$  equal 100, the  $\tan \phi$  function might be modeled for any  $\phi$  except in the  $1^\circ$  wide strips around  $\pm 90^\circ$ . Therefore, the crosstalk cancellation DFCRL might be realized with the practically available components.

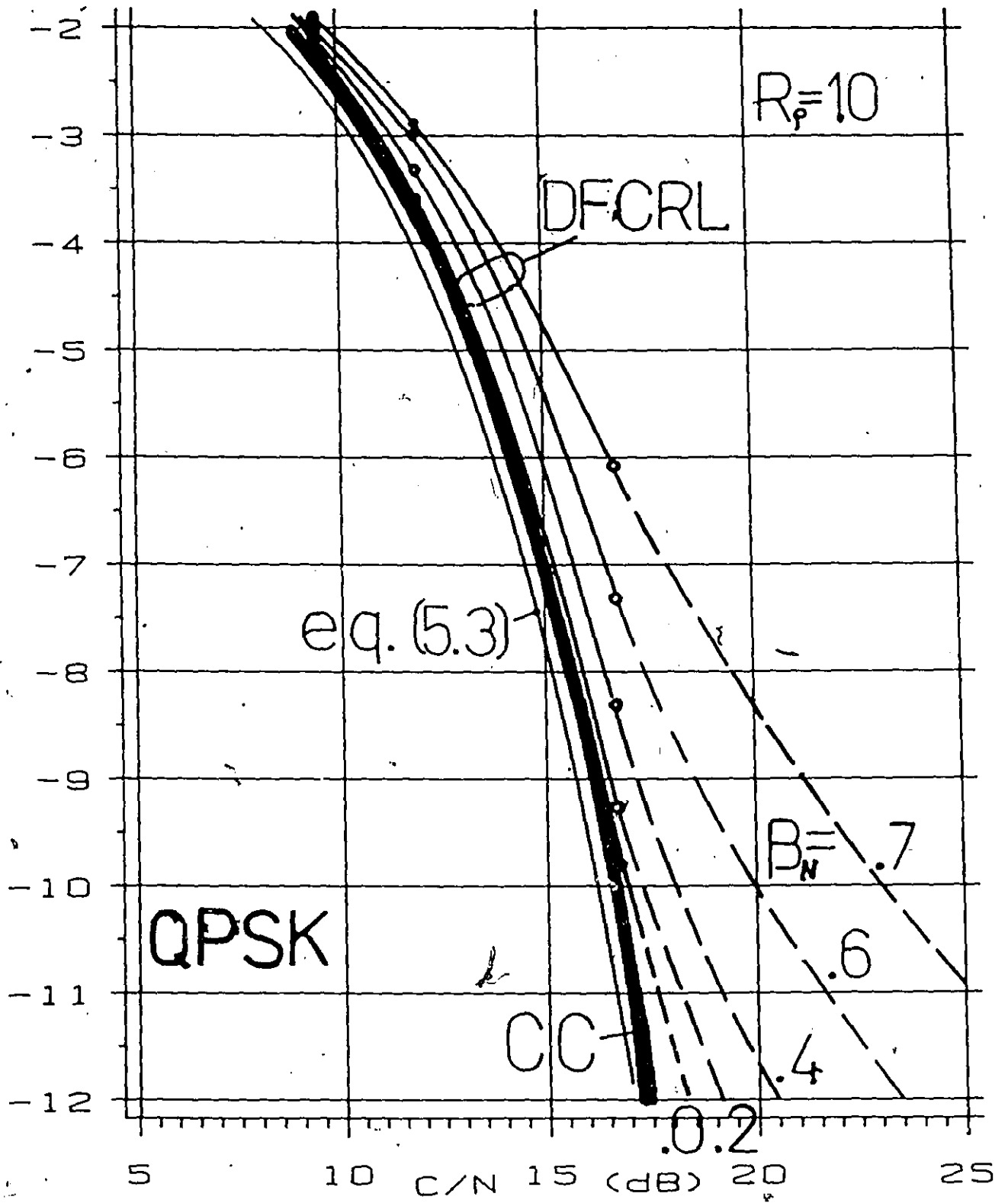


Figure 4.20. The QPSK  $\log_{10} P_e$  performance versus the carrier-to-noise ratio  $C/N$  in dB in the double-sided Nyquist bandwidth and the normalized loop detuning (loop stress)  $\beta_N$  as a parameter, employing classical or crosstalk cancellation (CC) decision feedback carrier recovery loop (DFCRL). The ratio  $R_p = SNR_L / SNR_{IF} = 10$  is assumed.

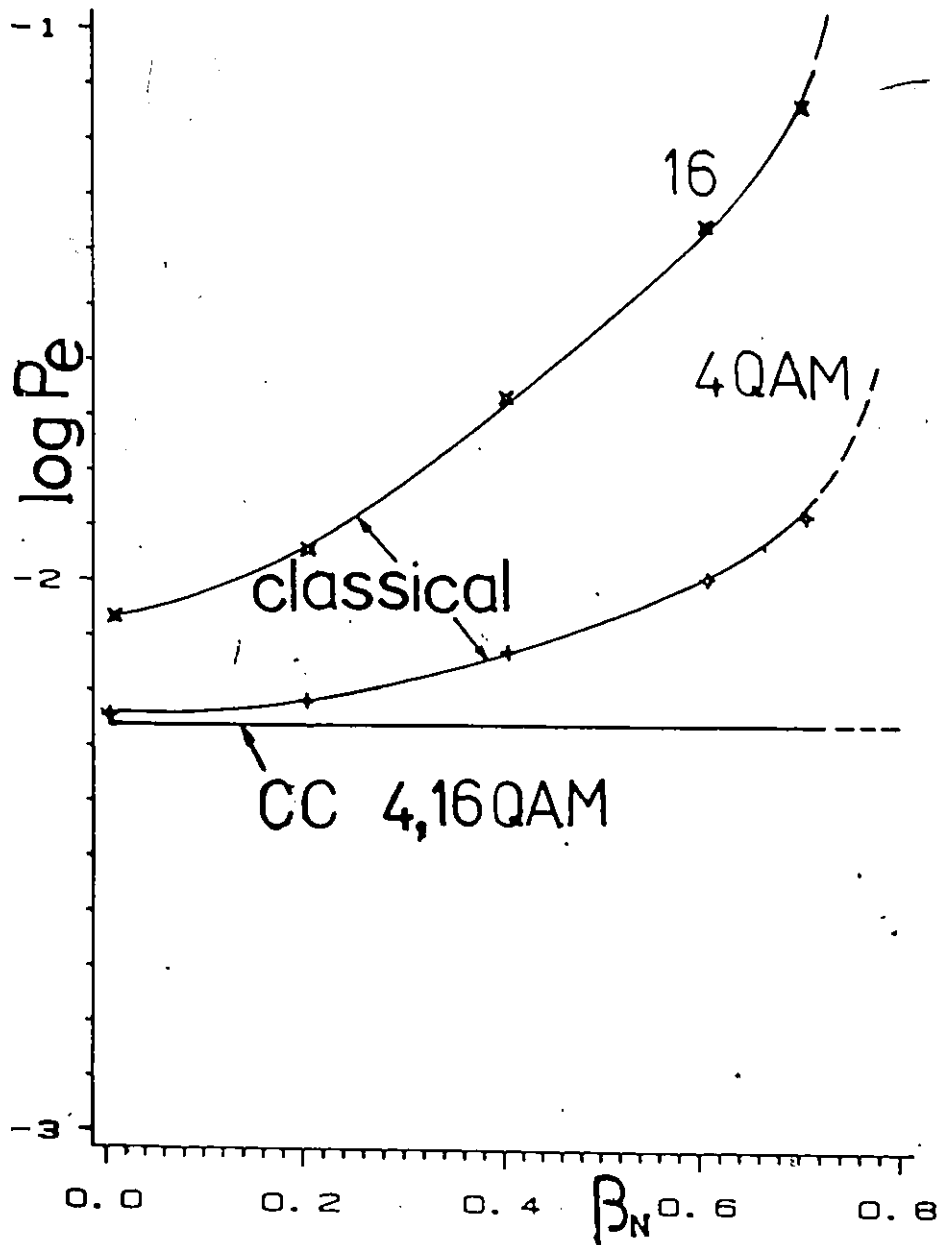


Figure 4.21. The 4 and 16QAM  $\log_{10} P_e$  performance versus the normalized loop detuning (loop stress)  $\beta_N$ , employing classical or crosstalk cancellation (CC) decision feedback carrier recovery loop (DFCRL). The ratio  $R_p = SNR_L/SNR_{IF} = 10$  is assumed.

### 4.3.2 Timing ISI Cancellation DFRCR Loop

By observing equation (4.34), it is easy to see that a timing uncertainty  $\lambda$  causes complex ISI. As an example, these negative effects might be partially overcome by employing a simple 3-tap equalizer, whose central tap gain is proportional to  $+1/R(|\lambda|)$  and the gains of two neighboring taps are proportional to the product of  $-R(1 - |\lambda|)$  and the corresponding step function ( $c_{-1} = 0$  for  $\lambda \geq 0$ , while  $c_{+1} = 0$  for  $\lambda \leq 0$ ), Fig.4.17b. In a system employing narrowband filtering, an equalizer with more taps will be necessary. The resultant CR loop is called **timing ISI cancellation DFRCR**, Fig.4.22. The loops in Fig.4.15 and Fig.4.22 are the same except for the different tap gains of the corresponding equalizers. Here we have assumed perfect knowledge of  $\lambda$  and have ignored crosstalk terms proportional to  $\sin \phi$ . The noise after the equalizer is Gaussian but not white with variance  $\sigma_n^2 = [R^{-2}(|\lambda|) + R^2(1 - |\lambda|)]N_o$ . However, SNR is proportional to

$$\frac{R^2(|\lambda|)}{1 + R^2(|\lambda|)R^2(1 - |\lambda|)} \quad (4.45)$$

Timing ISI pattern jitter is cancelled but SNR and the conditional probability of error deteriorate as  $\lambda$  increases. However, this deterioration is not as severe as in the classical DFRCR. The relative improvement increases as the number of baseband levels increases. A decision feedback equalizer which cancels timing ISI on the previous symbol(s) and a transversal equalizer which acts on future symbol(s) might give better results. Further improvements might be expected with an optimization of the TR circuit.

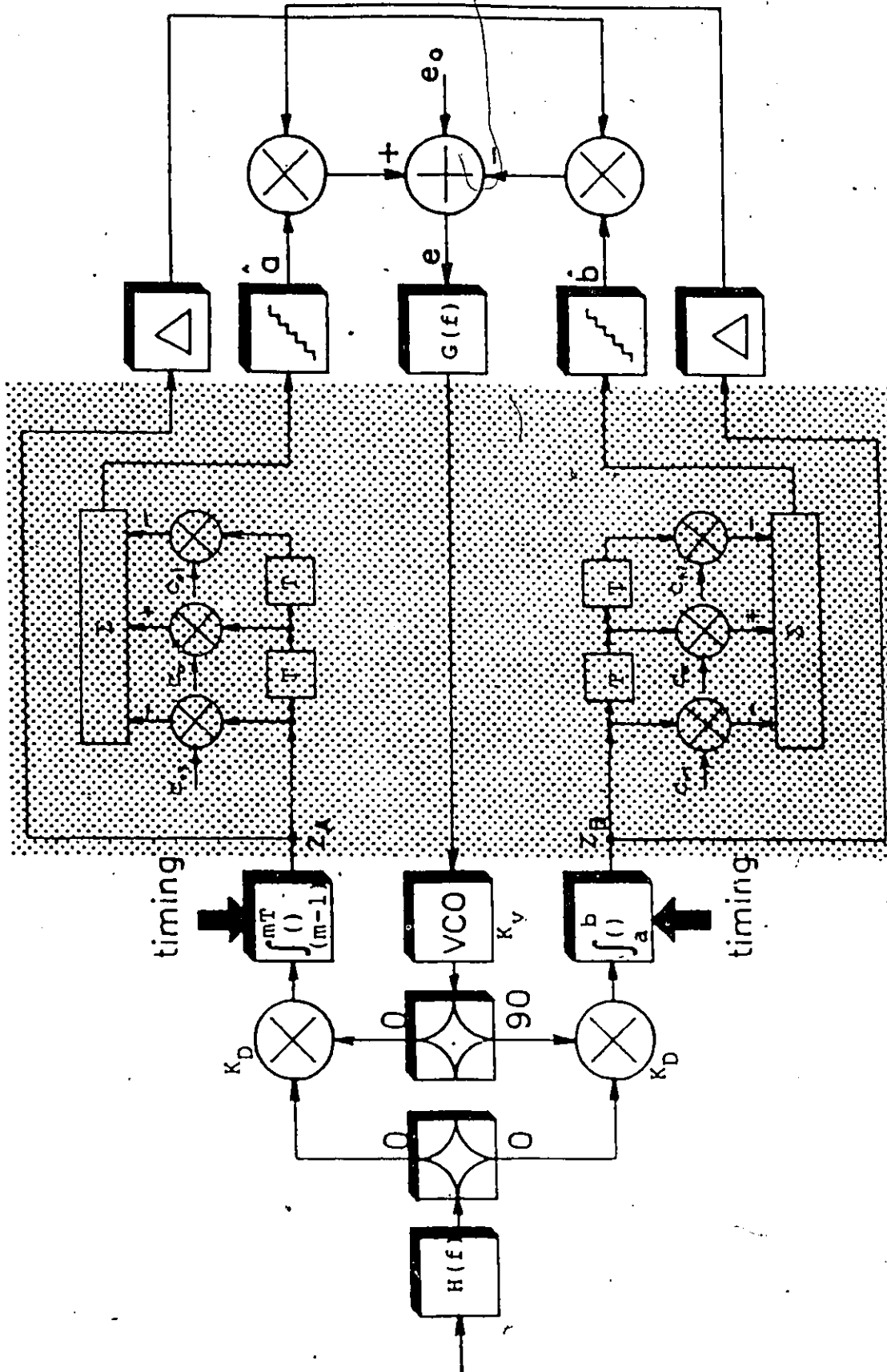


Figure 4.22. The timing intersymbol interference cancellation DFCRL.

### 4.3.3 FEEDLOOP

By using knowledge of both  $\phi$  and  $\lambda$  accumulated over  $V_c$  and  $V_T$  symbols respectively, a new feedback structure which uses an estimation of phase and an estimation of timing to improve detection is suggested in Fig.4.23. We call this loop FEEDLOOP, as an acronym for Feedback of data, Estimation of phase, Estimation of timing, and Detection LOOP. The uncertainty diagram of FEEDLOOP is independent of  $\phi$  and dependence on  $\lambda$  is significantly reduced, which becomes particularly important for multilevel schemes. SNR at the decision device input is proportional to

$$\frac{R^2(|\lambda|) \cos \phi}{\cos \phi + R^2(|\lambda|)R^2(1 - |\lambda|)} \quad (4.46)$$

for a FEEDLOOP employing a transversal equalizer, Fig.4.23. Based on the results of the Monte Carlo simulation, the UD of 256QAM scheme employing a FEEDLOOP is given in Fig.4.24. Note the deeps around the singular points at  $\phi = \pm 90$  degrees. The width of these deeps depend on the practical limitations of the components within the loop. The advantages of the FEEDLOOP, as seen in the results presented in Fig.4.24, and Fig.4.1c, over the classical DFCRL, Fig.4.10a-b, and Fig.4.1a, are obvious.

The SNR for the FEEDLOOP employing a decision feedback equalizer is rather difficult to calculate, in general. However, regarding  $\lambda$  as a slow varying process relative to the symbol rate, i.e.  $\lambda$  is constant during one symbol period,

$$\text{ISI} \propto a_{k\pm 1} R(1 - |\lambda|) P(e_k|\lambda) \quad (4.47a)$$

$$\text{signal} \propto a_k \{1 - [1 - R(|\lambda|)] P(e_k|\lambda)\} \quad (4.47b)$$

$$\text{noise} \propto \sigma_n^2 \quad (4.47c)$$

where  $\propto$  means proportional to. Crosstalk is reduced by  $P(e_k|\lambda)$ , the drop in signal is reduced in the same proportion, and noise remains the same.

A few more sentences are devoted to the choice of UD and nonlinearity surface as figures of merit: An UD independent of phase uncertainty  $\phi$  and timing uncertainty  $\lambda$  represents the best possible performance, i.e. a CW loop. Any dependence on  $\phi$  and  $\lambda$  represents a degradation caused by the presence of data, which has been called in the literature "data introduced ISI," "data dependent pattern jitter," "squaring loss," "self noise," etc. The nonlinearity surface determines the probability of error function of the loop and other properties such as acquisition, skipping rate, etc. Therefore, both the UD and nonlinearity surface describe the performance of the particular signal format-carrier recovery loop combination.

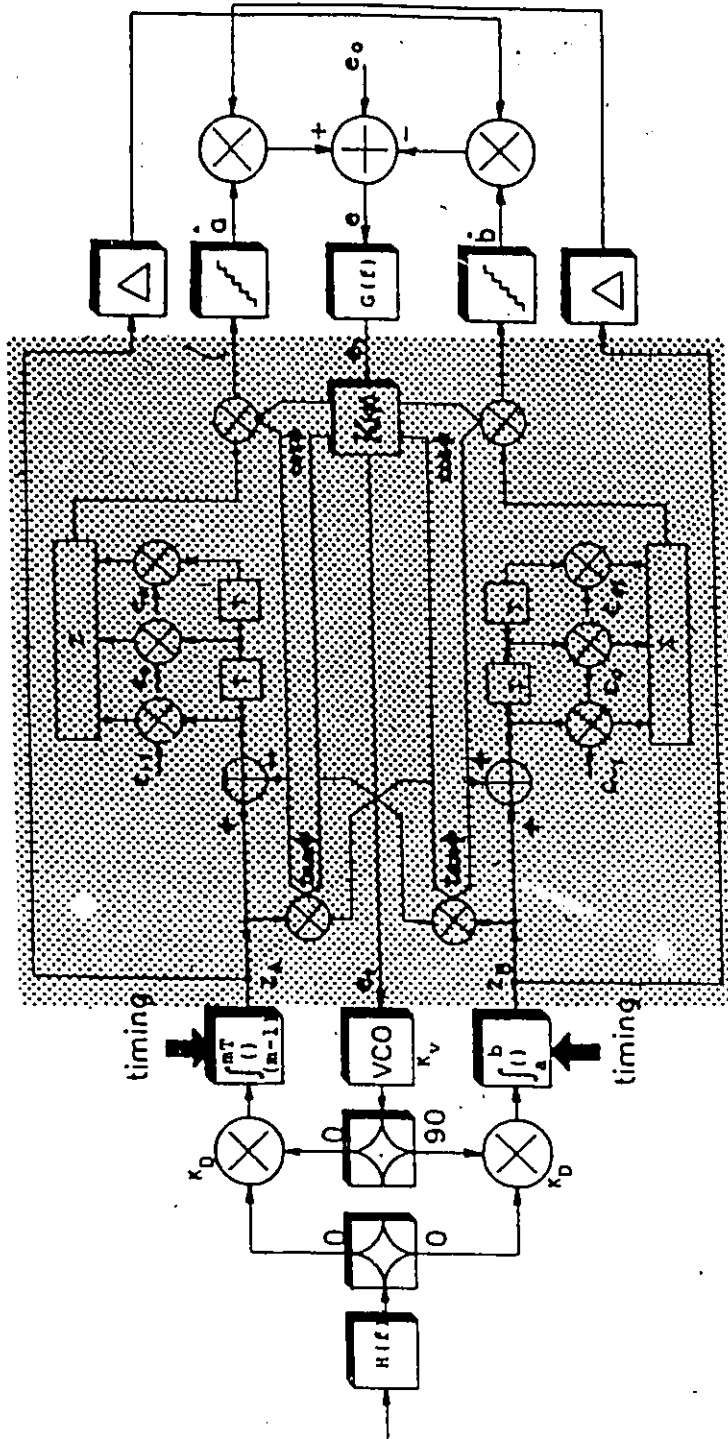


Figure 4.23. The FEEDLOOP.

# 256QAM Uncertainty Diagram @ $P_e = 10^{-2}$

FEEDLOOP. Monte Carlo Simulation.

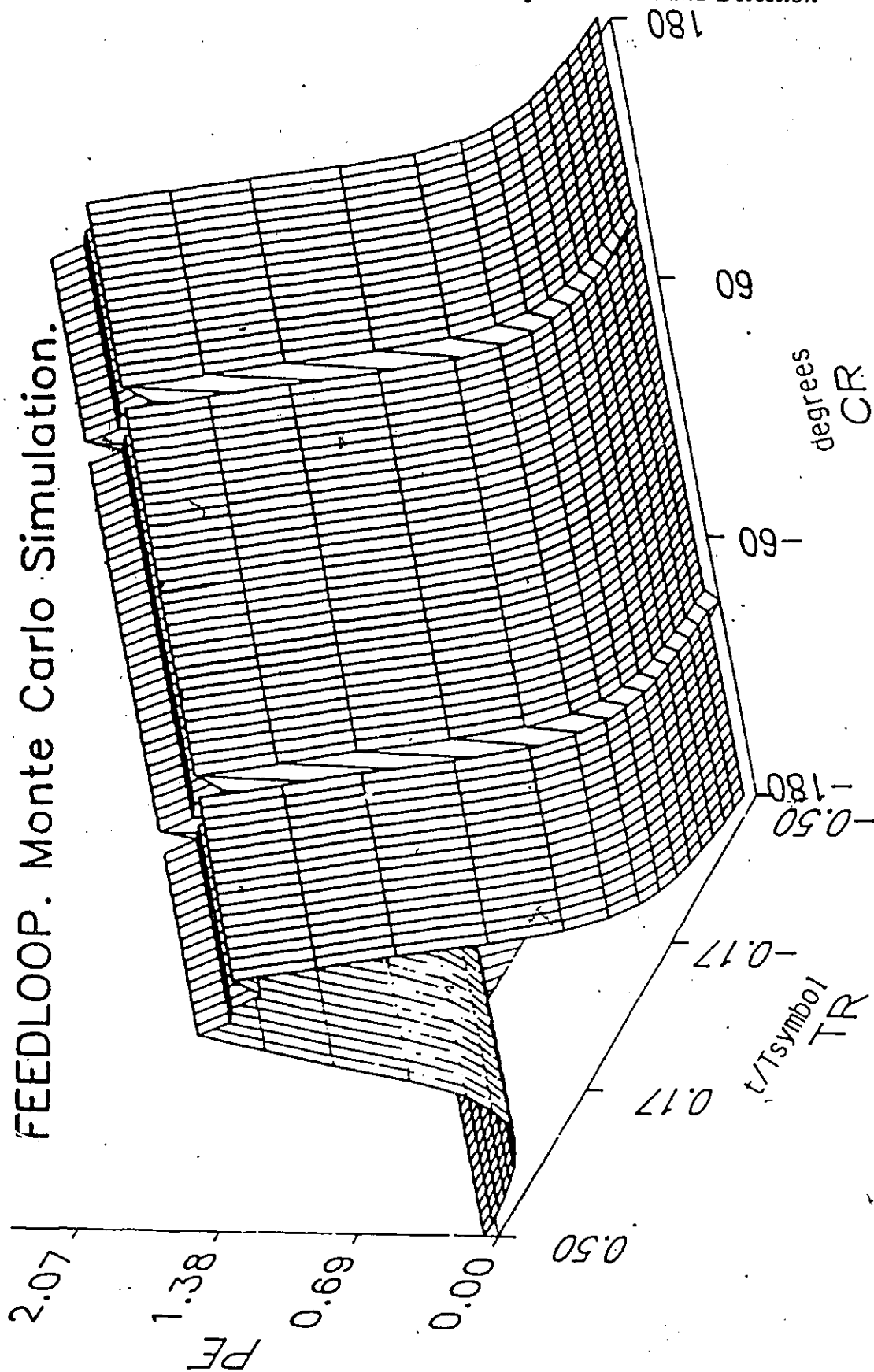


Figure 4.24. The 256QAM uncertainty diagram employing FEEDLOOP. The results of Monte Carlo simulation with 8124 symbols.  $P(e|\phi, \lambda) = -10 \log(PF)$ . TR ( $t/T$  symbols). CR (degrees).

## 4.4 CONCLUSION

In this chapter a composite phase and timing estimation and data detection of WQAM signal sets is analyzed. By using a maximum likelihood (ML) approach, four new joint phase and timing estimators are derived. The performance of the classical decision feedback carrier recovery loop (DFCRL) employing an integrate-and-sample device in each quadrature arm (active loop) is evaluated in the presence of both carrier uncertainty  $\phi$  and timing uncertainty  $\lambda$ . Results are presented in the following new forms: the Uncertainty diagram  $U(\phi, \lambda)$ , the equal (iso) probability of error isoper curves, and the nonlinearity surface  $h(\phi, \lambda)$  which becomes loop's nonlinearity S-curve when  $\lambda \rightarrow 0$ . The performance of overlapped schemes is degraded if classical carrier recovery (CR) schemes are employed. The theoretical results are experimentally verified on our Intersymbol-Jitter-Free (IJF) 64 kb/s modem. New equalized DFCRL which employs a simple 3-tap transversal equalizer in each quadrature arm is proposed for CR and the detection of overlapped schemes. Our new loop does not exhibit performance degradation associated with classical CR loops. By using the MAP probability approach and knowledge of  $\phi, \lambda$ , and  $h(\phi, \lambda)$  accumulated over corresponding observation intervals, improved loops, i.e. crosstalk cancellation DFCRL, timing intersymbol interference cancellation DFCRL, and FEEDLOOP, are introduced and analyzed. The theoretical results are verified by the Monte Carlo simulation. These loops perform almost as well as a continuous wave CR loop, do not exhibit quadrant ambiguities, and might be employed for phase and timing estimation and the detection of balanced and unbalanced WQAM schemes. The advantages of the new loops over the classical one become greater at lower probabilities of error and when higher state schemes are employed. E.g. at  $P_e = 10^{-6}$  and in the presence of a normalized loop detuning of 0.7, the crosstalk cancellation loop (and FEEDLOOP) outperform the classical one by 2.4 dB, assuming QPSK modulation scheme is employed.

However, we are aware that our analysis is far to be complete. In practice, the total phase error might be composed of many (usually independent) components such as Doppler shift, angle modulation, instabilities of the transmitter and receiver frequency sources, additive noise (usually Gaussian), etc. Herein we dealt with the digital data modulated signals with suppressed carrier in the presence of white Gaussian noise. We analyzed the interaction of data and noise and introduced a method to wipe-off the data — in order to improve the performance. The analysis of effects of Doppler, ACI, discrete spurious, and other

impairments on the tracking and detection performance of the loop was not the part of this presentation. In the next chapter, we present a simplified performance analysis of the multistate modulation schemes influenced by the phase noise, i.e. instabilities of the frequency sources.

PERFORMANCE  
OF M-ARY MODULATION SYSTEMS  
IN THE PRESENCE OF PHASE NOISE

In the Chapter 2 WQAM family is introduced. The performance of 4 state WQAM schemes was evaluated in the presence of different impairments typical for the satellite channels such as ACI and hardlimiter nonlinearity. In the Chapter 3 the performance of 256QAM and 1024QAM schemes is evaluated in the presence of the group delay and amplitude response impairments typical for the terrestrial radio and cable systems. An a priori knowledge of the carrier phase and symbol timing has been assumed. Chapter 4 deals with the estimation of the carrier phase and symbol timing of WQAM schemes, and a few new receivers are introduced and analyzed. In this chapter, the performance of WQAM and M-ary quadrature partial response (MQPR) systems is analyzed in the presence of phase noise. Herein we adopt a practical approach, which yields useful performance curves in which the degradation due to phase noise can be readily seen.

An outline of the chapter follows. In Section 5.1 the phase noise characterisation is given. In Section 5.2 the results for probability of error performance of MPSK, MQAM and MQPR modulation systems in the presence of thermal and phase noise are presented.

## 5.1 PHASE NOISE CHARACTERIZATION

The expressions for the performance of coherent digital modulation systems in a Gaussian channel are well known [B15]. However, in practice we rarely have a perfect knowledge of the local phase reference. The output signals from carrier and symbol timing recovery circuits are really random processes and produce errors in the estimation of phase and time, respectively. These random processes consist of two components: first contributed by thermal white Gaussian noise, and second contributed by all other random sources which is termed phase noise. The effects on the error probability performance due to this phase noise can be obtained in principle. However, this is a formidable task with only a few rather complex solutions existing [B3], [B12], [B16] for two- and four-state modulation systems only.

We compute the degradation of a system in the presence of phase noise in the following manner. Considering the sources of phase noise as independent random variables, the central-limit theorem says that, under certain general conditions, the resultant equivalent phase noise probability density function approaches a normal Gaussian curve as number of sources increase, [B25, p.267]. Since the number of individual sources tends to be large in practice, and their magnitudes are of the comparable order, the assumptions of the central limit theorem should apply. This is the case of a well designed system. However, in a particular example, an individual source might dictate the overall system performance and Gaussianity might be destroyed, which might result in an increased degradation of the performance. The phase noise is combined with assumed white Gaussian noise channel to produce a total carrier-to-noise ratio  $(C/N)_T$  given by

$$(C/N)_T = [(N/C) + (N/C)_p]^{-1} \quad (5.1a)$$

$$(N/C)_p = (N/C)_1 + (N/C)_2 + \dots + (N/C)_n \quad (5.1b)$$

where  $(N/C)$  is the thermal noise-to-carrier ratio,  $(N/C)_i$  ( $i = 1, \dots, n$ ) is the noise-to-carrier ratio of the  $i$ -th random source and  $(N/C)_p$  is the equivalent phase noise-to-carrier ratio. We use known expressions [B15] to calculate performance of coherent digital modulation systems in the presence of phase noise by replacing  $(C/N)$  by  $(C/N)_T$  and having  $(C/N)_p$  as a variable parameter.

Because of a simplistic phase noise model, the accuracy of results might depend how close the assumed Gaussian probability density function fits the probability density function of the real phase noise. However, in practice we are dealing with the small amount of phase noise which causes degradations less than 1 dB at  $P_e = 10^{-6}$ . In that case and for our purpose the Gaussian probability density function seems to be a good approximation for a real but unknown distribution of a phase noise. Our results of the measurement presented in Section 5.2 are in a close agreement with previous assumptions.

## 5.2 PERFORMANCE EVALUATION

The probability of error performance of Binary PSK (BPSK=2PSK), MPSK ( $M > 2$ ), MQAM and MQPR modulation schemes are given by the following expressions [B15]

$$P_B \doteq \frac{1}{2} \operatorname{erfc}(\sqrt{\gamma_b}), \quad (\text{BPSK}) \quad (5.2)$$

$$P_M \doteq \operatorname{erfc}\left(\sqrt{k\gamma_b} \sin \frac{\pi}{M}\right), \quad (\text{MPSK}, M > 2) \quad (5.3)$$

$$P_L \doteq \left(1 - \frac{1}{L}\right) \operatorname{erfc}\left(\sqrt{\frac{3}{M-1} \frac{1}{2} \gamma_{av}}\right), \quad (\text{MQAM}) \quad (5.4a)$$

$$P_L \doteq \left(1 - \frac{1}{M}\right) \operatorname{erfc}\left(\sqrt{\frac{3}{M-1} \frac{1}{2} \left(\frac{\pi}{4}\right)^2 \gamma_{av}}\right), \quad (\text{MQPR}) \quad (5.5a)$$

$$P_M = 2P_L \left(1 - \frac{1}{2} P_L\right) \quad \text{MQAM and MQPR} \quad (5.4b, 5.5b)$$

where [B8,p.254]

$$\gamma_b = \frac{E_b}{N_o} = \frac{C}{N} \frac{B}{f_b} \quad (5.6)$$

$\doteq$  stands for the approximately equal,  $P_B$  is the probability of error performance of BPSK,  $P_M$  is the corresponding symbol error rate for the MPSK ( $M > 2$ ), MQAM and MQPR systems, while  $P_L$  corresponds to the probability of error of the baseband signal in each of the two quadrature components of QAM or QPR.  $\gamma_{av}$  is the average signal-to-noise ratio per  $k$ -bit symbol, where  $k = \log M$  and  $M$  is the number of levels.  $\gamma_b$  is the energy per bit-to-noise ratio,  $(C/N)$  is the carrier-to-thermal noise ratio;  $f_b$  is the bit rate bit/s and  $B$  is the double-sided noise bandwidth in Hz.

We assume  $B$  is equal to the double-sided Nyquist bandwidth. The expressions (5.2)-(5.5) give the probability of error performance curves illustrated in Fig.5.1. Inclusion of  $(C/N)_p$  as a variable parameter produces a series of curves, one of which (256QAM) is shown for illustration in Fig.5.2. The degradations  $(C/N)_T - (C/N)$  for  $P_e = 10^{-6}$ , dB, vs. the  $(C/N)_p$  are summarized in Figs.5.3—5.5. Fig.5.3 applies for the MPSK systems, the MQAM systems are shown in Fig.5.4 and the MQPR systems in Fig.5.5.

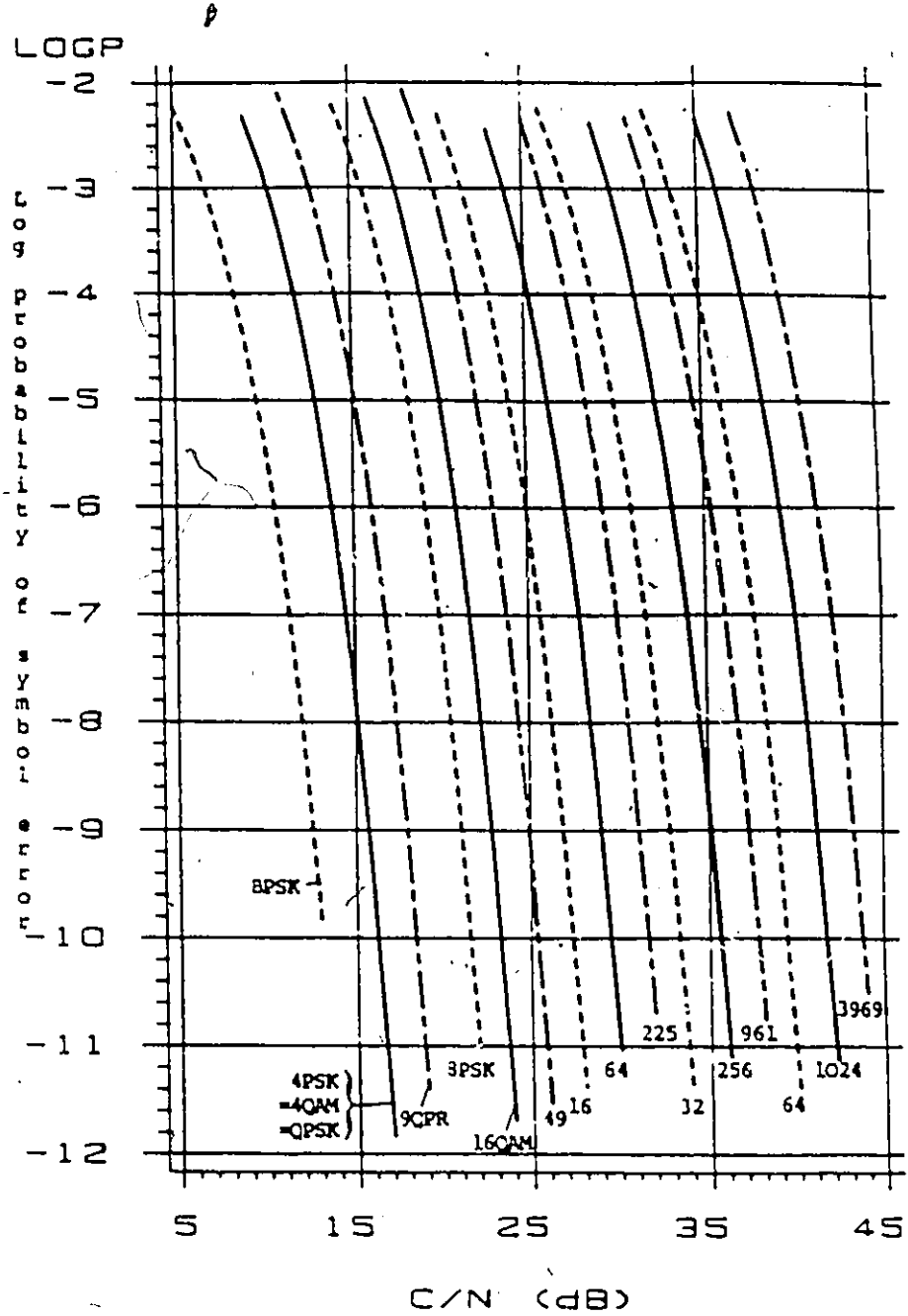


Figure 5.1. The average probability of error performance of the M-ary schemes versus the carrier-to-thermal noise ratio. The white Gaussian channel only (no phase noise). The double-sided Nyquist bandwidth. — MQAM schemes,

- - - - - MPSK schemes,
- · - · - MQPR schemes.

2

# 256QAM

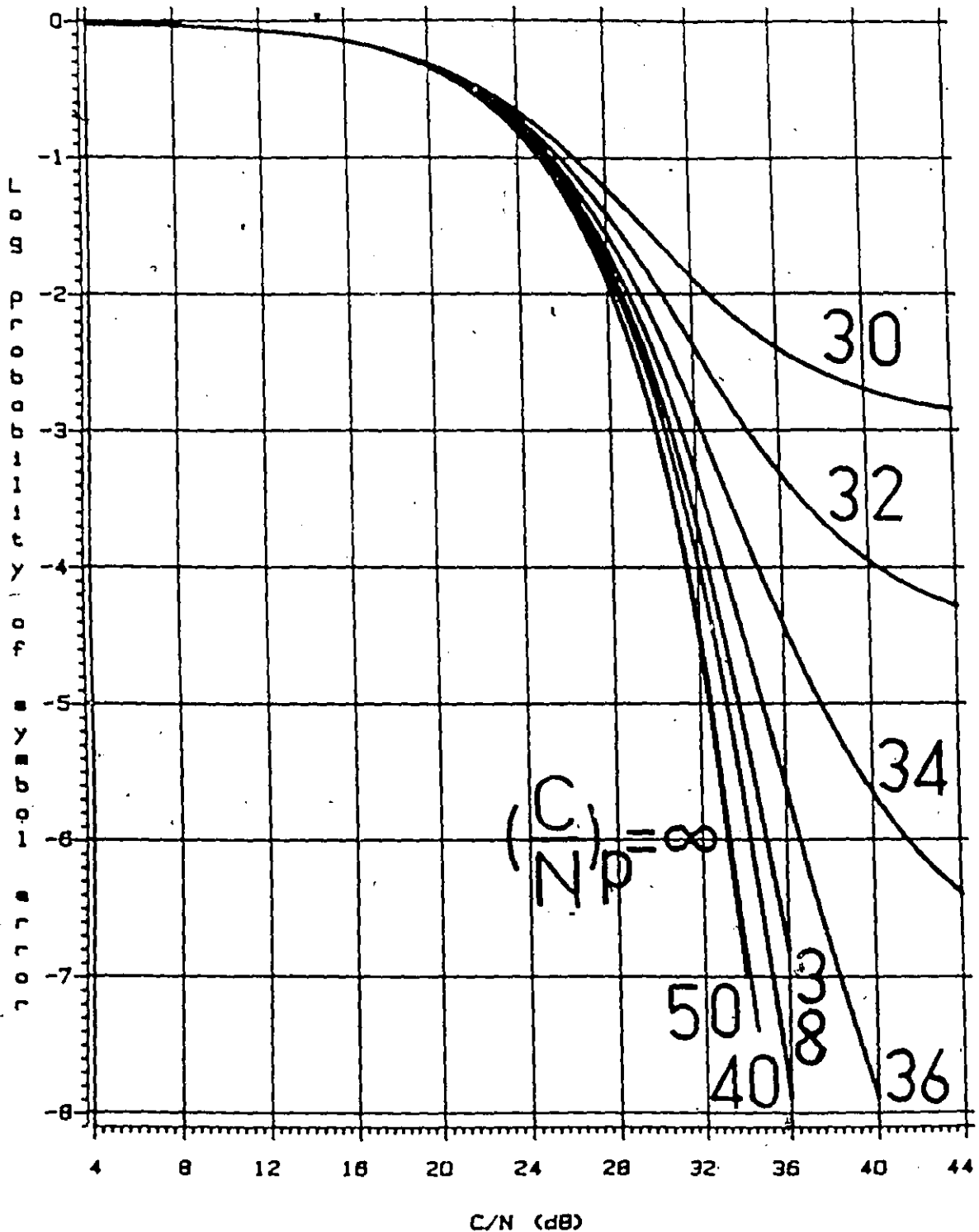


Figure 5.2. The 256QAM average probability of error performance versus the carrier-to-thermal noise ratio with the carrier-to-phase noise ratio as a parameter. The double-sided Nyquist bandwidth.

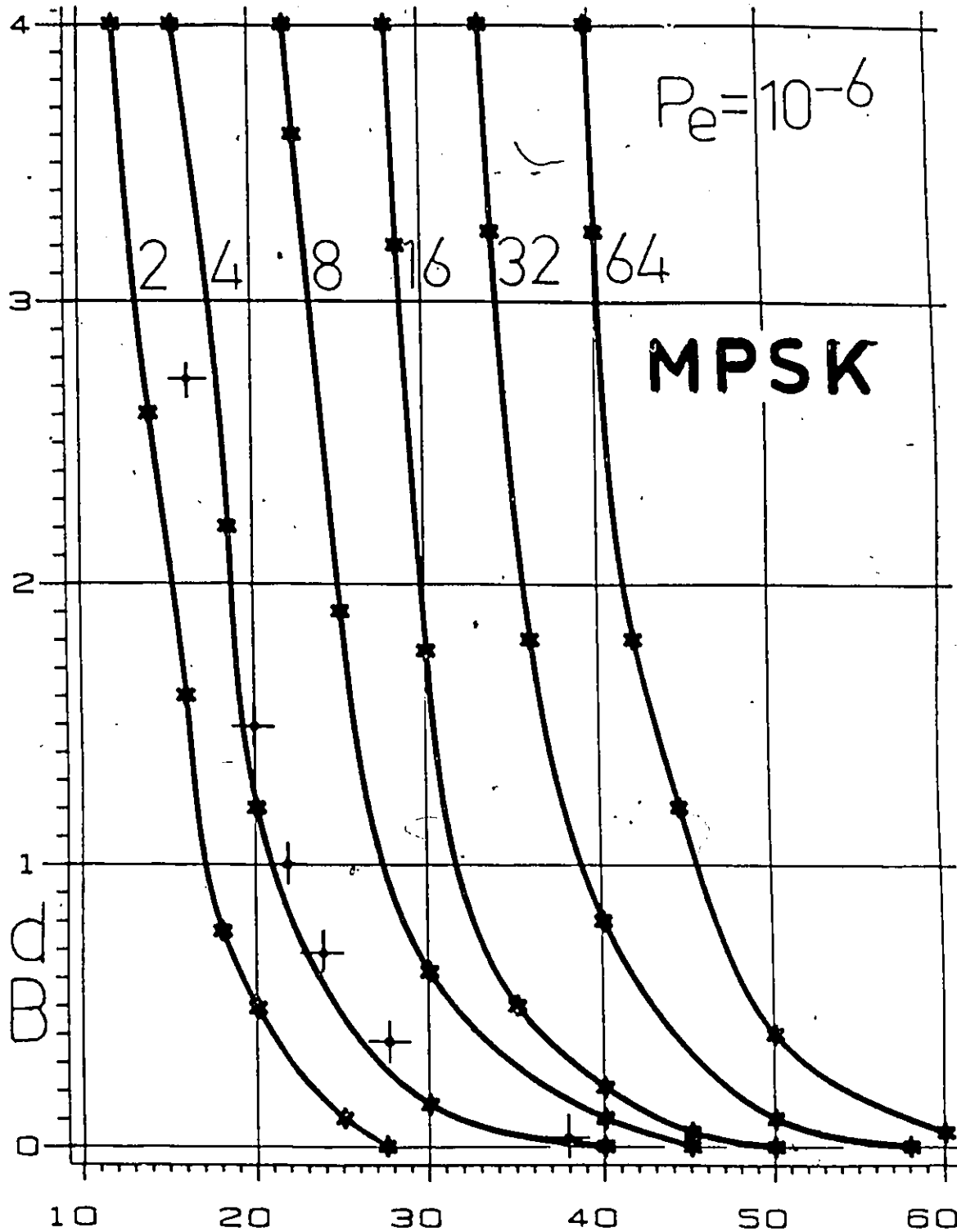


Figure 5.3. The degradation of the MPSK systems in dB, with respect to the theoretical value necessary to achieve the  $P_e = 10^{-6}$  performance, versus the carrier-to-phase noise ratio in the double-sided Nyquist bandwidth in dB. The pluses (+ + +) represent the results of measurements on 4 state SCPC satellite modems.

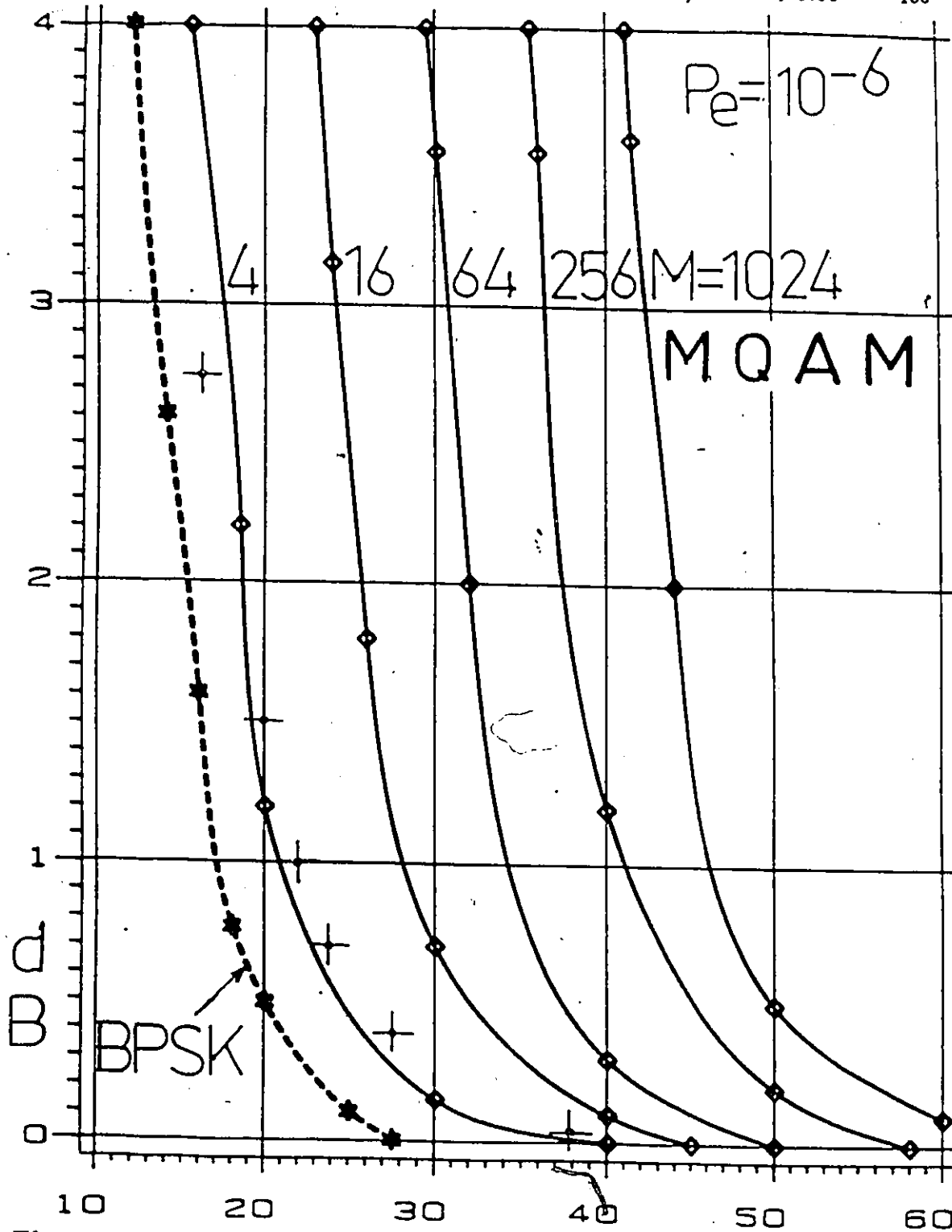


Figure 5.4. The degradation of the MQAM systems in dB, with respect to the theoretical value necessary to achieve the  $P_e = 10^{-6}$  performance, versus the carrier-to-phase noise ratio in the double-sided Nyquist bandwidth in dB. The pluses (+ + +) represent the results of measurements on 4 state SCPC satellite modems.

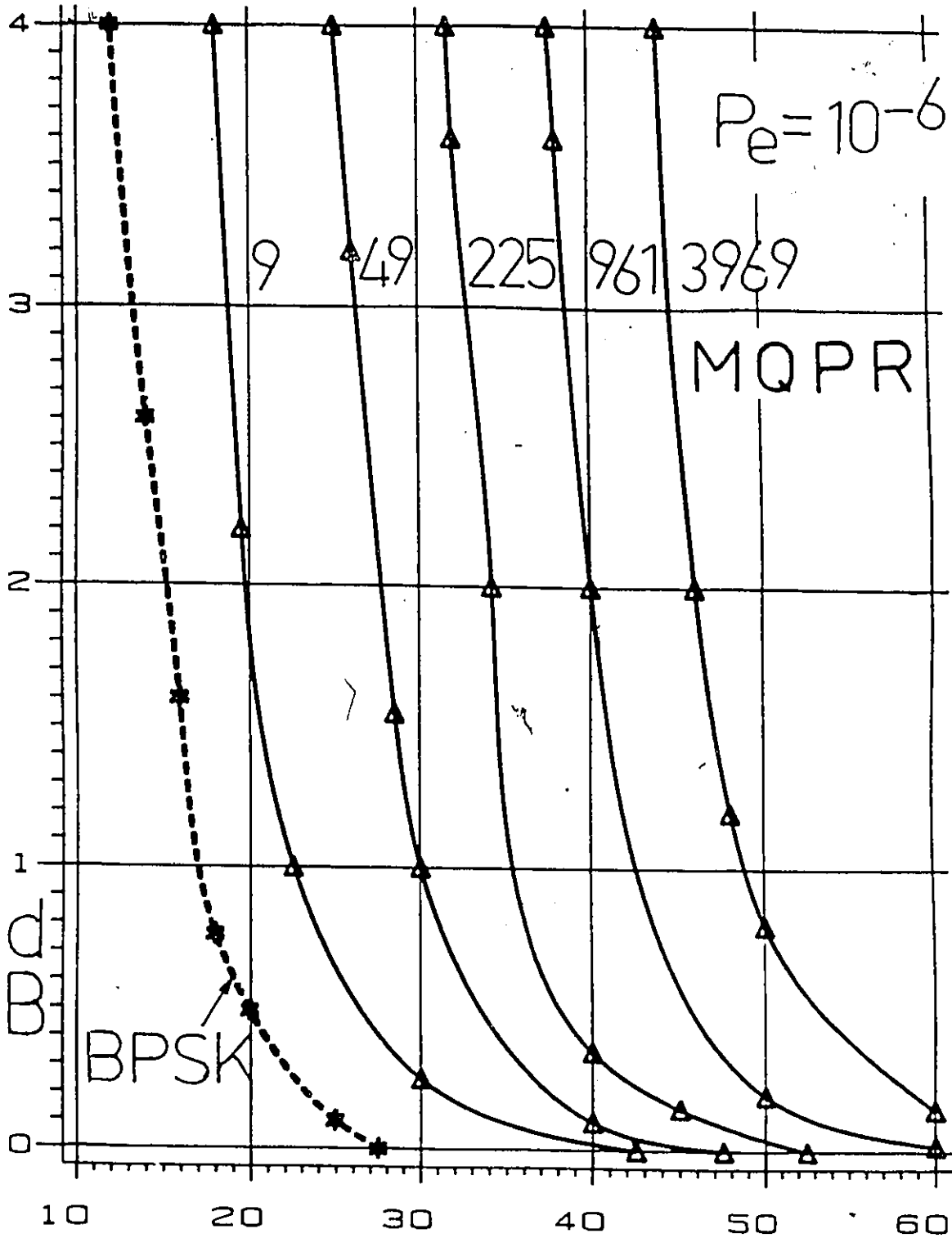


Figure 5.5. The degradation of the MQPR systems in dB, with respect to the theoretical value necessary to achieve the  $P_e = 10^{-6}$  performance, versus the carrier-to-phase noise ratio in the double-sided Nyquist bandwidth in dB.

In the BPSK system, Fig. 5.3, a  $(C/N)_p > 20$  dB causes the degradation to be less than 0.5 dB. If  $(C/N)_p > 30$  dB the degradation is negligible. This is an easily achievable goal, except in very low speed systems, where the spectral purity of signal source(s) could be critical [B28]. However, the 256QAM system — Fig. 5.2 and Fig. 5.4 — requires  $(C/N)_p > 45$  dB to limit the phase noise caused degradation to the amount below 1 dB. Additionally, the high-ary modulation schemes are more fragile in a multiple fading and interference environment. Further, the interference equalizer, carrier and symbol timing recovery and data generation and decision circuits are more complex for the case of high-ary modulation schemes. Consequently, the performance required of each component in the high-ary system should be higher. In all practical cases we find that if we take  $(C/N)_p$  to be 10 dB higher than the  $(C/N)_6$ , the degradation is less than 1 dB (Figs. 5.2—5.5). If  $(C/N)_p > (C/N)_6 + 20$  dB the degradation is negligible.

Results of measurements, Figs. 5.3—5.4, which will be briefly assessed, are in a close agreement with our engineering rule-of-thumb approximation. In a low speed data system (e.g. single-channel-per-carrier SCPC satellite link) a phase noise of frequency sources might limit an overall performance of the system. To verify this, we performed sets of measurements on SCPC satellite links consisting of two different 70 MHz 32 ksymbols/s 4-state modems (staggered QPSK and IJF), University of Ottawa earth station with 70 MHz/14 GHz up-converter and 12 GHz/70 MHz down-converter and two different "space segments". (Telesat Canada ANIK 14/12 GHz satellite transponder and a laboratory transponder with a similar performance). Each link consisted of five local oscillators of a comparable quality, which phase noises were measured by an automated spectrum analyzer. Phase noise power of each oscillator was integrated over the error transfer function  $[1-H(f)]$  of modem's carrier recovery loop (Costas loop type with a second order passive filter). The average of multiple measurements gave a noise power within the 16 kHz Nyquist bandwidth, which after multiplying by 2 and dividing by a total carrier power gave an  $(N/C)_i$  of a particular phase noise contributor. Although a phase noise of frequency source itself is nonwhite (it might be represented by  $\sum c_i f^{-\nu_i}$ ), after it passes through an "whitening filter" (i.e. error transfer function of the loop, which might be approximated by the  $cf^\nu$  near the carrier where the noise contribution is the most important) it becomes near white, but not necessary Gaussian. To get different values of  $(N/C)_i$ , the frequency stability of one of five local oscillators was intentionally degraded. Even with these unbalanced phase noise sources the measured results were in a close resemblance with previously assumed curves, Fig. 5.3—5.4.

### 5.3 CONCLUSION

In this chapter, the performance of MPSK, MQAM and MQPR modulation systems in the presence of phase noise and additive white Gaussian noise is presented in-graphic forms. If a carrier-to-phase noise ratio is at least 10 dB higher than a carrier-to-thermal noise ratio required for the  $P_e = 10^{-6}$ , the degradation due to phase noise will be less than 1 dB. If  $(C/N)_p > (C/N)_\theta + 20$  dB the degradation is negligible. The analysis is supported with results of measurements on 4-state SCPC satellite modems. Based on previous results a first order estimation of components requirements might be made. To minimize the degradation in the higher-ary modulation schemes the rigorous selection of components and use of advanced technologies is necessary.

## THESIS SUMMARY

In the **Introduction**, the purpose of this study was outlined. It was the author's goal to find power-bandwidth efficient modulation schemes, which will perform superiorly in composite ACI, linear and nonlinear, channel environments. Synthesis and analysis of both, transmitter and receiver, were performed. The results, achievements, and our own contributions which are presented in the chapters 2—5 are summarized as follows.

In the **Chapter 2**, the weighted quadrature amplitude modulation (WQAM) was introduced. By using the gradient search technique, a family of pulse shapes with a narrow mainlobe and minimal sidelobe levels within an equivalent baseband  $|fT_s| = 0$  to 5 (this corresponds to 1 to 2 adjacent channels in practice) was found. The performance of 4-state WQAM schemes was evaluated in the ACI linear and nonlinear channel environments, with the channel spacing and fading depth (signal attenuation) as parameters, by means of the computer simulation. One of the new staggered WQAM schemes, termed **S3MQAM**, outperforms other known members of the WQAM family, i.e. (S)QPSK, MSK and (S)QORC in almost all practical situations.

In the **Chapter 3** the performance analysis of 256 and 1024QAM schemes is performed in the presence of amplitude and group delay impairments. A brief feasibility study of the transmission of North American T1 (DS1) 1544 kb/s or CCITT 2048 kb/s data stream over the analog 240 kHz wide CCITT supergroup is given. Staggered QAM schemes perform better in the presence of linear group delay impairments, but nonstaggered schemes are less sensitive to linear amplitude gain impairments.

In **Chapter 4**, a composite phase and timing estimation and data detection of WQAM signal sets is analyzed. By using a maximum likelihood (ML) approach, four new joint phase and timing estimators are derived. The performance of the classical decision feedback carrier recovery loop (DFCRL) employing an integrate-and-sample device in each quadrature arm (active loop) is evaluated in the presence of both carrier uncertainty  $\phi$  and timing uncertainty  $\lambda$ . Results are presented in the following new forms: the **Uncertainty diagram**  $U(\phi, \lambda)$ , the equal (iso) probability of error **isoper curves**, and the **nonlinearity surface**  $h(\phi, \lambda)$  which becomes loop's nonlinearity S-curve when  $\lambda \rightarrow 0$ . The performance of overlapped schemes is degraded if classical carrier recovery (CR) schemes are employed. The theoretical results are experimentally verified on our Intersymbol-Jitter-Free (IJF) 64 kb/s modem. New equalized DFCRL which employs a simple 3-tap transversal equalizer in each quadrature arm is proposed for CR and the detection of overlapped schemes. Our new loop does not exhibit performance degradation associated with classical CR loops. By using the MAP probability approach and knowledge of  $\phi$ ,  $\lambda$ , and  $h(\phi, \lambda)$  accumulated over corresponding observation intervals, improved loops, i.e. **crossstalk cancellation DFCRL**, **timing intersymbol interference cancellation DFCRL**, and **FEEDLOOP**, are introduced and analyzed. The theoretical results are verified by the Monte Carlo simulation. These loops perform almost as well as a continuous wave CR loop, do not exhibit quadrant ambiguities, and might be

employed for phase and timing estimation and the detection of balanced and unbalanced WQAM schemes. The advantages of the new loops over the classical one become greater at lower probabilities of error and when higher state schemes are employed. E.g. at  $P_e = 10^{-6}$  and in the presence of a normalized loop detuning of 0.7, the crosstalk cancellation loop (and FEEDLOOP) outperform the classical one by 2.4 dB, assuming QPSK modulation scheme is employed.

In Chapter 5, the impact of phase noise on the performance of MQAM, M-ary phase shift keying and M-ary quadrature partial response systems in a Gaussian noise environment is computed. For all cases the degradation due to phase noise is found to be less than 1 dB if a carrier-to-phase noise ratio in a double-sided Nyquist bandwidth  $(C/N)_p$  is at least 10 dB higher than the carrier-to-thermal noise ratio  $(C/N)_t$  required for the probability of error performance  $P_e = 10^{-6}$ . Performance graphs are presented which enable a fast first order approximation of the phase noise requirements of a system to be estimated. Our engineering rule-of-thumb approximations are in a close agreement with the results of measurements performed on the single-channel-per-carrier (SCPC) satellite links consisting of two different 70 MHz 32 ksymbols/s 4-state modems (SQPSK and IJF), University of Ottawa earth station with 70 MHz/14 GHz up-converter and 12 GHz/70 MHz down-converter and two different "space segments" (Telesat Canada ANIK 14/12 GHz satellite transponder and a laboratory transponder with a similar performance).

Thesis concludes with an extensive list of references, and a copy of the computer programs printout.

We highlighted some of the so far unresolved problems associated with data transmission over power and bandwidth limited nonlinear channels, we proposed new WQAM schemes at the transmitter and new CR loops at the receiver, and we have shown that our novel schemes outperform previously known devices.

**RESEARCH PROPOSAL**

This thesis outlined some of the so far unresolved problems related to the generation and reception of power-bandwidth efficient coherent digital modulation schemes. Several new modulation schemes were proposed and analyzed, including several new receivers for the corresponding WQAM schemes. In this chapter, a brief research proposal for future studies is given.

- The optimization of the signal shapes (i.e. the minimization of the spectral sidelobes) might be extended to include a cascade of nonlinearities, filters, and channel noise sources — typical in the satellite link. This might allow one to match the modulation scheme to the particular power amplifier nonlinearity, and as a result, improve the power and spectral efficiency of the system. Modulation might be combined with coding type — block, convolutional, or Ungerböck trellis.
- The synthesis and analysis of the WQAM schemes might be extended to the multipath selective fading channels — typical for terrestrial radio systems, and to the Doppler effected channels — typical for mobile radio communications.
- The detailed study of different receivers might include stochastic Fokker-Planck-Kolmogorov partial differential equation analysis of the receiver behaviour in the presence of channel noise and intersymbol interferences, for acquisition performance during transients such as selective fading, discrete occasional interferences, etc.
- Possible application of the new decision feedback loops to coherent fiber optics and radionavigation, and further optimization of these devices might be investigated.

REFERENCES

A list of references consists of books (presented in the Section 8.1 and referred as Bxx), special issues (presented in the Section 8.2 and referred as Sxx) and other general publications (presented in the Section 8.3 and referred as Pxxx).

Further references on synchronous communications systems, particularly phase locked loops, might be found in

- [a] Kucar, A.: Synchronous Communications Systems: Introduction and Bibliography. Elektrotehniski vestnik, Vol.49, pp:165-187, No.4, 1982. In Sloven and Croato-Serb with English abstract.

**8.1 Books**

- [B1] Bennett, W.R., J.R.Davey: Data Transmission. McGraw-Hill Book Company, New York,1965.
- [B2] Lucky, R.W., J. Salz, E.J. Weldon Jr.: Principles of Data Communication. McGraw-Hill Book Company, New York,1968.
- [B3] Lindsey, W.C., M.K. Simon: Telecommunication Systems Engineering. Prentice-Hall, Inc., Englewood Cliffs, N.J.,1973.
- [B4] Spilker, J.J., Jr.: Digital Communications by Satellite. Prentice-Hall, Inc., Englewood Cliffs, N.J.,1977.
- [B5] Shanmugam, K.S.: Digital and Analog Communication Systems. John Wiley & Sons, Inc., New York,1979.
- [B6] Bhargava, V.K., D. Haccoun, R. Matyas, P.P. Nuspl: Digital Communications by Satellite. Modulation, Multiple Access and Coding. John Wiley & Sons, Inc., New York,1981.
- [B7] Feher, K.: Digital Communications, Microwave Applications. Prentice-Hall, Inc., Englewood Cliffs, N.J.,1981.
- [B8] Feher, K.: Digital Communications, Satellite/Earth Station Engineering. Prentice-Hall, Inc., Englewood Cliffs, N.J.,1983.
- [B9] Gagliardi, R.M.: Satellite Communications. Lifetime Learning Publications, Belmont, California, 1984.
- [B10] Wu, W.W.: Elements of Digital Satellite Communications. Volume I. Computer Science Press, Rockville, Maryland, 1984.
- [B11] Wu, W.W.: Elements of Digital Satellite Communications. Volume II. Computer Science Press, Rockville, Maryland, 1985.
- [B12] Yuen, J.H. (Editor): Deep Space Telecommunications Systems Engineering. New York: Plenum Press, 1983.
- [B13] Feher, K.: Digital Modulation Techniques in an Interference Environment. Don White Consultants, Inc., Germantown, Maryland, 1977.
- [B14] Lukatela, G., D. Drajić, G. Petrović: Digital Telecommunications. Gradjevinska knjiga, Beograd 1978. In Serbo-Croat: Digitalne Telekomunikacije.
- [B15] Proakis, J.G.: Digital Communications. McGraw-Hill Book Company, New York,1983.
- [B16] Lindsey, W.C.: Synchronization Systems in Communication and Control. Prentice-Hall, Inc., Englewood Cliffs, N.J.,1972.

- [B17] Balakrishnan, A.V. (Series Editor), A.J. Viterbi (Volume Editor): *Advances in Communication Systems. Theory and applications. Volume 4.* Academic Press, Inc., New York, 1975.
- [B18] Viterbi, A.J., J.K. Omura: *Principles of Digital Communication and Coding.* McGraw-Hill Book Company, New York, 1979.
- [B19] Clark, G.C., Jr., J.B. Cain: *Error — Correction Coding for Digital Communications.* Plenum Press, New York, 1981.
- [B20] Robins, W.P.: *Phase Noise in Signal Sources (Theory and Applications).* London: Peter Peregrinus, 1982.
- [B21] Helstrom, C.W.: *Statistical Theory of Signal Detection. Second Edition.* Pergamon Press, Hungary 1968.
- [B22] Van Trees, H.L.: *Detection, Estimation, and Modulation Theory. Part I.* John Wiley & Sons, Inc., New York, 1968.
- [B23] Van Trees, H.L.: *Detection, Estimation, and Modulation Theory. Part III.* John Wiley & Sons, Inc., New York, 1971.
- [B24] Papoulis, A.: *The Fourier Integral and its Applications.* McGraw-Hill Book Company, New York, 1962.
- [B25] Papoulis, A.: *Probability, Random Variables, and Stochastic Processes.* McGraw-Hill Book Company, New York, Kogakusha, 1965.
- [B26] Abramowitz, M., I.A. Stegun: *Handbook of Mathematical Functions.* Dover Publications, Inc., New York 1972.
- [B27] Middleton, D.: *An Introduction to Statistical Communication Theory.* McGraw-Hill Book Company, New York, 1960.
- [B28] Jakes, W.C., Jr. (Editor): *Microwave Mobile Communications.* John Wiley & Sons, Inc., New York, 1974.
- [B29] Lee, W.C.Y.: *Mobile Communications Engineering.* McGraw-Hill Book Company, New York, 1982. 1967.

## 8.2 Special Issues

- [S1] Lesh, J.R. (Guest Editor): Special Section on Communications over Nonlinear Channels. IEEE Trans. on Communications, Vol.COM-29, pp:537-620, May 1981.
- [S2] Kullstam, P. (Guest Editor): Special Issue on Satellite Communications and Direct Broadcast Satellite (DBS) Systems. IEEE Communications Magazine, Vol.22, No.3, March 1984.
- [S3] Feher, K., L.G.Greenstein, D.Lombard, L.Pollack (Guest Editors) : Special Issue on Digital Satellite Communications. IEEE Journal on Selected Areas in Communications, Vol.SAC-1, No.1, Jan. 1983.
- [S4] Feher, K., R.P. Tetarenko, P.R. Hartmann, V.K. Prabhu (Guest Editors) : Special Issue on Digital Radio. IEEE Trans. on Communications, Vol.COM-27, No.12, Dec. 1979.
- [S5] Anderson, J.B., J.R. Lesh (Guest Editors): Special Section on Combined Modulation and Encoding. IEEE Trans. on Communications, Vol.COM-29, No.3, March 1981.
- [S6] Falconer, D.D., R.D. Gitlin (Guest Editors): Special Issue on Voiceband Telephone Data Transmission. IEEE Journal on Selected Areas in Communications, Vol.SAC-2, No.5, September 1984.
- [S7] Gardner, F.M., W.C. Lindsey (Guest Editors) : Special Issue on Synchronization. IEEE Trans. on Communications, Part I, Vol.COM-28, Aug. 1980.
- [S8] Lindsey, W.C., C.M.Chie (Guest Editors) : Special Issue on Phase-Locked Loops. IEEE Trans. on Communications, Vol.COM-30, Oct. 1982.
- [S9] Davis, J.H. (Guest Editor) , J.J. Mikulski and P.T. Porter (Associated Guest Editors) , B.L. King (Guest Editorial Assistant) : Special Issue on Mobile Radio Communications. IEEE Journal on Selected Areas in Communications, Vol.SAC-2, No.4, July 1984.
- [S10] Okumura, Y., M.Shinji (Guest Editors): Mobile Radio Communications. IEEE Communications Magazine, Vol.24, No.2, February 1986.

## 8.3 Other Publications

- [P1] Nyquist, H.: Certain Topics in Telegraph Transmission Theory. Trans. AIEE, Vol.47, pp: 617-644, February 1928.
- [P2] Cahn, C.R.: Performance of Digital Phase-Modulation Communication Systems. IRE Trans. Communication Systems, Vol.CS-7, pp: 3-6, May 1959.
- [P3] Arthurs, E., H. Dym : On the Optimum Detection of Digital Signals in the Presence of White Gaussian Noise-A Geometric Interpretation and a Study of Three Basic Data Transmission Systems. IRE Trans. Communication Systems, Vol.CS-10, pp: 336-372, Dec. 1962.
- [P4] Lender, A.: Correlative Digital Communication Techniques. IEEE Tr. on Communication Technology, Vol.COM-12, pp: 128-135, Dec. 1964.
- [P5] DeBuda, R.: Coherent Demodulation of Frequency-Shift Keying with Low Deviation Ratio. IEEE Trans. on Communications, Vol.COM-20, pp: 429-435, June 1972.
- [P6] Thomas, C.M., M.Y. Weidner, S.H. Durrani: Digital Amplitude-Phase Keying with M-ary Alphabets. IEEE Trans. on Communications, Vol.COM-22, pp: 168-180, Feb. 1974.
- [P7] Mathwisch, H.R., J.F. Balcewicz, M. Hecht: The Effect of Tandem Band and Amplitude Limiting on the  $E_b/N_o$  Performance of Minimum (Frequency) Shift Keying (MSK). IEEE Trans. on Communications, Vol.COM-22, pp: 1525-1540, Oct. 1974.
- [P8] Gitlin, R.D., E.Y. Ho: The Performance of Staggered Quadrature Amplitude Modulation in the Presence of Phase Jitter. IEEE Trans. on Communications, Vol.COM-23, pp: 348-352, March 1975.
- [P9] Hill, F.S. Jr.: Optimum Pulse Shapes for Pulse-Amplitude Modulation Data Transmission Using Vestigial Sideband Modulation. IEEE Trans. on Communications, Vol. COM-23, pp: 352-361, March 1975.
- [P10] Thomas, C.M., C.L. May, G.R. Welti: Hybrid Amplitude-and-Phase Modulation for Analog Data Transmission. IEEE Trans. on Communications, Vol.COM-23, pp: 634-645, June 1975.
- [P11] Amoroso, F.: Pulse and Spectrum Manipulation in the Minimum (Frequency) Shift Keying (MSK) Format. IEEE Trans. on Communications, Vol.COM-24, pp: 381-384, March 1976.
- [P12] Gronemeyer, S.A., A.L. McBride: MSK and Offset QPSK Modulation. IEEE Trans. on Communications, Vol.COM-24, pp: 809-820, Aug. 1976.

- [P13] Simon, M.K.: A Generalization of Minimum-Shift-Keying (MSK) Type Signaling Based Upon Input Data Symbol Pulse Shaping. IEEE Trans. on Communications, Vol.COM-24, pp: 845-856, Aug. 1976.
- [P14] Amoroso, F., J.A. Kivett: Simplified MSK Signaling Technique. IEEE Trans. on Communications, Vol. COM-25, pp: 433-441, April 1977.
- [P15] Prabhu, V.K.: PSK Type Modulation with Overlapping Baseband Pulses. IEEE Trans. on Communications, Vol. COM-25, pp: 980-990, Sept.1977.
- [P16] Rabzel, M., S. Pasupathy: Spectral Shaping in Minimum Shift Keying (MSK)-Type Signals. IEEE Trans. on Communications, Vol. COM-26, pp: 189-195, Jan. 1978.
- [P17] DeJager, F., C.B. Dekker: Tamed Frequency Modulation, A novel method to achieve spectrum economy in digital transmission. IEEE Trans. on Communications, Vol.COM-26, pp:534-542, May 1978.
- [P18] Feher, K., M.Gendron: Une nouvelle famille de filtre non-lineaire. R. Can. Genie Elec. Vol.4, pp: 26-32, No.1, 1979.
- [P19] Pasupathy, S.: Minimum Shift Keying: A Spectrally Efficient Modulation. IEEE Communications Magazine, Vol.17, pp: 14-22, July 1979.
- [P20] Amoroso, F.: The Use of Quasi-Bandlimited Pulses in MSK Transmission. IEEE Trans. on Communications, Vol. COM-27, pp: 1616-1624, Oct. 1979.
- [P21] Huang, J.C.Y., K.Feher: Techniques to Generate ISI and Jitter — Free Bandlimited Nyquist Signals and a Method to Analyze Jitter Effects. IEEE Trans. on Communications, Vol. COM-27, pp: 1700-1711, Nov. 1979.
- [P22] Ryan, C.R., A.R. Hambley, E. Vogt: 760 Mbit/s Serial MSK Microwave Modem. IEEE Trans. on Communications, Vol. COM-28, pp: 771-777, May 1980.
- [P23] Yazdani, H., K. Feher, W. Steenaart: Constant Envelope Bandlimited BPSK Signal. IEEE Trans. on Communications, Vol. COM-28, pp: 889-897, June 1980.
- [P24] Amoroso, F.: The Bandwidth of Digital Data Signals. IEEE Communications Magazine, Vol.18, No.6, pp: 13-24, Nov. 1980.
- [P25] Rhodes, S.A.: FSOQ, a New Modulation Technique that Yields a Constant Envelope. NTC'80, pp: 5111-5117, Houston, Nov-Dec. 1980.
- [P26] Morais, D.H., K. Feher: The Effects of Filtering and Limiting on the Performance of QPSK, Offset QPSK, and MSK Systems. IEEE Trans. on Communications, Vol. COM-28, pp: 1999-2009, Dec. 1980.
- [P27] Deshpande, G.S., P.H. Wittke: Optimum Pulse Shaping in Digital Angle Modulation. IEEE Trans. on Communications, Vol. COM-29, pp: 162-168, Feb. 1981.

- [P28] Boutin, N., S. Morissette: Useful Signaling Waveforms and Related Transmit Filter Functions in Bandwidth Limited Channels. *IEEE Trans. on Communications*, Vol. COM-29, pp: 177-180, Feb. 1981.
- [P29] Anderson, J.B., C.-E. Sundberg, T. Aulin, N. Rydbeck: Power Bandwidth Performance of Smoothed Phase Modulation Codes. *IEEE Trans. on Communications*, Vol. COM-29, pp: 187-195, March 1981.
- [P30] Aulin, T., C.-E. Sundberg: Continuous Phase Modulation — Part I: Full Response Signaling. *IEEE Trans. on Communications*, Vol. COM-29, pp: 196-209. — Part II: Partial Response Signaling. pp: 210-225, March 1981.
- [P31] Muilwijk, D.: Correlative Phase Shift Keying—A Class of Constant Envelope Modulation Techniques. *IEEE Trans. on Communications*, Vol. COM-29, pp: 226-236, March 1981.
- [P32] Austin, M., M.U. Chang: Quadrature Overlapped Raised-Cosine Modulation. *IEEE Trans. on Communications*, Vol. COM-29, pp: 237-249, March 1981.
- [P33] Wilson, S.G., R.C. Gauss: Power Spectra of Multi-h Phase Codes. *IEEE Trans. on Communications*, Vol. COM-29, pp: 250-256, March 1981.
- [P34] Mazur, B.A., D.P. Taylor: Demodulation and Carrier Synchronization of Multi-h Phase Codes. *IEEE Trans. on Communications*, Vol. COM-29, pp: 257-266, March 1981.
- [P35] Taylor, D.P., H.C. Chan: A Simulation Study of Two Bandwidth-Efficient Modulation Techniques. *IEEE Trans. on Communications*, Vol. COM-29, pp: 267-275, March 1981.
- [P36] Johnston, D.A., S.K. Jones: Spectrally Efficient Communication via Fading Channels Using Coded Multilevel DPSK. *IEEE Trans. on Communications*, Vol. COM-29, pp: 276-284, March 1981.
- [P37] Divsalar, D., M.K. Simon: The Power Spectral Density of Digital Modulations Transmitted Over Nonlinear Channels. *IEEE Trans. on Communications*, Vol. COM-30, pp: 142-151, Jan. 1982.
- [P38] Le-Ngoc, T., K. Feher, H.P. Van: New Modulation Techniques for Low-Cost Power and Bandwidth Efficient Satellite Earth Stations. *IEEE Trans. on Communications*, Vol. COM-30, pp: 275-283, Jan. 1982.
- [P39] Ziemer, R.E., C.R. Ryan, J.H. Stilwell: Conversion and Matched Filter Approximations for Serial Minimum-Shift Keyed Modulation. *IEEE Trans. on Communications*, Vol. COM-30, pp: 495-509, March 1982.
- [P40] Morais, D.H., K. Feher: NLA-QAM: A Method for Generating High-Power QAM Signals Through Nonlinear Amplification. *IEEE Trans. on Communications*, Vol. COM-30, pp: 517-522, March 1982.
- [P41] Aulin, T., C.-E. Sundberg: Partially Coherent Detection of Digital Full Response Continuous Phase Modulated Signals. *IEEE Trans. on Communications*, Vol. COM-30, pp: 1096-1117, May 1982.

- [P42] Aulin, T., C.-E. Sundberg: Minimum Euclidian Distance and Power Spectrum for a Class of Smoothed Phase Modulation Codes with Constant Envelope. IEEE Trans. on Communications, Vol. COM-30, pp: 1721-1729, July 1982.
- [P43] Aulin, T., C.-E. Sundberg: Exact Asymptotic Behavior of Digital FM Spectra. IEEE Trans. on Communications, Vol. COM-30, pp: 2438-2449, Nov. 1982.
- [P44] Oshita, S., K. Feher:  $P_e$  Performance of Coherent M-ary PSK Systems in an Impulsive and Gaussian Noise Environment. IEEE Trans. on Communications, Vol. COM-30, pp: 2458-2464, Nov. 1982.
- [P45] Oshita, S., K. Feher: Combined Effect of the Carrier Recovery and Symbol Timing Recovery Error on the  $P_e$  Performance of QPR and Offset QPR Systems. IEEE Trans. on Communications, Vol. COM-30, pp: 2534-2540, Dec. 1982.
- [P46] Oshita, S., K. Feher: Performance of Coherent PSK and DPSK Systems in an Impulsive and Gaussian Noise Environment. IEEE Trans. on Communications, Vol. COM-30, pp: 2540-2546, Dec. 1982.
- [P47] Dickerson, E.T., W.B. Warren: Generation of Constant Envelope Signals. IEEE Trans. on Communications, Vol. COM-30, pp: 2554-2556, Dec. 1982.
- [P48] Le-Ngoc, T., K. Feher: Performance of IJF-OQPSK Modulation Schemes in a Complex Interference Environment. IEEE Trans. on Communications, Vol. COM-31, pp: 137-144, Jan. 1983.
- [P49] Amoroso, F.: Experimental Results on Constant Envelope Signaling with Reduced Spectral Sidelobes. IEEE Trans. on Communications, Vol. COM-31, pp: 157-160, Jan. 1983.
- [P50] Korn, I., B. Seth: Adjacent-Channel and Quadrature-Channel Interference in Minimum Shift Keying. IEEE Journal on Selected Areas in Communications, Vol. SAC-1, No.1, pp: 21-28, Jan. 1983.
- [P51] Vandamme, P., T. Le-Ngoc, K. Feher: Performance of IJF-OQPSK and Partial Response (PR) IJF-OQPSK Modems in a Nonlinearly Amplified and Adjacent-Channel Interference Satellite Environment. IEEE Journal on Selected Areas in Communications, Vol. SAC-1, No.1, pp: 29-38, Jan. 1983.
- [P52] Austin, M.C., M.U. Chang, D.F. Horwood, R.A. Maslov: QPSK, Staggered QPSK, and MSK-A Comparative Evaluation. IEEE Trans. on Communications, Vol. COM-31, pp: 171-182, Feb. 1983.
- [P53] Le-Ngoc, T., K. Feher: Performance of an IJF-OQPSK Modem in Cascaded Nonlinear and Regenerative Satellite Systems. IEEE Trans. on Communications, Vol. COM-31, pp: 296-301, Feb. 1983.
- [P54] Van, H.P., K. Feher: A Class of Two-Symbol-Interval Modems for Nonlinear Radio Systems. IEEE Trans. on Communications, Vol. COM-31, pp: 433-441, March 1983.

- [P55] Kato, S., K. Feher: XPSK: A New Cross-Correlated Phase-Shift Keying Modulation Technique. *IEEE Trans. on Communications*, Vol. COM-31, pp: 701-707, May 1983.
- [P56] Seo, J.S., K. Feher: Modified Minimum Shift Keyed (MMSK) Modem for Mobile Satellite Systems. 1st Canadian Satellite Comm. Conference SCC'83, pp: 551-556. North Holland. Ottawa, June 1983.
- [P57] Abe, R., I. Sasase, S. Mori: Bandwidth Efficient Quadrature Overlapped Squared Raised-Cosine Modulation. 1st Canadian Satellite Comm. Conference SCC'83, pp: 2471-2474. Ottawa, June 1983. Distributed by Nort Holland.
- [P58] Sklar, B.: A Structured Overview of Digital Communications — a Tutorial Review — Part I. *IEEE Communications Magazine*, Vol.21, No.5, pp: 4-17, Aug. 1983. Part II. No.7, pp: 6-21, Oct. 1983.
- [P59] Sundberg, C.-E.: On Continuous Phase Modulation in Cellular Digital Mobile Radio Systems. *B.S.T.J.*, Vol.62, pp: 2067-2089, Sept. 1983.
- [P60] Ziemer, R.E., C.R. Ryan: Minimum-Shift Keyed Modem Implementations for High Data Rates. *IEEE Communications Magazine*, Vol.21, No.7, pp: 28-37, Oct. 1983.
- [P61] Vaisey, D.J., P.J. McLane: Passive Arm Filters in I and Q Receivers for MSK-Type Continuous Phase Modulations. *IEEE Trans. on Communications*, Vol. COM-31, pp: 1235-1240, Nov. 1983.
- [P62] Boutin, N., S. Morissette, L. Dussault: Optimum Discrete Pulse Shaping in MSK-Type Signals. *IEEE Trans. on Communications*, Vol. COM-31, pp: 1251-1253, Nov. 1983.
- [P63] Harris, F.J.: On the Use of Windows for Harmonic Analysis with the Discrete Fourier Transform. *Proceedings IEEE*, Vol.66, No.1, pp: 51-83, Jan. 1978.
- [P64] Kabal, P., S. Pasupathy: Partial-Response Signaling. *IEEE Trans. on Communications*, Vol. COM-23, pp: 921-934, Sept. 1975.
- [P65] Pasupathy, S.: Correlative Coding. A Bandwidth Efficient Signalling Scheme. *IEEE Communications Magazine*, Vol. 15, pp: 4-11, July 1977.
- [P66] Halpern, P.H.: Optimum Finite Duration Nyquist Signals. *IEEE Trans. on Communications*, Vol. COM-27, pp: 884-888, June 1979.
- [P67] Korn, I.: Error Probability and Bandwidth of Digital Modulation. *IEEE Trans. on Communications*, Vol. COM-28, pp: 287-290, Feb. 1980.
- [P68] Palmer, L.C., S.A. Rhodes, S.H. Lebowitz: Synchronization for QPSK Transmission via Communications Satellites. *IEEE Trans. on Communications*, Vol. COM-28, pp: 1302-1314, Aug. 1980.
- [P69] Wilson, S.G.: Joint MAP Data/Phase Sequence Estimation for Trellis Phase Codes. *ICC'80*, Seattle, pp: 2611-2615, June 1980.

- [P70] Cruz, J.R., R.S. Simpson: Cochannel and Intersymbol Interference in Quadrature-Carrier Modulation Systems. IEEE Trans. on Communications, Vol. COM-29, pp: 285-297, March 1981. Comments on... COM-30, p. 2482, Nov. 1982.
- [P71] Ekanayake, N., D.P. Taylor: A Decision Feedback Receiver Structure for Bandlimited Nonlinear Channels. IEEE Trans. on Communications, Vol. COM-29, pp: 539-548, May 1981.
- [P72] Devieux, C. Jr., M.E. Jones: A Practical Optimization Approach for QPSK/TDMA Satellite Channel Filtering. IEEE Trans. on Communications, Vol. COM-29, pp: 556-566, May 1981.
- [P73] Fang, R.J.: Quaternary Transmission Over Satellite Channels with Cascaded Nonlinear Elements and Adjacent Channel Interference. IEEE Trans. on Communications, Vol. COM-29, pp: 567-582, May 1981.
- [P74] Kennedy, D.J., O. Shimbo: Cochannel Interference in Nonlinear QPSK Satellite Channel. IEEE Trans. on Communications, Vol. COM-29, pp: 582-592, May 1981.
- [P75] Huang, T.-C., J.K. Omura, W.C. Lindsey: Analysis of Coherent Satellite Communication Systems in the Presence of Interference and Noise. IEEE Trans. on Communications, Vol. COM-29, pp: 593-604, May 1981.
- [P76] Korn, I., Y. Tsang: Effect of Intersymbol and Quadrature Channel Interference on Error Probability of 16-ary Offset Quadrature Amplitude Modulation with Sinusoidal and Rectangular Shaping. IEEE Trans. on Communications, Vol. COM-31, pp: 264-269, Feb. 1983.
- [P77] Lim, T.L., J.K. Omura: Error Rate Estimates in Digital Communication Over a Nonlinear Channel with Memory. IEEE Trans. on Communications, Vol. COM-31, pp: 407-412, March 1983.
- [P78] Laurent, P.A.: Exact and Approximate Construction of Digital Phase Modulation by Superposition of Amplitude Modulated Pulses (AMP). IEEE Trans. on Communications, Vol. COM-34, No.2, pp: 150-160, Feb. 1986. IEEE Log Number 8406879.
- [P79] Natali, F.D.: Noise Performance of a Cross-Product AFC with Decision Feedback for DPSK Signals. IEEE Trans. on Communications, Vol. COM-34, No.3, pp: 303-307, March 1986. IEEE Log Number 8407419.
- [P80] Helstrom, C.W.: Calculating Error Probabilities for Intersymbol and Cochannel Interference. IEEE Trans. on Communications, Vol. COM-34, No.5, pp: 430-435, May 1986. IEEE Log Number 8607998.
- [P81] Padovani, R., J.K. Wolf: Coded Phase/Frequency Modulation. IEEE Trans. on Communications, Vol. COM-34, No.5, pp: 446-453, May 1986. IEEE Log Number 8607995.

- [P82] Lee, P.J.: Computation of the Bit Error Rate of Coherent M-ary PSK with Gray Code Bit Mapping. *IEEE Trans. on Communications*, Vol. COM-34, No.5, pp: 488-491, May 1986. IEEE Log Number 8707997.
- [P83] Kam, P.Y.: Maximum Likelihood Carrier Phase Recovery for Linear Suppressed-Carrier Digital Data Modulation. *IEEE Trans. on Communications*, Vol. COM-34, No.6, pp: 522-527, June 1986. IEEE Log Number 8608511.
- [P84] Hirosaki B., S.Hasegawa, A.Sabato: Advanced Groupband Data Modem Using Orthogonally Multiplexed QAM Technique. *IEEE Trans. on Communications*, Vol. COM-34, No.6, pp: 587-592, June 1986. IEEE Log Number 8608514.
- [P85] Forney, G.D., Jr., R.G.Gallager, G.R.Lang, F.M.Longstaff, S.U.Quereshi: Efficient Modulation for Band-Limited Channels. *IEEE Journal on Selected Areas in Communications*, Vol. SAC-2, No.5, pp: 632-647, September 1984.
- [P86] Thapar, H.K.: Real-Time Application of Trellis Coding to High-Speed Voiceband Data Transmission. *IEEE Journal on Selected Areas in Communications*, Vol. SAC-2, No.5, pp: 648-658, September 1984.
- [P87] Hirosaki, B.: A Maximum Likelihood Receiver for an Orthogonally Multiplexed QAM System. *IEEE Journal on Selected Areas in Communications*, Vol. SAC-2, No.5, pp: 757-764, September 1984.
- [P88] Pawula, R.F.: Asymptotics and Error Rate Bounds for M-ary DPSK. *IEEE Trans. on Communications*, Vol. COM-32, No.1, pp: 93-94, January 1984.
- [P89] Das, J.: A Technique for Improving the Efficiency of M-ary Signaling. *IEEE Trans. on Communications*, Vol. COM-32, No.2, pp: 199-201, February 1984.
- [P90] Pawula, R.F.: Offset DPSK and a Comparison of Conventional and Symmetric DPSK with Noise Correlation and Power Imbalance. *IEEE Trans. on Communications*, Vol. COM-32, No.3, pp: 233-240, March 1984.
- [P91] Taylor, D.P., M.Shafi: Decision Feedback Equalization for Multipath Induced Interference in Digital Microwave LOS Links. *IEEE Trans. on Communications*, Vol. COM-32, No.3, pp: 267-279, March 1984.
- [P92] Hambley, A.R., O.Tanaka: Generalized Serial MSK Modulation. *IEEE Trans. on Communications*, Vol. COM-32, No.3, pp: 305-308, March 1984.
- [P93] Ishizuka, M., Y.Yasuda: Improved Coherent Detection of GMSK. *IEEE Trans. on Communications*, Vol. COM-32, No.3, pp: 308-311, March 1984.
- [P94] McMillen, G.R., M. Shafi, D.P. Taylor: Simultaneous Adaptive Estimation of Carrier Phase, Symbol Timing, and Data for a 49-QPRS DFE Radio Receiver. *IEEE Trans. on Communications*, Vol. COM-32, No.4, pp: 429-443, April 1984.

- [P95] Boutin, N.: Constant Envelope Signal Generator with Improved Phase Linearity. IEEE Trans. on Communications, Vol. COM-32, No.4, pp: 488-490, April 1984.
- [P96] Ekanayake, N.: DPSK Signaling Over Hard Limiting Channel in the Presence of Intersymbol Interference. IEEE Trans. on Communications, Vol. COM-32, No.5, pp: 503-510, May 1984.
- [P97] Bello, P.A., K.Pahlavan: Adaptive Equalization for SQPSK and SQPR Over Frequency Selective Microwave LOS Channels. IEEE Trans. on Communications, Vol. COM-32, No.5, pp: 609-615, May 1984.
- [P98] Biglieri, E.: High-Level Modulation and Coding for Nonlinear Satellite Channels. IEEE Trans. on Communications, Vol. COM-32, No.5, pp: 616-626, May 1984.
- [P99] Sasase, I., Y.Harada, S.Mori: Bandwidth Efficient Quadrature Overlaped Modulation. IEEE Trans. on Communications, Vol. COM-32, pp: 638-640, May 1984.
- [P100] Pawula, R.F.: On M-ary DPSK Transmission Over Terrestrial and Satellite Channels. IEEE Trans. on Communications, Vol. COM-32, No.7, pp: 752-761, July 1984.
- [P101] Van, H.P., K.Feher: TSI-OQPSK fo. Multiple Carrier Satellite Systems. IEEE Trans. on Communications, Vol. COM-32, No.7, pp: 818-825, July 1984.
- [P102] Moeneclaey, M.: A Fundamental Lower Bound on the Performance of Practical Joint Carrier and Bit Synchronizers. IEEE Trans. on Communications, Vol. COM-32, No.9, pp: 1007-1012, September 1984.
- [P103] Moeneclaey, M.: Synchronizability of a General Class of PCM Formats, Including NRZ, Manchester, and Miller Coding. IEEE Trans. on Communications, Vol. COM-32, No.9, pp: 1020-1024, September 1984.
- [P104] Meidan, R.: Comment on 'Optimal Design of PLL with Two Separate Phase Detectors'. IEEE Trans. on Communications, Vol. COM-32, No.9, pp: 1056-1058, September 1984. Heiman, A., Y.Bar-Ness: Autors' Reply. IEEE Trans. on Communications, Vol. COM-32, No.9, pp: 1058-1060, September 1984.
- [P105] Jeruchim, M.C.: On the Application of Importance Sampling to the Simulation of Digital Satellite and Multihop Links. pp: 1088-1092, October 1984.
- [P106] Moeneclaey, M.: Two Maximum Likelihood Symbol Synchronizers with Superior Tracking Performance. IEEE Trans. on Communications, Vol. COM-32, No.11, pp: 1178-1185, November 1984.
- [P107] Moeneclaey, M.: The Influence of Four Types of Symbol Synchronizers on the Error Probability of a PAM Receiver. IEEE Trans. on Communications, Vol. COM-32, No.11, pp: 1186-1190, November 1984.
- [P108] Sandoz, J.P., W.Steenart: Performance Improvement of a Binary Quantized All-Digital Phase-Locked Loop with a New Aided-Acquisition Technique. IEEE Trans. on Communications, Vol. COM-32, No.12, pp: 1269-1276, December 1984.

- [P109] Wilson, S.G., H.A.Sleeper, II, P.J.Schottler, M.T.Lyons: Rate 3/4 Convolutional Coding of 16-PSK: Code Design and Performance Study. IEEE Trans. on Communications, Vol. COM-32, No.12, pp: 1308-1315, December 1984.
- [P110] Aulin, T., C.-E.Sundberg: On the Minimum Euclidean Distances for a Class of Signal Space Codes. IEEE Tr. on Information Theory, Vol.IT-28, No.1, pp: 43-55, January 1982.
- [P111] Ungerboeck, G.: Channel Coding with Multilevel/Phase Signals. IEEE Tr. on Information Theory, Vol.IT-28, No.1, pp: 55-67, January 1982.
- [P112] Prabhu, V.K.: Modified Chernoff Bounds for PAM Systems with Noise and Interference. IEEE Tr. on Information Theory, Vol.IT-28, No.1, pp: 95-100, January 1982.
- [P113] Stallings, W.: Digital Signaling Techniques. IEEE Communications Magazine, Vol.22, No.12, pp: 21-25, December 1984.
- [P114] Sundberg, C.-E.: Continuous Phase Modulation. IEEE Communications Magazine, Vol.24, No.4, pp: 25-38, April 1986.
- [P115] Hagmann, W.C.: Carrier synchronizer for overlapped raised cosine pulse amplitude modulation. COMSAT Tech. Review, Vol.14, No.1, pp: 25-52, Spring 1984.
- [P116] Kucar, A.D., K.Feher: Performance of Weighted QAM in the Presence of Phase and Timing Error: Uncertainty Diagrams and Isoper Curves. ICDS-7, Munchen, W. Germany, May 11-17, 1986.
- [P117] Kucar, A.D., K.Feher: Performance of MQAM in the presence of CR and TR uncertainty: Part I — Wideband systems. IEEE ELECTRONICOM'85, pp: 542-545, Toronto, Oct.7-9, 1985.
- [P118] Harris, R.A., P.Kristiansen: The Generation and Use of Bit Error Rate Surface Plots. IEEE Journal on Selected Areas in Comm., Vol. SAC-2, pp: 185-190, Jan.1984.
- [P119] Rhodes, S.A.: Effect of Noisy Phase Reference on Coherent Detection of Offset-QPSK Signals. IEEE Trans. on Communications, Vol. COM-22, pp: 1046-1055, Aug.1974.
- [P120] Davarian, F.: Imperfect phase and timing transfer effects on MSK and OQPSK signals. National TeleSystems Conf., NTC'82, Galveston Texas, pp: E231-5, Nov. 7-10, 1982.
- [P121] Lindsey, W.C., M.K.Simon: Carrier Synchronization and Detection of Polyphase Signals. IEEE Trans. on Communications, Vol. COM-20, pp: 441-454, June 1972.
- [P122] Simon, M.K., J.G.Smith: Carrier Synchronization and Detection of QASK Signal Sets. IEEE Trans. on Communications, Vol. COM-22, pp: 98-106, Feb.1974.
- [P123] Simon, M.K., J.G.Smith: Offset Quadrature Communications with Decision-Feedback Carrier Synchronization. IEEE Trans. on Communications, Vol. COM-22, pp: 1576-1584, Oct. 1974.

- [P124] Simon, M.K.: Further Results on Optimum Receiver Structures for Digital Phase and Amplitude Modulated Signals. ICC'78, Toronto, pp: 4211-4217, June 4-7, 1978.
- [P125] Leclert, A., P.Vandamme: Universal Carrier Recovery Loop for QASK and PSK Signal Sets. IEEE Trans. on Communications, Vol. COM-31, pp: 130-136, Jan. 1983.
- [P126] Qshita, S., K.Feher: Combined Effect of the Carrier Recovery and Symbol Timing Recovery Error on the  $P_e$  Performance of QPR and Offset QPR Systems. IEEE Trans. on Communications, Vol. COM-30, pp: 2534-2540, Dec. 1982.
- [P127] Braun, W.R., W.C.Lindsey: Carrier Synchronization Techniques for Unbalanced QPSK Signals-Part I. IEEE Trans. on Communications, Vol. COM-26, No.9, pp: 1325-1333, September 1978.
- [P128] Braun, W.R., W.C.Lindsey: Carrier Synchronization Techniques for Unbalanced QPSK Signals-Part II. IEEE Trans. on Communications, Vol. COM-26, No.9, pp: 1334-1341, September 1978.
- [P129] Simon, M.K., W.K.Alem: Tracking Performance of Unbalanced QPSK Demodulators: Part I-Biphase Costas Loop with Passive Arm Filters. IEEE Trans. on Communications, Vol. COM-26, No.8, pp: 1147-1156, August 1978.
- [P130] Simon, M.K.: Tracking Performance of Unbalanced QPSK Demodulators: Part II-Biphase Costas Loop with Active Arm Filters. IEEE Trans. on Communications, Vol. COM-26, No.8, pp: 1157-1166, August 1978.
- [P131] Kobayashi, H.: Simultaneous Adaptive Estimation and Decision Algorithm for Carrier Modulated Data Transmission Systems. IEEE Tr. on Comm. Technology, Vol. COM-19, pp: 268-280, June 1971.
- [P132] Falconer, D.D., J.Salz: Optimal Reception of Digital Data over the Gaussian Channel with Unknown Delay and Phase Jitter. IEEE Tr. on Information Theory, Vol.IT-23, pp: 117-126, Jan. 1977.
- [P133] Mengali, U.: Joint Phase and Timing Acquisition in Data-Transmission. IEEE Trans. on Communications, Vol. COM-25, No.10, pp: 1174-1185, October 1977.
- [P134] Franks, L.E.: Carrier and Bit Synchronization in Data Communication-A Tutorial Review. IEEE Trans. on Communications, Vol. COM-28, No.8, pp: 1107-1121, August 1980.
- [P135] Meyers, M.H., L.E.Franks: Joint Carrier Phase and Symbol Timing Recovery for PAM Systems. IEEE Trans. on Communications, Vol. COM-28, No.8, pp: 1121-1129, August 1980.
- [P136] Poklemba, J.J.: A joint estimator-detector for QPSK data transmission. COMSAT Technical Review, Vol.14, No.2, pp: 211-259, Fall 1984.

- [P137] Foschini, G.T., R.D.Gitlin, S.B.Weinstein: Optimization of Two-Dimensional Signal Constellations in the Presence of Gaussian Noise. IEEE Trans. on Communications, Vol. COM-22, No.1, pp: 28-38, Jan.1974.
- [P138] Booth, R.W.D.: An Illustration of the MAP Estimation Method for Deriving Closed-Loop Phase Tracking Topologies: The MSK Signal Structure. IEEE Trans. on Communications, Vol. COM-28, No.8, pp: 1137-1142, August 1980.

A

**APPENDIX A**

**COMPUTER PROGRAMS PRINTOUT**

This appendix contains a copy of the computer programs printout, which has been used in this thesis for the simulation purposes. Since joining Dr. Feher's Digital Communications Group at the Department of Electrical Engineering, University of Ottawa, in September 1982, the author has been developing computer software for the Amdahl 470 ( IBM 370 compatible ) system in the CMS environment.

The functional software has been written in the FORTRAN 66 and FORTRAN 77 languages. PLOTCOMM plotter, Hewlett-Packard hp 7470 plotter, and Tektonix 4105 color graphic terminal have been used as the output devices. The author wrote the software in the corresponding languages. In addition, SAS language has been used for graphic outputs.

The software is organized in the functional subroutines, whose model particular black-boxes ( modulator, filter, channel, nonlinearity, demodulator, synchronizer, equalizer, etc. — in practice ). The main programs use these subroutines ( black-boxes ) and make appropriate connections, according to the author's wishes. Most of the programs have been written in an interactive form, which allows an user-friendly approach to the simulation. Program description is given in the program printout captions ( comment lines ).

It is assumed that a potential user of these programs is familiar with the mentioned computer languages and the CMS environment.

130

FILE: ASINC FORTRAN A UNIV D'OF OTTAWA CMS RPLPASE A

```

C C C C C
A.KUCAR, 1983 08 10
Subroutine calculates the Arcsin(x)/x function
Singular point ASINC(0)=1.0
*****
SUBROUTINE ASINC(X)
IF (X.EQ.0.) GO TO 1
Y=ARSIN(X)/X
RETURN
1 Y=1.
RETURN
END

```

```

ASI000010
ASI000020
ASI000030
ASI000040
ASI000050
ASI000060
ASI000070
ASI000080
ASI000090
ASI000100
ASI000110
ASI000120
ASI000130

```

5

A

FILE: ATT      FORTRAN A      UNIV D:/CF 2TIAWA CMS RELEASE 4

```

CCCC
A.KUCAR, 1984 01 04, 12 08
**ATTENDUATES the signal pover
**SUBROUTINE ATT(LD, DATA, K)
**COMPLET. DATA(LD)
**DO 1 I=1, LD
**DATA(I)=DATA(I)*AT
**RETURN
**END
ATT000010
ATT000020
ATT000030
ATT000040
ATT000050
ATT000060
ATT000070
ATT000080
ATT000090
ATT000100
ATT000110
ATT000120

```

FILE: BERPHP PORTAN A UNIV D'OF OTTAWA CMS RELEASEP 4

```

C C C C C
A.KUCAR, 1983 10 10, 1985 02 25
Subroutine DRAWS Probability of error curves for a Pe(Eb/No) as
low as TH
*****
SUPERROUTINE BERPHP(IPEN,PEI,IPR,ITC,TH)
DIMENSION PEI(50)
M=ITC-IPR+1
DO I=1,KR-1
  J=K+IPR-I
  IF(PEI(J).LT.TH) RETURN
  A2=FLOAT(J)
  A1=ALOS(10){PEI(J)}
  WRITE(2,2){A2,A1,IPEN}
2 FORMAT(2E15.6,I2)
1 RETURN
END
BER00010
BER00020
BER00030
BER00040
BER00050
BERC0060
BER00070
BER00080
BER00090
BER00100
BER00110
BER00120
BER00130
BER00140
BER00150
BER00160
BER00170

```

FILE: CHANN PORTAN A UNIV D'CF OTTAWA CMS RELEASE A

```

CUCUCUC
A.KUCAR, 1984 12 20
Subroutine GENERATES the noise of
JTYPE=1. .GAUSSIAN
and ADD it to the data
SUBROUTINE CHANN(LD, DATA, SNR, JTYPE)
COMMON /I1/ IOFF, LSAMPL, NSYMB, NO1, NO2, NDMR(4,20), FT(A,4096)
COMMON /R1/ SAM, PI, BAUD, BW, AMPL(14,4), FT1BL(4,4), FT1PK(4,30)
COMPLEX I(2), DATA(LD)
REAL R(2)
DOUBLE PRECISION PID, DSEED
PID=3.141592653589793D0
DSEED=4569286.D0
DO I=1, LD
  CALL GSNML(DSEED, 2, R)
  R(1)=R(1)/SNR
  R(2)=R(2)/SNR
  DATA(I)=DATA(I)+CMPLX(R(1), R(2))
1 RETURN
END

```

```

BRA000010
CHA000020
CHA000030
CHA000040
CHA000050
CHA000060
CHA000070
CHA000080
CHA000090
CHA000100
CHA000110
CHA000120
CHA000130
CHA000140
CHA000150
CHA000160
CHA000170
CHA000180
CHA000190
CHA000200
CHA000210

```

FILE: CURPHP FORTRAN A UNIV D'OF OTTAWA CMS RELEASE 4

```

C C C
C A. KUCAR, 1984 01 26, 12 08
C Subroutine PLOTS:1)Pe=0.5*erfc(SORT(Ib/wo))
C *****
C SUBROUTINE CURPHP(I,IFROM,ITO)
C DO 1 J=I,IPROM,ITO
C A1=PL0A(I)*A1)
C A2=10.*SQR(T(E0))/2.
C A2=ERFC(A2)
C WRITE(2,2)A1,A2,IPEN
C 1 RETURN
C 2 RETURN
C END
CDR000010
CDR000020
CDR000030
CDR000040
CDR000050
CDR000060
CDR000070
CDR000080
CDR000090
CDR000100
CDR000110
CDR000120
CDR000130
CDR000140

```

```

A KUCAR, 1984 11 19 1985 03 11
Subroutine DECODES: LARY=1, WOA= data
> 1... HQAM data

C NEB=0. VS.Eb/NO
=1. VS.C/N
SUBROUTINE DECODE(LD, DATA, PNOISE, PRI, IFR, ITO, ER, MI, NO, LARY, CN, WEP)
COMMON /R1/ IOP, LSAMPL, NSY, HB, NO1, NO2, NUMB(4,30), NI(4,4095)
COMMON /R2/ SA, SA1, SA2, SA3, SA4, SA5, SA6, SA7, SA8, SA9, SA10, SA11, SA12, SA13, SA14, SA15, SA16, SA17, SA18, SA19, SA20, SA21, SA22, SA23, SA24, SA25, SA26, SA27, SA28, SA29, SA30, SA31, SA32, SA33, SA34, SA35, SA36, SA37, SA38, SA39, SA40, SA41, SA42, SA43, SA44, SA45, SA46, SA47, SA48, SA49, SA50
DIMENSION DATA(1:LD), PEI(1:50)
ARY=FLOAT(LARY)
IF (LARY.EQ.1) ARY=2.0
IF (LARY.EQ.0) ARY=1.0
IF (CN.EQ.0) EB=EB/ALOG(ARY)*ALOG(2.0)
SNR=SQRT(2.0*PNOISE*EB)
NER=1.0-1./ARY
DO 1 N=IFR, ITO
PEI(N)=0.0
IF (LARY.GT.1) GOTO 4
DO 2 K=1, NSYMB
JI={K-1}*LSAMPL+MI
JB=REAL(DATA(JI))
JD=AIMAG(DATA(JI))
INDI=NO(3,K)*JB.LE.0.) INDI=1
INDO=NO(4,K)*YB.LE.0.) INDO=1
IF (INDI.EQ.1.OR.INDO.EQ.1) NER=NER+1
YB=ABS(YB)/SNR
--- compute the probability of error for this symbol ---
DO 2 N=IFR, ITO
ARG=XB*IN
IF (ARG.GT.12.) ARG=12.
EI=ERFC(ARG)/2.
IF (INDI.EQ.1) EI=1.-EI
IF (YB*IN)
IF (ARG.GT.12.) ARG=12.
EQ=ERFC(ARG)/2.
IF (INDO.EQ.1) EQ=1.-EQ
PEI(N)=PEI(N)+(EI+EQ)/2.
GOTO 9
HIGH=FLOAT(LARY-1)
DO 7 K=1, NSYMB
JI={K-1}*LSAMPL+MI
JB=REAL(DATA(JI))
YB=AIMAG(DATA(JI))

```

FILE: DECODE FORTRAN A UNIV D'/OF OTTAWA CMS RELFASP &

```

DECC0005580
DECC0005590
DECC0005600
DECC0005610
DECC0005620
DECC0005630
DECC0005640
DECC0005650
DECC0005660
DECC0005670
DECC0005680
DECC0005690
DECC0005700
DECC0005710
DECC0005720
DECC0005730
DECC0005740
DECC0005750
DECC0005760
DECC0005770
DECC0005780
DECC0005790
DECC0005800
DECC0005810
DECC0005820
DECC0005830
DECC0005840
DECC0005850
DECC0005860
DECC0005870
DECC0005880
DECC0005890
DECC0005900
DECC0005910
DECC0005920
DECC0005930
DECC0005940
DECC0005950
DECC0005960
DECC0005970
DECC0005980
DECC0005990
DECC0010100
DECC0010200
DECC0010300
DECC0010400
DECC0010500
DECC0010600
DECC0010700
DECC0010800
DECC0010900
DECC0011000

```

```

X1=ABS(YB)
DY1=ABS(YB)
INDI=0
IF (PLOAT(NI(3,K)) LE.O.) INDI=1
AI=ABS(AI)
THRI1=AI-1.
THRI2=A+AI+1.
LAI=AI.EQ.HIGH GOTO 30
IF (AI GE.THRI2.OR.DY1.LE.THRI1) INDI=1
COTO 40
IF (DX1 LE.THRI1) INDI=1
30 LAGI=1
40 INDI=0
AI=PLOAT(NI(4,K))
IF (YB*AI) LE.O.) INDO=1
AI=ABS(AI)
THRO2=A+AI+1.
LAI=AI.EQ.HIGH GOTO 50
IF (AI GE.THRO2.OR.DY1.LE.THRO1) INDO=1
COTO 60
IF (DY1 LE.THRO1) INDO=1
50 LAG=1
60 INDI=1
OR.INDQ.EQ.1) NER=NER+1
COTO 9
C .-----compute the probability of error for this symbol-----
DX2=ABS(DX1-THRI2)//SNR
DY2=ABS(DY1-THRO2)//SNR
DY17=ABS(DY1-THRO1)//SNR
DYM=10.*YM*(PLOAT(M)/20.)
IF (ARG GT.12.) ARG=12.
EI=ERFC(ARG)/PEF
IF (LAG2*YM) GOTO 5
ARG=DI1*YM
EI=EI+ERFC(ARG)/PEF
IF (ARG GT.12.) ARG=12.
EI=EI+EI*YM
IF (INDI*YM) ARG=12.
EI=ERFC(ARG)/PEF
IF (LAG2*YM) GOTO 6
ARG=ARG3*YM
EI=EI+ERFC(ARG)/PEF
IF (ARG GT.12.) ARG=12.
EI=EI+EI*(M/6./3)NER
WRITE(8,3)NER
FORNAT(81,.....ERRORS=,I5, ' TRY again')

```

FILE: DECODE PORTRAN A UNIV D'OF OTTAWA CMS RELEASE A

RETURN  
END

DEC01110  
DEC01120



FILE: DECODO FORTRAN \* UNIV D'OF OTTAWA CMS RELEASE 0

```

THRI1=AI-1.
THRI2=AI+1.
IF (AI.EQ.HIGH) GOTO 30
IF (DX1.GE.THRI2.OR.DX1.LE.THRI1) INDT=1
GOTO 40
IF (DX1.LE.THRI1) INDI=1
30 INDO=0
IF (YB*AI) .LE.0.} INDO=1
AIF (ABS(AI-1).
THRO1=AI-1.
THRO2=AI+1.
IF (AI.EQ.HIGH) GOTO 50
IF (DY1.GE.THRO2.OR.DY1.LE.THRO1) INDO=1
GOTO 5
IF (DY1.LE.THRO1) INDO=1
5 NI(1,I)=NI(1,I)+INDI
NI(2,I)=NI(2,I)+INDO
C..... IF error is detected WRITE sample number generated, received samp.
C      IF (INDI.EQ.1.OR.INDO.EQ.1) WRITE(2,10) JI,NI(1,K),YR,JO,NI(4,K)
C      *CONTINUE
7 FORMAT(2(I10,I6,F10.2))
10 RETURN
END

```

```

DECC00560
DECC00570
DECC00580
DECC00590
DECC00600
DECC00610
DECC00620
DECC00630
DECC00640
DECC00650
DECC00660
DECC00670
DECC00680
DECC00690
DECC00700
DECC00710
DECC00720
DECC00730
DECC00740
DECC00750
DECC00760
DECC00770
DECC00780
DECC00790
DECC00800

```



FILE: ENCODE FORTRAN A UNIV D'OP OTTAWA CMS PRLPASR Q

```

ENC000560
ENC000570
ENC000580
ENC000590
ENC000600
ENC000610
ENC000620
ENC000630
ENC000640
ENC000650
ENC000660
ENC000670
ENC000680
ENC000690
ENC000700
ENC000710
ENC000720
ENC000730

```

```

DO 6 K=1, NSYMB
  J=1+(K-1)*LSAMPL
  DO 8 I=1, LSAMPL
    DATA(JI+I)=CMPLX(FLOAT(NI(1,K)),FLOAT(NI(2,K)))
  -----
  C 8 IF (N.NE.1) GOTO 4
    DO 7 I=1, NSYMB
      NI(3,I)=NI(1,I)
      NI(4,I)=NI(2,I)
      RETURN
    L2=LD-1
    DO 11 I=1, IOFF
      A=AIMAG3(DATA(I))
      DO 12 L=1, L2
        DATA(L)=CMPLX(REAL(DATA(L)),AIMAG(DATA(L+1)))
        DATA(LD)=CMPLX(REAL(DATA(LD)),A)
      11 RETURN
    END

```

FILE: ENCODO PORTRAN \* UNIX D:/OF OTTAWA CMS RELEASE 4

```

CUCUCUC
A.KUCAR, 1987 01 01
*****
SUBROUTINE GENERATES two channels of: *NAM signal. M=LAPY**2
*****
SUBROUTINE ENCODO(LD,DATA,N,LARY)
COMMON /R1/SAMPL,NSYMB,N01,N02,NUMR(4,20),VI(4,4,C96)
COMPLEX /DATA(LD),BAUD,BW,AMPL(4,4),TIMPK(4,30)
DOUBLE PRECISION PID,DSEED
PID=3.141592653589793DO
DSEED=4569286.DO
N1=LARY-1
DO 2 I=1,NSYMB
  NI(1,I)=2*INT(LARY*GGUBPS(DSEED))-M1
  DO 6 K=1,NSYMB
    J1=(K-1)*LSAMPL
    DO 6 I=1,LSAMPL
      DATA(J1+I)=CMPLX(FLOAT(NI(1,K)),FLOAT(NI(2,K)))
    IF (M.NE.1) GOTO 4
  DO 3 I=1,NSYMB
    NI(3,I)=NI(1,I)
  NI(4,I)=NI(2,I)
  IF (IOFF.EQ.0) RETURN
  L2=LD-1
  DO 11 I=1,IOFF
    A=AIMAG(DATA(I))
    DO 12 L=1,CMPLX(REAL(DATA(L)),AIMAG(DATA(L+1)))
      DATA(LD)=CMPLX(REAL(DATA(L)),A)
    RETURN
  11
  12
END

```

```

ENC000010
ENC000020
ENC000030
ENC000040
ENC000050
ENC000060
ENC000070
ENC000080
ENC000090
ENC000100
ENC000110
ENC000120
ENC000130
ENC000140
ENC000150
ENC000160
ENC000170
ENC000180
ENC000190
ENC000200
ENC000210
ENC000220
ENC000230
ENC000240
ENC000250
ENC000260
ENC000270
ENC000280
ENC000290
ENC000300
ENC000310
ENC000320
ENC000330
ENC000340

```



FILE: FEEDLOOP FORTRAN \* UNIV D'OF OTTAWA CMS RELRASP 8

```

CALL MRFPCI(SER,EB1,IER)
EB=EB1*SQRT(2.)
C Generate data
CALL ENCODO(LD,DATA,NCH,LARY)
C..... Generate Gaussian noise,add it to the DATA and store it in DATA1
DO 1 I=1,LD
  CALL IGENML(DSEED,2,R)
  DATA(I)=DATA(I)+EB*R(2)/ER)
C Introduce ISI
CALL TREQ(3,LSAMPL,LD,DATA,TF,C,LS2,JOF)
DO 3 I=1,LD
  DATA(I)=DATA(I)
C 5 degrees phase steps
DO 5 J=1,73
  DEG1=FLOAT(J-37)*5.
  PI=DEG1/PI
  CY=SIN(PI)
  SCALCUI=1
DO 2 DATA(I)=CMPLX(CX*REAL(DATA1(I))+SY*AIMAG(DATA1(I)),
  5 CX*AIMAG(DATA1(I))-SY*REAL(DATA1(I)))
C..... Crosstalk and timing ISI compensation.....
IF (JACK.EQ.90) OR (PI.EQ.-90) TPI=TAW(PI)
IF (PI.EQ.90) OR (PI.EQ.-90) TPI=1.R+I
IF (ESTPI.GT.999) GOTO 21
CALL IGENML(DSEED,1,R)
CTPI=TPI+I/LSORT(ESTPI)
21 DO DATA(I)=LD
  11 DATA(I)=CMPLX(REAL(DATA(I))-TPI*AIMAG(DATA(I)),
  11 AIMAG(DATA(I))+TPI*REAL(DATA(I)))
  12 IF (JACK.EQ.90) CALL TREQ(3,LSAMPL,LD,DATA,TP,C,LS2,?)
  DO DATA(I)=LD
  15 DATA(I)=DATA(I)*CX
  14 DATA(I)=VE
C ONTE DECODO once per sample and compare with sent sample
C Make DECODO(LD,DATA,NCH,LARY)
C Calculate signal before loop filter then filter it
C DATA(I)=CMPLX(REAL(DATA(I))*AD-AIMAG(DATA(I))*RD,0.)
C CALL 99 K=1/LSAMPL
DO SAMB=FLOAT(K-1)/SAM-0.5
  PEATE=-ALOG10(FLOAT(NI(1,K)+NI(2,K)))+ALD
  WRITE(17,SAMPL) WRITE(1,7) SAMB+SAY1,NPG1,PPA
C CONMAT(99E10.3)
  99 FORMAT(2F5.0,5X,2F5.0,I3)
  10 PND
  END

```

```

PEEEOO06100
PEEEOO06200
PEEEOO06300
PEEEOO06400
PEEEOO06500
PEEEOO06600
PEEEOO06700
PEEEOO06800
PEEEOO06900
PEEEOO07000
PEEEOO07100
PEEEOO07200
PEEEOO07300
PEEEOO07400
PEEEOO07500
PEEEOO07600
PEEEOO07700
PEEEOO07800
PEEEOO07900
PEEEOO08000
PEEEOO08100
PEEEOO08200
PEEEOO08300
PEEEOO08400
PEEEOO08500
PEEEOO08600
PEEEOO08700
PEEEOO08800
PEEEOO08900
PEEEOO09000
PEEEOO09100
PEEEOO09200
PEEEOO09300
PEEEOO09400
PEEEOO09500
PEEEOO09600
PEEEOO09800
PEEEOO09900
PEEEO10000
PEEEO10100
PEEEO10200
PEEEO10300
PEEEO10400
PEEEO10500
PEEEO10600
PEEEO10700

```

FILE: FILTER PORTRAW A UNIV D'OF OTTAWA CMS RELPASP A

```

1 100000000000
2 100000000000
3 100000000000
4 100000000000

A.KUCAR, 1984, 01, 04, 1985, 05, 08
Subroutine performs the FILTERING of data
*****
SUBROUTINE FILTER(LD, L3, DATA, TF, IWK, N, NPTI)
COMMON /R1/ IOPP, LS, AMPL, NSYMB, NO1, NO2, NUMR(4, 20), VI(N, 4, 0, 96)
COMPLEX DATA(LD), PI, BAUD, BW, AMPL(N, 4), TIMPL(N, 30)
INTEGER IWK(L3), FF(ED)
N1=NP#3+2
N2=NP#2+3
DIN=PLDAT(LD)
BW1=BW/DIN
TWOPI=2.*PI
N0=NUMB(N, M1)
CALL FPIZ(N, DATA, L3, IWK)
IPOP=FIX(TIMEXDATA, TF, IPOF)
CALL TIMESH(LD, 5, 6, 7, 8, 9, 10, 11, 12, 13, 14, 15, 16), NO
RETURN
*****
Phase equalized BUTTERWORTH filter
Mod(H(L))=-----
\ / 1+(f/PN)**2n
A2=1./SQRT(1.+(FLOAT(J)/PN)**NA1)
PN=3
a = filter order
PN=TIMEK(N, M2+1)/BW1
NA1=2*NUMB(N, M1+1)
TF(1)=CMPLX(1.0, 0.0)
DO 100 I=2, NO1
J=I-1
A2=1./SQRT(1.+(FLOAT(J)/PN)**NA1)
FF(I)=CMPLX(A2, 0.)
3 RETURN
*****
Phase equalized SQUARE ROOT COSINE FILTER with arbitrary alpha
ITP(L)=1, 0<=f<=(P1=PN(1-alpha))
ITP(L)=.5/|1-sin(PI/2/alpha*(f/PN-1))|, P1<=f<=(P2=PN(1+alpha))
ITP(L)=.5/|sinx equalizer| included
VPI>0...
IF (TIMEK(N, M2), EQ 0.) TIMEK(N, M2)=0.0001
PN=TIMEK(N, M2+1)/BW1
P1=(1.-TIMEK(N, M2))*PN
*****

```

CCCCCCCCCCCC CCCCCCCCCCCC CCCCCCCCCCCC CCCCCCCCCCCC

FILE: FILTER FORTRAN A UNIV D'OP OTTAWA CMS RELEASE A

```

110 F2=(1.+TIMEX(N,M2))*PN
    IPN=IPXX(FN)
    IPN1=PLCAT(I,IPN)
    IP1=IPXX(F1)+1
    IP2=IPXX(F2)+1
    A1=PI/2.
    A2=1.
    A3=PI/2./TIMEX(N,M2)
    IP(F1)=CMPLX(1.0,6.0)
    DO 110 I=2,IP1
    IP(NPIL.LF.0) GOTO 110
    IP=FLOAT(I-1)*A1
    A2=PI/SIN(FI)
    IP(I)=CMPLX(A2,0.0)
    JK=IP1+1
    DO 120 J=JK,IF2
    PI1=PLCAT(J-1)
    A=A3*(PI1/FN1)-1.
    IP(J)=CMPLX(SOPT(0.5*(1.0-SIN(A))),0.0)
    IP(NPIL.LT.0) GOTO 120
    PI=PI1*A1
    A2=PI/SIN(FI)
    IP(J)=CMPLX(A2,0.0)
    JK=IP2+1
    DO 130 I=JK,NO1
    IP(I)=CMPLX(0.0,0.0)
    GOTO 99
5 RETURN
6 RETURN
7 RETURN
8 LINEAR Group Delay
  PI1=PI*1.E-3*TIMEX(N,M2)
  DO 31 I=1,NO1
  PHI1=(PI1)*RW1
  PHI1=AMOD(PHI1,TWOPI)
  IP(I)=CMPLX(COS(PHI1),-SIN(PHI1))
  GOTO 98
9 PARABOLIC Group Delay
  PI2=TWOPI/3.*1.E-3*TIMEX(N,M2)
  DO 32 I=1,NO1
  PHI1=(I-1)*BW1
  PHI1=AMOD(PHI1,TWOPI)
  IP(I)=CMPLX(COS(PHI1),-SIN(PHI1))
  GOTO 99
10 LINEAR GalB
  A1=BW1*TIMEX(N,M2)/20.
  DO 34 I=1,NO1
  IP(I)=CMPLX(10.**((I-1)*A1),0.0)
  DO

```

IL00560  
 IL00570  
 IL00580  
 IL00590  
 IL00600  
 IL00610  
 IL00620  
 IL00630  
 IL00640  
 IL00650  
 IL00660  
 IL00670  
 IL00680  
 IL00690  
 IL00700  
 IL00710  
 IL00720  
 IL00730  
 IL00740  
 IL00750  
 IL00760  
 IL00770  
 IL00780  
 IL00790  
 IL00800  
 IL00810  
 IL00820  
 IL00830  
 IL00840  
 IL00850  
 IL00860  
 IL00870  
 IL00880  
 IL00890  
 IL00900  
 IL00910  
 IL00920  
 IL00930  
 IL00940  
 IL00950  
 IL00960  
 IL00970  
 IL00980  
 IL00990  
 IL01000  
 IL01010  
 IL01020  
 IL01030  
 IL01040  
 IL01050  
 IL01060  
 IL01070  
 IL01080  
 IL01090  
 IL01100

FILE: FILTER FORTRAN A UNIV D'OF OTTAWA CMS RELFASP 4

```

41  FP(I)=CMPLX(10.**((I-2-LD)*A1),0.)
3010 199
C *****
C PARABOLIC GAIN
11  A1=BW1*BW1*TIMEK(N,M2)/20.
DO 36 I=1,NO1
PI=FLOAT(I-1)
AM1={A1*PI*PI}
36  FP(I)=CMPLX(10.**AM1,0.)
3010 99
C *****
C RETURN
13  RETURN
14  RETURN
15  RETURN
C *****
C RUNMLER'S SELECTIVE FADING MODEL
H(f)=a(1-b*exp(+j2PI(f-fo)tau))
a=flat fading depth (normalized to 1)
b=db (flat fading)/(1-b) (is a notch depth)
+ - nonflat fading, minimum phase
fo=notch offset
tau=delay of second path
-----
16  ARO=THOPAI*TIMEK(N,15)*1.E-3
TT=TIMEK(N,M2+1)
B=10.**{ABS(TT)}/20.)
DO 57 I=1,NO1
AR1=AR0*(PI*COAT(I-1)/BW1-TIMEK(N,M2))
AR2=-SIGN(AR2,TT)*8*SIN(AR1)/{.-R*C}S(AR1)
57  TF(I)=SQRT(1.+R*B-2.**B*COS(AR1))*
*CMPLX(COS(AR2),-SIN(AR2))
C *****
C DO 20 I=NO2,LD
20  TFP(I)=CONJG(TF(LD+2-I))
3010 199
C *****
C DO 21 I=NO2,LD
21  FP(I)=TF(LD+2-I)
199  DO 111 I=1,LD
111  DATA(I)=CONJG(DATA(I)*TF(I))
DO 222 I=1,LD
222  DATA(I)=CONJG(DATA(I))/DIN
END

```

PILLO11120  
PILLO11130  
PILLO11140  
PILLO11150  
PILLO11160  
PILLO11170  
PILLO11180  
PILLO11190  
PILLO11200  
PILLO11210  
PILLO11220  
PILLO11230  
PILLO11240  
PILLO11250  
PILLO11260  
PILLO11270  
PILLO11280  
PILLO11290  
PILLO11300  
PILLO11310  
PILLO11320  
PILLO11330  
PILLO11340  
PILLO11350  
PILLO11360  
PILLO11370  
PILLO11380  
PILLO11390  
PILLO1400  
PILLO1410  
PILLO1420  
PILLO1430  
PILLO1440  
PILLO1450  
PILLO1460  
PILLO1470  
PILLO1480  
PILLO1490  
PILLO1500  
PILLO1510  
PILLO1520  
PILLO1530  
PILLO1540  
PILLO1550  
PILLO1560  
PILLO1570  
PILLO1580



FILE: INP1 FORTRAN A UNIV D'OF OTTAWA CMS RELEASE 4

```

WRITE(8,5)(AMPL(J,I),TIME(J,I),TIME(J,I),I=1,KH)
6 CONTINUE
IF(IWAY.EQ.1) WRITE(6,5)(AMPL(J,I),TIME(J,I),TIME(J,I),I=1,KH)
RETURN
END
INP00560
INP00570
INP00580
INP00590
INP00600

```

FILE: INP2    PORTAN    A    UNIV D'/OF OTTAWA CMS RELEASE 4

```

A.KUCAR,1983,12,13,1985,05,02
*** for the MAIN and ACI/CCI channels
input data for the channels,max 4
N is the modulation (window) type
NUMB(N,4) - number of filters in each of max 4 systems,max 4
      (N,5) - filter type #1
      (N,6) - filter order #2
      (N,8) - filter #3
      (N,11) - filter #4
      (N,14) - nonlinearity type
      (N,20) - 1st filter parameter,
OF LINEAR GD:ns/MHZ,
OI PARABOLIC GD:ns*ns/MHZ,
OI PARABOLIC DG:db/MHZ,
OI NOTCH OFFSET:MHZ,
      (N,6) - filter bandwidth MHZ #1, or notch depth:db,
      (N,7) - filter #2
      (N,9) - filter #3
      (N,11) - filter #4
      (N,13) - frequency level dbi
      (N,14) - channel delay:ns
      (N,15) - 2nd parameter
***
SUBROUTINE INP2(N)
COMMON /R1/SAM,PI,BAUD,BW,AMPL(4,4),TIMEL(4,4),TIMPK(4,30)
TIMPK(1,15)=0.
IF (N.BE.1) GOTO 22
DORITE(8,CH,I)
FORNAT(7,15) I,I1,':OFFSET-MHZ.:'
WRITE(8,12) I,TIMEK(I,13)
FORNAT(7,15) I,I1,':LEVEL-dbi.:'
WRITE(8,12) I,TIMEK(I,14)
IF (NUMB(N,4).GT.0) GO TO 13
DORITE(8,CH,I)
FORNAT(7,15) I,I1,':NONLINEARITY:0=linear,18X,1=hard limiter,18X,2=soft limiter,18X,3=HP,18X,4=GaAs PFT.:'
WRITE(8,12) I,TWNUMB(I,20)
FORNAT(7,15) I,I1,':NUMB.of filters-max 4:'
WRITE(8,12) I,NUMB(I,4)
READ(8,17) KK
KK=NUMB(I,4)
IF (KK.EQ.0) GO TO 8
DO 8 J=1,KK
M=J*3+2
N1=J*2+3
NUMB(I,1+M)=0

```

CCCCCCCCCCCCCCCCCCCCCCCCCCCCCCCCCCCC

```

INP000010
INP000020
INP000030
INP000040
INP000050
INP000060
INP000070
INP000080
INP000090
INP000100
INP000110
INP000120
INP000130
INP000140
INP000150
INP000160
INP000170
INP000180
INP000190
INP000200
INP000210
INP000220
INP000230
INP000240
INP000250
INP000260
INP000270
INP000280
INP000290
INP000300
INP000310
INP000320
INP000330
INP000340
INP000350
INP000360
INP000370
INP000380
INP000390
INP000400
INP000410
INP000420
INP000430
INP000440
INP000450
INP000460
INP000470
INP000480
INP000490
INP000500
INP000510
INP000520
INP000530
INP000540
INP000550

```



FILE: INP2      PORTAN A      UNIV D\*/OP OTTAWA CMS RELEASE A

```

WRITE(8,14) I, TIMEK(I,13), TIMEK(I,14)
WRITE(6,6)
WRITE(8,6)
K=NUMB(I,4)
DO 10 J=1,K
M=J*3+2
M1=J*2+3
WRITE(6,214) NUMB(I,M), NUMB(I,M+1), TIMEK(I,M1+1), TIMEK(I,M1)
WRITE(8,214) NUMB(I,M), NUMB(I,M+1), TIMEK(I,M1+1), TIMEK(I,M1)
CONTINUE(I,1)
FORMAT(I,2)
FORMAT(I,3,7)
FORMAT(I,15,2F15.7)
FORMAT(2I15,2F15.7)
RETURN
END
10 14
44 12
14 14
214 214

```

```

INP01120
INP01130
INP01140
INP01150
INP01160
INP01170
INP01180
INP01190
INP01200
INP01210
INP01220
INP01230
INP01240
INP01250
INP01260
INP01270

```

FILE: MCARL4 FORTRAN A UNIV D'/OF OTTAWA CMS RELEASE 4

CCCC

```

A. KUCAR, 1984 12 19 1985 04 18
*** DECODES the 4QAM data using MONTE CARLO techniques
Subroutine MCARL4(LD,DATA,NSYMB,NO1,NO2,NUMB(4,20),NT(4,4096),
SBRONN, /I1/SAMP,PI,BAUD,BW,AMPL(4,4),TIME(4,30))
COMMON /R1/SA(LB),DATA(LB)
DO 1 K=1,NSYMB
  JI=(K-1)*LSAMPL+MI
  JB=NI(3,K)*AREAL(DATA(JI))
  IF(YB(4,4)) K,MCA
  WRITE(6,4) K,MCA
  IF(YB(6,4)) K,GOTO 6
  IF(YB(7,4)) K,GOTO 6
  IF(YB(5,5)) K,GOTO 6
  IF(YB(LE,0)) OR(YB,LE,0.) NFROR=NERROR+1
  I CHANNEL error in symbol, IS, I
  Q channel error in symbol, IS, I
FORMAT(10,15,15)
PRINT*
RETURN
END

```

MCA0000010  
MCA000020  
MCA000030  
MCA000040  
MCA000050  
MCA000060  
MCA000070  
MCA000080  
MCA000090  
MCA000100  
MCA000110  
MCA000120  
MCA000130  
MCA000140  
MCA000150  
MCA000160  
MCA000170  
MCA000180  
MCA000190  
MCA000200  
MCA000210  
MCA000220  
MCA000230  
MCA000240





FILE: MDPL1 PORTAN X UNIV D'OF OTTAWA CMS RELFASP R

```

DO 11 N9=1,L2,2
M1=N9-LRA
RAM=(RAM1+RAM)*CX
YA1=(RAM1+RAM)*CX
DO 11 N9=1,L2,2
N3=N9-LRB
RAM=N3*RAM1+RAM)*SX
YB1=(RAM1+YB1)
YAB1=(MO.EQ.LM1) PEA=ERRFC((PPI-YAB1)*ERN)
YAB1=(MO.EQ.LM1) PEA=ERRFC((YAB1-PM1)*ERN)
IF (M.EQ.LM1) PEA=ERRFC((YAB1-PM1)*ERN)
IF (M.EQ.LM1) PEA=ERRFC((YAB1-PM1)*ERN)
PEA1=PEA+PEA1
PEIN=PEIN+PEA1
PEB=PEB+PEIN
G2=G2+M*M*PEN
GC1=C1+M*M*PEN
DO 14 I9=1,L2,2
O I9=1,L2,2
I I9=1,L2,2
PPI=FLOAT(I1+1)
PM1=PP1-2.
IA=IABS(I1)
PENI=0.
PEJ1=0.
DO 13 N0=1,L2,2
N=N0-L*RB1
RAM1=N*RAM1+RAM)*CX
YA1=(RAM1+RAM)*CX
DO 16 N9=1,L2,2
N1=N9-LRB
RAM=N1*RAM1+RAM)*SX
YB1=(RAM1+YB1)
YAB1=(MO.EQ.LM1) PEA=ERRFC((YAB1-FPI1)*ERN)
YAB1=(MO.EQ.LM1) PEA=ERRFC((YAB1-FPI1)*ERN)
IF (M.EQ.LM1) PEA=ERRFC((YAB1-FPI1)*ERN)
IF (M.EQ.LM1) PEA=ERRFC((YAB1-FPI1)*ERN)
*PEI=ERRFC((YAB1-FPI1)*ERN)
*PEI=ERRFC((YAB1-FPI1)*ERN)
PEI1=PEI+PEI1
PENI=PEJ1+N*PEI1
PEJ1=PEJ1+PEI1
G2=G2+I1*M*PENI
CONTINUE
G1=C1-PEI2
AN1=C1-PEI2

```

MDP011110  
MDP011120  
MDP011130  
MDP011140  
MDP011150  
MDP011160  
MDP011170  
MDP011180  
MDP011190  
MDP011200  
MDP011210  
MDP011220  
MDP011230  
MDP011240  
MDP011250  
MDP011260  
MDP011270  
MDP011280  
MDP011290  
MDP011300  
MDP011310  
MDP011320  
MDP011330  
MDP011340  
MDP011350  
MDP011360  
MDP011370  
MDP011380  
MDP011390  
MDP011400  
MDP011410  
MDP011420  
MDP011430  
MDP011440  
MDP011450  
MDP011460  
MDP011470  
MDP011480  
MDP011490  
MDP011500  
MDP011510  
MDP011520  
MDP011530  
MDP011540  
MDP011550  
MDP011560  
MDP011570  
MDP011580  
MDP011590  
MDP011600  
MDP011610  
MDP011620  
MDP011630  
MDP011640

C-----



FILE: MDP11 PORTMAN A UNIV D'OF OTTAWA CMS RELEASE SP. 4

MDP022210  
 MDP022230  
 MDP022240  
 MDP022250  
 MDP022260  
 MDP022270  
 MDP022280  
 MDP022290  
 MDP023100  
 MDP023200  
 MDP023300  
 MDP023400  
 MDP023500

```

26 PEI1=PEI1+PEI1
'23 PEJ1=PEJ1+N*PEI1
'24 C2=G2+I1*PEJ1
C-----
G2=G2*P3/2
G1=1-.31*P3
AN1=1.-AN1*P3
PEA=-ALOG10(PEB*P2)
SFI=G1*SI+G2*CX
GFIN=2.*GFI/AN1
P=GFIN
R=TURN
END
  
```

C-----



FILE: MOAM FORTRAN A UNIV D/OF OTTAWA CMS RELRASP A

```

1  I (LARY, EQ, 1) CALL INP1(NCH, 1)
2  L INP2(NCH)
3  WRITE(8, 4)
4  FORNMA(1, 102) IPEN type:1 TO 9')
5  LPEN=IPEN+4
6  WRITE(8, 6) IPEN, IOFF, NUMB(1, 20), LARY
7  WRITE(8, 6) IPEN, IOFF, NUMB(1, 20), LARY
8  FORNMA(1, 102) IPEN, IOFF, NUMB(1, 20), LARY, AT 5)
9  DBER(I)=1 FROM, ITO
10 DBER(I)=0 SORT(1.)
11 ANO RH=SQ=1 NR LD, DATA, 1, LARY)
12 ALL ENCODE(LD, L1, L2, L3, L4, L5, DATA, YA, XB, PSY, NWK, WK, 3, IPEV, 1)
13 CALL P1(LD) GOTO 10
14 J NEPLTSAS(LD, DATA, 60 MI, MO, JKL, IJK, LARY, 2)
15 ALL PLTSAS(LD, DATA, 250 MI, MO, JKL, IJK, LARY, 1)
16 CALL NCH(LD, DATA, ANORN, 1)
17 IPEN, ITO, LD, L1, L2, L3, L4, L5, DATA, YA, XB, PSY, NWK, WK, 3, IPEV, 1)
18 FIM(LD, L1, L2, L3, L4, L5, DATA, YA, XB, PSY, NWK, WK, 3, IPEV, 1)
19 NUMB(1, 1, 1) : POP, 4) CALL FILTER(LD, L3, DATA, TP, IWK, 1, 2)
20 NCH(LD, L1, L2, L3, L4, L5, DATA, YA, XB, PSY, NWK, WK, 3, IPEV, 1)
21 CH=INT(1) LD, DATA, ANORN, 1)
22 NCH(LD, L1, L2, L3, L4, L5, DATA, YA, XB, PSY, NWK, WK, 3, IPEV, 1)
23 ENCODE(LD, DATA, 1, LARY)
24 NONLIN(LD, DATA, 1, ANORN, K)
25 PSH=PI2*SSHM*(LD, DATA, 1, PSH) (DSEED)=-.5))
26 TSH=INT(1) LD, DATA, 1, TP, ITSH)
27 ALL INT(LD, DATA, 1, TP, ITSH)
28 ALL INT(LD, DATA, 1, TP, ITSH)
29 DATA(1, 1) LTA(I) + DATA(1, I) PPEA, EB, 0)
30 DATA(1, 1) PPEA, EB, 0)
31 DATA(1, 1) PPEA, EB, 0)
32 DATA(1, 1) PPEA, EB, 0)
33 DATA(1, 1) PPEA, EB, 0)
34 DATA(1, 1) PPEA, EB, 0)
35 DATA(1, 1) PPEA, EB, 0)
36 DATA(1, 1) PPEA, EB, 0)
37 DATA(1, 1) PPEA, EB, 0)
38 DATA(1, 1) PPEA, EB, 0)
39 DATA(1, 1) PPEA, EB, 0)
40 DATA(1, 1) PPEA, EB, 0)
41 DATA(1, 1) PPEA, EB, 0)
42 DATA(1, 1) PPEA, EB, 0)
43 DATA(1, 1) PPEA, EB, 0)
44 DATA(1, 1) PPEA, EB, 0)
45 DATA(1, 1) PPEA, EB, 0)
46 DATA(1, 1) PPEA, EB, 0)
47 DATA(1, 1) PPEA, EB, 0)
48 DATA(1, 1) PPEA, EB, 0)
49 DATA(1, 1) PPEA, EB, 0)
50 DATA(1, 1) PPEA, EB, 0)
51 DATA(1, 1) PPEA, EB, 0)
52 DATA(1, 1) PPEA, EB, 0)
53 DATA(1, 1) PPEA, EB, 0)
54 DATA(1, 1) PPEA, EB, 0)
55 DATA(1, 1) PPEA, EB, 0)
56 DATA(1, 1) PPEA, EB, 0)
57 DATA(1, 1) PPEA, EB, 0)
58 DATA(1, 1) PPEA, EB, 0)
59 DATA(1, 1) PPEA, EB, 0)
60 DATA(1, 1) PPEA, EB, 0)
61 DATA(1, 1) PPEA, EB, 0)
62 DATA(1, 1) PPEA, EB, 0)
63 DATA(1, 1) PPEA, EB, 0)
64 DATA(1, 1) PPEA, EB, 0)
65 DATA(1, 1) PPEA, EB, 0)
66 DATA(1, 1) PPEA, EB, 0)
67 DATA(1, 1) PPEA, EB, 0)
68 DATA(1, 1) PPEA, EB, 0)
69 DATA(1, 1) PPEA, EB, 0)
70 DATA(1, 1) PPEA, EB, 0)
71 DATA(1, 1) PPEA, EB, 0)
72 DATA(1, 1) PPEA, EB, 0)
73 DATA(1, 1) PPEA, EB, 0)
74 DATA(1, 1) PPEA, EB, 0)
75 DATA(1, 1) PPEA, EB, 0)
76 DATA(1, 1) PPEA, EB, 0)
77 DATA(1, 1) PPEA, EB, 0)
78 DATA(1, 1) PPEA, EB, 0)
79 DATA(1, 1) PPEA, EB, 0)
80 DATA(1, 1) PPEA, EB, 0)
81 DATA(1, 1) PPEA, EB, 0)
82 DATA(1, 1) PPEA, EB, 0)
83 DATA(1, 1) PPEA, EB, 0)
84 DATA(1, 1) PPEA, EB, 0)
85 DATA(1, 1) PPEA, EB, 0)
86 DATA(1, 1) PPEA, EB, 0)
87 DATA(1, 1) PPEA, EB, 0)
88 DATA(1, 1) PPEA, EB, 0)
89 DATA(1, 1) PPEA, EB, 0)
90 DATA(1, 1) PPEA, EB, 0)
91 DATA(1, 1) PPEA, EB, 0)
92 DATA(1, 1) PPEA, EB, 0)
93 DATA(1, 1) PPEA, EB, 0)
94 DATA(1, 1) PPEA, EB, 0)
95 DATA(1, 1) PPEA, EB, 0)
96 DATA(1, 1) PPEA, EB, 0)
97 DATA(1, 1) PPEA, EB, 0)
98 DATA(1, 1) PPEA, EB, 0)
99 DATA(1, 1) PPEA, EB, 0)
100 DATA(1, 1) PPEA, EB, 0)
101 DATA(1, 1) PPEA, EB, 0)
102 DATA(1, 1) PPEA, EB, 0)
103 DATA(1, 1) PPEA, EB, 0)
104 DATA(1, 1) PPEA, EB, 0)
105 DATA(1, 1) PPEA, EB, 0)
106 DATA(1, 1) PPEA, EB, 0)
107 DATA(1, 1) PPEA, EB, 0)
108 DATA(1, 1) PPEA, EB, 0)
109 DATA(1, 1) PPEA, EB, 0)
110 DATA(1, 1) PPEA, EB, 0)
111 DATA(1, 1) PPEA, EB, 0)

```

-----prob.of symbol error-----  
 -----prob.of symbol error-----  
 -----C/N-----  
 -----prob.of symbol error-----

FILE: MQAM    FORTRAN A    UNIV D'/OF OTTAWA CMS RELEASE 0

```

172  PEI(I) = BER(I)/PUNS
173  CALL BERPH(I, IPEN, PEI, IFROM, ITO, I.E-12)
173  WRITE(8, 173)
173  IF (NEW PA RAM > 0) NEW BB SIGNAL<0...')
11  READ(7, 100, 11, 2)
12  IF (GO)
102  CON TIT (I1)
222  FORMAT (F15.7)
      END

```

```

MQAO11110
MQAO11120
MQAO11130
MQAO11140
MQAO11150
MQAO11160
MQAO11170
MQAO11180
MQAO11190
MQAO12100
MQAO12200
MQAO12300
MQAO1240

```

2

FILE: NOISE1 FORTRAN A UNIV D'OF OTTAWA CMS RELPASP a

```

CCCCCCCC
A.KUCAR, 1984 01 04, 1985 04 18 *****
***** COMPUTES the effective noise (PNOISE)
SUBROUTINE INTEGRAL(I,TF,PI,BAUD,BW,AMPL,NO1,NO2,NUMB,HI)
PNOISE=NO*INTEGRAL(I,TF,PI,BAUD,BW,AMPL,NO1,NO2,NUMB,HI)
NO=0.5 *****
***** (White Gaussian Noise) *****
***** *****
SUBROUTINE NOISE1(LD,TF,PNOISE)
COMMON /I1/IOFF,LSAMPL,NO1,NO2,NUMB,HI
COMPLET=TF/LD
SUM=0.0
DO 1 L=1,LD
  SUM=SUM+(CABS(TF(L)))**2
PNOISE=SUM*BW/PI/LD
RETURN
END

```

```

NOI000010
NOI000020
NOI000030
NOI000040
NOI000050
NOI000060
NOI000070
NOI000080
NOI000090
NOI000100
NOI000110
NOI000120
NOI000130
NOI000140
NOI000150
NOI000160
NOI000170

```

FILE: NONLIN FORTRAN A UNIV D'/OF OTTAWA CMS RELEASE A

```

CCCCC
A.KUCIAR, 1984 01 04, 1985 04 18
****
Subroutine simulates an ideal HARDIMITPP:Out=|I|*npi|
****
SUBROUTINE NONLIN(LD,DATA,ANORM,N)
COMMON /I1/IOFF,LSAMPL,NSYMB,NO1,NO2,NUMB(4,20),VI(4,4096)
COMPLEX DATA(LD)
IF (NUMB(N,20).EQ.0) RETURN
DO I=1,LD
DATA(I)=ANORM*DATA(I)/CABS(DATA(I))
RETURN
END
NON000010
NON000020
NON000030
NON000040
NON000050
NON000060
NON000070
NON000080
NON000090
NON000100
NON000110
NON000120
NON000130

```

FILE: PHASSH PORTAN A UNIV D\*/OP OTTAWA CMS RELEASE 4

```

CCCCC
A.KUCAR, 1984 01 04, 12985 04 18
*****
Subroutine COMPENSATES the PHASE SHFT due to the Carrier offset
*****
SUBROUTINE PHASSH(LD,DATA,PSHIFT)
  COMPLEX DATA(LD),EPS
  EPS=CMPLX(COS(PSHIFT),-SIN(PSHIFT))
  DO 1 I=1,LD
    DATA(I)=DATA(I)*EPS
  RETURN
  END
1
PHA000010
PHA000020
PHA000030
PHA000040
PHA000050
PHA008060
PHA000070
PHA000080
PHA000090
PHA000100
PHA000110
PHA000120

```

FILE: PLTSAS FORTRAN A UNIV D'/OF OTTAWA CMS RELEASE

```

C C C C C
A.KUCAR, 1984 01 20, 1985 04 18
Subroutine DRAWS:IWHAT=1...EYE-PATTERN for 2 SYMBOL duration
2...POLAR (state space) DIAGRAM
*****
SUBROUTINE PLTSAS(LD,DATA,M2,MI,NO,IKL,IJK,LARY,IHRRAT)
COMMON /R1/SAMPL,NSYMB,NO1,N62,NHUMB(4,20),NIT(4,4,096)
COMPLEX /DATA(LD)
ARY=FLOAT(LARY)-1.
IF (ARY.EQ.0.) ARY=1.
SOFO (1,2),IWHAT
----- E Y E -----
C 1
JJ=2*LSAMPL+1
DO 11 JJ-1
K1=KK-1
JKL=JKL+1
DO 11 I=1,JJ
II=K1+J1+I+MI
A2=REAL(DATA(II))/ARY
A1=(FLOAT(12))/A1,A2,JKL
WRITE(2F10.6,1B)
RETURN
C 2
JJ=LSAMPL+1
IF (IJK.GT.0) JJ=1
DO 13 KAMPL
K1=KK+LSAM-1
K2=K+MI-1
IJK=IJK+1
JJ=IJK(K1+I))/ARY
A1=REAL(DATA(K2+I))/ARY
A2=AIMAG(9,12)A1,A2,IJK
WRITE(9,12)
RETURN
END
PLT000010
PLT000020
PLT000030
PLT000040
PLT000050
PLT000060
PLT000070
PLT000080
PLT000090
PLT000100
PLT000110
PLT000120
PLT000130
PLT000140
PLT000150
PLT000160
PLT000170
PLT000180
PLT000190
PLT000200
PLT000210
PLT000220
PLT000230
PLT000240
PLT000250
PLT000260
PLT000270
PLT000280
PLT000290
PLT000300
PLT000310
PLT000320
PLT000330
PLT000340
PLT000350
PLT000360
PLT000370
PLT000380
PLT000390
PLT000400
PLT000410

```

FILE: POWER FORTRAN A UNIV D:/OF OTTAWA CMS RELEASE a

```

C C C C C
A.KUCAR, 1984 01 22, 1985 04 18
* * * * *
SUBROUTINE COMPUTES THE MEAN AND PEAK POWER AND PR
* * * * *
SUBROUTINE POWER(LD, DATA, PAVE, PEAK, EB, N)
COMMON /I1/ IOPF, LSAMPL, NSYMB, NO1, NO2, NUMB(4,20), NI(4,4096)
COMMON /R1/ SAM, PI, BAUD, BW, AMPL(4,4), TIMEP(4,40)
COMPLEX DATA(LD)
PEAK=0.
PAVE=0.
DO 1 I=1, LD
  A=CABS(DATA(I))
  PAVE=PAVE+A*A
  IF (PEAK.LT.A) PEAK=A
  ICONTINUE
PAVE=PAVE/FLOAT(LD)/2.
PEAK=PEAK/PAVE
IF (N.EQ.1) EB=PAVE/BAUD*2.
IF (RETURN)
  RETURN
  < END

```

```

POW000010
POW000020
POW000030
POW000040
POW000050
POW000060
POW000070
POW000080
POW000090
POW000100
POW000110
POW000120
POW000130
POW000140
POW000150
POW000160
POW000170
POW000180
POW000190
POW000200
POW000210

```

FILE: P1 PORTAN A UNIV D/OF OTTAWA CMS RELRASP Q

```

A.KUCAR,1984 02 02,1985 04 17
SUBROUTINE COMPUTES PRINTS, AND PLOTS
1.)POWER SPECTRUM DENSITY AND OUT-OF-BAND ENERGY
IWBAT=0 -->OUT-OF-BAND ENERGY
      =1 -->SPECTRUM
      =2 -->BOTH
2.)POWER SPECTRUM DENSITY OF Weighted cosine signal
   Kaiser-Bessel signal
IWBAT=3
3.)N=-1 -->TRIANGULAR SIGNAL SHAPE
-----
LD2=2*LD
L1=LD/64
L3=L2G(L1)**.2**L3=L1
L4=L1/2
L5=L1+2
*****
SUBROUTINE P1(LD,LD2,L1,L2,L3,L4,L5,DATA,XA,XB,PSY,BWK,WK,IV,IP,W)
COMMON /I1/IOPE,LSAMPL,NSYMB,NO1,NO2,HUMB(4,20),RT(4,4696)
COMMON /R1/SAMP,PI,BAUD,BW,AMPL(4,4),TIMREL(4,4),ATMRF(4,30)
COMPLEI ON YB(LD2),PSY(L2),NBK(L3),WK(L4)
DIMENSION IO(3) GOTO 98
IF (JW.EQ.3) GOTO 98
LL1=L2+1
LL2=L2-2
P=0
DO 1 I=1,LD
  I1=I-1
  I2=I+1
  IF(I1.LE.0) I1=I1+LD
  YB(I)=REAL(DATA(I))
  XBP=XB(I)+XBI(I)+XBI(I+LD)
  P=P/LD2
DO 9 I=1,LD2
  I1=I
  I2=I+1
  XB(I1)=XB(I1)-P
WRITE(6)I,I1,I2,THE MEAN OF I+O channel:R17.5)
CALL P1(PPS(XB,Y,LD2,L1,0,PSY,PSY,XPS,NBK,WK,XA,IP,P)
P1=PSY(I1)
DO 2 I=1,L2
  YP=PSY(I1)/P
  IF(PSY(I1).EQ.0) Y=1.E-10
  PSY(I1)=10.*ALOG10(Y)
  XB(I1)=0
DO 3 I=1,L2
  XB(L3-I)=P1
  XB(L2-I)=XB(L1-I)+2.*10.**(PSY(L2-I)*.1)
  YB(I1)=XB(I1)
DO 4 I=1,L2
  Y=XB(I1)/P1

```

CCCCCCCCCCCCCCCCCCCC

```

P1 00010
P1 00020
P1 00030
P1 00040
P1 00050
P1 00060
P1 00070
P1 00080
P1 00090
P1 00100
P1 00110
P1 00120
P1 00130
P1 00140
P1 00150
P1 00160
P1 00170
P1 00180
P1 00190
P1 00200
P1 00210
P1 00220
P1 00230
P1 00240
P1 00250
P1 00260
P1 00270
P1 00280
P1 00290
P1 00300
P1 00310
P1 00320
P1 00330
P1 00340
P1 00350
P1 00360
P1 00370
P1 00380
P1 00390
P1 00400
P1 00410
P1 00420
P1 00430
P1 00440
P1 00450
P1 00460
P1 00470
P1 00480
P1 00490
P1 00500
P1 00510
P1 00520
P1 00530
P1 00540
P1 00550

```

FILE: P1 PORTRAN A UNIV D'OF OTTAWA CMS RELEASE P

```

4  Y=LE-10. Y=1.E-10
C  X=ALOG10(Y)
5  WRITE(6,5) Spectrum X Out-of-band energy
C  WRITE(6,6) (PSX(I),XB(I),I=1,L2)
6  FORMAT(2P16.7)
X=INTE(FLOAT(L2-1)*10)/(SAM)+1
SS=SUM(FLOAT(NSYMB))
DO 22 I=1,SS
22  Y=I-1
23  Y=PSX(I),IP
98  RETURN
C  TRIANG=0
IF (NUMB(N,1).EQ.-1) TRIANG=1.
ITIMEL(N,1)=TIMEL(N,1)/(1.+TRIANG)
NNH=IABS(NUMB(N,1))
P=0.
CALL PSD(N,NNH,TRIANG,P,SLOG,SZ)
J1=2001
IF (IP.GT.2) J1=1001
DO 12 J=1,J1
P=FLOAT(J-1001)/200.
CALL PSD(N,NNH,TRIANG,P,SLOG,SZ)
12  WRITE(3,23) P,SLOG,IP
END
-----
SUBROUTINE PSD(N,NNH,TRIANG,P,SLOG,SZ)
COMMON /R1/SAM,PL,NSYMB,NO1,NR6?,NUMB(4,20),RTA(4096)
C  COMMON /R1/SAM,BADD,BW,AMPL(4,4),TIMEL(4,4),TFPK(4,30)
IF (NNH.GT.0) GOTO 77
PL=PI*TIMEL(N,1)/SINH(TIMEX(N,1))
X=PI*SQRT(ABS(AMPL(N,1)*AMPL(N,1)-PL*PL))
IF (AMPL(N,1).LE.PL) GOTO 66
X=SQRT(ABS(X)/X)
GOTO 67 SINC(X)
66  CALL SINC(X)
67  SLIN=NO*X
IF (SLIN.EQ.0) SZ=SLIN
SLIN=SLIN/SZ
GOTO 78
78  Y=PI*TIMEL(N,1)*P
79  CALL SINC(X)
80  AMPL(N,1)*TIMEL(N,1)*X
GN=0.
C  TRIANG.EQ.1. GM=GN*GM
IF (NRH.EQ.1) GO TO 17
DO 16 K=2,NNH
DO 16 L=1,362
X=PI*TIMEL(N,K)*(P+(FLOAT(L)-2.)*TI*PK(N,K)/TIMEL(N,K)/2.)
CALL SINC(X)

```

```

P1 00560
P1 00570
P1 00580
P1 00590
P1 00600
P1 00610
P1 00620
P1 00630
P1 00640
P1 00650
P1 00660
P1 00670
P1 00680
P1 00690
P1 00700
P1 00710
P1 00720
P1 00730
P1 00740
P1 00750
P1 00760
P1 00770
P1 00780
P1 00790
P1 00800
P1 00810
P1 00820
P1 00830
P1 00840
P1 00850
P1 00860
P1 00870
P1 00880
P1 00890
P1 00900
P1 00910
P1 00920
P1 00930
P1 00940
P1 00950
P1 00960
P1 00970
P1 00980
P1 00990
P1 01000
P1 01010
P1 01020
P1 01030
P1 01040
P1 01050
P1 01060
P1 01070
P1 01080
P1 01090
P1 01100

```

FILE: P1 FORTRAN A UNIV D'/OP OTTAWA CMS RELEASE B

P1	011118
P1	011120
P1	011130
P1	011140
P1	011150
P1	011160
P1	011170
P1	011180
P1	011190

```

16 GN=GN+TIMEI(N,K)*AMPL(N,K)*X
17 CONTINUE
18 C=GN+GN/2
19 IF (P.EQ.0.) SZ=2.*G*G
20 SLIN=2.*G*G/SZ
78 IF (SLIN.LT.1E-10) SLIN=1.0E-10
   SLOG=10.*ALOG10(SLIN)
   RETURN
   END

```

FILE: SIGPHP FORTRAN A UNIV D'OP OTTAWA CMS RELEASE A

```

C C C C C C C C
A*KUCAR,1984,01,29,1985,04,18
Subroutine PLOTS (JOE=0) Y=SUM(A*COE,PI**t**K/L)) signal
      (JOE=1) I and 2 ch. 20 symbols
*****
SUBROUTINE SIGPHP(LD,DATA,JOE,IPEN,N)
COMMON /R1/LSAMPL,NSYMB,N01,N02,NUMR(4,20),HI(4,4096)
COMPLEX X,DATA(LD)
REAL MBSIO
IF (MBSIO.EQ.1) GO TO 4
DO 3 K=1,N
  DO 3 L=1,1081
    I=L-541
    I=PL0AN(I)*TIMEL(K,J)/1080.
    I=KNN(GT.0)GOTO 1
    I=AMPL(K,1)*SQRT(1.-4*T*T/TIMPL(K,1)/TIMPL(K,1))
    A1=MBSIO(1,A1,IER)/MBSIO(1,A0,IER)
    GO TO 3
    A2=AMPL(K,J)*COS(PI*T*TIME(K,J)/TIMEL(K,J))
    I=TIME(108)T,A2,KPEN
    RETURN
  DO 5 I=1,K
    DATA(I)
    A1=AREAL(DATAN-1)/SIN
    A2=7.5*PL0AN(TREAL(DATA(I)))
    A3=4.0+CABS(DATA(I))
    WRITE(10,F10.4,I2)
  RETURN
END

```

```

SIG000010
SIG000020
SIG000030
SIG000040
SIG000050
SIG000060
SIG000070
SIG000080
SIG000090
SIG000100
SIG000110
SIG000120
SIG000130
SIG000140
SIG000150
SIG000160
SIG000170
SIG000180
SIG000190
SIG000200
SIG000210
SIG000220
SIG000230
SIG000240
SIG000250
SIG000260
SIG000270
SIG000280
SIG000290
SIG000300
SIG000310
SIG000320
SIG000330
SIG000340
SIG000350
SIG000360
SIG000370
SIG000380
SIG000390
SIG000400
SIG000410
SIG000420
SIG000430
SIG000440

```

```

11
13
8
4
5
6

```

FILE: SINC PORTAN A UNIV D'/OF OTTAWA CFS RELEASE 4

```

C C C C C
A. KDCAR, 1983 07 31 *****
Subroutine CALCULATES sin(x)/x *****
Singular point x=0 is included, i.e. sin(0)/0=1. *****
*****
SUBROUTINE SINC(X)
IF (X.EQ.0.0) GO TO 1
Y=SIN(X)/X
RETURN
X=1.
RETURN
END
1

```

```

SINH00010
SINH00020
SINH00030
SINH00040
SINH00050
SINH00060
SINH00070
SINH00080
SINH00090
SINH00100
SINH00110
SINH00120
SINH00130

```

FILE: SYNCH PORIRAN A UNIV D°/OF OTTAWA CMS RELEASE Q

```

C C C C C
A.KUCAR, 1984 10 21, 1985 04 18
Subroutine SYNCHRONIZES the N-ary JAM received data
*****
SUBROUTINE SYNCH(LD, DATA, TP, PNOISE, MT, MQ, ER, LARY)
COMMON /I1/ IOFF, LSAMPL, NSYMB, NO1, NO2, YNMB(4,20), NI(4,40,96)
COMMON /R1/ SAM, PI, BAUD, BW, AMPL(4,4), TEMPL(4,30)
COMPLEX DATA(LD), EQ(0)
IF (IOFF.EQ.0) GOTO 111
DO I=1, IOFF
  A=AIMAG(DATA(LD))
  DO J=2, LD
    J1=LD-J+2
    DATA(J1)=CMPLX(REAL(DATA(J1)), AIMAG(DATA(J1-1)))
    DATA(J)=CMPLX(REAL(DATA(J)), A)
  WOLD=0
  NS2=2*NSYMB
  K=1
  NEW=0
  J=1
  NSYMB
  J1=J-1
  J=J+1
  IF(J1.LD) J1=J1-LD
  YB=REAL(DATA(J1))+REAL(DATA(J1+1))/2.
  YBC=AIMAG(DATA(J1))*XB
  YPC=ABS(3.6T.O.)
  YPB=ABS(4.6T.O.)
  YPC=ABS(5.6T.O.)
  YPB=ABS(6.6T.O.)
  COPI=INOE
  IF(WOLD.NE.NEW) GOTO 5
  WOLD=NEW
  K=K+1
  IF(WOLD.LT.NS2.AND.K.LE.LD) GOTO 3
  NOP=NOP-1
  CALL TIMESH(LD, DATA, TP, NOP)
  EQ=EQ+1
  EQ2=EQ
  HI=1
  SNR=SQRT(PNOISE*EB/10.)
IF (LARY.GT.1) GOTO 2
DO J=1, LSAMPL
  EQ=0.
  EQ2=0.
  K=1
  NSYMB
  J1=J
  LSAMPL
  J1=J-1
  J=J+1
  YB=REAL(DATA(J1))+REAL(DATA(J1+1))/2.
  YPB=AIMAG(DATA(J1))*XB
  YPC=SIGN(1., YB)
  YPB=ABS(YB)/SNR

```

SYN000010  
SYN000020  
SYN000030  
SYN000040  
SYN000050  
SYN000060  
SYN000070  
SYN000080  
SYN000090  
SYN000100  
SYN000110  
SYN000120  
SYN000130  
SYN000140  
SYN000150  
SYN000160  
SYN000170  
SYN000180  
SYN000190  
SYN000200  
SYN000210  
SYN000220  
SYN000230  
SYN000240  
SYN000250  
SYN000260  
SYN000270  
SYN000280  
SYN000290  
SYN000300  
SYN000310  
SYN000320  
SYN000330  
SYN000340  
SYN000350  
SYN000360  
SYN000370  
SYN000380  
SYN000390  
SYN000400  
SYN000410  
SYN000420  
SYN000430  
SYN000440  
SYN000450  
SYN000460  
SYN000470  
SYN000480  
SYN000490  
SYN000500  
SYN000510  
SYN000520  
SYN000530  
SYN000540  
SYN000550

C C C C C

C

FILE: SYNCH PORTAN A UNIV D'OF OTTAWA CMS RELEASE A

```

IP (XB.GT.12.) XB=12.
EI=EI+ERPC(XB)/2.
XB=ABS(YB)/SNR
IP (XB.GT.12.) XB=12.
EQ=EQ+ERPC(XB)/2.
CONTINUE
6 IP(EI.LE.EI) GO TO 8
EI=EI
HI=J
8 EQ=EQ
EQ=EQ
CONTINUE
7 GO TO 1
-----
2 HIGH=FLOAT(LARY-1)
DO 17 J=1,LSAMPL
EI=0.
EO=0.
DO 16 K=1,NSYMB
J1=(K-1)*LSAMPL+J
XB=((REAL(DATA(J1))+REAL(DATA(J1+1)))/2.
YB=((AIMAG(DATA(J1))+AIMAG(DATA(J1+1)))/2.
DX1=ABS(XB)
DY1=ABS(YB)
INDI=0
AI=FLOAT(NI(3,K)) INDI=1
IP((YB*AI).LE.0.) INDI=1
ATHR1=AI-1.
ATHR2=AI+1.
THRI=0
IF (AI.EQ.HIGH) GOTO 30
IF (DY1.GE.THR2.OR.DX1.LE.THR1) INDI=1
COT 0 40
IF (DY1.LE.THR1) INDI=1
30 LAGI=1
40 INDI=0
AI=FLOAT(NI(4,K)) INDO=1
IP((YB*AI).LE.0.) INDO=1
ATHR1=AI-1.
ATHR2=AI+1.
THRQ=0
IF (AI.EQ.HIGH) GOTO 50
IF (DY1.GE.THR2.OR.DX1.LE.THRQ) INDO=1
COT 0 60
IF (DY1.LE.THRQ) INDO=1
50 LAG2=1
60 DX2=ABS(DX1-THR1)/SNR
DY2=ABS(DY1-THRQ)/SNR
EIF=(EI+ERPC(DX2))/2.
IF (LAG3(DX1-THR1)/SNR

```

SYN00560  
SYN00570  
SYN00580  
SYN00590  
SYN00600  
SYN00610  
SYN00620  
SYN00630  
SYN00640  
SYN00650  
SYN00660  
SYN00670  
SYN00680  
SYN00690  
SYN00700  
SYN00710  
SYN00720  
SYN00730  
SYN00740  
SYN00750  
SYN00760  
SYN00770  
SYN00780  
SYN00790  
SYN00800  
SYN00810  
SYN00820  
SYN00830  
SYN00840  
SYN00850  
SYN00860  
SYN00870  
SYN00880  
SYN00890  
SYN00900  
SYN00910  
SYN00920  
SYN00930  
SYN00940  
SYN00950  
SYN00960  
SYN00970  
SYN00980  
SYN00990  
SYN01000  
SYN01010  
SYN01020  
SYN01030  
SYN01040  
SYN01050  
SYN01060  
SYN01070  
SYN01080  
SYN01090  
SYN01100

FILE: SYNCH PORTAN A UNIV D'/OP OTTAWA CMS RELEASE P A

```

10 IF (DX2.GT.12.} /2.} DI2=12.
    IF (EI+EREC(DY2.} /2.} EI=EI+1.
    IF (INDI.EQ.1.} EI=DY2=12.
    EQ=EQ+EREC(DY2.} /2.} GOTO 12
    IF (LABS(DY1-THRQ2)/SNR.
    IF (DY2.GT.12.} /2.} EQ=EQ+1.
    EQ=EQ+EREC(DY2.} /2.} EQ=EQ+1.
12 CONTINUE
16 IF (EICI.LE.EI) GO TO 18
    IF (EI=J
    IF (EQ=EQ
18 IF (EQ2.LE.EQ) GO TO 17
    EQ=EQ+J
17 CONTINUE
    IF (MI) /SAM
    EQ=FLOAT(MO) /SAM
    WRITE(6,9) EI,EQ
    WRITE(8,9) EI,EQ
    9 PORTAN('Sampling points for I and Q channels',?PR.?)
    RETURN
    END

```

```

SYNO11110
SYNO11120
SYNO11130
SYNO11140
SYNO11150
SYNO11160
SYNO11170
SYNO11180
SYNO11190
SYNO11200
SYNO11210
SYNO11220
SYNO11230
SYNO11240
SYNO11250
SYNO11260
SYNO11270
SYNO11280
SYNO11290
SYNO11300
SYNO11310
SYNO11320
SYNO11330
SYNO11340
SYNO11350

```

FILE: TIMESH PORTAN A UNIV D./OF OTTAWA CMS RELEASE A

```

C C C C C
A.KUCAR,1984 01 04,1985 04 18
SUBROUTINE SHIFTS the signal in TIME DOMAIN
**
SUBROUTINE TIMESH(LD,DATA,TP,IFOP)
COMMON /I1/IOPF,LSAMPL,NSYMB,NO1,NO2,NUMR(4,20),RI(4,4096)
COMPLETE,DATA(LD),TF(LD)
IF (IFOP.EQ.0) RETURN
J=LD-IABS(IFOP)
K=J+1
IF (IPOP.LT.0) GOTO 4
DO 1 I=1,J
  DATA(I)=DATA(LD)
DO 2 I=1,J
  DATA(I)=DATA(I)
DO 3 I=1,J
  DATA(I)=TF(I)
RETURN
4
DO 4 I=1,IPOP
  LD=I-IFOP
  DATA(I)=DATA(I)
DO 5 I=1,IPOP
  DATA(I)=IFOP
DO 6 I=1,J
  DATA(I)=DATA(I)
DO 7 I=1,J
  DATA(I)=TF(I)
RETURN
END
TIM000010
TIM000020
TIM000030
TIM000040
TIM000050
TIM000060
TIM000070
TIM000080
TIM000090
TIM000100
TIM000110
TIM000120
TIM000130
TIM000140
TIM000150
TIM000160
TIM000170
TIM000180
TIM000190
TIM000200
TIM000210
TIM000220
TIM000230
TIM000240
TIM000250
TIM000260
TIM000270
TIM000280

```



FILE: WINDOW FORTRAN A UNIV.D'/OP OTTAWA CMS RELEASE P

```

C C C C C C C C
A KUCAR, 1983 10 28, 1985 04 18
SUBROUTINE CALCULATES WINDOW (WEIGHT) FUNCTIONS
MAX OVERLAPPING L=4TS
SUBROUTINE WINDOW(LD,M1,L1,M2,L2,IP,R,N,LOOP)
COMMON /I1/IOPP,LSAMPL,NSY,HB,NO1,NO2,NUMB(4,20),WI(4,4096)
COMMON /R1/SAM,PI,BAUD,BW,AMPL(4,4),TIMEI(4,4),TIMPR(4,30)
REAL LOOP,GT(.1) GOTO 4
L8=LSAMPL/2
L9=LSAMPL*2
KNN=NUMB(N,1)
KN=KNN
IP(KNN,EO,0) KN=1
TL=TIMEI(1,1)
DO 3 I=1,LSAMPL
  R(I)=0.
  DO 6 J=1,KNN
    IF (TIMEI(N,J).GT.TL) TL=TIMEI(N,J)
  DO 6 I=1,LSAMPL
    U=-.5+.5*FLOAT(I-1)/SAM
    CALL WIND1(J,U,Y,N,KNN,IP)
    R(I)=R(I)+Y
  IF (TL.LE.1.) RETURN
  DO 1 J=1,KNN
    ITL=(INT(EQ.0) + TIMEI(N,J)*SAM) - LSAMPL / 2
    IF (ITL.GT.L8) ITL=L8
    DO 1 I=1,ITL
      U=LSAMPL - I + 1
      U=.5+.5*FLOAT(I-1)/SAM
      CALL WIND1(J,U,Y,N,KNN,M1)
      R(I)=R(I)+Y
    CALL WIND1(J,U,Y,N,KNN,L1)
    R(I)=R(I)+Y
  IF (TL.LE.2.) RETURN
  DO 2 J=1,KNN
    ITL=(INT(EQ.0) + TIMEI(N,J)*SAM) - L9 / 2
    IF (ITL.GT.L8) ITL=L8
    DO 2 I=1,ITL
      U=LSAMPL - I + 1
      U=.5+.5*FLOAT(I-1)/SAM
      CALL WIND1(J,U,Y,N,KNN,L1)
      R(I)=R(I)+Y
      CALL WIND1(J,U,Y,N,KNN,M1)
      R(L8+I)=R(L8+I)+Y
  IF (TL.LE.3.) RETURN

```

```

WIN000010
WIN000020
WIN000030
WIN000040
WIN000050
WIN000060
WIN000070
WIN000080
WIN000090
WIN000100
WIN000110
WIN000120
WIN000130
WIN000140
WIN000150
WIN000160
WIN000170
WIN000180
WIN000190
WIN000200
WIN000210
WIN000220
WIN000230
WIN000240
WIN000250
WIN000260
WIN000270
WIN000280
WIN000290
WIN000300
WIN000310
WIN000320
WIN000330
WIN000340
WIN000350
WIN000360
WIN000370
WIN000380
WIN000390
WIN000400
WIN000410
WIN000420
WIN000430
WIN000440
WIN000450
WIN000460
WIN000470
WIN000480
WIN000490
WIN000500
WIN000510
WIN000520
WIN000530
WIN000540
WIN000550

```

FILE: WINDOW FORTRAN A UNIV D'/OP OTTAWA CMS RPLPASP A

```

O 7 J=1,KN
ITL=(INT{TIMEL(N,J)*SAM}-L8-LSAMPL)/?
IF (ITL.EQ.0) ITL=1
DO 7 I=1,ITL
L1=LSAMPL/I+1
L2=L1.5+FLOAT(I-1)/SAM
CALL WIND1(J,U,Y,N,KNN,H2)
CR(I1)=R(I1)+Y
CALL WIND1(J,U,Y,N,KNN,L2)
CR(I1)=R(I1)+Y
7 RETURN
END

*****
KAISER-BESSEL and WEIGHTED COSINE WINDOWS-->Subc.WINDOW
*****
SUBROUTINE WIND1(J,T,Y,N,KNN,JIP)
COMMON /R1/SAM,PI,BAUD,BA,AMPL(4,4),TIMEL(4,4),TIMEK(4,30)
REAL KNN,GT,0) GOTO 1
I=AMPL(N,1)}*SORT(1.-4.*T/TIMEL(N,1)/TIMEL(N,1))
Y=NMBSIO(1,Y,IER)/NMBSIO(1,Y,IER)
Y=JIP*Y
RETURN
1 Y=JIP*AMPL(N,J)*COS(PI*TIMEK(N,J)/TIMEL(N,J)*T)
RETURN
END

```

```

WIN00560
WIN00570
WIN00580
WIN00590
WIN00600
WIN00610
WIN00620
WIN00630
WIN00640
WIN00650
WIN00660
WIN00670
WIN00680
WIN00690
WIN00700
WIN00710
WIN00720
WIN00730
WIN00740
WIN00750
WIN00760
WIN00770
WIN00780
WIN00790
WIN00800
WIN00810
WIN00820
WIN00830
WIN00840

```

CCCCC



FILE: WDFL FORTRAN A UNIV D'OF OTTAWA CMS RELEASE 4

```

5 CALL UD1
6 WRITE(1,7)SAMB,DEG1,PEA,G1,G2,AN1,GPI,GPIN
7 FORMAT(1,# of levels L=04)
8 FORMAT(I2)
9 FORMAT(I4)
10 FORMAT(8E10.3)
11 FORMAT(PEBNO=,P7.2, at Pe=1E-,I2)
12 FORMAT(EBR exp=06)
13 FORMAT(Staggered=01,Non-staggered=00)
14 END
C
SUBROUTINE UD1
COMMON L1,L2,LM1,LM2,LM1SQ,L2L,L4L
COMMON P1,AMB,PEA,PEB,RA,RA1,RR,RR1,G1,G2,AN1,FI,F1,R2,R3
COMMON PEA1,PEB1,PEI1,RA1,RBL,GPI,GPIN,BD1,BD2,BD3,RA4
COMMON PIP1,PIP3
PEB=0.
PEI2=0.
I=0.
G2=0.
I2=0.
X=COS(PI)
Y=SIN(PI)
DO 14 N0=1,L2,2
M=M0-L*LOCAT(M-1)
PPI=PM1+2
IM=IABS(M)
PEN=0.
PEI12=N0=1,L2,2
DN=M0-L
PEA11=N9=1,L2,2
D01=N9-L*8=1,3,2
D07=M8-L
I3=IABS(M+M1+M7)
IIP={I13-NE.M*7}
IIP={M7-NE.M*1}
IIP={M7-NE.M*1}
D05=M6-L
I4=IABS(M+M1+M5)
IIP={I4-NE.M*5}
IIP={M-NE.M*5}
IIP={M-NE.M*5}
IY1={M+M1+RAM}*CI
D02=N9-L
D01=N9-L*8=1,3,2
RAM=M1*BD2
RAM=M1*RA
RAM=M1*BD7*PIP3

```

```

WDF000560
WDF000570
WDF000580
WDF000590
WDF000600
WDF000610
WDF000620
WDF000630
WDF000640
WDF000650
WDF000660
WDF000670
WDF000680
WDF000690
WDF000700
WDF000710
WDF000720
WDF000730
WDF000740
WDF000750
WDF000760
WDF000770
WDF000780
WDF000790
WDF000800
WDF000810
WDF000820
WDF000830
WDF000840
WDF000850
WDF000860
WDF000870
WDF000880
WDF000890
WDF000900
WDF000910
WDF000920
WDF000930
WDF000940
WDF000950
WDF000960
WDF000970
WDF000980
WDF000990
WDF01000
WDF01010
WDF01020
WDF01030
WDF01040
WDF01050
WDF01060
WDF01070
WDF01080
WDF01090
WDF01100

```



FILE: WDFL FORTRAN A UNIV D/OF OTTAWA CMS RELEASE A

```

IF (JN7.EQ.3) RAN1=N*RB1
IF (N7.EQ.N1) .AND. (N7.NE.N) } RAN1=V*RD3*PIP1
IF (N7.NE.N1) .AND. (N.EQ.N7) } RAN1=N*RD3
IF (N7.NE.N1) .AND. (N.NE.N7) } RAN1=V*RR1/PIP1
DO 16 N6=1,3,2
N5=N6-L
J4=IABS (N+N1+N5)
JIP ((J4.EQ.3) RAN=N1*RB
IF ((N.NE.N5) .AND. (N1.NE.N)) RAN=N1*RD4*PIP3
IF ((N.NE.N5) RAN=N1*BD4
YAB1=(RAN1+RB1)
IF (I9.EQ.1) PEI=ERFC ((YAB1-FPI1)*ERN)
IF ((I1.EQ.1) .OR. (LM1)) PEI=ERFC ((FMI1-YAB1)*RBN)
IF ((I1.EQ.1) .OR. (LM1)) .AND. (GT.MPC)
*PPI=RRP ((I1.FMI1-YAB1)*ERN)
IF ((I1.EQ.1) .OR. (LM1)) .AND. (I1.LT.M)
*PPI=ERFC ((YAB1-FPI1)*ERN)
16 PEI1=PEI1+PEI1
13 PEI1=PEI1+N*PEI1
32=CE2-I1*M*PENI
CONTINUE
14 AN1=CI1-PEI2
-----
DO 24 N0=1,L2,2
N=MOPLOCAT(M-1)
PPI=PH1+2
PM=IABS(M)
PEN=N0
DO 22 N0=1,L2,2
N=N0-L
PEA1=N0
DO 21 N9=1,L2,2
DO 21 N8=1,3,2
M7=M8-L
I3=IABS (M+N1+M7)
IF (I3.EQ.3) RAN1=N*RA1
IF (I3.NE.M7) RAN1=M*BD1
IF (N7.EQ.M1) .AND. (M7.NE.M)) RAN1=V*RD1*PIP3
DO 21 N7=1,3,2
N5=N6-L
I4=IABS (M+N1+M5)
IF (I4.EQ.3) RAN=N1*RA*PIP1
IF (I4.NE.M5) .AND. (M1.NE.M)) RAN=N1*RD2
IF (I4.NE.M5) .AND. (M1.EQ.M))
IF (I4.NE.M5) .AND. (M1.NE.M)) RAN=N1*RA
IF (I4.NE.M5) .AND. (M1.NE.M)) RAN=N1*RD2*PTP3
IA1=1
IAO

```

WDF01660  
WDF01670  
WDF01680  
WDF01690  
WDF01700  
WDF01710  
WDF01720  
WDF01730  
WDF01740  
WDF01750  
WDF01760  
WDF01770  
WDF01780  
WDF01790  
WDF01800  
WDF01810  
WDF01820  
WDF01830  
WDF01840  
WDF01850  
WDF01860  
WDF01870  
WDF01880  
WDF01890  
WDF01900  
WDF01910  
WDF01920  
WDF01930  
WDF01940  
WDF01950  
WDF01960  
WDF01970  
WDF01980  
WDF01990  
WDF02000  
WDF02010  
WDF02020  
WDF02030  
WDF02040  
WDF02050  
WDF02060  
WDF02070  
WDF02080  
WDF02090  
WDF02100  
WDF02110  
WDF02120  
WDF02130  
WDF02140  
WDF02150  
WDF02160  
WDF02170  
WDF02180  
WDF02190  
WDF02200



FILE: WDFL      FORTRAN A      UNIV D\* / OF OTTAWA CMS RELEASE A

```

IF ( J3.EQ.3 ) RAN1=N*RB1      RAN1=Y*RD3*PIP3
IF ( J3.EQ.3 ) .AND. ( N7.NE.N )      RAN1=M*RD3
IF ( J3.EQ.3 ) .AND. ( N7.EQ.N7 )      RAN1=Y*RR1/PIP1
DO 26 N6=1,3,2      .AND. ( N7.NE.N )      RAN1=Y*RR1/PIP1
N5=N6-L ( N+N1+N5 )
J4=IABS ( J4.EQ.3 ) RAN=N1*RB
IF ( J4.EQ.3 ) .AND. ( N1.NE.N )      RAN=M1*RD4*PIP3
IF ( J4.EQ.3 ) .AND. ( N1.NE.N )      RAN=N1*BD4
IF ( J4.EQ.3 ) .AND. ( N5.NE.N )      RAN=N1*BD4
YAB1=(YAN1+YB1) *SX
YAB1=I9.EQ.1) PEI=ERPC ( YAB1-PPI1)*ERN )
IF ( I9.EQ.1 ) PEI=ERPC ( (PMT1-YAB1)*ERN )
IF ( I9.EQ.1 ) PEI=ERPC ( (GT.M) )
IF ( I9.EQ.1 ) PEI=ERPC ( (EBN)-YAB1 )
IF ( I9.EQ.1 ) PEI=ERPC ( (PPT1-YAB1)*ERN )
IF ( I9.EQ.1 ) PEI=ERPC ( (I1.LT.M) )
IF ( I9.EQ.1 ) PEI=ERPC ( (YAB1-FPI1)*ERN )
IF ( I9.EQ.1 ) PEI=ERPC ( (YAB1-PMI1)*ERN )
26      PEI1=PEI1+PEI1
23      PEJ1=PEJ1+W*PEI1
24      IZ=G2+I1*PEJ1
C-----
32=G2*P3/2
G1=1-31*P3
AN1=1-AG10*F3
PEA=-ALOG10 (PBB*F2)
GPI=G1*SX+G2*CX
SPIN=2.*GPI/AN1
END

```

- WDF02760
- WDF02770
- WDF02780
- WDF02790
- WDF02800
- WDF02810
- WDF02820
- WDF02830
- WDF02840
- WDF02850
- WDF02860
- WDF02870
- WDF02880
- WDF02890
- WDF02900
- WDF02910
- WDF02920
- WDF02930
- WDF02940
- WDF02950
- WDF02960
- WDF02970
- WDF02980
- WDF02990
- WDF03000
- WDF03010
- WDF03020
- WDF03030
- WDF03040
- WDF03050
- WDF03060

C-----





